**Multiscale Modeling of Tuberculosis Disease and
Treatment to Optimize Antibiotic Regimens**

by

Joseph M. Cicchese

A dissertation submitted in partial fulfillment
of the requirements for the degree of
Doctor of Philosophy
(Chemical Engineering)
in the University of Michigan
2020

Doctoral Committee:

     Professor Jennifer J. Linderman, Chair
     Assistant Professor Bryan R. Goldsmith
     Professor Denise E. Kirschner
     Associate Professor Greg Thurber

Joseph M. Cicchese
cicchese@umich.edu
ORCID iD: 0000-0001-6145-3124

© Joseph M. Cicchese 2020

Acknowledgments

There are so many people whose support, both in research and in life, I have relied on to complete this work. I have so much gratitude for being advised by Jennifer Linderman. Her excellence as a mentor and dedication to her students exemplify what it means to be a research advisor. She cares about developing her students and producing excellent researchers. I cannot thank you enough for all the guidance you have given me. I am incredibly fortunate that I also had Denise Kirschner as my mentor. I gained so much by being welcomed into your lab, and I thank you for all you taught me. Your knowledge and experience helped develop me into a better researcher. And of course, thanks for all the lab snacks!

Thank you to all the members of the Linderman and Kirschner Labs, both current and former. I value all the conversations we had and relied on them to generate new ideas in my research. I can only hope I have helped you all as much as you have helped me.

To all my friends, both in Michigan and across the country, I thank you all for the countless memories and support you have given me. I am so lucky to have so many wonderful people in my life.

To my parents, the values you taught me have helped to shape me into the person I am today. The support you have always shown me give me the strength and confidence to take on any challenge. I thank you for always being there for me.

And finally, thank you to my wife, Jacqueline. I would not have been able to complete this journey without your unwavering love and support for me. Through all the challenges I faced along the way, you have given me true joy and meaning in my life. I could not ask for a better partner to build a life with.

Table of Contents

List of Figures

List of Tables

List of Appendices

Abstract

Tuberculosis (TB) is one of the world's deadliest infectious diseases. Caused by the pathogen *Mycobacterium tuberculosis* (Mtb), the standard regimen for treating TB consists of treatment with multiple antibiotics for at least six months. There are a number of complicating factors that contribute to the need for this long treatment duration and increase the risk of treatment failure. Person-to-person variability in antibiotic absorption and metabolism leads to varying levels of antibiotic plasma concentrations, and consequently lower concentrations at the site of infection. The structure of granulomas, lesions forming in lungs in response to Mtb infection, creates heterogeneous antibiotic distributions that limit antibiotic exposure to Mtb. Microenvironments in the granuloma can shift Mtb to phenotypic states that have higher tolerances to antibiotics. We can use computational modeling to represent and predict how each of these factors impacts antibiotic regimen efficacy and granuloma sterilization.

In this thesis, we utilize an agent-based, computational model called *GranSim* that simulates granuloma formation, function and treatment. We present a method of incorporating sources of heterogeneity and variability in antibiotic pharmacokinetics to simulate treatment. Using *GranSim* to simulate treatment while accounting for these sources of heterogeneity and variability, we discover that individuals that naturally have low plasma antibiotic concentrations and granulomas with high bacterial burden are at greater risk of failing to sterilize granulomas during antibiotic treatment. Importantly, we find that changes to regimens provide greater improvements in granuloma sterilization times for these individuals. We also present a new pharmacodynamic model that incorporates the synergistic and antagonistic interactions associated with combinations of antibiotics. Using this model, we show that *in vivo* antibiotic concentrations impact the strength of these interactions, and that accounting for the actual concentrations within

granulomas provides greater predictive power to determine the efficacy of a given antibiotic combination.

A goal in improving antibiotic treatment for TB is to find regimens that can shorten the time it takes to sterilize granulomas while minimizing the amount of antibiotic required. With the number of potential combinations of antibiotics and dosages, it is prohibitively expensive to exhaustively simulate all combinations to achieve these goals. We present a method of utilizing a surrogate-assisted optimization framework to search for optimal regimens using *GranSim* and show that this framework is accurate and efficient. Comparing optimal regimens at the granuloma scale shows that there are alternative regimens using the antibiotic combination of isoniazid, rifampin, ethambutol and pyrazinamide that could improve sterilization times for some granulomas in TB treatment. In virtual clinical trials, these alternative regimens do not outperform the regimen of standard doses but could be acceptable alternatives. Focusing on identifying alternative regimens that can improve treatment for high risk patients could help to significantly decrease the global burden for TB. Overall, this thesis presents a computational tool to evaluate antibiotic regimen efficacy while accounting for the complicating factors in TB treatment and improves our ability to predict new regimens that can improve clinical treatment of TB.

Chapter 1 Introduction

1.1 Motivation

Tuberculosis is one of the world's deadliest infectious diseases and has plagued humanity for thousands of years. Caused by the pathogen *Mycobacterium tuberculosis* (Mtb), it has waged a war of attrition against humanity, evading immune responses and drug therapies, while simultaneously surviving in human lungs for years. The current treatment for TB involves months of antibiotics, and while it is >95% effective against drug-susceptible Mtb when the regimen is properly adhered to, there is still a need to find ways to lessen the global disease burden [1]. TB treatment is further complicated by drug-resistant strains of Mtb, which require the use of alternative antibiotics and are becoming increasingly difficult to treat. Individuals have varying pharmacokinetics (PK) and complex lung lesions in TB disease that both generate variability and heterogeneity in antibiotic exposure at the site of infection. Combinations of antibiotics can lead to synergistic or antagonistic effects on the pharmacodynamic (PD) effect. Investigating all possible drug regimens to find an optimal therapy is difficult considering the number of drug candidates available for TB. Given the variability of disease, it is also difficult to know whether that optimal therapy will be optimal for all patients. In this thesis, I will present a multi-scale computational model that serves as a tool to integrate the PK and disease variability, PD drug interactions, and optimization algorithms to predict optimal antibiotic regimens. Using this model, I demonstrate how sources of heterogeneity in TB disease and treatment impact granuloma sterilization during antibiotic therapy, and how spatial gradients within the granuloma can impact antibiotic interactions and PD effect. Using surrogate-assisted optimization algorithms, I predict potential optimal antibiotic regimens and compare those regimens in a virtual clinical trial setting.

1.2 Global tuberculosis disease burden

TB is one of the world's most common infectious diseases and is the leading cause of death from a single infectious pathogen. According to the 2019 WHO Global Tuberculosis Report, an estimated 10 million new TB cases were reported in 2018, and approximately 1.5 million TB-related deaths [2]. The 'End TB' strategy is an initiative launched by the WHO that aims to reduce the number of TB-related deaths by 90% and the TB incidence rate by 80% by 2030 when compared to the 2015 statistics. Co-infection with TB and HIV is common, and approximately 250,000 of the 2018 TB-related deaths were HIV-positive people [2]. Risk factors associated with developing active TB disease include HIV, undernutrition, immunosuppressive therapies, as well as socioeconomic factors including overcrowding and poverty [3]. The majority of TB cases occurred in South-East Asia, Africa, and Western Pacific regions, with 86% of 2018 cases in those three regions [2].

1.3 Tuberculosis treatment

As a bacterial infection, the standard of care for TB treatment involves a regimen of antibiotics. The current recommended regimen for treating active TB disease involves treatment with four first-line antibiotics for up to six months: isoniazid (INH, H), rifampin (RIF, R), ethambutol (EMB, E) and pyrazinamide (PZA, Z) [4]. Multi-drug resistant TB (MDR-TB) has been an emerging problem, and there were a total of approximately 186,000 MDR-TB and rifampin-resistant TB in 2018 [2]. MDR-TB is classified as resistant to both INH and RIF. The introduction of fluoroquinolones, including moxifloxacin (MXF, M), levofloxacin (LVX, L) and gatifloxacin (GFX, G), have led to new regimens used to treat MDR-TB. While a fluoroquinolone is strongly recommended for use in MDR-TB treatment, extensively drug-resistant TB (XDR-TB) is additionally resistant to a fluoroquinolone and an injectable antibiotic and presents an even greater challenge to treatment. Depending on the specific antibiotics a strain of Mtb is resistant to, guidelines recommend building a regimen containing five or more drugs that contain either moxifloxacin or levofloxacin, bedaquiline, linezolid, clofazimine and cycloserine, with an extensive list of secondary antibiotics consisting of oral and injectable antibiotics if a regimen is unable to be built from those prioritized drugs [5]. Recently, the Nix-TB

regimen, consisting of bedaquiline, linezolid, and pretomanid, has shown success in leading to high percentages of favorable outcomes after 6 months of therapy in patients with XDR-TB or nonresponsive MDR-TB [6].

1.4 Tuberculosis disease pathology

1.4.1 Clinical description of tuberculosis

Individuals are infected with Mtb when they inhale aerosolized droplets that contain the pathogen, expelled from contagious individuals when they cough or breathe [7]. When someone is infected with the pathogen, they may not progress to active disease and instead harbor a latent infection [8]. Developing active disease is associated with symptoms such as fever, cough, night sweats and chest pains. While pulmonary TB is most common, extrapulmonary TB can occur, involving infection of other organs [9]. Extrapulmonary TB in also more common in children, who are more susceptible to progressive disease[10]. Individuals with latent infection are at risk of progressing to active disease, as latent infection can persist for years. Circumstances that lead to immune suppression, such as age, co-infection with HIV, or immune suppressive medication, can result in reactivation of latent disease [3]. While the clinical definition of latent versus active disease is traditionally binary, it is widely thought that individuals infected with Mtb lie on a spectrum from latent to active disease [11].

1.4.2 Immune response to infection and granuloma formation

The immune response in TB occurs over multiple organs and involves numerous cell types (Figure 1.1). Initially, Mtb in the lung are phagocytized by macrophages, initiating the immune response leading to granuloma formation. Antigen presenting cells, such as dendritic cells, will bring antigen to lymph nodes, and present to naïve T cells. Meanwhile, at the site of infection, cytokine secretion and signaling pathways recruit macrophages and neutrophils to fight the infection. The adaptive immune response recruits T cells from the lymph node to the granuloma site. T cells are then transported to the granuloma to aid in immune activation and cytotoxic function.
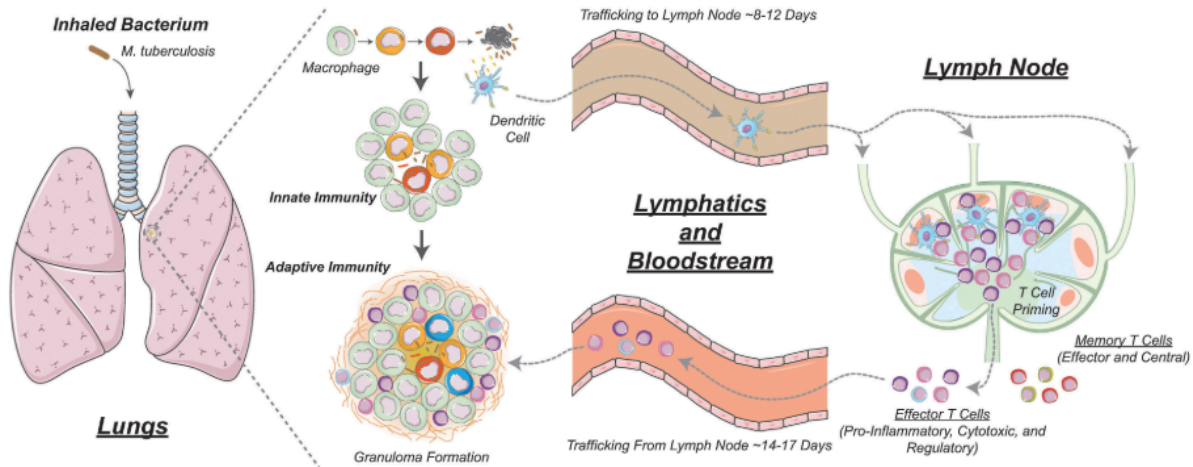
Figure 1.1 Multiscale immune response in TB.
The immune response in TB is complex and occurs over multiple length and time scales and involves multiple organs. The response is initiated when Mtb is inhaled into the lungs. Mtb infect macrophages in the lung, initiating the innate immune response and recruitment of other macrophages, neutrophils and dendritic cells to the cite of infection. Meanwhile, dendritic cells traffic antigen to the lymph nodes, where they prime a T cell response. T cells eventually travel to the lung, initiating the adaptive immune response at the infection site, and completing the formation of a granuloma. Figure adapted from reference [12].

One aspect of TB disease that allows for the latent infection is the granuloma. The granuloma is a collection of immune cells, bacteria, and necrotic tissue. It forms in response to the infection, in an attempt to both kill the pathogen and prevent the spread of infection [13]. In TB disease, multiple granulomas can form in the lungs, arising from multiple infection sites or developing due to the dissemination of existing infection [14]. The arrangement of a granuloma is classically viewed as containing macrophages and other leukocytic cells, surrounded by a lymphocyte cuff containing T cells [15,16]. As cells die in the granuloma, caseum, consisting of dead cell debris, can develop in the center of the granuloma [12]. These caseous regions are typically hypoxic, slowing the metabolism and increasing antibiotic tolerance of Mtb in these areas [17,18]. Fibrosis can also occur in granulomas, often associated with healing granulomas [16,19]. Pulmonary cavitation is another common pathological feature of TB that arises due to the liquification and degradation of the granuloma structure, and is associated with treatment failure [20,21].

1.5 Pharmacokinetics of TB antibiotics

The purpose of pharmacokinetic (PK) studies on TB drugs is to determine how the drug is absorbed and metabolized in the body, and how well the drug is able to reach the

granulomas where Mtb reside. These studies provide evidence to determine appropriate dosing, and other factors that influence plasma exposure for different antibiotics. Population PK studies seek to identify covariates that exist in populations to determine what doses are both safe and effective for individuals in a population [22]. These studies can help to identify conditions or patients that may be at risk for sub-therapeutic levels of antibiotic and thus at increased risk for resistance or treatment failure. The PK of the first-line antibiotics (INH, RIF, EMB and PZA) have been extensively studied [23–27]. Population PK studies have also been used to determine effective doses in populations for newer anti-TB drugs, such as fluoroquinolones [28], linezolid [29], bedaquiline [30] and pretomanid [31].

Sources of population variability come from numerous factors, such as genetic differences in the population, co-administration with other drugs (especially HIV medication), and even nutrition [25,32–34]. Understanding the population-level variability and the factors that influence drug concentrations in plasma has important implications on treatment outcome [35]. Techniques such as the hollow-fiber model have provided a way to study how varying levels of drug concentration *in vitro* impact the pharmacodynamic effect and emergence of resistance for numerous antibiotics [36–40].

Understanding the sources and impact of variability in plasma concentrations is important because it is a potential cause of sub-therapeutic antibiotic concentrations in granulomas [41]. As Mtb reside inside granulomas in TB disease, the ultimate target for antibiotics are these lesions, and antibiotics must travel from blood into the lung environment, and ultimately distribute throughout the granuloma in sufficient concentrations to be effective [42]. The granuloma itself, and in particular caseous and necrotic portions of the granuloma, can present a physiological barrier to antibiotic diffusion, which can impact an antibiotic's ability to sterilize a granuloma [43]. While *in vitro* and physiochemical properties can influence distribution in tissue, attempts to find strong correlations between these measurements and effective *in vivo* concentrations have failed [44]. Studies looking at distribution of INH, RIF, EMB and fluroquinolones in

rabbit granulomas have uncovered important trends and patterns in how these antibiotics distribute in lesions, and potential relationships to sterilizing ability [45–47]. Another important aspect in determining drug distribution in granulomas is binding to macromolecules, in particular those present in caseum. Advances in assays that can measure binding to this material have greatly increased our understanding and ability to predict drug distribution in a granuloma [48].

1.6 Pharmacodynamics of TB antibiotics

Pharmacodynamics (PD) describes the relationship between drug concentration and its therapeutic effect. With regards to antibacterial effect on Mtb, this refers to either the growth inhibition or bactericidal effect of anti-TB drugs. PD parameters, such as the minimum inhibitory concentration and minimum bactericidal concentration, measure the concentration at which a certain level of inhibition or killing is achieved [44]. Other types of assays also measure effective concentrations in hypoxic or nutrient starved conditions, such as the Wayne cidal concentration [49] and Loebel cidal concentration [50,51]. These measures are of particular importance to determine the PD effect a given antibiotic has on Mtb, as Mtb harvested from caseum have been shown to exhibit tolerance to high concentration to certain antibiotics [18]. Given the complex nature of the granuloma, and the hypoxic and nutrient starved environments it can present to Mtb, translating *in vitro* measurements directly to *in vivo* efficacy is difficult, as the necessary concentration for killing Mtb can vary greatly depending on the specific environment [43].

Another important aspect of determining PD effect is that antibiotic therapy for TB consists of multiple antibiotics. The presence of multiple drugs to achieve some therapeutic activity can lead to non-linear effects in their action, resulting in synergistic or antagonistic effects [52,53]. With regards to TB antibiotics, there is growing evidence that these drug-drug interactions could be predictive of clinical efficacy for TB regimens [54]. These drug-drug interactions can be measured in checkerboard assays that combine varying concentrations of antibiotics together and measure the resulting PD effect. The combinatorics involved with screening high-order (3 or more drugs)

6

interactions requires a prohibitively large number of experiments, even with recent advancements that limit the number of concentration combinations needed to measure the drug interactions [55,56]. To more efficiently predict drug interactions for any drug combination, machine-learning algorithms have been used to identify drug-gene expression patterns from transcriptomics data to predict synergy or antagonism for novel combinations of antibiotics [54,57–59].

1.7 Animal Models of TB

Numerous animal models have been used to contribute to the understanding of tuberculosis pathology, immunological response and treatment, using species such as mice, guinea pigs, rabbits, non-human primates and zebrafish [60].These models have varying utility depending on the specific scientific study in question, as they can vary greatly in terms of similarity to human immune response, granuloma formation, and cost.

1.7.1 Mice
Mice are useful models in studying immune responses in infectious diseases. With regards to TB research, they typically fail to develop necrotic lesions and fail to develop the same latent infection present in humans [61]. More recently, the C3HeB/FeJ mouse model for TB was developed that can form necrotic lesions and potentially be used to study antibiotic treatment [62]. The C3HeB/FeJ mouse was used to show that clofazimine as a single-drug treatment lacked efficacy if granulomas progressed to hypoxic and necrotic granulomas [63]. The mouse model has also shown that PZA can contribute to a sterilizing effect in combination with first-line TB antibiotics, but is likely inactive in neutral pH caseum [64,65]. The ability of the C3HeB/FeJ mouse to develop necrotic lesions allows for the ability to study the dependence of drug distribution in granulomas on efficacy.

1.7.2 Rabbits
Rabbits are relatively resistant to infection with Mtb, but they do produce granuloma heterogeneity and structure that is very similar to human lesions in TB [66–68].

Although rabbits are resistant to chronic infection and therefore fail to provide a model to study disease progression and reactivation, rabbits are frequently used to study tissue specific distribution. PK models built and calibrated to concentration data for isoniazid, rifampin, pyrazinamide and moxifloxacin helped to describe the differences in lesion concentrations for those different agents, and identified lesion-specific indices to apply PK studies [45]. Studies with rabbits analyzed ethambutol cellular accumulation in granulomas, and partially explained the disconnect between observed ethambutol clinical efficacy and lack of *in vitro* efficacy [46]. Using matrix-assisted laser desorption/ionization mass spectrometric (MALDI-MS) imaging in rabbit studies has provided a powerful tool to visualize the qualitative distribution of antibiotics, and identify the critical PK properties of antibiotics and physiological granuloma characteristics that influence antibiotic distribution [43,69]. MALDI-MS imaging, together with computational modeling of antibiotic distribution, characterized the differences in distribution between the fluoroquinolones moxifloxacin, levofloxacin, and gatifloxacin and their relative efficacies [47].

1.7.3 Non-human primates
Non-human primate models have provided an excellent model in studying the spectrum of disease and immune response in TB. Macaques, which are outbred, are a popular primate used in the study of TB disease, and studies show that there are variable outcomes in disease trajectory similar to humans [70]. Cynomolgus macaques infected with a low-dose of Mtb have been extensively characterized and shown to produce of spectrum of TB disease and granuloma types, providing a valuable model to study disease progression, reactivation and treatment [71], and mechanisms or markers that could predict disease progression or sterilization [72–74]. Macaque models have been used PET-CT imaging to monitor treatment progression and the efficacy of antibiotic regimens to protect against TB reactivation [75,76]. Recently, they have been useful to study new antibiotics, including linezolid [77,78].

1.8 Multi-scale modeling in TB

The entire immune response in TB disease relies on the integration of events occurring at the molecular, cellular and organ scales. As immune cells encounter Mtb, molecular signals recruit more immune cells to the site of infection, and T cells travel from lymph nodes through the blood and into the lung. As a way to address complexities of biological systems, and better understand the role different aspects of the immune response have on granuloma formation, maintenance, and function, systems biology and multi-scale modeling approaches have helped to connect these multiple phenomena. Multi-scale modeling is modeling that involves more than one level of resolution in the time, space or function [79]. Multi-scale modeling is used widely in the computational biology field, with applications in cancer [80,81], inflammatory responses [82], muscle regeneration [83], cellular and signaling trafficking [84,85] and more [79].

1.8.1 Granuloma simulation: GranSim
Multi-scale computational modeling in TB has been used to study many aspects of granuloma formation and disease progression [86]. *GranSim* is an agent-based model that captures the emergent behavior of granuloma formation and function to study the heterogeneity of TB lesions and the importance of various immune responses [87–91]. Briefly, *GranSim* simulates the immunology-inspired rules of interaction between immune cells and bacteria on a computational grid. Immune cells, including macrophages and T cells, can move, secrete cytokines and chemokines, and change states through interactions with their environment and other immune cells. Mtb exist as agents in the model and exist in subpopulations of intracellular (inside macrophages), replicating extracellular, or non-replicating extracellular. Cytokines, chemokines, and antibiotics can diffuse through the computational grid. Studies uncovered critical cytokines and signaling pathways that can lead to different TB outcomes, and how the balance between pro- and anti-inflammatory signals can control the disease response [89,92–94]. Inclusion of lymph node recruitment also helped to inform how and when immune cells are recruited to the site of infection, including recruitment to multiple granulomas, and provides a way to track potential biomarkers for infection outcome [73,95]. ODE models representing multiple granuloma formation in a single lung

9

environment, connected by blood and lymph node recruitment, have predicted how granuloma progression is linked to disease dissemination [96].

While TB computational modeling is used to study many of the aspects of the immune response, ranging from signaling pathways to cellular recruitment through the blood, multi-scale modeling has also been critical in studying aspects of Mtb and its role in the granuloma. Simulating Mtb as individual agents in an agent-based model gave the ability to show how mutations at the bacterial level leading to antibiotic resistance influence in treatment outcome and granuloma sterilization [97]. Additionally, metabolic pathways in Mtb influence growth rate, and the availability of nutrients and oxygen inside a granuloma influence the phenotypic state of Mtb [17].

1.8.2 Simulating antibiotic treatment in GranSim
Antibiotic distribution and concentration in granulomas involve events that occur over multiple organ, length and time scales, similar to the immune response in TB. Oral antibiotics are absorbed into the blood, where they can partition into peripheral tissues and are eliminated through hepatic or renal function. In the lung, antibiotics permeate through blood vessels into the lung tissue, where they can diffuse, bind to extracellular material, and partition into cells such as macrophages. Modeling PK at multi-scale resolutions is also beneficial and is required to capture the observed heterogeneity in antibiotic distribution in granulomas [41,42], and provides a tool to design new therapeutic approaches, including oral and inhaled regimens [12,98]. Using agent-based models to simulate the cellular-level interactions and organizational structure of the granuloma provides an environment to simulate antibiotic distribution, and has led to uncovering immune system mechanisms that impact sterilization during antibiotic treatment [91]. Linking the PK occurring in the blood with tissue-level PK/PD models provides a tool to explore how different regimens influence sterilization *in vivo* at a granuloma scale [99]. Adding another layer of complexity by simulating the dynamic binding of fluoroquinolones to extracellular material and partitioning into macrophages in granulomas has provided a model that accurately describes the unique distribution

characteristics of fluoroquinolones in granulomas and a tool to compare their efficacies [47].

1.8.3 Optimization in TB treatment

Research involving efforts to optimize TB treatment to find the appropriate combination of antibiotics and doses is an important step in improving TB treatment [55,100,101]. Based on the number of antibiotics available to treat TB, and the numerous possible combinations of antibiotics, is too large to test experimentally. Formalizing locating better antibiotic treatment regimens as an optimization problem and using computational modeling to compare regimen efficacies can provide a method to efficiently predict optimal regimens through a rational design approach. A variety of optimization algorithms are applied in science, math and engineering [102,103]. Of these algorithms, population-based algorithms, such as genetic algorithms, and surrogate-assisted optimization algorithms have been widely used across many fields of science and technology [104–106]. Because options for optimization algorithms are as variable as the types of problems they can solve, selecting the appropriate algorithm is essential. For the purpose of optimizing antibiotic regimens for TB, we must use an algorithm that can efficiently and accurately predict relevant regimens with good efficacy.

1.8.4 Virtual clinical trials

Previous studies using *GranSim* to simulate antibiotic treatment focus on treatment at the granuloma scale. However, treatment of a patient with TB requires treating and sterilizing multiple granulomas. Choosing the best regimen for TB treatment should ensure that it can sterilize all granulomas in an individual and perform well in a diverse population. When using computational models to predict regimen efficacies, simulating a virtual clinical trial can provide a way to compare different regimens or interventions in a way that mimics actual clinical trials [107–109]. Virtual clinical trials can be used to generate a virtual population of individuals that have the same characteristics and variability in disease and responses that exist in the real population. For the purpose of

TB treatment, individuals have variable PK and heterogeneous granulomas that both can impact treatment [110].

1.9 Thesis summary

In this thesis, I utilize a multi-scale computational model to simulate antibiotic treatment in TB granulomas. Using this model, I address how PK variability and granuloma heterogeneity impact granuloma sterilization with antibiotic treatment in Chapter 2. In Chapter 3, I present a PD model that adjusts antibiotic killing rates based on drug-drug interactions and discuss how these interactions are dependent on concentration distributions and how they impact regimen efficacy. In Chapter 4, I present a way of optimizing antibiotic regimens using computational simulations and compare the efficiency and accuracy of different optimization algorithms. In Chapter 5, I utilize a surrogate-assisted optimization algorithm to optimize the doses of isoniazid, rifampin, ethambutol, and pyrazinamide for treatment of primary TB, and compare optimal regimens at the granuloma and virtual population scale using virtual clinical trials. This thesis shows that incorporating multi-scale phenomena and appropriately representing the heterogeneity and variability in TB disease and treatment is critical in evaluating regimen efficacy at both the individual and population level.

1.10 References

1. Jindani A, Harrison TS, Nunn AJ, Phillips PPJ, Churchyard GJ, Charalambous S, et al. High-Dose Rifapentine with Moxifloxacin for Pulmonary Tuberculosis. N Engl J Med. 2014;371: 1599–1608. doi:10.1056/NEJMoa1314210
2. Global tuberculosis report 2019. 2019.
3. Dheda K, Barry CE, Maartens G. Tuberculosis. Lancet. 2016;387: 1211–1226. doi:10.1016/S0140-6736(15)00151-8
4. Nahid P, Dorman SE, Alipanah N, Barry PM, Brozek JL, Cattamanchi A, et al. Official American Thoracic Society/Centers for Disease Control and Prevention/Infectious Diseases Society of America Clinical Practice Guidelines: Treatment of Drug-Susceptible Tuberculosis. Clin Infect Dis. 2016;63: 853–867. doi:10.1093/cid/ciw566
5. Nahid P, Mase SR, Migliori GB, Sotgiu G, Bothamley GH, Brozek JL, et al. Treatment of drug-resistant tuberculosis. An official ATS/CDC/ERS/IDSA clinical practice guideline. American Journal of Respiratory and Critical Care Medicine. 2019. doi:10.1164/rccm.201909-1874ST
6. Conradie F, Diacon AH, Ngubane N, Howell P, Everitt D, Crook AM, et al. Treatment of highly drug-resistant pulmonary tuberculosis. N Engl J Med. 2020;382: 893–902. doi:10.1056/NEJMoa1901814
7. Williams CM, Abdulwhhab M, Birring SS, De Kock E, Garton NJ, Townsend E, et al. Exhaled Mycobacterium tuberculosis output and detection of subclinical disease by face-mask sampling: prospective observational studies. Lancet Infect Dis. 2020;20: 607–617. doi:10.1016/S1473-3099(19)30707-8
8. Barry III CE, Boshoff HI, Dartois V, Dick T, Ehrt S, Flynn J, et al. The spectrum of latent tuberculosis: rethinking the biology and intervention strategies. Nat Rev Microbiol. 2009;7: 845–855. doi:10.1038/nrmicro2236
9. Lee JY. Diagnosis and treatment of extrapulmonary tuberculosis. Tuberc Respir Dis (Seoul). 2015;78: 47–55. doi:10.4046/trd.2015.78.2.47
10. Newton SM, Brent AJ, Anderson S, Whittaker E, Kampmann B. Paediatric tuberculosis. Lancet Infect Dis. 2008;8: 498–510. doi:10.1016/S1473-3099(08)70182-8
11. Lin PL, Flynn JL. The End of the Binary Era: Revisiting the Spectrum of Tuberculosis. J Immunol. 2018;201: 2541–2548. doi:10.4049/jimmunol.1800993
12. Linderman JJ, Cilfone NA, Pienaar E, Gong C, Kirschner DE. A multi-scale approach to designing therapeutics for tuberculosis. Integr Biol. 2015;7: 591–609. doi:10.1039/C4IB00295D
13. Ramakrishnan L. Revisiting the role of the granuloma in tuberculosis. Nat Rev Immunol. 2012;12: 352–66. doi:10.1038/nri3211
14. Martin CJ, Cadena AM, Leung VW, Lin L, Maiello P, Hicks N, et al. Digitally barcoding Mycobacterium tuberculosis reveals in vivo infection dynamics in the macaque model of tuberculosis. MBio. 2017;8: 1–12.
15. O'Garra A, Redford PS, McNab FW, Bloom CI, Wilkinson RJ, Berry MPR. The immune response in tuberculosis. Annual review of immunology. 2013. doi:10.1146/annurev-immunol-032712-095939
16. Peters W, Ernst JD. Mechanisms of cell recruitment in the immune response to Mycobacterium tuberculosis. Microbes Infect. 2003;5: 151–158.

doi:10.1016/S1286-4579(02)00082-5

17. Pienaar E, Matern WM, Linderman JJ, Bader JS, Kirschner DE. Multiscale Model of Mycobacterium tuberculosis Infection Maps Metabolite and Gene Perturbations to Granuloma Sterilization. Infect Immun. 2016;84: 1650–1669. doi:10.1128/IAI.01438-15.Editor

18. Sarathy JP, Via LE, Weiner D, Blanc L, Boshoff H, Eugenin EA, et al. Extreme drug tolerance of mycobacterium tuberculosis in Caseum. Antimicrob Agents Chemother. 2018;62: 1–11. doi:10.1128/AAC.02266-17

19. Warsinske HC, DiFazio RM, Linderman JJ, Flynn JL, Kirschner DE. Identifying mechanisms driving formation of granuloma-associated fibrosis during Mycobacterium tuberculosis infection. J Theor Biol. 2017;429: 1–17. doi:10.1016/j.jtbi.2017.06.017.Identifying

20. Ong CWM, Elkington PT, Friedland JS. Tuberculosis, pulmonary cavitation, and matrix metalloproteinases. Am J Respir Crit Care Med. 2014;190: 9–18. doi:10.1164/rccm.201311-2106PP

21. Chatterjee A, D'Souza D, Vira T, Bamne A, Ambe GT, Nicol MP, et al. Strains of Mycobacterium tuberculosis from Western Maharashtra, India, exhibit a high degree of diversity and strain-specific associations with drug resistance, cavitary disease, and treatment failure. J Clin Microbiol. 2010;48: 3593–3599. doi:10.1128/JCM.00430-10

22. Sheiner LB, Ludden TM. Population pharmacokinetics/dynamics. Annu Rev Pharmacol Toxicol. 1992;32: 185–209.

23. Jonsson S, Davidse A, Wilkins J, Van Der Walt JS, Simonsson USH, Karlsson MO, et al. Population pharmacokinetics of ethambutol in South African tuberculosis patients. Antimicrob Agents Chemother. 2011;55: 4230–4237. doi:10.1128/AAC.00274-11

24. Zhu M, Burman WJ, Starke JR, Stambaugh JJ, Steiner P, Bulpitt AE, et al. Pharmacokinetics of ethambutol in children and adults with tuberculosis. Int J Tuberc Lung Dis. 2004;8: 1360–1367.

25. Wilkins JJ, Savic RM, Karlsson MO, Langdon G, McIlleron H, Pillai G, et al. Population pharmacokinetics of rifampin in pulmonary tuberculosis patients, including a semimechanistic model to describe variable absorption. Antimicrob Agents Chemother. 2008;52: 2138–2148. doi:10.1128/AAC.00461-07

26. Denti P, Jeremiah K, Chigutsa E, Faurholt-Jepsen D, PrayGod G, Range N, et al. Pharmacokinetics of isoniazid, pyrazinamide, and ethambutol in newly diagnosed pulmonary TB patients in Tanzania. PLoS One. 2015;10: 1–19. doi:10.1371/journal.pone.0141002

27. Lalande L, Bourguignon L, Bihari S, Maire P, Neely M, Jelliffe R, et al. Population modeling and simulation study of the pharmacokinetics and antituberculosis pharmacodynamics of isoniazid in lungs. Antimicrob Agents Chemother. 2015;59: 5181–5189. doi:10.1128/AAC.00462-15

28. Peloquin CA, Hadad DJ, Molino LPD, Palaci M, Boom WH, Dietze R, et al. Population pharmacokinetics of levofloxacin, gatifloxacin, and moxifloxacin in adults with pulmonary tuberculosis. Antimicrob Agents Chemother. 2008;52: 852–857. doi:10.1128/AAC.01036-07

29. McGee B, Dietze R, Hadad DJ, Molino LPD, Maciel ELN, Boom WH, et al.

Population pharmacokinetics of linezolid in adults with pulmonary tuberculosis. Antimicrob Agents Chemother. 2009;53: 3981–3984. doi:10.1128/AAC.01378-08

30. Svensson EM, Dosne AG, Karlsson MO. Population Pharmacokinetics of Bedaquiline and Metabolite M2 in Patients with Drug-Resistant Tuberculosis: The Effect of Time-Varying Weight and Albumin. CPT Pharmacometrics Syst Pharmacol. 2016;5: 682–691. doi:10.1002/psp4.12147

31. Salinger DH, Subramoney V, Everitt D, Nedelman JR. Population pharmacokinetics of the antituberculosis agent pretomanid. Antimicrob Agents Chemother. 2019;63: 1–10. doi:10.1128/AAC.00907-19

32. Azuma J, Ohno M, Kubota R, Yokota S, Nagai T, Tsuyuguchi K, et al. NAT2 genotype guided regimen reduces isoniazid-induced liver injury and early treatment failure in the 6-month four-drug standard treatment of tuberculosis: A randomized controlled trial for pharmacogenetics-based therapy. Eur J Clin Pharmacol. 2013;69: 1091–1101. doi:10.1007/s00228-012-1429-9

33. Van Oosterhout JJ, Dzinjalamala FK, Dimba A, Waterhouse D, Davies G, Zijlstra EE, et al. Pharmacokinetics of antituberculosis drugs in HIV-positive and HIV-negative adults in Malawi. Antimicrob Agents Chemother. 2015;59: 6175–6180. doi:10.1128/AAC.01193-15

34. Saktiawati AMI, Sturkenboom MGG, Stienstra Y, Subronto YW, Sumardi, Kosterink JGW, et al. Impact of food on the pharmacokinetics of first-line anti-TB drugs in treatment-naive TB patients: A randomized cross-over trial. J Antimicrob Chemother. 2016;71: 703–710. doi:10.1093/jac/dkv394

35. Pasipanodya JG, McIlleron H, Burger A, Wash PA, Smith P, Gumbo T. Serum drug concentrations predictive of pulmonary tuberculosis outcomes. J Infect Dis. 2013;208: 1464–1473. doi:10.1093/infdis/jit352

36. Srivastava S, Musuka S, Sherman C, Meek C, Leff R, Gumbo T. Efflux-Pump–Derived Multiple Drug Resistance to Ethambutol Monotherapy in *Mycobacterium tuberculosis* and the Pharmacokinetics and Pharmacodynamics of Ethambutol. J Infect Dis. 2010;201: 1225–1231. doi:10.1086/651377

37. Srivastava S, Gumbo T. In Vitro and In Vivo Modeling of Tuberculosis Drugs and its Impact on Optimization of Doses and Regimens. Curr Pharm Des. 2011;17: 2881–2888. doi:10.2174/138161211797470192

38. Gumbo T, Louie A, Liu W, Brown D, Ambrose PG, Bhavnani SM, et al. Isoniazid bactericidal activity and resistance emergence: Integrating pharmacodynamics and pharmacogenomics to predict efficacy in different ethnic populations. Antimicrob Agents Chemother. 2007;51: 2329–2336. doi:10.1128/AAC.00185-07

39. Gumbo T, Dona CSWS, Meek C, Leff R. Pharmacokinetics-pharmacodynamics of pyrazinamide in a novel in vitro model of tuberculosis for sterilizing effect: A paradigm for faster assessment of new antituberculosis drugs. Antimicrob Agents Chemother. 2009;53: 3197–3204. doi:10.1128/AAC.01681-08

40. Magombedze G, Pasipanodya JG, Srivastava S, Deshpande D, Visser ME, Chigutsa E, et al. Transformation Morphisms and Time-to-Extinction Analysis That Map Therapy Duration from Preclinical Models to Patients with Tuberculosis: Translating from Apples to Oranges. Clin Infect Dis. 2018;67: S349–S358. doi:10.1093/cid/ciy623

41. Lenaerts A, Barry CE, Dartois V. Heterogeneity in tuberculosis pathology,

microenvironments and therapeutic responses. Immunol Rev. 2015;264: 288–307. doi:10.1111/imr.12252

42. Dartois V. The path of anti-tuberculosis drugs: from blood to lesions to mycobacterial cells. Nat Rev Microbiol. 2014;12: 159–167. doi:10.1038/nrmicro3200

43. Prideaux B, Via LE, Zimmerman MD, Eum S, Sarathy J, O'Brien P, et al. The association between sterilizing activity and drug distribution into tuberculosis lesions. Nat Med. 2015;21: 1223–7. doi:10.1038/nm.3937

44. Lakshminarayana SB, Huat TB, Ho PC, Manjunatha UH, Dartois V, Dick T, et al. Comprehensive physicochemical, pharmacokinetic and activity profiling of anti-TB agents. J Antimicrob Chemother. 2015;70: 857–867. doi:10.1093/jac/dku457

45. Kjellsson MC, Via LE, Goh A, Weiner D, Low KM, Kern S, et al. Pharmacokinetic evaluation of the penetration of antituberculosis agents in rabbit pulmonary lesions. Antimicrob Agents Chemother. 2012;56: 446–457. doi:10.1128/AAC.05208-11

46. Zimmerman M, Lestner J, Prideaux B, O'Brien P, Dias-freedman I, Chen C, et al. Ethambutol Partitioning in Tuberculous Pulmonary Lesions Explains Its Clinical Efficacy. Antimicrob Agents Chemother. 2017;61: 1–12.

47. Pienaar E, Sarathy J, Prideaux B, Dietzold J, Dartois V, Kirschner DE, et al. Comparing efficacies of moxifloxacin, levofloxacin and gatifloxacin in tuberculosis granulomas using a multi-scale systems pharmacology approach. PLOS Comput Biol. 2017;13. doi:10.1371/journal.pcbi.1005650

48. Sarathy JP, Zuccotto F, Hsinpin H, Sandberg L, Via LE, Marriner GA, et al. Prediction of Drug Penetration in Tuberculosis Lesions. ACS Infect Dis. 2016;2: 552–563. doi:10.1021/acsinfecdis.6b00051

49. Wayne LG, Hayes LG. An in vitro model for sequential study of shiftdown of Mycobacterium tuberculosis through two stages of nonreplicating persistence. Infect Immun. 1996;64: 2062–2069. doi:10.1128/iai.64.6.2062-2069.1996

50. Loebel RO, Shorr E, Richardson HB. The influence of foodstuffs upon the respiratory metabolism and growth of human tubercle bacilli. J Bacteriol. 1932;26: 139–166.

51. Gengenbacher M, Rao SPS, Pethe K, Dick T. Nutrient-starved, non-replicating Mycobacterium tuberculosis requires respiration, ATP synthase and isocitrate lyase for maintenance of ATP homeostasis and viability. Microbiology. 2010;156: 81–87. doi:10.1099/mic.0.033084-0

52. Berenbaum MC. What is Synergy? Pharmacol Rev. 1989;1989: 93–141.

53. Berenbaum MC. A method for testing for synergy with any number of agents. J Infect Dis. 1978;137: 122–130. doi:10.1093/infdis/137.2.122

54. Ma S, Jaipalli S, Larkins-Ford J, Lohmiller J, Aldridge BB, Sherman DR, et al. Transcriptomic signatures predict regulators of drug synergy and clinical regimen efficacy against tuberculosis. MBio. 2019;10: 1–16. doi:10.1128/mBio.02627-19

55. Silva A, Lee B-Y, Clemens DL, Kee T, Ding X, Ho C-M, et al. Output-driven feedback system control platform optimizes combinatorial therapy of tuberculosis using a macrophage cell culture model. PNAS. 2016;113: 2172–2179. doi:10.1073/pnas.1600812113

56. Cokol M, Kuru N, Bicak E, Larkins-Ford J, Aldridge BB. Efficient measurement

and factorization of high-order drug interactions in Mycobacterium tuberculosis. Sci Adv. 2017;3: e1701881. doi:10.1126/sciadv.1701881

57. Chandrasekaran S, Cokol-Cakmak M, Sahin N, Kazan H, Yilancioglu K, Collins JJ, et al. Chemogenomics and orthology-based design of antibiotic combination therapies. Mol Syst Biol. 2016;12: 872. doi:10.15252/msb.20156777

58. Cokol M, Li C, Chandrasekaran S. Chemogenomic model identifies synergistic drug combinations robust to the pathogen microenvironment. PLoS Comput Biol. 2018;14: 1–24. doi:10.1371/journal.pcbi.1006677

59. Chandrasekaran S. Predicting Drug Interactions From Chemogenomics Using INDIGO. Systems Chemical Biology Methods in Molecular Biology. 2019. pp. 219–231.

60. Flynn JL. Lessons from experimental Mycobacterium tuberculosis infections. Microbes Infect. 2006;8: 1179–1188. doi:10.1016/j.micinf.2005.10.033

61. Scanga CA, Mohan VP, Joseph H, Yu K, Chan J, Flynn JL. Reactivation of Latent Tuberculosis : Variations on the Cornell Murine Model. Infect Immun. 1999;67: 4531–4538.

62. Driver ER, Ryan GJ, Hoff DR, Irwin SM, Basaraba RJ, Kramnik I, et al. Evaluation of a mouse model of necrotic granuloma formation using C3HeB/FeJ mice for testing of drugs against Mycobacterium tuberculosis. Antimicrob Agents Chemother. 2012;56: 3181–3195. doi:10.1128/AAC.00217-12

63. Irwin SM, Gruppo V, Brooks E, Gilliland J, Scherman M, Reichlen MJ, et al. Limited activity of clofazimine as a single drug in a mouse model of tuberculosis exhibiting caseous necrotic granulomas. Antimicrob Agents Chemother. 2014;58: 4026–4034. doi:10.1128/AAC.02565-14

64. Lanoix JP, Ioerger T, Ormond A, Kaya F, Sacchettini J, Dartois V, et al. Selective inactivity of pyrazinamide against tuberculosis in C3HeB/FeJ mice is best explained by neutral pH of caseum. Antimicrob Agents Chemother. 2016;60: 735–743. doi:10.1128/AAC.01370-15

65. Lanoix JP, Betoudji F, Nuermberger E. Sterilizing activity of pyrazinamide in combination with first-line drugs in a C3HeB/FeJ mouse model of tuberculosis. Antimicrob Agents Chemother. 2016;60: 1091–1096. doi:10.1128/AAC.02637-15

66. Bishai WR, Dannenberg AM, Parrish N, Ruiz R, Chen P, Zook BC, et al. Virulence of Mycobacterium tuberculosis CDC1551 and H37Rv in rabbits evaluated by Lurie's pulmonary tubercle count method. Infect Immun. 1999;67: 4931–4934. doi:10.1128/iai.67.9.4931-4934.1999

67. Converse PJ, Dannenberg AM, Estep JE, Sugisaki K, Abe Y, Schofield BH, et al. Cavitary Tuberculosis Produced in Rabbits by Aerosolized Virulent Tubercle Bacilli. Infect Immun. 1996;64: 4776–4787.

68. Converse PJ, Dannenberg AM, Shigenaga T, McMurray DN, Phalen SW, Stanford JL, et al. Pulmonary Bovine-Type Tuberculosis in Rabbits : Bacillary Virulence , Inhaled Dose Effects , Tuberculin Sensitivity , and Mycobacterium vaccae Immunotherapy. Clin Diagn Lab Immunol. 1998;5: 871–881.

69. Prideaux B, Dartois V, Staab D, Weiner DM, Goh A, Via LE, et al. High-sensitivity MALDI-MRM-MS imaging of moxifloxacin distribution in tuberculosis-infected rabbit lungs and granulomatous lesions. Anal Chem. 2011;83: 2112–2118. doi:10.1021/ac1029049

70. Capuano III S V, Croix DA, Pawar S, Zinovik A, Myers A, Lin PL, et al. Experimental Mycobacterium tuberculosis Infection of Cynomolgus Macaques Closely Resembles the Various Manifestations of Human M . tuberculosis Infection. Infect Immun. 2003;71: 5831–5844. doi:10.1128/IAI.71.10.5831

71. Lin PL, Rodgers M, Smith L, Bigbee M, Myers A, Bigbee C, et al. Quantitative comparison of active and latent tuberculosis in the cynomolgus macaque model. Infect Immun. 2009;77: 4631–4642. doi:10.1128/IAI.00592-09

72. Gideon HP, Phuah J, Myers AJ, Bryson BD, Rodgers MA, Coleman MT, et al. Variability in tuberculosis granuloma T cell responses exists, but a balance of pro- and anti-inflammatory cytokines is associated with sterilization. PLoS Pathog. 2015;11. doi:10.1371/journal.ppat.1004603

73. Marino S, Gideon HP, Gong C, Mankad S, McCrone JT, Lin PL, et al. Computational and Empirical Studies Predict Mycobacterium tuberculosis-Specific T Cells as a Biomarker for Infection Outcome. PLoS Comput Biol. 2016;12: 1–30. doi:10.1371/journal.pcbi.1004804

74. Gideon HP, Skinner JA, Baldwin N, Flynn JL, Lin PL. Early Whole Blood Transcriptional Signatures Are Associated with Severity of Lung Inflammation in Cynomolgus Macaques with *Mycobacterium tuberculosis* Infection. J Immunol. 2016; 1601138. doi:10.4049/jimmunol.1601138

75. Lin PL, Coleman T, Carney JPJ, Lopresti BJ, Tomko J, Fillmore D, et al. Radiologic responses in cynomolgus macaques for assessing tuberculosis chemotherapy regimens. Antimicrob Agents Chemother. 2013;57: 4237–4244. doi:10.1128/AAC.00277-13

76. Lin PL, Dartois V, Johnston PJ, Janssen C, Via L, Goodwin MB, et al. Metronidazole prevents reactivation of latent Mycobacterium tuberculosis infection in macaques. Proc Natl Acad Sci. 2012;109: 14188–14193. doi:10.1073/pnas.1121497109

77. Coleman MT, Chen RY, Lee M, Lin PL, Dodd LE, Maiello P, et al. PET/CT imaging reveals a therapeutic response to oxazolidinones in macaques and humans with tuberculosis. Sci Transl Med. 2014;6: 265ra167. doi:10.1126/scitranslmed.3009500

78. Winchell CG, Mishra BB, Phuah JY, Saqib M, Nelson SJ, Maiello P, et al. Evaluation of IL-1 Blockade as an Adjunct to Linezolid Therapy for Tuberculosis in Mice and Macaques. Front Immunol. 2020;11: 1–18. doi:10.3389/fimmu.2020.00891

79. Walpole J, Papin JA, Peirce SM. Multiscale Computational Models of Complex Biological Systems. Annu Rev Biomed Eng. 2013;15: 137–154. doi:10.1146/annurev-bioeng-071811-150104

80. Cilliers C, Menezes B, Nessler I, Linderman J, Thurber GM. Improved Tumor Penetration and Single-Cell Targeting of Antibody – Drug Conjugates Increases Anticancer Efficacy and Host Survival. Cancer Res. 2018;78: 758–769. doi:10.1158/0008-5472.CAN-17-1638

81. Menezes B, Cilliers C, Wessler T, Thurber GM, Linderman JJ. An Agent-Based Systems Pharmacology Model of the Antibody-Drug Conjugate Kadcyla to Predict Efficacy of Different Dosing Regimens. AAPS J. 2020;22: 1–13. doi:10.1208/s12248-019-0391-1

82. An G, Mi Q, Dutta-Moscato J, Vodovotz Y. Agent-based models in translational systems biology. Wiley Interdiscip Rev Syst Biol Med. 2009;1: 159–171. doi:10.1002/wsbm.45

83. Martin KS, Virgilio KM, Peirce SM, Blemker SS. Computational modeling of muscle regeneration and adaptation to advance muscle tissue regeneration strategies. Cells Tissues Organs. 2015;202: 250–266. doi:10.1159/000443635

84. Bailey AM, Lawrence MB, Shang H, Katz AJ, Peirce SM. Agent-based model of therapeutic adipose-derived stromal cell trafficking during ischemia predicts ability to roll on p-selectin. PLoS Comput Biol. 2009;5. doi:10.1371/journal.pcbi.1000294

85. Spinosa PC, Luker KE, Luker GD, Linderman JJ. The CXCL12/CXCR7 signaling axis, isoforms, circadian rhythms, and tumor cellular composition dictate gradients in tissue. PLoS One. 2017;12: 1–17. doi:10.1371/journal.pone.0187357

86. Kirschner D, Pienaar E, Marino S, Linderman JJ. A review of computational and mathematical modeling contributions to our understanding of Mycobacterium tuberculosis within-host infection and treatment. Curr Opin Syst Biol. 2017;3: 170–185. doi:10.1016/j.coisb.2017.05.014

87. Segovia-Juarez JL, Ganguli S, Kirschner D. Identifying control mechanisms of granuloma formation during M. tuberculosis infection using an agent-based model. J Theor Biol. 2004;231: 357–376. doi:10.1016/j.jtbi.2004.06.031

88. Ray JCJ, Flynn JL, Kirschner DE. Synergy between individual TNF-dependent functions determines granuloma performance for controlling Mycobacterium tuberculosis infection. J Immunol. 2009;812: 3706–37017. doi:10.4049/jimmunol.0802297

89. Fallahi-Sichani M, El-Kebir M, Marino S, Kirschner DE, Linderman JJ. Multiscale computational modeling reveals a critical role for TNF-α receptor 1 dynamics in tuberculosis granuloma formation. J Immunol. 2011;186: 3472–3483. doi:10.4049/jimmunol.1003299

90. Cilfone NA, Perry CR, Kirschner DE, Linderman JJ. Multi-scale modeling predicts a balance of tumor necrosis factor-a and interleukin-10 controls the granuloma environment during Mycobacterium truberculosis infection. PLoS One. 2013;8: e68680. doi:10.1371/journal.pone.0068680

91. Pienaar E, Cilfone NA, Lin PL, Dartois V, Mattila JT, Butler JR, et al. A computational tool integrating host immunity with antibiotic dynamics to study tuberculosis treatment. J Theor Biol. 2015;367: 166–179. doi:10.1016/j.jtbi.2014.11.021

92. Fallahi-Sichani M, Schaller MA, Kirschner DE, Kunkel SL, Linderman JJ. Identification of key processes that control tumor necrosis factor availability in a tuberculosis granuloma. PLoS Comput Biol. 2010;6: 1–19. doi:10.1371/journal.pcbi.1000778

93. Cicchese JM, Evans S, Hult C, Joslyn LR, Wessler T, Millar JA, et al. Dynamic balance of pro- and anti-inflammatory signals controls disease and limits pathology. Immunol Rev. 2018;285: 147–167. doi:10.1111/imr.12671

94. Cilfone NA, Ford CB, Marino S, Mattila JT, Gideon HP, Flynn JL, et al. Computational modeling predicts IL-10 control of lesion sterilization by balancing early host immunity-mediated antimicrobial responses with caseation during mycobacterium tuberculosis infection. J Immunol. 2015;194: 664–77.

doi:10.4049/jimmunol.1400734

95. Marino S, Kirschner D. A Multi-Compartment Hybrid Computational Model Predicts Key Roles for Dendritic Cells in Tuberculosis Infection. Computation. 2016;4: 39. doi:10.3390/computation4040039

96. Wessler T, Joslyn LR, Jacob Borish H, Gideon HP, Flynn JAL, Kirschner DE, et al. A computational model tracks whole-lung Mycobacterium tuberculosis infection and predicts factors that inhibit dissemination. PLoS Comput Biol. 2020;16: 1–25. doi:10.1371/journal.pcbi.1007280

97. Pienaar E, Linderman JJ, Kirschner DE. Emergence and selection of isoniazid and rifampin resistance in tuberculosis granulomas. PLoS One. 2018;13: 1–29. doi:10.1371/journal.pone.0196322

98. Cilfone NA, Pienaar E, Thurber GM, Kirschner DE, Linderman JJ. Systems Pharmacology Approach Toward the Design of Inhaled Formulations of Rifampicin and Isoniazid for Treatment of Tuberculosis. CPT Pharmacometrics Syst Pharmacol. 2015;4: 1–11. doi:10.1002/psp4.22

99. Pienaar E, Dartois V, Linderman JJ, Kirschner DE. In silico evaluation and exploration of antibiotic tuberculosis treatment regimens. BMC Syst Biol. 2015;9: 1–12. doi:10.1186/s12918-015-0221-8

100. Egelund EF, Alsultan A, Peloquin CA. Optimizing the Clinical Pharmacology of Tuberculosis Medications. Clin Pharmacol Ther. 2015;98: 387–393. doi:10.1002/cpt.180

101. Lee B-Y, Clemens DL, Silva A, Dillon BJ, Masleša-Galić S, Nava S, et al. Drug regimens identified and optimized by output-driven platform markedly reduce tuberculosis treatment time. Nat Commun. 2017;8. doi:10.1038/ncomms14183

102. Man KF, Tang KS, Kwong S. Genetic algorithms: Concepts and applications. IEEE Trans Ind Electron. 1996;43: 519–534. doi:10.1109/41.538609

103. Jin Y. Surrogate-assisted evolutionary computation : Recent advances and future challenges. Swarm Evol Comput. 2011;1: 61–70. doi:10.1016/j.swevo.2011.05.001

104. Alba E, Luque G, Nesmachnow S. Parallel metaheuristics: recent advances and new trends. Int Trans Oper Res. 2013;20: 1–48. doi:10.1111/j.1475-3995.2012.00862.x

105. Forrester AIJ, Sóbester A, Keane AJ. Engineering Design via Surrogate Modelling: A Practical Guide. John Wiley & Sons; 2008.

106. Sóbester A, Forrester AIJ, Toal DJJ, Tresidder E, Tucker S. Engineering design applications of surrogate-assisted optimization techniques. Optim Eng. 2014;15: 243–265. doi:10.1007/s11081-012-9199-x

107. Brown D, Namas RA, Almahmoud K, Zaaqoq A, Sarkar J, Barclay DA, et al. Trauma in silico: Individual-specific mathematical models and virtual clinical populations. Sci Transl Med. 2015;7. doi:10.1126/scitranslmed.aaa3636

108. Clermont G, Bartels J, Kumar R, Constantine G, Vodovotz Y, Chow C. In silico design of clinical trials: A method coming of age. Crit Care Med. 2004;32: 2061–2070. doi:10.1097/01.CCM.0000142394.28791.C3

109. Marino S, Sud D, Plessner H, Lin PL, Chan J, Flynn JL, et al. Differences in reactivation of tuberculosis induced from anti-tNF treatments are based on bioavailability in granulomatous tissue. PLoS Comput Biol. 2007;3: 1909–1924.

doi:10.1371/journal.pcbi.0030194

110. Cicchese JM, Dartois V, Kirschner DE, Linderman JJ. Both Pharmacokinetic Variability and Granuloma Heterogeneity Impact the Ability of the First-Line Antibiotics to Sterilize Tuberculosis Granulomas. Front Pharmacol. 2020;11: 1–15. doi:10.3389/fphar.2020.00333

Chapter 2 Both Pharmacokinetic Variability and Granuloma Heterogeneity Impact the Ability of the First-Line Antibiotics to Sterilize Tuberculosis Granulomas

This chapter is a published work:

2.1 Abstract

Tuberculosis (TB) remains as one of the world's deadliest infectious diseases despite the use of standardized antibiotic therapies. Recommended therapy for drug-susceptible TB is up to six months of antibiotics. Factors that contribute to lengthy regimens include antibiotic underexposure in lesions due to poor pharmacokinetics (PK) and complex granuloma compositions, but it is difficult to quantify how individual antibiotics are affected by these factors and to what extent these impact treatments. We use our next-generation multi-scale computational model to simulate granuloma formation and function together with antibiotic pharmacokinetics and pharmacodynamics, allowing us to predict conditions leading to granuloma sterilization. In this work, we focus on how PK variability, determined from human PK data, and granuloma heterogeneity each quantitatively impact granuloma sterilization. We focus on treatment with the standard regimen for TB of four first-line antibiotics: isoniazid, rifampin, ethambutol and pyrazinamide. We find that low levels of antibiotic concentration due to naturally occurring PK variability and complex granulomas leads to longer granuloma sterilization times. Additionally, the ability of antibiotics to distribute in granulomas and kill different subpopulations of bacteria contributes to their

specialization in the more efficacious combination therapy. These results can inform strategies to improve antibiotic therapy for TB.

2.2 Introduction

Tuberculosis (TB) continues to be one of the world's deadliest infectious diseases, leading to the death of 1.3 million people in 2017, about 2-3 people per minute [1]. Caused by infection with the pathogen *Mycobacterium tuberculosis* (Mtb), TB most commonly presents as a pulmonary disease in adults when individuals inhale aerosolized Mtb transmitted by other infected individuals. The immune response in the lungs leads to the formation of multiple lesions called granulomas, collections of immune cells that act to contain the infection both immunologically and physically but also present a barrier to antibiotic diffusion and delivery [2–4]. Understanding penetration and distribution of antibiotics in granulomas is critical to understanding how best to treat TB.

The current recommended regimen to treat active, drug-susceptible TB disease requires up to six months of multiple antibiotics [5]. For the first two months, patients take daily doses of isoniazid (INH, H), rifampin (RIF, R), ethambutol (EMB, E), and pyrazinamide (PZA, Z), referred to as HRZE. Each of these antibiotics has side effects associated with their use that, together with the lengthy treatment duration, make it difficult for patients to properly adhere to the regimen [6,7]. Efforts such as directly observed therapy (DOT) attempt to increase patient adherence but are not tractable on a global scale [8,9]. Emergence of multidrug-resistant (defined as resistant to INH and RIF) and extensively drug-resistant TB (resistant to INH, RIF and a second-line injectable) further complicates treatment [1]. There is a need for improved antibiotic therapy for TB and to understand what causes treatment failure.

There are two key factors outside of drug resistance that have been identified as contributing to drug failure in TB: pharmacokinetic (PK) variability (acting at population scale) and granuloma heterogeneity (acting at the host scale). How these factors interact to affect both the rate and extent of sterilization during treatment is not well-understood. PK variability is defined as differences in plasma antibiotic exposure,

typically measured as variability in plasma area under the curve (AUC) measurements. Population PK models can help determine appropriate dosing of TB antibiotics and represent this variability based on distributions of PK model parameters [10–13]. These distributions can be related to natural differences in populations through covariates such as weight, age or overall health. Additionally, PK variability can be due to differences at the genetic scale, such as in N-acetyltransferase 2 involved in the metabolism of INH [14,15]. This PK variability can lead to poor exposure in granuloma lesions, reducing the amount of time antibiotic concentrations are above therapeutic thresholds during therapy [16].

Host-scale heterogeneity encompasses host-level variations in granuloma number, size, and composition. Granuloma size and composition can lead to slower diffusion of antibiotics, spatial gradients of concentration and underexposure at the host tissue scale [3,4,17,18]. Granuloma composition can affect how antibiotics accumulate or fail to accumulate within lesions [3]. For example, EMB's clinical efficacy may partially be explained by its ability to accumulate in cellular regions of the granuloma [19]. Structural differences in lesions affect the sterilizing ability of PZA, as shown in different strains of mice [20]. Caseous regions of the granuloma may also harbor bacteria that are phenotypically more tolerant, and may be less accessible, to many TB antibiotics [21].

Capturing both PK variability at the population scale and granuloma heterogeneity at the host scale in a computational model can help predict granuloma sterilization and design antibiotic regimens. Our group previously developed a computational model that incorporates the host formation of granulomas and antibiotic PK to predict the sterilization of granulomas using different regimens with INH and RIF [4,22]. Using this multi-scale, systems pharmacology model, we have also highlighted major differences between members of the fluoroquinolone drug class and simulated TB therapy with development of antibiotic resistance [23,24]. Using this computational framework provides a way to include both PK variability and granuloma heterogeneity to predict whether a treatment can achieve granuloma sterilization in primary, pulmonary TB in adults.

Here we use our hybrid, multi-scale agent-based model to capture PK variability and granuloma heterogeneity and to simulate antibiotic treatment of primary, lung granulomas. For the first time with this model, we simulate treatment based on human PK and with the combination of the four first-line antibiotics used to treat TB: INH, RIF, EMB and PZA. We also present a sequential calibration scheme that captures spatial distributions of antibiotics within granulomas and known PK variability that exists across the population scale and at the host scale within granulomas. Using this highly detailed model, we discuss the role of first-line antibiotics (HRZE) in sterilizing granulomas and how PK variability and granuloma heterogeneity impact distributions of sterilization times.

2.3 Methods

2.3.1 Computational model of granuloma formation and function
GranSim is a well-established hybrid, multi-scale computational model that produces the emergent behavior of granuloma formation in Mtb infection [25–28]. Briefly, this agent-based model simulates immune cell movement and interactions, and bacterial growth on a spatial grid representing an area of lung tissue. The immune cell agents, such as different classes of macrophages and T cells, move in response to chemokine gradients and interact with each other according to immunology-derived rules to activate or deactivate immune cells/responses. Bacteria in the model are simulated as individual agents, and they exist in three distinct subpopulations: extracellular replicating, extracellular non-replicating, or intracellular (inside macrophages). The effective growth rate of bacteria in these three subpopulations is influenced by extracellular or intracellular location and availability of nutrients and oxygen [29]. Non-replicating Mtb represent bacteria trapped within caseum, which presents hypoxic conditions with limited nutrient resources [21,30]. A more detailed explanation of *GranSim* and the simulation rules and assumptions can be found online (http://malthus.micro.med.umich.edu/GranSim/). *GranSim* simulates lung granulomas that form due to primary, pulmonary infection in adults and captures a wide diversity of granulomas through variations in host immune system parameters and stochastic events in the agent-based model. The boundary of the granuloma is defined by regions

25

of high cell density, and outlines of the granuloma are drawn to enclose these regions. Parameters that were varied to generate our library of heterogeneous granulomas are listed in Table 2.1.

2.3.2 In silico granuloma library

We generate two distinct libraries of granulomas that are heterogeneous in bacterial load and cellular composition: one categorized as low-CFU (colony-forming unit, equal to the number of bacteria in the simulation) granulomas and the other as high-CFU granulomas. The low-CFU granulomas are smaller in size and have CFU/granuloma that are more stable over time, whereas the high-CFU granulomas are larger in size, have increasing CFU over time, and have higher levels of caseum. To generate the low-CFU granulomas, we sampled 500 parameter sets based on ranges for host immune system parameters listed in Table 2.1 using Latin Hypercube Sampling (LHS) [4]. Using the simulation outputs at day 300 for granuloma size and CFU, we performed sensitivity analysis using partial rank correlation coefficients to determine parameters that have the most significant impact on those two outcomes [31]. A total of 400 high-CFU granulomas were generated by increasing or decreasing the upper and lower bounds of the parameter ranges that have the strongest correlation with granuloma size and CFU, as well as initializing simulations with multiple infection locations to generate larger granulomas. Parameter ranges for all granulomas are shown in Table 2.1. Low-CFU granulomas are simulated on a 200 by 200 compartment square grid representing a 4 by 4 mm section of lung tissue (each grid compartment has a side-length of 20 microns), whereas the high-CFU are run on 300 by 300 compartment grid representing 6 by 6 mm. Note that we simulate the small granulomas on a smaller grid for computational efficiency, as the larger is not required. At day 300, a total of 354 low-CFU granulomas and 352 high-CFU granulomas still had bacteria and were selected for treatment simulations. Figure 2.1 shows CFU per granuloma of these two groups.
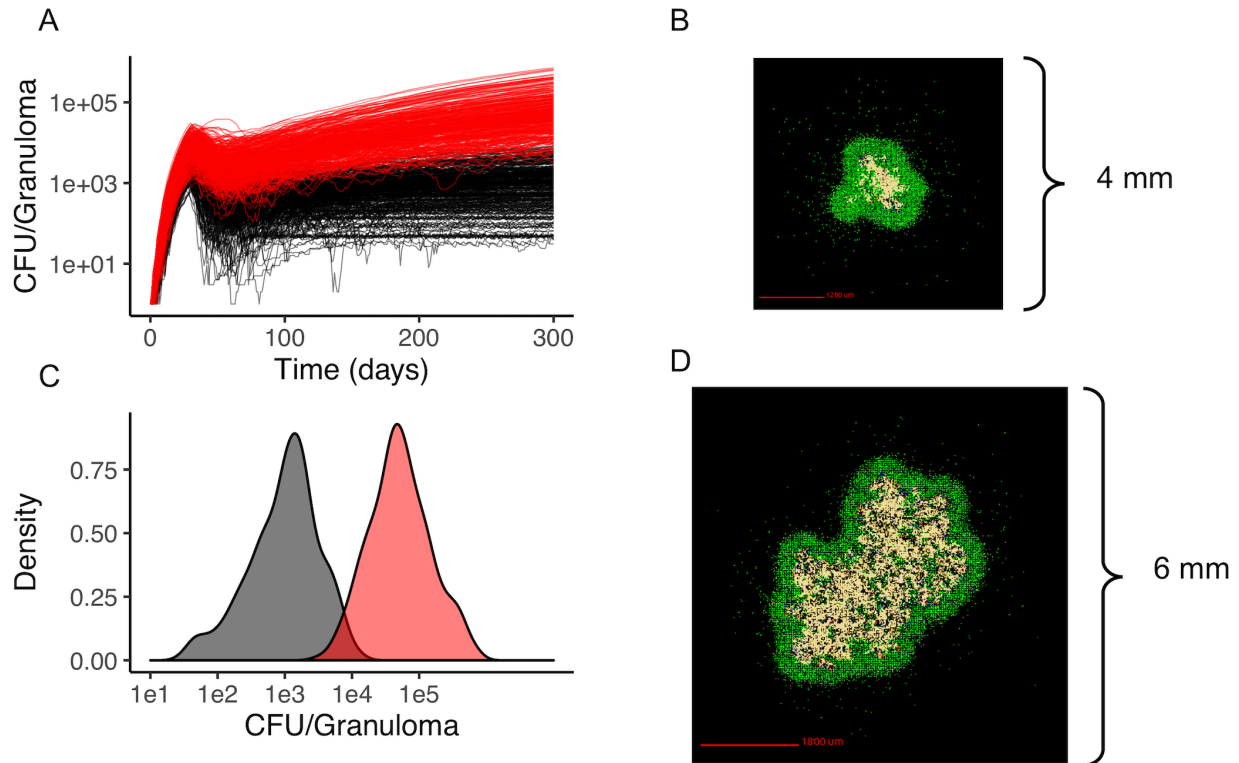
Figure 2.1 Heterogeneous granulomas generated using the computational model *GranSim*.
There are two groups of in silico granulomas at day 300 post infection: low CFU granulomas (black/gray, n=354) and high CFU granulomas (red, n=352). High CFU granulomas have increasing CFU over time relative to the more stable lower CFU granulomas (A). (C) shows the distribution of CFU per granuloma in the low CFU group (black) and the high CFU group (red) at day 300. (B) shows an example of a low CFU *in silico* granuloma and (D) shows an example of a high CFU granuloma. In both simulations the colors represent: macrophages green; resting; blue, active; orange, infected; red, chronically infected), T cells (IFN-gamma producing; pink, cytotoxic, purple; regulatory, light blue), and caseated regions (tan).

2.3.3 Plasma pharmacokinetic model

The plasma PK model is comprised of a two-compartmental model with one or two transit compartments that simulate oral absorption. INH and RIF follow a two-absorption compartment model based on previously developed PK models, whereas EMB and PZA are simulated with one absorption compartment based on best fits and other PK models [4,11,12,19,32]. The two-compartment model simulates distribution between plasma and peripheral tissue, and antibiotics are eliminated with a first-order clearance rate constant (Figure 2.2). Pharmacokinetic variability can be introduced by varying the parameters of the plasma PK model based on reported variability in the parameters (Table 2.2).
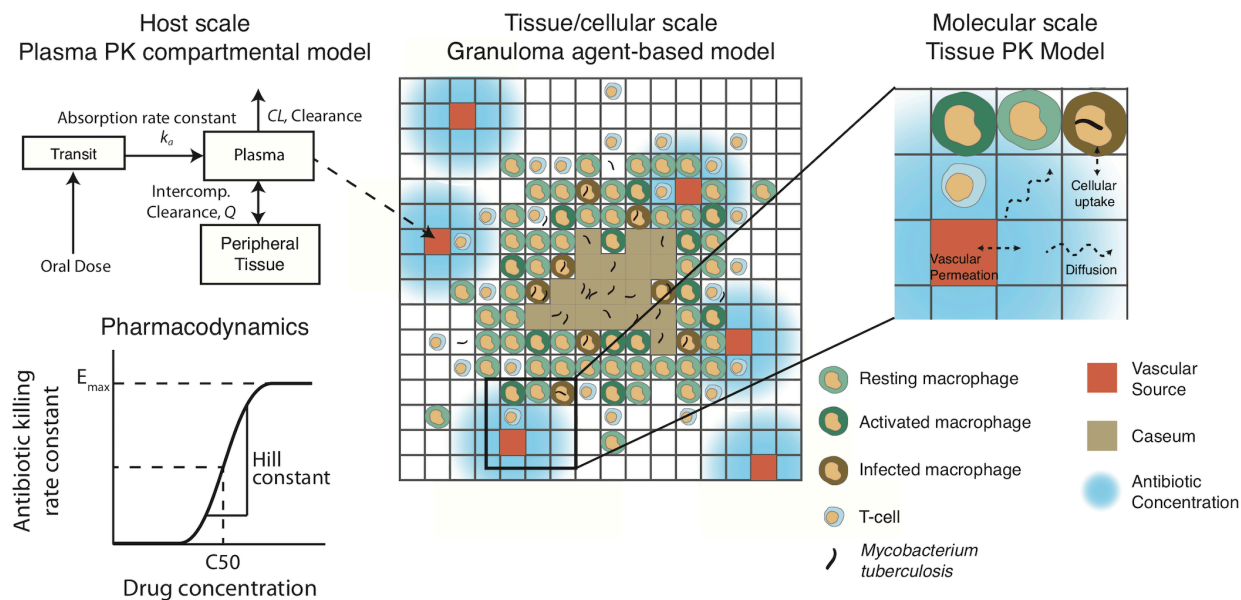
Figure 2.2 Pharmacokinetic/pharmacodynamic dynamics in *GranSim*.
Plasma concentration is simulated with a two-compartment PK model with one (EMB and PZA) or two (INH and RIF) transit compartments to capture oral absorption. The amount of drug added or subtracted through the vascular sources in the agent-based spatial grid depends on local gradients of antibiotics. Antibiotics on the grid can diffuse, degrade, bind to extracellular material (such as caseum) and partition into macrophages. Based on intra- or extracellular concentrations in each grid compartment, a killing rate constant based on a Hill curve determines the probability per time step that a given bacterium will die due to exposure to antibiotics.

2.3.4 Tissue pharmacokinetic model

The plasma PK model is linked to the agent-based environment through blood vessels placed on the simulation grid (Figure 2.2). Based on the difference between the plasma concentration and local tissue concentration in the compartments surrounding a blood vessel and the permeability of the antibiotic through blood vessel walls, a flux of antibiotic through the vessel wall is calculated as in previous work [4]. Antibiotics in the tissue (on the simulation grid) undergo a series of distribution events: diffusion, binding to extracellular material such as caseum, partitioning into macrophages, and degradation. Implementation of vascular permeation, diffusion, binding and degradation is as previously published [4,33]. Antibiotics on the simulation grid can be tracked as free molecules, bound to extracellular material, or partitioned into macrophages. When calibrating and fitting to data, we use total drug concentration in a grid compartment, but

only free or intracellular antibiotic is used to determine antimicrobial activity, depending on the location of bacteria. Calibrated tissue PK parameters are given in Table 2.3 (see below for calibration datasets).

2.3.5 Sequential pharmacokinetic model calibration scheme

Gradients between plasma and tissue concentrations drive the amount of antibiotic delivered into the agent-based model simulation through blood vessels, so fitting tissue PK parameters to match the experimentally observed spatial distribution and average antibiotic concentrations in granuloma lesions requires incorporating both plasma PK variability and granuloma heterogeneity. We have devised a pipeline for incorporating these factors into *GranSim* (Figure 2.3). Using our *in silico* granuloma library, each granuloma is assigned a different plasma PK set sampled using LHS from parameter ranges that capture biological variability (Table 2.2). Next, changes in antibiotic tissue concentrations over time are simulated for each granuloma with 200 tissue PK parameter sets sampled using LHS. For each tissue PK parameter set, the results from each granuloma are averaged at each time point, and then compared to experimental data. The tissue PK parameter set that both minimizes the sum of the squared error between average granuloma concentration and the experimental lesion concentrations, as well as provides a good visual fit to the data is chosen as the calibrated tissue PK parameter set. Tissue PK parameter ranges for calibration sampling are listed in Table 2.3.
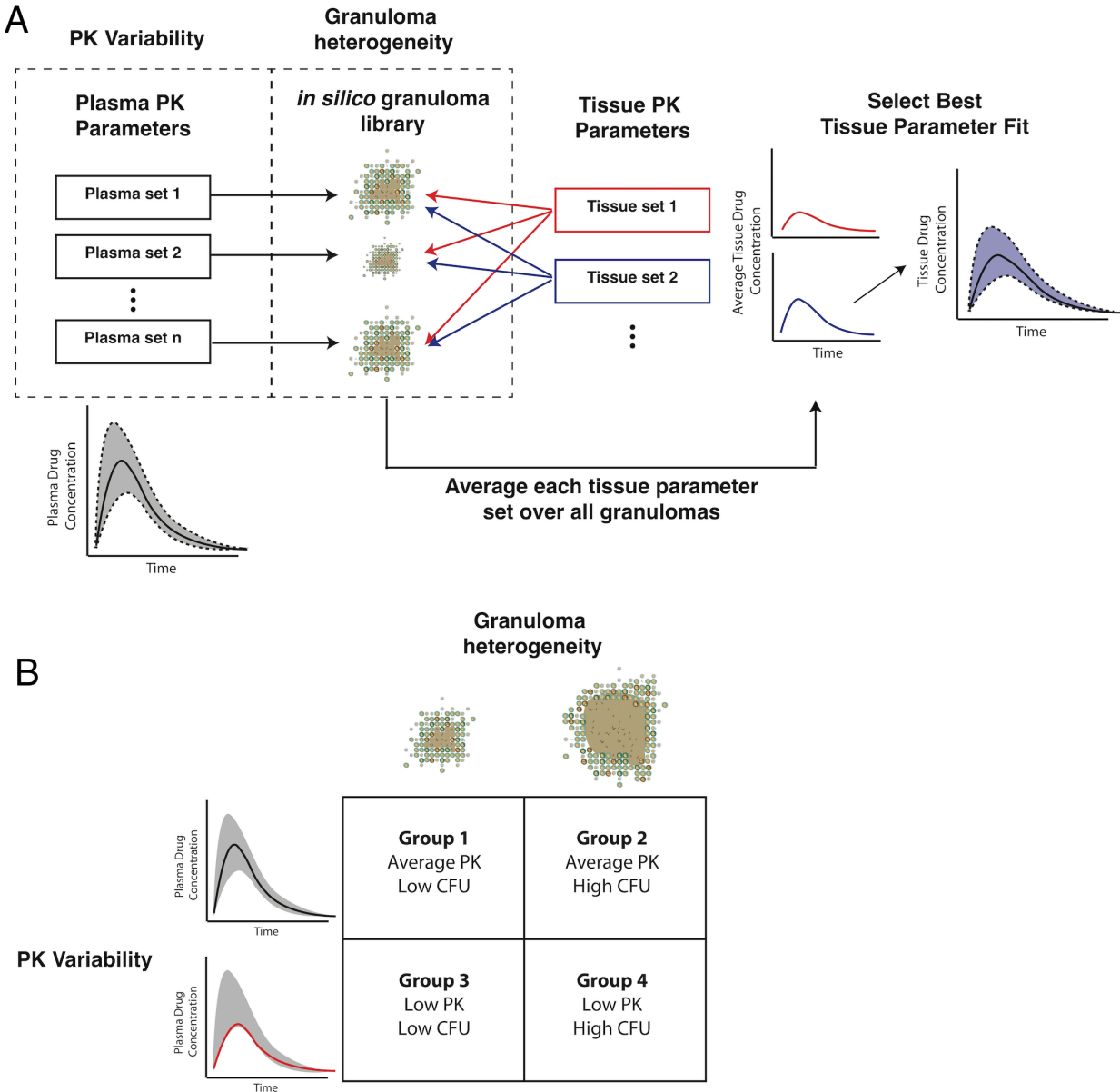
Figure 2.3 Capturing pharmacokinetic variability and granuloma heterogeneity in PK calibration and treatment simulations.
(A) shows our strategy. Based on population variability and ranges in plasma PK parameters, sets of plasma PK parameters are sampled and assigned to a set of *in silico* granulomas. Based on experimentally guided ranges for tissue PK parameters, a set of tissue PK parameters is obtained using LHS. Simulations then predict antibiotic concentrations in the tissue. The average concentration over all granulomas for a given tissue PK parameter set is calculated and compared to experimental lesion concentrations. (B) shows the four types of treatment simulations that capture biologically relevant PK variability and granuloma heterogeneity: average PK exposure with low or high CFU granulomas and low PK exposure with low or high CFU granulomas.

2.3.6 Pharmacokinetic Data
Plasma and tissue PK parameters for INH, RIF and PZA are calibrated using plasma and lesion antibiotic concentrations measured in resected lung samples from patients with drug-refractory TB [18]. EMB concentrations in rabbit TB granulomas are used to calibrate tissue PK parameters, based on rabbit plasma PK parameters [19]. Since tissue PK parameters are based on physical properties and interactions between drug molecules and tissue, we assume that tissue PK parameters in rabbits and humans are similar. To simulate human treatment with EMB, we replace the rabbit plasma PK parameters with human parameters fit to population PK measurements [12].

2.3.7 Pharmacodynamic model
The pharmacodynamic model involves evaluating a concentration-dependent killing rate constant derived from a Hill curve:

$$k = E_{max} \frac{C^h}{C^h + C_{50}^h}$$

The killing rate constant *k* (units of 1/timestep or 1/10 min) is dependent on the variable concentration (*C*), the maximum killing rate constant (*E_{max}*), the concentration at half maximal killing (*C_{50}*) and the Hill curve constant (*h*). The concentration used to determine the antibiotic killing rate constant is based only on free drug concentration. Parameters *E_{max}*, *C_{50}*, and *h* need to be determined for each antibiotic and for each bacterial subpopulation (replicating extracellular, non-replicating extracellular, and intracellular). To fit these parameters, we use *in vitro* dose-response assays from individual experiments from the literature of Mtb growth/death under varying antibiotic concentrations (see Table 2.4 for parameters and references for data and refer to Figure A.1 (Appendix A) for calibrated fits to dose-response curves). In the present model, we do not include drug-drug interactions, so the highest single antibiotic killing rate constant for each antibiotic within a specific grid compartment in the simulation is used as the effective antibiotic killing rate constant for that location [22,34]. This assumption isolates the impact of PK variability and granuloma heterogeneity on granuloma sterilization within this study.

2.3.8 In silico antibiotic treatment of granulomas

Treatment simulations are executed by choosing the non-sterile set of low and high

CFU *in silico* granulomas that have formed 300 days post infection (in the absence of

antibiotics). The doses for the standard regimen are based on CDC recommended adult

doses for each of the four antibiotics: INH, 5 mg/kg; RIF, 10 mg/kg; EMB, 17 mg/kg;

PZA 21 mg/kg [5]. Simulated treatments use daily doses of each antibiotic. Treatment

simulations are administered for a maximum of 180 days, which are based on standard

regimen length [5]; simulations are stopped once granulomas sterilize to reduce

computational resource use. After treatment, we calculate a simulated early bactericidal

activity (EBA), which is defined as the rate of decrease of $\log_{10}$(CFU) per day. For

example, the EBA for 0-2 days is calculated as $(\log_{10}(\text{CFU day 0}) - \log_{10}(\text{CFU day 2}))/2$.

We simulate four groups of granulomas to incorporate PK variability and granuloma

heterogeneity (Figure 2.3). Group 1 has population average plasma PK exposure (AUC)

with low-CFU granulomas and Group 2 has average PK exposure with high-CFU

granulomas. Groups 3 and 4 both have low plasma PK exposure, with low and high-

CFU granulomas respectively. Plasma PK parameter values for the low and average PK

exposure are listed in Table 2.2.

2.4 Results

2.4.1 Pharmacokinetic model captures plasma and lesion variability in antibiotic concentrations

Heterogeneity in antibiotic exposure within granulomas is the result of two factors.

Differences in plasma drug concentrations among individuals can be due to differences

in drug absorption and elimination rates, and these are reflected in distributions of

plasma PK parameters across a population. Additionally, granuloma structural

heterogeneity (including differences in size and composition) can lead to differences in

antibiotic exposure at the lesion level. To capture both sources of heterogeneity, which

occur at different length scales, we devised a sequential calibration scheme to calibrate

the PK model from data (Figure 2.3; parameters in Table 2.2 and Table 2.3).

Figure 2.4 shows antibiotic total concentrations (sum of free and bound) within both

plasma and granulomas for all four first-line antibiotics (INH, RIF, EMB and PZA).

Results are shown for 24 hours following an oral dose and compared to experimental data. Using our sequential calibration scheme, we capture a large proportion of the experimentally observed antibiotic concentration data in both plasma and granulomas. The C_{50} values for each bacterial subpopulation, obtained by fitting the data referenced in Table 2.3, indicate the free-drug concentration when a given antibiotic is at half its maximum bacterial killing rate. INH, RIF and EMB achieve sufficient concentrations to kill extracellular replicating Mtb for a majority of the dosing period. Both INH and EMB can achieve concentrations above the C_{50} for intracellular Mtb. Only RIF approaches concentrations necessary to achieve bactericidal activity against non-replicating Mtb. Based on average granuloma concentrations, PZA appears to have little sterilizing activity in granulomas.

Figure 2.4 also shows antibiotic total concentrations as a function of position throughout the grid, at the time of maximal average granuloma drug concentration following a single oral dose of each antibiotic in the same *in silico* granuloma, shown in grayscale to allow for the illustration of gradual concentration changes. INH shows a relatively homogenous distribution in the lesion that rapidly clears as INH is eliminated in the plasma. RIF accumulates poorly in granulomas at early time points but can slowly accumulate in the caseum following multiple doses (Figure A.2, Appendix A). EMB tends to accumulate in regions with a high density of macrophages but fails to diffuse into caseum significantly. PZA shows a slight accumulation in caseum relative to the macrophage-rich regions of the granuloma. To further validate our model, Figure 2.5 shows PZA distribution identified experimentally using matrix-assisted laser desorption/ionization mass spectrometry imaging (MALDI-MSI) as we have done previously [18] and compares the PZA signal intensity distribution to two simulated granulomas. Overall, our simulated distributions for other antibiotics agree with observations made through MALDI-MSI in TB granulomas [18,19]. These qualitative features observed in the simulations for each antibiotic were not used in calibrating the tissue PK parameters, but rather resulted from estimating and fitting the tissue PK parameters to average granulomas concentrations (Table 2.1).
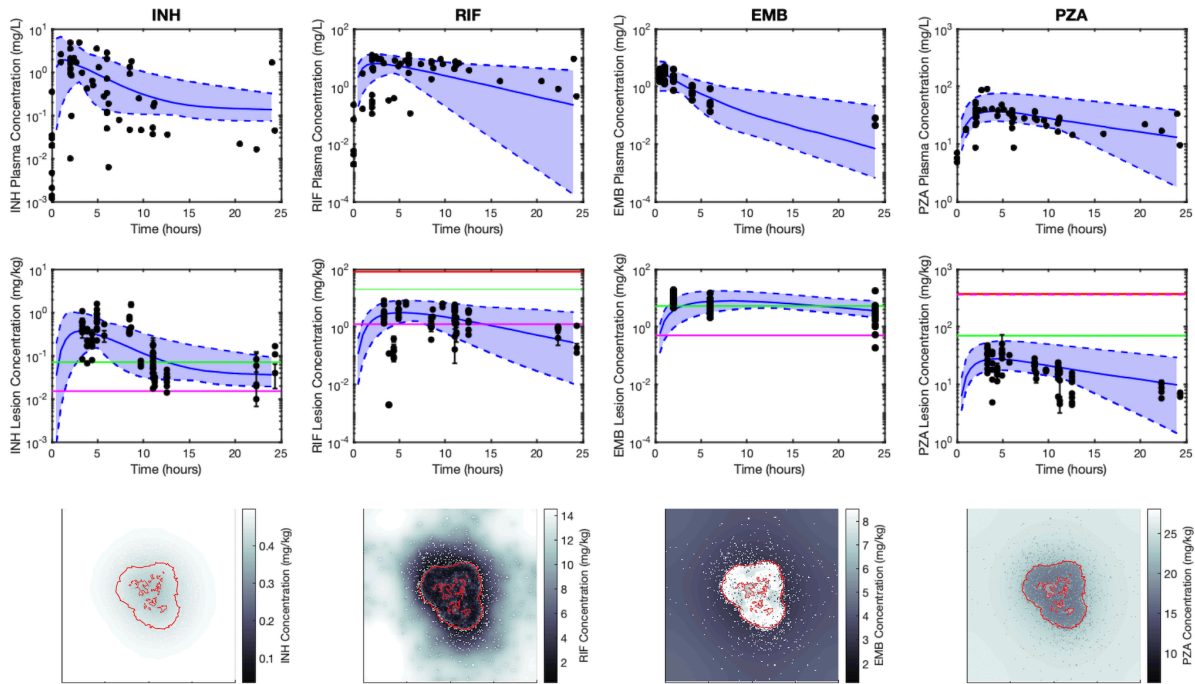
Figure 2.4 Simulations capture both the experimentally observed temporal and spatial antibiotic concentrations.
Simulations and data for each antibiotic (INH, RIF, EMB and PZA), dosed singly, are shown in different columns, respectively. The top row shows plasma concentrations and the middle row shows average lesion concentrations with varying plasma PK parameters (median, solid blue line; range between minimum and maximum of simulations, blue shade) and experimentally measured antibiotic concentrations (black points). Concentrations in granulomas are in mg/kg (assuming tissue density is approximately 1 kg/L), and reflect the sum of concentrations of free, bound and intracellular drug. Horizontal lines represent the C_{50} values for intracellular (green), extracellular replicating (magenta) and non-replicating (red) subpopulations of Mtb (C_{50} values not shown are above the range of lesion concentrations displayed on the plot). Data in the middle row are measurements from human granulomas (INH, RIF and PZA (Prideaux et al. 2015) [18]) and rabbit granulomas (EMB (Zimmerman et al. 2017) [19]). The bottom row shows spatial distribution of antibiotics in *GranSim* at the time of the maximal average lesion concentration. Red outlines indicate edge of granuloma (outer line) and caseated locations (inner lines).
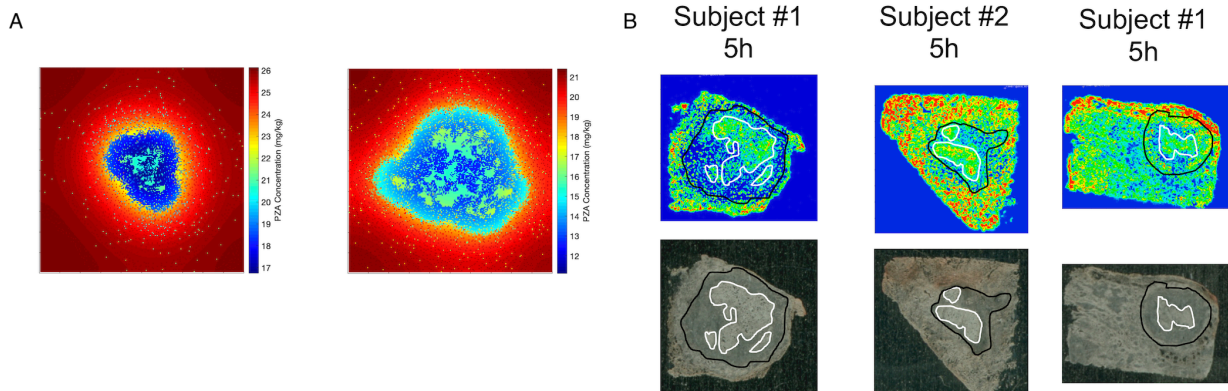
Figure 2.5 Comparison of spatial distribution of PZA in GranSim
(**A**) and in experimental images of granulomas using MALDI-MSI (**B**). The simulation images show heat maps of the spatial distribution of PZA at 5 hours after a single-PZA dose. In the simulated concentration heat maps, shown in color to mimic the images from MALDI-MSI (**A**), the red area corresponds to lung tissue outside of the granuloma, the darker blue regions indicates regions inside the granuloma with higher densities of macrophages, and the lighter blue to green sections show correspond to caseated regions. Both simulation images are on a 200 by 200 grid,

34

representing a 4 mm by 4 mm section of lung tissue. Experimental images (**B**) show PZA distribution in granulomas imaged with MALDI-MSI, with granuloma boundary outlined in black, and caseated regions outlined in white. Both simulation and experiments show some accumulation of PZA inside caseous regions, relative to the cellular portions of the granuloma.

2.4.2 Single-drug treatments sterilize granulomas at different rates and to different extents

We next tested the abilities of each first-line antibiotic, when dosed alone, to sterilize granulomas with average plasma PK exposure and low or high-CFU (Groups 1 and 2 of Figure 2.3). The rates and extents of sterilization differ for each antibiotic in low-CFU granulomas, as shown in Figure 2.6, due to differences in sterilizing activity against various subpopulations of bacteria as well as the antibiotic distribution within granulomas. After 180 days of treatment, single-drug therapy with RIF sterilizes all low-CFU granulomas. INH sterilized 93% low-CFU granulomas. EMB and PZA each sterilize just 32% and 1.7% of low-CFU granulomas, respectively. INH and EMB all have early sterilizing ability and were able to sterilize 29% and 31% of granulomas after two weeks, respectively. RIF alone only sterilized 5% by two weeks, and PZA failed to sterilize any granulomas by two weeks.

Our simulations show that INH can quickly distribute within granulomas, and in sufficient concentrations to kill both intracellular and extracellular replicating bacteria, and therefore provides rapid sterilization for some granulomas, as shown in Figure 2.4 and Figure 2.5. However, with poor sterilizing ability against non-replicating Mtb found in caseum [21], INH usually requires many months to sterilize granulomas that have a high number of non-replicating Mtb and leads to the drawn-out sterilization of non-replicating Mtb in INH-treated granulomas. EMB, similar to INH, has poor ability to kill non-replicating Mtb, so our simulations show it is only able to sterilize a subset of granulomas, even though it distributes throughout cellular regions of the granuloma. However, it does rapidly kill both extracellular replicating and intracellular Mtb, indicated by the percentage of granulomas sterilized by two weeks, which is consistent with favorable early bactericidal activity (EBA) for EMB [35]. Because INH and EMB are bacteriostatic and have low ability to kill non-replicating Mtb, sterilization time (for INH) and total Mtb remaining in the granuloma (for EMB) are highly correlated with the initial number of non-replicating bacteria present in the granuloma (Figure A.3, Appendix A).

RIF shows more complete sterilization of low-CFU granulomas than any other individual antibiotic as it has some sterilizing ability against each subpopulation of bacteria.

We observe similar trends with single-drug treatments in high-CFU granulomas (Figure 2.6). Overall, the sterilization times are longer when compared to low-CFU granulomas. INH and RIF both sterilize lower percentages of the high-CFU granulomas than they do low-CFU granulomas. High-CFU granulomas are also more likely to have higher total numbers of non-replicating Mtb, decreasing the ability of INH to completely sterilize these granulomas. RIF, with weakened ability to kill intracellular Mtb due to low granuloma concentrations, fails to kill all intracellular Mtb in some granulomas. This weakness is amplified in larger granulomas, slowing diffusion of antibiotics into the granulomas.

Figure 2.6 Single-antibiotic treatments and combination therapy of low-CFU
(A, C) and high-CFU (B, D) granulomas show different sterilizing rates and extents for each of the first-line antibiotics and all four antibiotics together (HRZE). (A) and (B) show the percentage of granulomas sterilized over the course of treatment for both groups of granulomas. (C) and (D) show the distribution of sterilization times for only the

granulomas that sterilized for each treatment, with the time when 90% of granulomas were sterilized indicated by a red line. Percentage below each treatment indicates the total percentage of granulomas that sterilized. For example, EMB sterilized 32% of low-CFU granulomas (C), and of those sterilized granulomas, a majority of them sterilized in the first few days (indicated by the box plot collapsing to a line).

2.4.3 Specialization of individual antibiotics contributes to success of combination therapy

Combination therapy – all four first-line antibiotics – sterilizes low-CFU granulomas at nearly the same rate as the best single-antibiotic treatment (RIF) (Figure 2.6). All granulomas are sterilized after 147 days of combination therapy, with 33% sterilized after 2 weeks. The difference in early versus late sterilizing ability for the single-drug treatments is one reason why the combination therapy shows faster and more complete sterilization than any one drug on its own. Early in treatment, INH and EMB do much of the killing, and the presence of RIF completes the sterilization.

The benefit of combination therapy is more dramatic for high-CFU granulomas (Group 2 of Figure 2.3). Here, treatment with INH or RIF show only 33% and 39% sterilization after 180 days of therapy, respectively, compared to 97% of granulomas sterilized with HRZE (Figure 2.6). Although RIF is able to sterilize granulomas as well as HRZE in low-CFU granulomas, the same behavior is not observed in high-CFU granulomas. RIF is relatively slow at killing intracellular bacteria. In the low-CFU granulomas, the number of intracellular Mtb is low enough where RIF can kill these bacteria eventually. In high-CFU granulomas, RIF is not always able to kill intracellular Mtb fast enough to keep up with its replication, and therefore fails to sterilize all high-CFU granulomas. The presence of INH and EMB provide assistance in killing the intracellular Mtb, so the combination of antibiotics allows for more complete sterilization. Our model predicts that the different abilities to kill each of the subpopulations of bacteria and the different distributions within granulomas complement each other in combination therapy.

During combination therapy (HRZE), a majority of bacterial death is due to antibiotics; antibiotics are responsible for roughly an order of magnitude more bacterial death than the immune response, and two orders more than bacterial death in caseum representing a lack of oxygen and nutrients (Figure A.4, Appendix A). This trend is consistent across the single-drug treatments with the exception of PZA, which shows the poorest efficacy and thus allows for continued bacteria growth and continued slow killing via the immune response.

2.4.4 High-CFU and low PK exposure lengthen sterilization times during combination therapy

We next tested how sterilization time and thus the necessary length of treatment is affected by plasma PK variability between individuals and granuloma heterogeneity. We compared the sterilization times of all four granuloma groups (Figure 2.3) when treated with daily doses of HRZE. Figure 2.7 shows the distribution of sterilization times for each of these treatment scenarios. Simulating the low-CFU granulomas with low PK exposure (Group 2) results in a shift in the distribution towards longer sterilization times relative to average PK exposure (Group 1), with the 90% sterilization time increasing from 97 to 133 days. In contrast, 165 days of HRZE are required to sterilize 90% of the high-CFU granulomas with average PK exposure, and 90% sterilization cannot be reached within 6 months of treatment when those same granulomas have low PK exposure.

With some granulomas failing to sterilize after 180 days of treatment, we sought to analyze the characteristics of those granulomas. We grouped our granulomas into four different 'risk' categories: low (sterilize in under 90 days of HRZE), medium (sterilize between 90 and 150 days), high (sterilize after 150 days), and unsterilized. For each of these groups, we compared characteristics of the granulomas before treatment to see what types of granulomas have different levels of risk. Unsterilized and high-risk granulomas tend to be higher in CFU, size, and amount of caseation (Figure A.5, Appendix A), with median CFU/granuloma levels before treatment of 1.1×10^5, 6.0×10^4, 2.1×10^4, and 1×10^3 for the unsterilized, high, medium and low risk categories. However, these pretreatment characteristics are not sufficient in predicting whether a specific granuloma will fail to sterilize during treatment, as there are some granulomas with high CFU, diameter and caseation that sterilize within 90 days. Although these low risk granulomas look like high risk or unsterilized granulomas, they have higher percentages of intracellular Mtb. At the beginning of treatment with HRZE, these intracellular bacteria can be quickly killed, making the granulomas easier to sterilize.

Variation in plasma PK exposure may impact treatment with some antibiotics more profoundly than others. To test this, we sampled a set of 200 plasma PK parameters from the ranges used in calibrating the PK model (Table 2.2). With each of these

plasma PK parameter sets that generate different levels of exposure in plasma, we treated the same granuloma with each single-drug treatment (Figure 2.8). Overall, RIF is most impacted by natural variability in plasma exposure, and varying plasma PK parameters for RIF results in a wider spread of treatment outcomes than other antibiotics, ranging from a minimum sterilization time of 38 days to unsterilized granulomas by the end of treatment (Figure 2.8). This indicates that optimizing dose for RIF and other antibiotics that are particularly sensitive to variations in PK existing in human populations may be critical in designing better regimens.
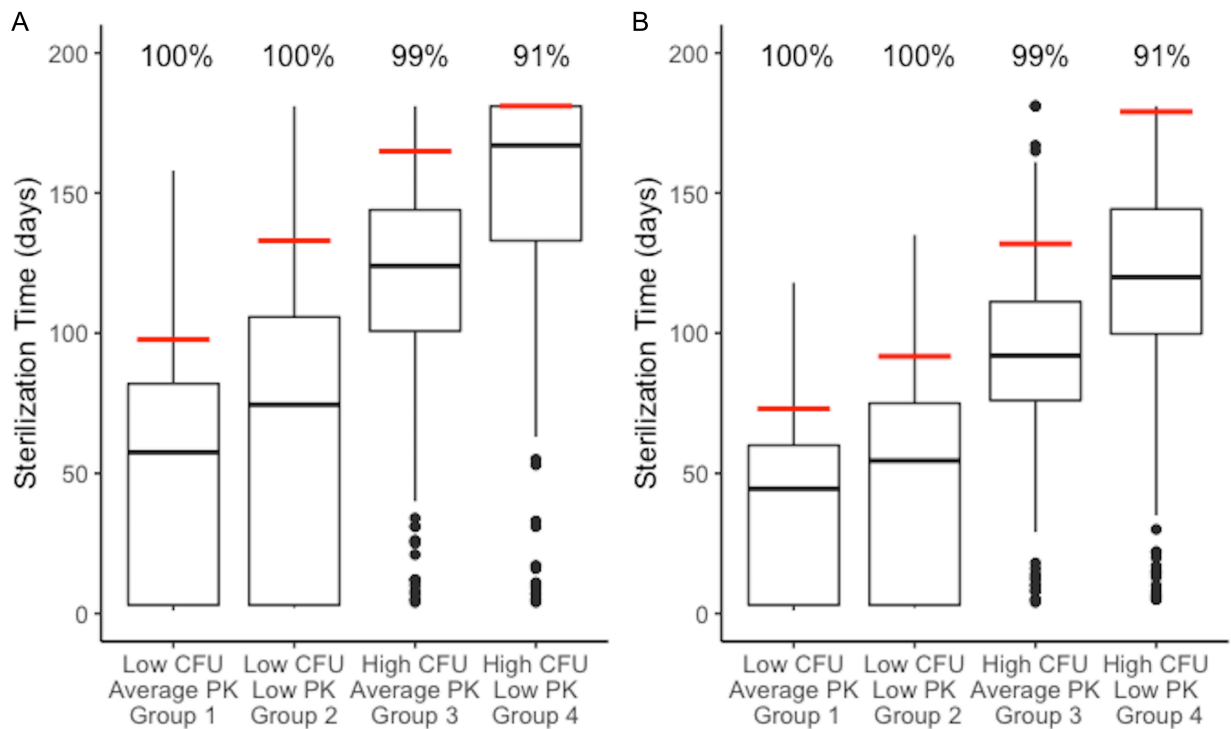
Figure 2.7 Distributions of sterilization times for different granuloma treatment groups,
Distributions of sterilization times for different granuloma treatment groups referenced in Figure 2.3, treated with HRZE indicate factors that negatively impact sterilization. (A) shows simulations of the standard regimen (HRZE). (B) shows the simulations of high RIF dose treatments (20 mg/kg). Each dot is the sterilization time of a specific granuloma simulation, with the red line indicating the time of 99% sterilization. Low CFU granulomas with average PK exposure sterilize the fastest. Low CFU granulomas with low PK exposure show a shift to longer sterilization times compared with average exposure. Similarly, high CFU granulomas with average exposure sterilize faster than high CFU granulomas with low exposure. Results for low CFU and high CFU with average PK are shown in Figure 2.6 and are plotted again here for comparison.
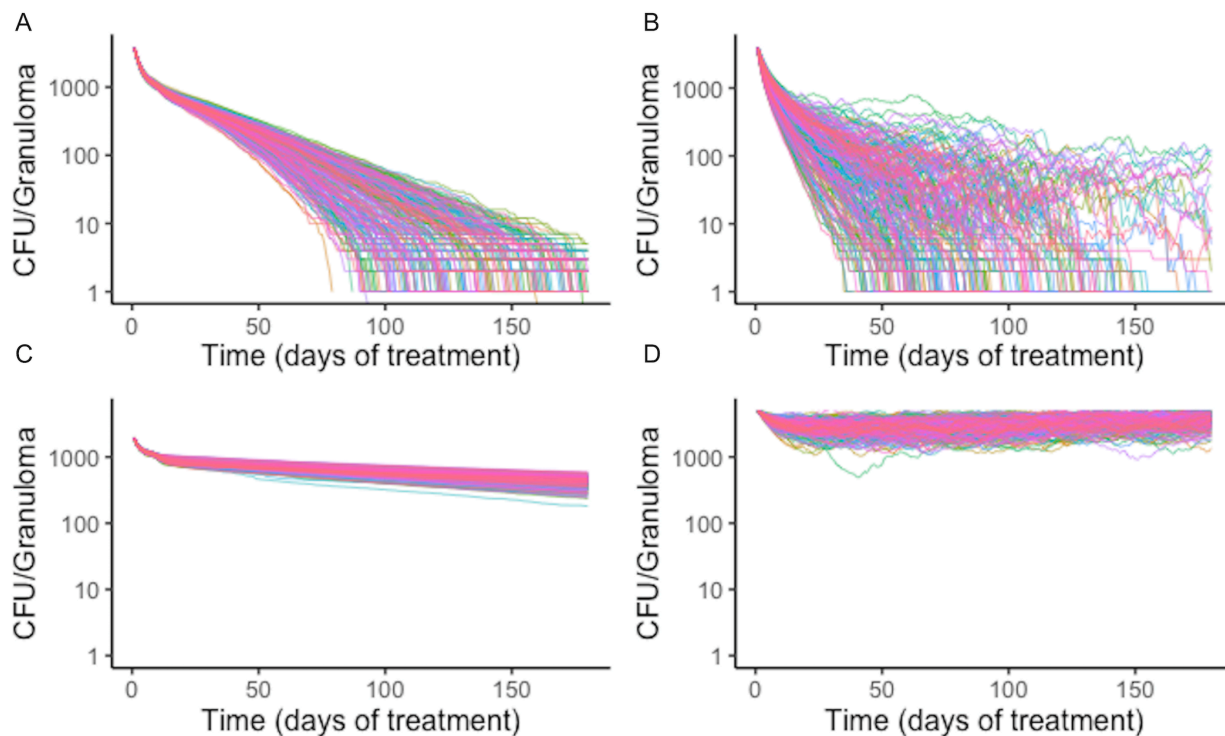
Figure 2.8 Simulation treatment outcomes of single-drug treatments of the same *in silico* granuloma vary with different plasma PK parameter sets.
A single granuloma was treated with each of the single-drug treatments with 200 different plasma PK parameter sets. Above shows the CFU for each granuloma simulation over time during treatment for INH (A), RIF (B), EMB (C) and PZA (D). The standard deviation of sterilization times for different plasma PK parameter sets for RIF normalized to mean sterilization time is 0.40. This indicates greater variability in sterilization times due to changes in plasma PK for RIF compared to INH, for which the value is 0.19. EMB and PZA have standard deviations of log-transformed CFU normalized to the mean at the end of treatment standard deviations of 0.033 and 0.034, respectively.

2.4.5 Treatment time can be shortened for some granulomas by increasing the dose of RIF

There have been numerous efforts to shorten TB treatment regimens and clinical trials that involve replacing one or more antibiotics in the standard regimen or increasing doses of the first-line antibiotics [36,37]. Increasing RIF dosage to 20 mg/kg is a strategy applied in several clinical trials [38–40], and is rational because it could lessen the impact PK variability has on RIF given our results (Figure 2.7). We investigated how increasing the RIF dose impacts granuloma sterilization time while accounting for granuloma heterogeneity and PK variability. To simulate high RIF dose treatments, we simulated each treatment group of granulomas with the same combination regimen as before but increased the RIF dose to 20 mg/kg.

Increasing the RIF dose in combination therapy results in shorter average sterilization times as compared to the standard combination therapy (Figure 2.7). The 90%

sterilization times for low-CFU granulomas decrease by 25 days for average PK and 41 days for low PK exposure. High-CFU granulomas with average PK exposure showed a decrease in 90% sterilization times by 33 days when treated with a high RIF dose, and the low PK exposure simulations increased the percent of sterilized granulomas from 62% to 91% (the latter giving a 90% sterilization time of 179 days). Overall, the improvement observed is greater in the low PK exposure simulations than in average PK simulations.

2.5 Discussion

Treatment of drug-susceptible TB requires multiple months of antibiotics, after which treatment may still fail due to unsterilized granulomas. A better understanding of the first-line combination therapy, HRZE, will help to develop rational approaches to reduce treatment duration and improve cure rates. To analyze the use of first-line antibiotics and the factors that impact granuloma sterilization and conditions of treatment failure, we developed a computational framework that captures both granuloma heterogeneity and PK variability observed in human studies to determine the rate and extent of sterilization during treatment with first-line TB antibiotics at the granuloma scale.

To place the findings of our work into better context with clinical evidence that has been gathered on first-line TB antibiotics, we compared our simulations for single-drug treatments and combination treatments to early bactericidal activities (EBA) measured in multiple studies (Table 2.5). The EBA estimates based on the simulations are shown as the decrease in $\log_{10}$(CFU)/day for each treatment. Many of our simulated estimates are near the clinically measured EBA values (given as reported ranges or confidence intervals). For simulated EBA estimates that do not match clinical results, our simulations tend to predict lower EBA values than those observed clinically. Our EBA estimates account for the entire granuloma's CFU count, and it is possible that we predict lower EBAs as our simulations detect more remaining bacteria than those that would be detected clinically in sputum due to limitations of detection in assays used.

We found that typical PK variability and granuloma heterogeneity can create scenarios that profoundly impact sterilization rates and treatment success. The level of antibiotic concentration in plasma leads to commensurate concentrations within granulomas,

41

creating differences in sterilization rates. Individuals with lower plasma PK exposure are at higher risk of antibiotic underexposure in selected granulomas. When coupled with complex and caseous granuloma structure with impaired vascular supply, this can lead to longer sterilization times using standard HRZE TB therapy (Figure 2.7). Other models using various experimental data, including hollow fiber experiments, show that low drug exposure can lead to decreased rates in bacterial killing [41], and have used variability in PK to predict variability in required treatment durations [42]. The model we present builds on these findings by providing the ability to simulate sterilization in a granuloma, while accounting for human-based PK variability and granuloma structure. The benefit of simulating treatment in the context of the whole granuloma is that it includes the spatial microenvironments that can influence both antibiotic distribution and bacterial susceptibility or tolerance to antibiotics. Treating each Mtb as an individual agent also provides the ability to simulate treatment while accounting specifically for antibiotic resistance [24]. Our model is a tool that can provide quantitative predictions and sterilization times for a given regimen at a granuloma level, the possibility to predict entire host treatment through linking of plasma pharmacokinetics, and the potential to search for optimal treatment regimens [43].

We show that treatment with any of the current first-line TB antibiotics alone is not sufficient to sterilize all granulomas, and that combinations of antibiotics result in more rapid and complete sterilization. Although RIF shows the best sterilizing ability on its own and is about as effective as HRZE in low-CFU granulomas, RIF alone fails to sterilize many of the high-CFU granulomas, where it only sterilizes 39% of granulomas compared to 97% with HRZE. Although our simulations predict that PZA sterilizes very few granulomas on its own, evidence suggests that PZA does show sterilizing ability when administered on its own, and suggests that our simulations underestimate its activity and that there is discrepancy between the *in vitro* activity of PZA and *in vivo* efficacy that our model does not capture [20,44,45].

Granulomas with increased CFU and lower antibiotic exposure can dramatically increase sterilization time and increase the risk of granulomas that do not completely sterilize. Granulomas with high risk of not sterilizing tend to be larger and have more CFU; however, the type of bacteria present in those granulomas may affect the risk of

treatment failure as well. Granulomas with high CFU may still have a low risk of treatment failure if they have high percentages of intracellular Mtb. Because some of the antibiotics in HRZE are good at quickly killing this subpopulation, these granulomas that look like high risk granulomas pretreatment, quickly become low risk granulomas as treatment begins.

RIF is the antibiotic that provides the best sterilizing ability on its own, but also is the antibiotic that shows the highest inter-individual PK variability [46] and is most impacted by PK variability. To reduce the impact the sensitivity RIF has to PK variability, we simulated HRZE treatment while doubling the RIF dose. Indeed, we did observe faster granuloma sterilization and more complete sterilization in high-CFU, low PK granulomas, yet some granulomas in that group still failed to sterilize. Additionally, there was only a slight improvement in sterilization times for granulomas that were already easy to treat, indicating there might only be a modest improvement in treatment for a subset of those granulomas. Understanding an individual's PK profile for different drugs would be an important step in developing a personalized medicine approach to treatment.

While our model can recapitulate key experimental observations and also predict TB treatment outcomes, there are several limitations to our findings. Clinical results measure outcomes at the host level, and *GranSim* fundamentally simulates treatment and sterilization at the granuloma scale. The relevance of our results relies on the assumption that treatment at the granuloma scale is indicative of treatment at a host scale. Our model simulates primary granulomas and does not fully capture the full complexity of multiple pulmonary lesions as is observed during TB disease. It is appreciated that non-replicating and persisting Mtb are critical targets to achieve full sterilization of lesions, and while we observe this in our model, their importance could be amplified in cavitary disease or fibrotic lesions that are not captured in our model. Further, directly relating *in vitro* antimicrobial activity to *in vivo* efficacy does not necessarily capture the full range of antimicrobial activity that occurs within granulomas and may partially account for any discrepancies between our simulation results and clinical observations. An additional limitation of our model is that it currently assumes there are no interactions occurring between antibiotics, and synergistic or antagonistic

combinations may be relevant in determining regimen efficacy [47,48]. Going forward, we are currently introducing synergistic and antagonistic antibiotic interactions to improve the PD model and further refine our estimates and predictions of granuloma sterilization [49–51]. The current model also does not include the development of antibacterial resistance, which may profoundly impact granuloma sterilization; see [24] for a previously published model examining development of resistance and a discussion of modeling resistance development. Finally, this work drew on data sets from a variety of human and animal studies, and predictions of treatment efficacy for other and newer drugs is dependent on the acquisition of similar data sets.

The significant impact that population PK variability and granuloma heterogeneity have on granuloma sterilization highlights the continued need for new approaches and drugs for treatment, and optimization of new regimens. Close collaboration between wet lab and computational scientists will help facilitate the evaluation of these new approaches and provide a more efficient and comprehensive development of new ways to treat TB.

Table 2.1. Host immune parameters for in silico granulomas.
Timestep units represent 10-minute time steps in the agent-based simulation. Parameter values based on previously published work [4].

Parameter definition	Units	Low CFU Granulomas		High CFU Granulomas	
		Min	Max	Min	Max
# immune cell deaths causing compartment caseation		6	10	6	10
Time to heal caseated compartment	Timesteps	909	1365	901	1398
TNF threshold for causing immune cell apoptosis	Molecules	690	1035	690	1200
Rate constant for TNF-induced apoptosis	1/s	1.36e-6	2.04e-6	1.00e-6	2.00e-6
Minimum chemokine concentration to induce chemotaxis	Molecules	0.27	0.41	0.27	0.41
Maximum chemokine concentration to induce chemotaxis	Molecules	392	588	392	588
Initial density of macrophages	Fraction of grid compartments	0.019	0.029	0.019	0.029
Time between resting macrophage movements	Timesteps	4	6	4	6
Time between active macrophage movements	Timesteps	15	23	15	23
Time between infected macrophage movements	Timesteps	169	255	169	255
TNF threshold to induce NFkB activation	Molecules	42.8	64.1	35.1	65.0
Rate constant for NFkB activation	1/s	6.77e-6	1.01e-5	6.00e-6	1.00e-5
Probability resting macrophage kills extracellular Mtb		0.0738	0.111	0.0738	0.111
Killing probability adjustment for resting macrophages with NFkB activation		0.129	0.194	0.129	0.194
# bacteria to cause NFkB activation		236	354	236	354
# bacteria for macrophage to become chronically infected		12	18	12	18
# bacteria to cause macrophage to burst		19	29	19	29

		3	5	3	5
# bacteria activated macrophage can phagocytose		3	5	3	5
Probability activated macrophage will will heal a caseated compartment		0.00459	0.00687	0.00459	0.00687
Probability a T-cell will move to same compartment as a macrophage		0.0367	0.0550	0.0251	0.0550
Probability IFNγ producing T-cell induces Fas/FasL apoptosis		0.0293	0.0439	0.0290	0.0440
Probability IFNγ producing T-cell also produces TNF		0.0514	0.0770	0.0510	0.0779
Probability cytotoxic T-cell kills macrophage		0.00505	0.0121	0.00806	0.0121
Probability cytotoxic T-cell kills a macrophage and all its intracellular bacteria		0.619	0.928	0.611	0.920
Probability regulatory T-cell deactivates macrophage		0.00584	0.00876	0.00580	0.00880
Time when T-cell recruitment begins	Timesteps	3225	4722	3225	4397
Time delay after T-cell recruitment begins until maximal recruitment rate	Timesteps	650	976	650	849
Macrophage maximal recruitment probability		0.0241	0.0361	0.0240	0.0500
Macrophage threshold for recruitment by chemokines	Molecules	0.641	0.960	0.640	0.960
Macrophage threshold for recruitment by TNF	Molecules	0.00859	0.0129	0.00851	0.0130
Macrophage half sat for recruitment by TNF	Molecules	1.22	1.82	1.21	1.83
Macrophage half sat for recruitment by chemokine	Molecules	1.68	2.52	1.68	2.52
IFNγ producing T-cell maximal recruitment probability		0.0484	0.0726	0.0300	0.0620
IFNγ producing T-cell threshold for recruitment by chemokine	Molecules	0.0535	0.0802	0.0530	0.0800
IFNγ producing T-cell threshold for recruitment by TNF	Molecules	1.01	1.51	1.00	1.51
IFNγ producing T-cell half sat for recruitment by TNF	Molecules	1.22	1.82	1.21	1.82

IFNγ producing T-cell half sat for recruitment by chemokine	Molecules	1.64	2.46	1.63	2.45
Probability a IFNγ producing T-cell is cognate		0.0437	0.0655	0.0201	0.0650
Cytotoxic T-cell maximal recruitment probability		0.0370	0.0554	0.0370	0.0550
Cytotoxic T-cell threshold for recruitment by chemokine	Molecules	3.55	5.32	3.54	5.32
Cytotoxic T-cell threshold for recruitment by TNF	Molecules	0.920	1.38	0.922	1.38
Cytotoxic T-cell half sat for recruitment by TNF	Molecules	0.715	1.07	0.711	1.07
Cytotoxic T-cell half sat for recruitment by chemokine	Molecules	5.24	7.86	5.25	7.85
Probability a cytotoxic T-cell is cognate		0.0414	0.0620	0.0410	0.0619
Regulatory T-cell maximal recruitment probability		0.0246	0.0369	0.0242	0.0618
Regulatory T-cell threshold for recruitment by chemokine	Molecules	2.03	3.04	2.02	3.04
Regulatory T-cell threshold for recruitment by TNF	Molecules	1.65	2.47	1.65	2.47
Regulatory T-cell half sat for recruitment by TNF	Molecules	2.00	3.00	2.00	3.00
Regulatory T-cell half sat for recruitment by chemokine	Molecules	1.23	1.84	1.22	1.84
Probability a regulatory T-cell is cognate		0.0400	0.0600	0.0401	0.0600

Table 2.2 Plasma pharmacokinetic parameters
Plasma pharmacokinetic parameters listed with the ranges used to calibrate the tissue pharmacokinetic parameters, as well as the parameter values for the average and low PK exposure treatment groups.

Parameter	Units	Min	Max	Average PK	Low PK	Source
INH Absorption rate constant	1/h	0.50	6.0	3.25	0.57	Fit to data from [18]
INH Intercompartmental clearance rate constant	L/(h*kg)	0.20	0.70	0.45	0.67	Fit to data from [18]
INH Central compartment volume of distribution	L/kg	0.50	3.0	1.75	2.5	Fit to data from [18]

INH Peripheral compartment volume of distribution	L/kg	25	40	32.5	37	Fit to data from [18]
INH Plasma clearance rate constant	L/(h*kg)	0.0080	0.070	0.039	0.061	Fit to data from [18]
RIF Absorption rate constant	1/h	0.40	2.5	1.5	0.41	Fit to data from [18]
RIF Intercompartmental clearance rate constant	L/(h*kg)	2.0	5.9	3.9	3.95	Fit to data from [18]
RIF Central compartment volume of distribution	L/kg	0.18	0.57	0.38	0.48	Fit to data from [18]
RIF Peripheral compartment volume of distribution	L/kg	0.32	0.97	0.64	0.9	Fit to data from [18]
RIF Plasma clearance rate constant	L/(h*kg)	0.050	0.30	0.175	0.3	Fit to data from [18]
EMB Absorption rate constant	1/h	0.10	0.80	0.45	0.1	Fit to data from [12]
EMB Intercompartmental clearance rate constant	L/(h*kg)	0.45	0.70	0.57	0.56	Fit to data from [12]
EMB Central compartment volume of distribution	L/kg	0.80	1.95	1.37	1.7	Fit to data from [12]
EMB Peripheral compartment volume of distribution	L/kg	8.1	12.7	10.4	12.6	Fit to data from [12]
EMB Plasma clearance rate constant	L/(h*kg)	0.3	1.0	0.65	0.99	Fit to data from [12]
PZA Absorption rate constant	1/h	0.55	0.75	0.65	0.60	Fit to data from [18]
PZA Intercompartmental clearance rate constant	L/(h*kg)	0.10	0.70	0.40	0.35	Fit to data from [18]
PZA Central compartment volume of distribution	L/kg	0.25	0.75	0.50	0.74	Fit to data from [18]
PZA Peripheral compartment volume of distribution	L/kg	0.010	0.050	0.030	0.050	Fit to data from [18]
PZA Plasma clearance rate constant	L/(h*kg)	0.010	0.050	0.030	0.050	Fit to data from [18]

Table 2.3 Calibrated tissue PK parameters for each antibiotic.

Parameter	INH	RIF	EMB	PZA	Source
degRateConst Extracellular degradation rate constant (1/s)	6.94e-8	3.90e-8	1.73e-8	1.34e-8	Fit to data from [18,19]
degRateConstInt Intraceullar degradation rate constant (1/s)	2.84e-6	2.59e-4	8.75e-6	2.26e-3	Fit to data from [18,19]
Diffusivity Effective diffusivity* (cm^2/s)	6.58e-7	5.08e-8	5.20e-7	3.24e-6	Fit to data from [18,19]
cellUptake Cellular accumulation ratio	1.13	24	5.95	0.593	Fit to data from [18,19]
vascularPermeability Vascular permeability (cm/s)	1.34e-6	2.65e-7	1.33e-7	8.62e-6	Fit to data from [18,19]
permCoeff Permeability coefficient	0.25	3.3	7.4	1	Fit to data from [18,19]
caseumUnboudFraction Fraction unbound to caseum	1	0.052	0.35	1	Fit to data from [17–19]

* Guided by estimates from [52]

Table 2.4 Pharmacodynamic parameters

Pharmacodynamic parameters and sources for data used for parameter fitting/estimation. Units of 1/timestep represent per model timestep of 10 minutes.

Parameter	INH	RIF	EMB	PZA	Sources
Intracellular C_{50} (mg/L)	0.070	20	5.22	70	[21,53–55]
Extracellular, replicating C_{50} (mg/L)	0.015	1.23	0.05	370	[21,53–55]
Extracellular, Non-replicating C_{50} (mg/L)	17.7	81	1000	370	[21,56]
Intracellular Emax (1/timestep)	0.0056	0.014	0.026	0.0006	[21,53–55]
Extracellular Emax (1/timestep)	0.0056	0.019	0.025	0.007	[21,53–55]
Intracellular hill constant, h	1	0.5	2.5	3.2	[21,53–55]
Extracellular hill constant, h	1	0.5	1.5	1	[21,53–55]

Table 2.5 Comparison of antibiotic treatment simulations to clinical early bactericidal activity (EBA) data.
Table shows the simulation EBA, calculated as the decrease in $\log_{10}$(CFU) per day over the day intervals indicted. Values reported are the mean daily decrease in CFU over all granulomas simulated with the standard regimen doses and average PK. Standard deviation is indicated in parenthesis. The clinical EBA values reported are taken from a number of studies and reviews. The simulation EBA for (0-x) days is calculated as ($\log_{10}$(CFU day 0)- $\log_{10}$ (CFU day x))/x.

Antibiotic	Simulation, Mean (SD)			Clinical		
	EBA 0-2 Days	EBA 0-5 Days	EBA 0-14 Days	EBA 0-2 Days	EBA 0-5 Days	EBA 0-14 Days
INH	0.16 (0.062)	0.13 (0.066)	0.079 (0.051)	Ranges from 0.37-0.77 involving 13 studies summarized in [35]	0.25 (range of 0.19-0.40) as summarized in [35]	Ranges from 0.189-0.192 involving 2 studies summarized in [35]
RIF	0.15 (0.044)	0.12 (0.037)	0.086 (0.027)	Ranges 0.174-0.631 involving 8 studies summarized in [35]	0.226 (SD 0.144) reported in [57]	[b]0.11 (SD 0.096) reported in [35] from (Jindani et al., 1980)
EMB	0.45 (0.36)	0.20 (0.16)	0.082 (0.061)	0.25 (95% CI: 0.06-0.45) pooled in [58]	NA	[b]0.16 (SD 0.090) reported in [59]
PZA	0.014 (0.009)	0.014 (0.007)	0.012 (0.006)	0.01 (95% CI: -0.07-0.09) pooled in [58]	NA	[b]0.11 (SD 0.038) reported in [59]
HRZE	0.49 (0.34)	0.24 (0.15)	0.11 (0.052)	0.3 (95% CI: 0.09 – 0.50) pooled in [58]	[a]0.16 (95% CI: 0.09 – 0.24) pooled in [58]	0.16 (95% CI: 0.11-0.21) pooled in [58]

[a]EBA 0-7 Days
[b]EBA 2-14 Days

2.6 References

1. Global tuberculosis report. Geneva; 2018.
2. Ramakrishnan L. Revisiting the role of the granuloma in tuberculosis. Nat Rev Immunol. 2012;12: 352–66. doi:10.1038/nri3211
3. Dartois V. The path of anti-tuberculosis drugs: from blood to lesions to mycobacterial cells. Nat Rev Microbiol. 2014;12: 159–167. doi:10.1038/nrmicro3200
4. Pienaar E, Cilfone NA, Lin PL, Dartois V, Mattila JT, Butler JR, et al. A computational tool integrating host immunity with antibiotic dynamics to study tuberculosis treatment. J Theor Biol. 2015;367: 166–179. doi:10.1016/j.jtbi.2014.11.021
5. Nahid P, Dorman SE, Alipanah N, Barry PM, Brozek JL, Cattamanchi A, et al. Official American Thoracic Society/Centers for Disease Control and Prevention/Infectious Diseases Society of America Clinical Practice Guidelines: Treatment of Drug-Susceptible Tuberculosis. Clin Infect Dis. 2016;63: 853–867. doi:10.1093/cid/ciw566
6. Munro SA, Lewin SA, Smith HJ, Engel ME, Fretheim A, Volmink J. Patient Adherence to Tuberculosis Treatment: A Systematic Review of Qualitative Research. PloS Med. 2007;4: 1230–1245. doi:10.1371/journal.pmed.0040238
7. Yee D, Valiquette C, Pelletier M, Parisien I, Rocher I, Menzies D. Incidence of Serious Side Effects from First-Line Antituberculosis Drugs among Patients Treated for Active Tuberculosis. Am J Respir Crit Care Med. 2003;167: 1472–1477. doi:10.1164/rccm.200206-626OC
8. McLaren ZM, Milliken AA, Meyer AJ, Sharp AR. Does directly observed therapy improve tuberculosis treatment? More evidence is needed to guide tuberculosis policy. BMC Infect Dis. 2016;16. doi:10.1186/s12879-016-1862-y
9. Steffen R, Menzies D, Oxlade O, Pinto M, de Castro AZ, Monteiro P, et al. Patients' costs and cost-effectiveness of tuberculosis treatment in DOT and non-DOT facilities in Rio de Janeiro, Brazil. PLoS One. 2010;5: 1–7. doi:10.1371/journal.pone.0014014
10. Zhu M, Burman WJ, Starke JR, Stambaugh JJ, Steiner P, Bulpitt AE, et al. Pharmacokinetics of ethambutol in children and adults with tuberculosis. Int J Tuberc Lung Dis. 2004;8: 1360–1367.
11. Denti P, Jeremiah K, Chigutsa E, Faurholt-Jepsen D, PrayGod G, Range N, et al. Pharmacokinetics of isoniazid, pyrazinamide, and ethambutol in newly diagnosed pulmonary TB patients in Tanzania. PLoS One. 2015;10: 1–19. doi:10.1371/journal.pone.0141002
12. Jonsson S, Davidse A, Wilkins J, Van Der Walt JS, Simonsson USH, Karlsson MO, et al. Population pharmacokinetics of ethambutol in South African tuberculosis patients. Antimicrob Agents Chemother. 2011;55: 4230–4237. doi:10.1128/AAC.00274-11
13. Lalande L, Bourguignon L, Bihari S, Maire P, Neely M, Jelliffe R, et al. Population modeling and simulation study of the pharmacokinetics and antituberculosis pharmacodynamics of isoniazid in lungs. Antimicrob Agents Chemother. 2015;59: 5181–5189. doi:10.1128/AAC.00462-15
14. Blum M, Demierre A, Grant DM, Heim M, Meyer UA. Molecular mechanism of

slow acetylation of drugs and carcinogens in humans. Proc Natl Acad Sci. 1991;88: 5237–5241. doi:10.1073/pnas.88.12.5237

15.   Kinzig-Schippers M, Tomalik-scharte D, Jetter A, Scheidel B, Jakob V, Rodamer M, et al. Should We Use N-Acetyltransferase Type 2 Genotyping To Personalize Isoniazid Doses? Antimicrob Agents Chemother. 2005;49: 1733–1738. doi:10.1128/AAC.49.5.1733

16.   Strydom N, Gupta S V, Fox WS, Via LE, Bang H, Lee M, et al. Tuberculosis drugs' distribution and emergence of resistance in patient's lung lesions : A mechanistic model and tool for regimen and dose optimization. PLoS Med. 2019;16. doi:10.1371/journal.pmed.1002773

17.   Sarathy JP, Zuccotto F, Hsinpin H, Sandberg L, Via LE, Marriner GA, et al. Prediction of Drug Penetration in Tuberculosis Lesions. ACS Infect Dis. 2016;2: 552–563. doi:10.1021/acsinfecdis.6b00051

18.   Prideaux B, Via LE, Zimmerman MD, Eum S, Sarathy J, O'Brien P, et al. The association between sterilizing activity and drug distribution into tuberculosis lesions. Nat Med. 2015;21: 1223–7. doi:10.1038/nm.3937

19.   Zimmerman M, Lestner J, Prideaux B, O'Brien P, Dias-freedman I, Chen C, et al. Ethambutol Partitioning in Tuberculous Pulmonary Lesions Explains Its Clinical Efficacy. Antimicrob Agents Chemother. 2017;61: 1–12.

20.   Irwin SM, Prideaux B, Lyon ER, Zimmerman MD, Brooks EJ, Schrupp CA, et al. Bedaquiline and Pyrazinamide Treatment Responses Are Affected by Pulmonary Lesion Heterogeneity in Mycobacterium tuberculosis Infected C3HeB/FeJ Mice. ACS Infect Dis. 2016;2: 251–267. doi:10.1021/acsinfecdis.5b00127

21.   Sarathy JP, Via LE, Weiner D, Blanc L, Boshoff H, Eugenin EA, et al. Extreme drug tolerance of mycobacterium tuberculosis in Caseum. Antimicrob Agents Chemother. 2018;62: 1–11. doi:10.1128/AAC.02266-17

22.   Pienaar E, Dartois V, Linderman JJ, Kirschner DE. In silico evaluation and exploration of antibiotic tuberculosis treatment regimens. BMC Syst Biol. 2015;9: 1–12. doi:10.1186/s12918-015-0221-8

23.   Pienaar E, Sarathy J, Prideaux B, Dietzold J, Dartois V, Kirschner DE, et al. Comparing efficacies of moxifloxacin, levofloxacin and gatifloxacin in tuberculosis granulomas using a multi-scale systems pharmacology approach. PLOS Comput Biol. 2017;13. doi:10.1371/journal.pcbi.1005650

24.   Pienaar E, Linderman JJ, Kirschner DE. Emergence and selection of isoniazid and rifampin resistance in tuberculosis granulomas. PLoS One. 2018;13: 1–29. doi:10.1371/journal.pone.0196322

25.   Fallahi-Sichani M, El-Kebir M, Marino S, Kirschner DE, Linderman JJ. Multiscale computational modeling reveals a critical role for TNF-α receptor 1 dynamics in tuberculosis granuloma formation. J Immunol. 2011;186: 3472–3483. doi:10.4049/jimmunol.1003299

26.   Linderman JJ, Cilfone NA, Pienaar E, Gong C, Kirschner DE. A multi-scale approach to designing therapeutics for tuberculosis. Integr Biol. 2015;7: 591–609. doi:10.1039/C4IB00295D

27.   Cilfone NA, Perry CR, Kirschner DE, Linderman JJ. Multi-scale modeling predicts a balance of tumor necrosis factor-a and interleukin-10 controls the granuloma environment during Mycobacterium truberculosis infection. PLoS One. 2013;8:

e68680. doi:10.1371/journal.pone.0068680

28. Segovia-Juarez JL, Ganguli S, Kirschner D. Identifying control mechanisms of granuloma formation during M. tuberculosis infection using an agent-based model. J Theor Biol. 2004;231: 357–376. doi:10.1016/j.jtbi.2004.06.031

29. Pienaar E, Matern WM, Linderman JJ, Bader JS, Kirschner DE. Multiscale Model of Mycobacterium tuberculosis Infection Maps Metabolite and Gene Perturbations to Granuloma Sterilization. Infect Immun. 2016;84: 1650–1669. doi:10.1128/IAI.01438-15.Editor

30. Nathan C, Barry III CE. TB drug development: Immunology at the table. Immunol Rev. 2015;264: 308–318. doi:10.1111/imr.12275

31. Marino S, Hogue IB, Ray CJ, Kirschner DE. A methodology for performing global uncertainty and sensitivity analysis in systems biology. J Theor Biol. 2008;254: 178–196. doi:10.1016/j.jtbi.2008.04.011

32. Kjellsson MC, Via LE, Goh A, Weiner D, Low KM, Kern S, et al. Pharmacokinetic evaluation of the penetration of antituberculosis agents in rabbit pulmonary lesions. Antimicrob Agents Chemother. 2012;56: 446–457. doi:10.1128/AAC.05208-11

33. Cilfone NA, Kirschner DE, Linderman JJ. Strategies for Efficient Numerical Implementation of Hybrid Multi-scale Agent-Based Models to Describe Biological Systems. Cell Mol Bioeng. 2015;8: 119–136. doi:10.1007/s12195-014-0363-6

34. Bhusal Y, Shiohira CM, Yamane N. Determination of in vitro synergy when three antimicrobial agents are combined against Mycobacterium tuberculosis. Int J Antimicrob Agents. 2005;26: 292–297. doi:10.1016/j.ijantimicag.2005.05.005

35. Donald PR, Diacon AH. The early bactericidal activity of anti-tuberculosis drugs: a literature review. Tuberculosis. 2008;88: S75–S83. doi:10.1016/S1472-9792(08)70038-6

36. Gillespie SH, Crook AM, McHugh TD, Mendel CM, Meredith SK, Murray SR, et al. Four-Month Moxifloxacin-Based Regimens for Drug-Sensitive Tuberculosis. N Engl J Med. 2014;371: 1577–1587. doi:10.1056/NEJMoa1407426

37. Jindani A, Harrison TS, Nunn AJ, Phillips PPJ, Churchyard GJ, Charalambous S, et al. High-Dose Rifapentine with Moxifloxacin for Pulmonary Tuberculosis. N Engl J Med. 2014;371: 1599–1608. doi:10.1056/NEJMoa1314210

38. Boeree MJ, Heinrich N, Aarnoutse R, Diacon AH, Dawson R, Rehal S, et al. High-dose rifampicin, moxifloxacin, and SQ109 for treating tuberculosis: a multi-arm, multi-stage randomised controlled trial. Lancet Infect Dis. 2017;17: 39–49. doi:10.1016/S1473-3099(16)30274-2

39. Diacon AH, Patientia RF, Venter A, Helden PD Van, Smith PJ, Mcilleron H, et al. Early Bactericidal Activity of High-Dose Rifampin in Patients with Pulmonary Tuberculosis Evidenced by Positive Sputum Smears. Antimicrob Agents Chemother. 2007;51: 2994–2996. doi:10.1128/AAC.01474-06

40. Peloquin CA, Velásquez GE, Lecca L, Calderón RI, Coit J, Milstein M, et al. Pharmacokinetic Evidence from the HIRIF Trial To Support Increased Doses of Rifampin for Tuberculosis. Antimicrob Agents Chemother. 2017;61: 1–6.

41. Srivastava S, Gumbo T. In Vitro and In Vivo Modeling of Tuberculosis Drugs and its Impact on Optimization of Doses and Regimens. Curr Pharm Des. 2011;17: 2881–2888. doi:10.2174/138161211797470192

42. Magombedze G, Pasipanodya JG, Srivastava S, Deshpande D, Visser ME, Chigutsa E, et al. Transformation Morphisms and Time-to-Extinction Analysis That Map Therapy Duration from Preclinical Models to Patients with Tuberculosis: Translating from Apples to Oranges. Clin Infect Dis. 2018;67: S349–S358. doi:10.1093/cid/ciy623

43. Cicchese JM, Pienaar E, Kirschner DE, Linderman JJ. Applying Optimization Algorithms to Tuberculosis Antibiotic Treatment Regimens. Cell Mol Bioeng. 2017;10: 523–535. doi:10.1007/s12195-017-0507-6

44. Lanoix JP, Betoudji F, Nuermberger E. Sterilizing activity of pyrazinamide in combination with first-line drugs in a C3HeB/FeJ mouse model of tuberculosis. Antimicrob Agents Chemother. 2016;60: 1091–1096. doi:10.1128/AAC.02637-15

45. Blanc L, Sarathy JP, Alvarez Cabrera N, O'Brien P, Dias-Freedman I, Mina M, et al. Impact of immunopathology on the antituberculous activity of pyrazinamide. J Exp Med. 2018;215: 1975–1986. doi:10.1084/jem.20180518

46. Stott KE, Pertinez H, Sturkenboom MGG, Boeree MJ, Aarnoutse R, Ramachandran G, et al. Pharmacokinetics of rifampicin in adult TB patients and healthy volunteers: a systematic review and meta-analysis. J Antimicrob Chemother. 2018;73: 2305–2313. doi:10.1093/jac/dky152

47. Ma S, Jaipalli S, Larkins-Ford J, Lohmiller J, Aldridge BB, Sherman DR, et al. Transcriptomic signatures predict regulators of drug synergy and clinical regimen efficacy against tuberculosis. MBio. 2019;10: 1–16. doi:10.1128/mBio.02627-19

48. Swaminathan S, Pasipanodya JG, Ramachandran G, Kumar AKH, Srivastava S, Deshpande D, et al. Drug Concentration Thresholds Predictive of Therapy Failure and Death in Children with Tuberculosis: Bread Crumb Trails in Random Forests. Clin Infect Dis. 2016;63: S63–S74. doi:10.1093/cid/ciw471

49. Cokol M, Li C, Chandrasekaran S. Chemogenomic model identifies synergistic drug combinations robust to the pathogen microenvironment. PLoS Comput Biol. 2018;14: 1–24. doi:10.1371/journal.pcbi.1006677

50. Chandrasekaran S, Cokol-Cakmak M, Sahin N, Kazan H, Yilancioglu K, Collins JJ, et al. Chemogenomics and orthology-based design of antibiotic combination therapies. Mol Syst Biol. 2016;12: 872. doi:10.15252/msb.20156777

51. Cokol M, Kuru N, Bicak E, Larkins-Ford J, Aldridge BB. Efficient measurement and factorization of high-order drug interactions in Mycobacterium tuberculosis. Sci Adv. 2017;3: e1701881. doi:10.1126/sciadv.1701881

52. Pruijn FB, Patel K, Hay MP, Wilson WR, Hicks KO. Prediction of tumour tissue diffusion coefficients of hypoxia-activated prodrugs from physicochemical parameters. Aust J Chem. 2008;61: 687–693. doi:10.1071/CH08240

53. Jayaram R, Shandil RK, Gaonkar S, Kaur P, Suresh BL, Mahesh BN, et al. Isoniazid pharmacokinetics-pharmacodynamics in an aerosol infection model of tuberculosis. Antimicrob Agents Chemother. 2004;48: 2951–2957. doi:10.1128/AAC.48.8.2951-2957.2004

54. Jayaram R, Gaonkar S, Kaur P, Suresh BL, Mahesh BN, Jayashree R, et al. Pharmacokinetics-Pharmacodynamics of Rifampin in an Aerosel Infection Model of Tuberculosis. Antimicrob Agents Chemother. 2003;47: 2118–2124. doi:10.1128/AAC.47.7.2118

55. Hartkoorn RC, Chandler B, Owen A, Ward SA, Bertel Squire S, Back DJ, et al.

Differential drug susceptibility of intracellular and extracellular tuberculosis, and the impact of P-glycoprotein. Tuberculosis. 2007;87: 248–255. doi:10.1016/j.tube.2006.12.001

56. Lakshminarayana SB, Huat TB, Ho PC, Manjunatha UH, Dartois V, Dick T, et al. Comprehensive physicochemical, pharmacokinetic and activity profiling of anti-TB agents. J Antimicrob Chemother. 2015;70: 857–867. doi:10.1093/jac/dku457

57. Sirgel FA, Fourie PB, Donald PR, Padayatchi N, Rustomjee R, Levin J, et al. The early bactericidal activities of rifampin and rifapentine in pulmonary tuberculosis. Am J Respir Crit Care Med. 2005;172: 128–135. doi:10.1164/rccm.200411-1557OC

58. Bonnett LJ, Ken-dror G, Koh GCKW, Davies GR. Comparing the Efficacy of Drug Regimens for Pulmonary Tuberculosis: Meta-analysis of Endpoints in Early-Phase Clinical Trials. Clin Infect Dis. 2017;65: 46–54. doi:10.1093/cid/cix247

59. Jindani A, Doré CJ, Mitchison DA. Bactericidal and sterilizing activities of antituberculosis drugs during the first 14 days. Am J Respir Crit Care Med. 2003;167: 1348–1354. doi:10.1164/rccm.200210-1125OC

Chapter 3 A multi-scale pipeline linking drug transcriptomics with pharmacokinetics predicts *in vivo* interactions of tuberculosis drugs

This chapter has been submitted for publication

Authors: Joseph Cicchese, Awanti Sambarey, Denise Kirschner, Jennifer Linderman, Sriram Chandrasekaran

3.1 Abstract

Tuberculosis (TB) is the deadliest infectious disease worldwide. The design of new treatments for TB is hindered by the large number of candidate drugs, drug combinations, dosing choices, and complex pharmaco-kinetics/dynamics (PK/PD). Here we study the interplay of these factors in designing combination therapies by linking a machine-learning model, INDIGO-MTB, which predicts *in vitro* drug interactions using drug transcriptomics, with a multi-scale model of drug PK/PD and pathogen-immune interactions called *GranSim*. We calculate an *in vivo* drug interaction score (iDIS) from dynamics of drug diffusion, spatial distribution, and activity within lesions against various pathogen sub-populations. The iDIS of drug regimens evaluated against non-replicating bacteria significantly correlates with efficacy metrics from clinical trials. Our approach identifies mechanisms that can amplify synergistic or mitigate antagonistic drug interactions *in vivo* by modulating the relative distribution of drugs. Our mechanistic framework enables efficient evaluation of *in vivo* drug interactions and optimization of combination therapies.

3.2 Introduction

Tuberculosis (TB), caused by inhalation of *Mycobacterium tuberculosis* (Mtb), remains the world's deadliest infectious disease, infecting 30% of all people world-wide and leading to ~1.3 million deaths annually [1,2]. The emergence of multidrug resistance

coupled with slow progress in developing new drugs has created a pressing need to identify new approaches to treat TB. The current standard TB treatment regimen is a combination of 4 first-line anti-TB drugs – the antibiotics isoniazid (H), rifampicin (R), pyrazinamide (Z), and ethambutol (E). This treatment has remained unchanged over 50 years [3–5]. Typical combination therapy for TB is administered for at least six months, while treating drug-resistant strains may take up to two years. New drugs, such as bedaquiline, linezolid, and pretomanid, are being tested in new regimens to potentially shorten TB treatment [6,7] The WHO has called for entirely new strategies to meet the goals for 'End TB', which aims to reduce TB deaths by 95% by 2035.

The large number of potential drug combinations greatly complicates TB treatment design [8]. Therapy involving drug combinations can lead to surprising non-linear effects; some drugs can enhance each other's action leading to higher potency (synergy), or drugs can interfere with their action leading to reduced potency (antagonism) [9,10]. These drug interactions can impact treatment efficacy and emergence of drug resistance [11]. Such synergistic or antagonistic drug interactions can be determined using checkerboard assays by screening a panel of drug combinations in multiple doses against Mtb [12]. However, such experimental screening of drug interactions has limited throughput despite recent developments in reducing the number of doses required for measurement [13–15]. Designing an optimal 4-drug combination from a set of just 50 candidate drugs at a single dose requires ~200,000 drug interaction experiments. The dosage and dosing frequency further increase the space of possible regimens exponentially [16].

Measuring *in vivo* drug interactions is even more challenging as it requires mice, primates, or other model organisms infected with Mtb [17]. Consequently, the number of drug candidates that can be screened through these model organisms is very limited. Further, current drug screening strategies for TB do not consider a patient's immune system. Once Mtb is inhaled, it triggers a cascade of immune responses that result in the accumulation of an immune cell-rich mass around infected cells and bacteria known as a granuloma. Mtb can persist for decades within granulomas, and there are multiple

58

granulomas within lungs of infected patients [18]. Granulomas also create a physical barrier altering the penetration of drugs, which can greatly impact relative drug concentrations at the site of infection and lead to effective mono-therapies in granulomas [19–22]. Granulomas also produce nutrient-starved and hypoxic environments that contain Mtb that are phenotypically tolerant to antibiotics, further complicating treatment [23,24].

This study addresses these challenges by creating a multi-scale pipeline combining two cutting-edge computational approaches, operating at different biological scales, to evaluate combination therapies using drug transcriptomics and pharmacokinetics /pharmacodynamics (PK/PD) (Figure 3.1). First, to rapidly predict drug-drug interactions (synergy/antagonism) among combinations of two or more drugs, we utilize the existing *in silico* tool —inferring drug interactions using chemogenomics and orthology (INDIGO) optimized for Mtb (INDIGO-MTB) [8,12]. INDIGO-MTB uses a training data of known drug interactions along with drug transcriptomics data as inputs. INDIGO-MTB then utilizes a machine-learning algorithm to identify gene expression patterns that are predictive of specific drug-drug interactions. Once trained, INDIGO-MTB can determine if new drugs in combination have synergistic or antagonistic interactions using transcriptomics data. We previously used INDIGO-MTB to identify synergistic drug regimens for treating TB from over a million possible drug combinations using the pathogen response transcriptome elicited by individual drugs. The INDIGO-MTB model contains 164 drugs with anti-TB activity and it accurately predicted novel interactions of two-drug and three-drug combinations *in vitro* [8].
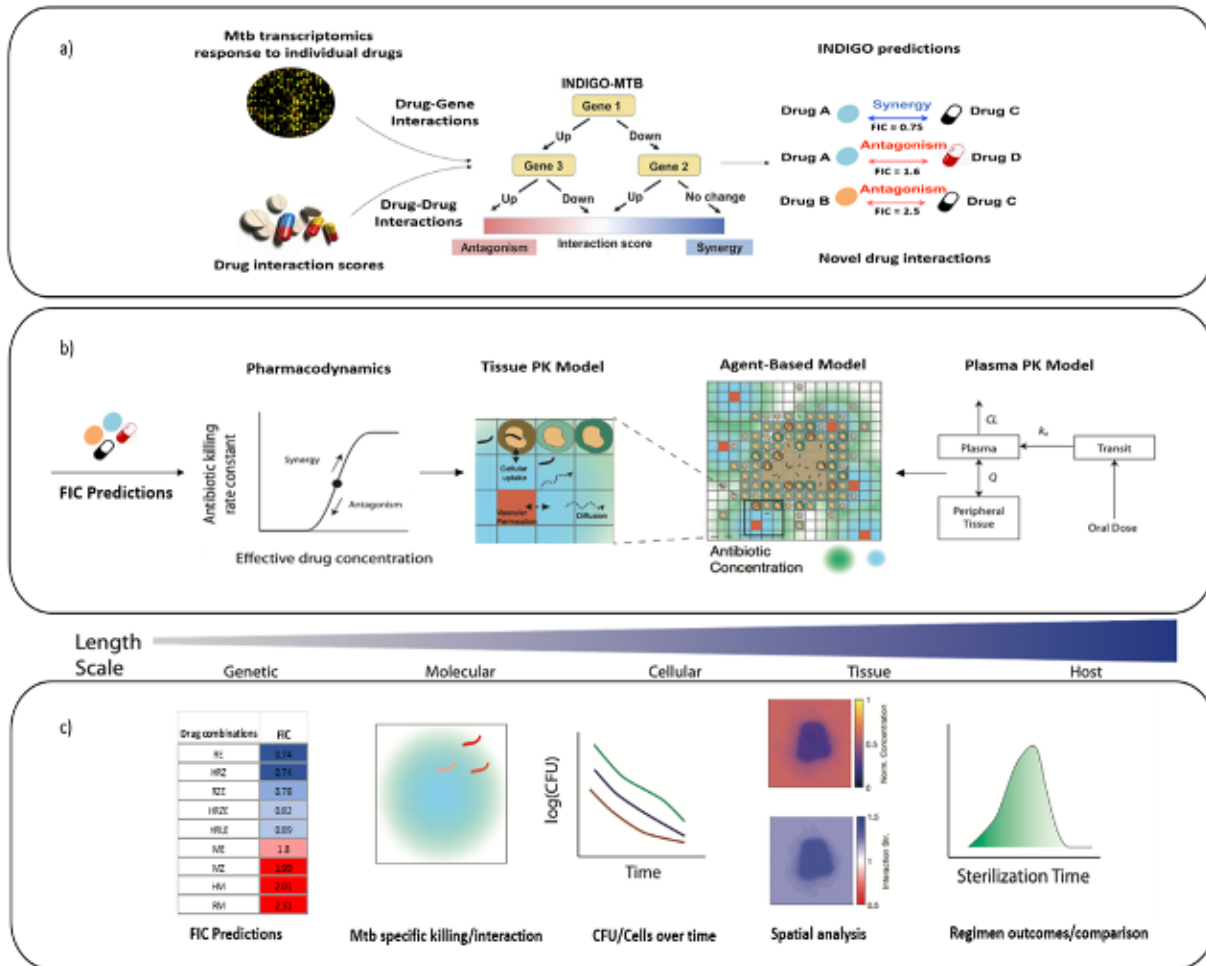
Figure 3.1 Overview of our multiscale pipeline to predict in vivo drug interactions.
a) INDIGO-MTB uses Mtb transcriptomic responses to drugs and experimentally measured drug-drug interactions as inputs for training a machine-learning model, inferring synergistic and antagonistic interactions between new drug combinations as output [8,25]. b) Components of the model integrating GranSim and INDIGO-MTB. From right to left, the plasma PK model determines the time-dependent concentration of all antibiotics following oral doses, which in turn determines the amount of antibiotic delivered onto the agent-based model grid. The computational grid is 200x200 square grid spaces, representing 4mm by 4mm of lung. Within the agent-based model, the tissue PK model describes antibiotic diffusion and binding as well as immune cell accumulation. Based on the local concentration of antibiotics, the PD model evaluates an antibiotic killing rate constant based on an effective concentration that is calculated from each individual antibiotic concentration. The corresponding FIC predicted from INDIGO-MTB either increases or decreases this effective concentration, depending on whether the combination is synergistic or antagonistic. c) Different predictions and outcomes, with the gradient above corresponding to the relevant length scale for the model/prediction. From left to right, predictions made by integration of GranSim and INDIGO-MTB are shown, including FIC predictions from INDIGO-MTB, Mtb-specific killing rate and interactions, number of cells/Mtb overtime used to evaluate simulated EBA, spatial analysis of antibiotic concentration and interactions, and sterilization time distributions from a collection of granulomas.

Next, to predict *in vivo* interactions and efficacy, here we integrate INDIGO-MTB predicted drug interactions within an existing multi-scale model of pathogen-immune dynamics leading to granuloma formation, known as *GranSim* [22,26–29]. *GranSim* integrates spatio-temporal host immunity, pathogen growth and drug PK/PD into a

single computational framework. *GranSim* uses a hybrid agent-based model to describe interactions between immune cells and cytokines with bacteria and antibiotic delivery to granulomas, and provides a dynamic picture of pathogen clearance leading to granuloma sterilization [22]. Previously, we modeled PK/PD in *GranSim* and explored regimens with isoniazid and rifampin, three fluoroquinolones, and more recently HRZE [30–32]. However, in these studies we assumed no interaction between antibiotics. Hence, we now integrate INDIGO-MTB predictions of drug interactions within the *GranSim* framework, allowing the full characterization of drug interaction dynamics at the molecular and cellular scales, and verify our results against patient-level data. This allows us to evaluate how drug interactions and PK/PD at the molecular scale influence *in vivo* efficacy at the granuloma scale.

Our study herein represents the first pipeline that incorporates both *in vitro* drug interactions and *in vivo* PK/PD to simulate treatment dynamics of numerous drug regimens. Our study overcomes the limitation of prior studies that have focused on variation in PK/PD parameters alone to predict treatment outcome [33–35]. Combining INDIGO-MTB with *GranSim* allows us to compare different regimens based on the impact of their interactions on various simulated metrics such as rate of pathogen load decline in granulomas and granuloma sterilization rates. Our approach provides a measurement of drug interactions within lung granulomas based on concentrations that different bacterial populations are experiencing in their individual granuloma environment.

3.3 Methods

3.3.1 INDIGO-MTB model for predicting drug interactions
INDIGO-MTB identifies interactions between drugs in a combination regimen by utilizing pathogen transcriptomics in response to individual drugs. INDIGO-MTB was built using drug response transcriptome data for 164 drugs, including well known drugs rifampicin, isoniazid, streptomycin, and several fluoroquinolones [8]. The model first generates a drug-gene association network using the transcriptomics data, and the machine-learning algorithm, Random Forest. The algorithm identifies genes that are predictive of

drug interaction outcomes using a training data set of known interactions [25]. This trained network model is used to predict interactions for novel drug combinations and provides the Fractional Inhibitory Concentration (FIC) as an output (Figure 3.1). The model can identify all possible 2-way, 3-way, 4-way and 5-way synergistic, additive and antagonistic drug interactions after *in silico* screening of more than 1 million potential drug combinations. INDIGO-MTB predicted FIC scores to be integrated within *GranSim* were generated for all possible combinations of the first line drugs and two fluoroquinolones (H, R, Z, E, Levofloxacin (L) and Moxifloxacin (M)), as listed in Table B.1 (Appendix B).

3.3.2 GranSim model of granuloma formation and function

GranSim is a well-established agent-based model of granuloma formation and function [22,26–29]. It simulates the spatial heterogeneity and bacterial burden of primary TB lesions by simulating the immune response to infection with Mtb in a computational grid representing a small section of lung tissue, with formation of a granuloma as an emergent behavior (Figure 3.1). The simulation begins with a single infected macrophage at the center of the grid, and macrophages and T cells are recruited to the site of infection and interact with each other according to immunology-based rules that describe cell movement, activation, cytokine secretion, and killing of bacteria (for a full list of rules see referenced webpage [36]). Bacteria are tracked individually and modeled as individual agents in the simulation, existing in three distinct subpopulations: intracellular (inside macrophages), extracellular replicating and extracellular non-replicating. The effective growth rates of extracellular bacteria are modulated by the number of bacteria in a given grid compartment. The growth rate becomes zero when the carrying capacity for that compartment is reached to reflect the relative availability of nutrients and physical space limitations [28]. Growth rates of extracellular Mtb are also slowed by the presence of caseum (dead cell debris), as a way to estimate the effect of lack of oxygen [37]. The parameter values describing rules and interactions are based on previous *GranSim* studies and evidence from experimental literature and datasets on non-human primates [22,32,38].

3.3.3 Simulation of antibiotic delivery and concentrations within granuloma

We simulate antibiotic delivery within the *GranSim* computational framework as previously described [22,30,32]. Briefly, a plasma PK model simulates absorption into plasma following an oral dose, exchange with peripheral tissue, and first-order elimination from plasma. Flux of antibiotics into the simulation grid is based on the local gradient between the average drug concentration surrounding vascular sources on the agent-based grid and the plasma concentration. Here we use a 200x200 grid representing a 4 mm x 4 mm lung section. The flux is calculated over time as plasma concentrations change within and around each vascular source and allows for delivery or subtraction from the computational lung environment, depending on the direction of the concentration gradient. Once on the grid, antibiotics diffuse, bind to extracellular material (epithelial tissue and caseum), partition within macrophages and degrade (Figure 3.1). Based on relative binding and partitioning rates into macrophages, concentrations of intracellular and bound antibiotic are modeled at pseudo-steady state for isoniazid, rifampin, ethambutol and pyrazinamide. The drugs moxifloxacin and levofloxacin exhibit slower rates of binding and partitioning relative to diffusion. Hence the dynamic binding and partitioning of these drugs are modeled using ordinary differential equations [30]. We determined plasma PK parameters by calibration to human data as previously described [20,32,39]. We calibrated tissue PK parameters based on concentrations in rabbit or human lesions [20,30,32,40].

3.3.4 Calculation of antibiotic killing rate and in vivo drug interaction

We calculate the antibiotic killing rate constant using an Emax model (Hill equation) as we have done previously [22]. This antibiotic killing rate constant is evaluated at each time step for every Mtb in the simulation based on the local grid concentrations as they change over time. The antibiotic killing rate constant (k) is evaluated as

$$k(t) = E_{max} \frac{C_{eff}(t)^h}{C_{eff}(t)^h + C_{50}{}^h}$$

Eq. 3.1

where E_{max} is the maximal killing rate constant, C_{50} is the concentration at which half maximal killing is achieved, h is the Hill coefficient, and C_{eff} is the effective concentration of the antibiotic (or combination of antibiotics). To reflect each antibiotic's unique levels of activity against different sub-populations of bacteria, the PD parameters C_{50}, E_{max} and h vary depending on the location of the bacteria within the granuloma (intracellular, extracellular replicating, or extracellular non-replicating).The relationship between a combination of drug concentrations and pharmacodynamic effect (such as killing and inhibition) is described using the Loewe Additivity model [14,41]. In the Loewe additivity model, a simply additive interaction between two antibiotics is described by

$$\frac{C_1}{IC_{x,1}} + \frac{C_2}{IC_{x,2}} = 1 \qquad \text{Eq. 3.2}$$

where $IC_{x,1}$ and $IC_{x,2}$ are the inhibitory concentrations of drugs 1 and 2 that achieve x% inhibition on their own, and C_1 and C_2 are the concentrations that achieve the same level of inhibition in combination. We can convert the concentration of drug 2 to an equipotent concentration of drug 1, shown in Figure 3.2 and denoted $C_{2,adj}$. This gives the concentration of drug 1 that results in the same antibiotic killing rate constant as the given concentration of drug 2 (C_2), which we define as the adjusted concentration for drug 2 ($C_{2,adj}$).

$$C_1 = C_{2,adj} = \left(\frac{C_{1,50}{}^{h_1} C_2{}^{h_2}}{\frac{E_{max,1}}{E_{max,2}}\left(C_2{}^{h_2} + C_{50,2}{}^{h_2}\right) - C_2{}^{h_2}} \right)^{1/h_1} \qquad \text{Eq. 3.3}$$

The corresponding inhibitory concentrations for a given x% inhibition for drugs 1 and 2 are now both equivalent to $IC_{x,1}$, because both C_1 and $C_{2,adj}$ are expressed in terms of

concentration of drug 1. Substituting $C_{2,adj}$ for C_2 and $IC_{x,2}$ for $IC_{x,1}$, Eq. 3.2 can be rewritten as

$$C_1 + C_{2,adj} = IC_{x,1}$$

Eq. 3.4

If there are 3 or more drugs under consideration, we define this sum of concentrations as the effective concentration (C_{eff}) of a combination of *n* antibiotics:

$$C_{eff} = \sum_{i=1}^{n} C_{i,adj}$$

Eq. 3.5

We define synergy or antagonism between two or more drugs based on deviations from simple additivity, as assumed above. This deviation is represented using the Fractional Inhibitory Concentration (FIC) [42]:

$$FIC = \frac{C_o}{C_e}$$

Eq. 3.6

where C_o represents the observed combined drug concentration to yield a given level of inhibition, and C_e is the expected combined drug concentration to yield the same level of inhibition if the two drugs or more drugs were simply additive [14]. The FIC measures changes in potency, i.e. how much drug is needed to produce a certain pharmacodynamic effect. Based on the value of FIC, synergistic or antagonistic combinations result in a lower or higher effective drug concentration to achieve the same level of killing. To incorporate drug interactions into our model, we assume the effective concentration for a combination of n drugs is adjusted from Eq.3.5 based on the FIC value:

$$C_{eff} = \left(\sum_{i=1}^{n} C_{i,adj}{}^{FIC} \right)^{1/FIC}$$

Eq. 3.7

Eq. 3.7 adjusts effective concentration so that synergistic combinations (FIC < 1) result in a higher effective concentration, and antagonistic combinations (FIC > 1) result in a lower effective concentration. Using our defined effective concentration, we substitute Eq. 3.7 into Eq. 3.1 to evaluate the antibiotic killing rate constant for combinations of antibiotics while also accounting for drug interactions. Our drug interaction model and effective concentration formulae accurately recreate *in vitro* drug interaction behavior observed in checkerboard assays (Figure 3.2) [14].

To evaluate the impact that each drug interaction has on the calculated killing rate constant (Eq. 3.1) for a given combination of antibiotics in our *in vivo* simulation, we define an *in vivo Drug Interaction Score* (iDIS). The iDIS is the ratio of the bacterial killing rate constant with a predicted FIC to the killing rate constant if FIC was equal to 1, i.e. no or additive drug interactions. This allows us to quantify the impact that drug interactions have on bacterial killing for each individual Mtb at each time step during simulated treatment.
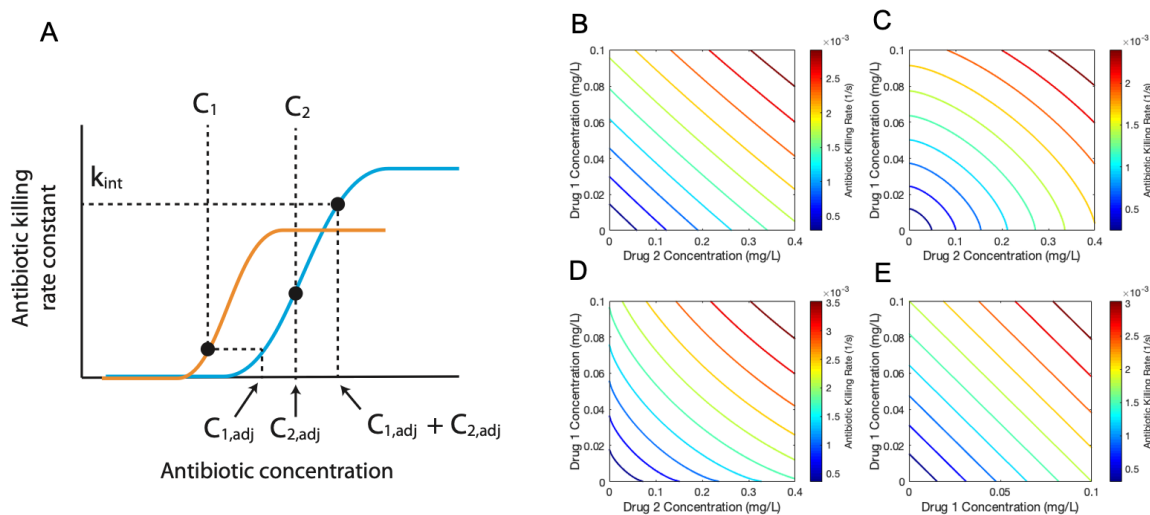
Figure 3.2 Graphical representation of computing the adjusted concentration and killing rate constant (Eq. 3.1 and 3.3).

The adjusted concentration of a drug is found by computing the equipotent concentration for another drug. The plot of two Hill curves for three different drugs (drug 1, orange; drug 2, blue) shows the relationship between concentrations of the two antibiotics and their adjusted concentration (A). The effective concentration, evaluated as the sum of the adjusted concentrations, determines the antibiotic killing rate constant. Antibiotic killing rate constant contours show the behavior of the drug interaction model for a combination of two theoretical drugs. Drug 1 has a c50 of 1 mg/L, Emax of 0.02 1/s, and a hill coefficient of 1. Drug 2 has a c50 of 2 mg/L, Emax of 0.01 1/s, and a hill coefficient of 1. When the two drugs have an FIC of 1.0 (B), 1.5 (C), or 0.6 (D), the contours show the characteristic straight line or curved contours characteristic of checkerboard assays for additive, antagonistic, or synergistic combinations. A sham combination of Drug 1 (E) results in a simply additive case.

3.3.5 Antibiotic treatment simulations and calculation of regimen efficacy

To simulate treatment with different antibiotic combinations, we first created an *in silico* granuloma library to generate a set of granulomas. Each library consists of 500 granulomas simulations, generated from 100 parameter sets sampled with Latin Hypercube Sampling (LHS), and each parameter set was replicated five times [43,44]. Table B.2 (Appendix B) lists the parameters varied and their ranges, which have been established in previous work [22,32]. Parameter ranges capture natural variability in the immune response and lung environment, such as differences in cellular recruitment and immune cell activation. In addition, replicating simulations with the same parameter set incorporates variability due to stochasticity in the simulations. Granulomas are simulated for 300 days in the absence of antibiotics. At day 300, a random sample of 100 unsterilized granulomas is selected from the relevant library for treatment. The prescribed regimens are simulated for 180 days or until the granuloma is sterilized. See Table B.1 (Appendix B) for the full list of regimens tested.

We evaluate three metrics from our simulations to assess the efficacy of each regimen tested: log decrease in CFU per day, percent of simulated granulomas that are sterilized after eight weeks of treatment (sterilization percent), and average time at which those granulomas become sterile (sterilization time). For each regimen, 100 granulomas are simulated and results from those simulations are used to calculate 3 outcomes measures: simulated log decrease in CFU per day, sterilization percent, and sterilization time.

3.3.6 Comparison to clinical trials

To validate our model results, we compared our treatment simulation outcomes to Phase IIb clinical trial data [45]. We compared the clinical datasets outcomes for each

regimen with our simulated granuloma sterilizations after 8 weeks of treatment. We used the percent of granulomas that are completely sterilized at 8 weeks as a lower bound estimate. Our upper bound estimate is the percentage of granulomas with fewer than 10 CFU after 8 weeks. We chose this value as these granulomas with low bacterial load would not be detectable in sputum. Additionally, we compared the rank of clinically tested regimens, ranked by sputum conversion, to the rank of regimens based on simulation results. Simulated regimen rankings were ranked by average sterilization time, FIC, and average iDIS for non-replicating Mtb. Further, we compared our predicted treatment sterilization times for fluoroquinolone-containing regimens with clinical endpoints (up to 6 months) from recent phase III clinical trials that include fluoroquinolones for treating drug-susceptible TB [46–48].

3.3.7 Plasma PK sensitivity analysis on interaction strength
We performed a sensitivity analysis to evaluate how PK parameters impact the predicted iDIS for regimens with different levels of synergy. For four regimens (HRZE, RE, HE, RM), we selected a single granuloma to simulate treatment for one day to measure an iDIS. For each regimen, we simulated the granuloma 500 times with different plasma PK parameters sampled using LHS. For each plasma PK parameter set, we calculated the average iDIS over the first day of dosing over all non-replicating Mtb. Finally, we evaluated the partial ranked correlation coefficient (PRCC) between each plasma PK parameter and the predicted iDIS to determine the impact each parameter has on the drug interactions [44,49].

3.4 Results

3.4.1 Drug interactions significantly impact in vivo treatment dynamics in GranSim
We focus on combinations of 2, 3 or 4 drugs involving the first-line antibiotics and two fluoroquinolones (Table B.1, Appendix B). These drugs include isoniazid (H), rifampin (R), ethambutol (E), pyrazinamide (Z), moxifloxacin (M), and levofloxacin (L). We chose these drugs as they are part of the current standard-of-care for treating TB. Further, transcriptomics and PK/PD parameters are available for these drugs for simulation using both INDIGO-MTB and *GranSim*.

68

Using INDIGO-MTB, we first predicted all possible *in vitro* interaction outcomes for these combinations. The combinations are predicted to have FIC values that range from synergistic (e.g. HRZ – FIC of 0.74) to antagonistic (e.g. RM – FIC of 2.31). The standard regimen (HRZE) is predicted to be synergistic (FIC – 0.82) while moxifloxacin-containing regimens were mostly antagonistic (Table B.2, Appendix B).

Given the various factors that can impact antibiotic efficacy *in vivo* that are captured in *GranSim*, the relative impact of drug interactions on treatment outcomes is unclear. We hypothesized that analysis of various drug regimens with different drug interaction scores (FIC) can help tease out the impact on treatment outcome. Our previous studies of antibiotic treatment using *GranSim* did not consider drug interactions. Here we explore how either antagonistic or synergistic affects overall efficacy. We tested the impact of incorporating drug interactions on treatment dynamics using *GranSim*.

We input FIC values into *GranSim* and simulated the immune response and antibiotic delivery to granulomas (Methods). The plasma and tissue PK parameters for these drugs within the *GranSim* computational framework were derived from previous studies calibrating PK parameters to experimental plasma and lesion drug concentrations (Methods). For each regimen tested, 100 simulated granulomas were treated for up to 180 days with daily doses of each antibiotic in the specified regimen. To compare the efficacy of each of these regimens, we evaluate three measures: the log decrease in CFU per day, percent sterilization of granulomas, and average sterilization time.

The *in vitro* FIC value of each combination is correlated with each of the three simulated efficacy outcomes that we calculated (Figure 3.3). For our simulated log decrease in CFU per day from 0-14 days and the sterilization percent, we observe that both outcomes tend to decrease as FIC values go from synergistic to antagonistic (correlation R = -0.52 and -0.59 respectively, Figure 3.3). The average sterilization time is positively correlated with FIC value (correlation R = 0.59, Figure 3.3). Overall, this

indicates that synergistic regimens are more likely to sterilize a greater percentage of granulomas in a shorter time at both early and later time points.

Although these relationships show moderate levels of correlation, there are a few notable deviations. Interestingly, the regimen RM (FIC = 2.31) performs better than the less antagonistic regimen HE (FIC = 1.46). The best regimen in terms of average sterilization time is HRZE (FIC = 0.82); however, the regimen RE (FIC = 0.74) has a lower FIC but does not perform as well as HRZE. These results suggest that FIC values are not the only factor impacting granuloma sterilization. Because these results are based on sterilization in granulomas, the concentrations of each antibiotic in the granuloma compartment (based on dosage and PK) also impact the ability of each regimen to sterilize.
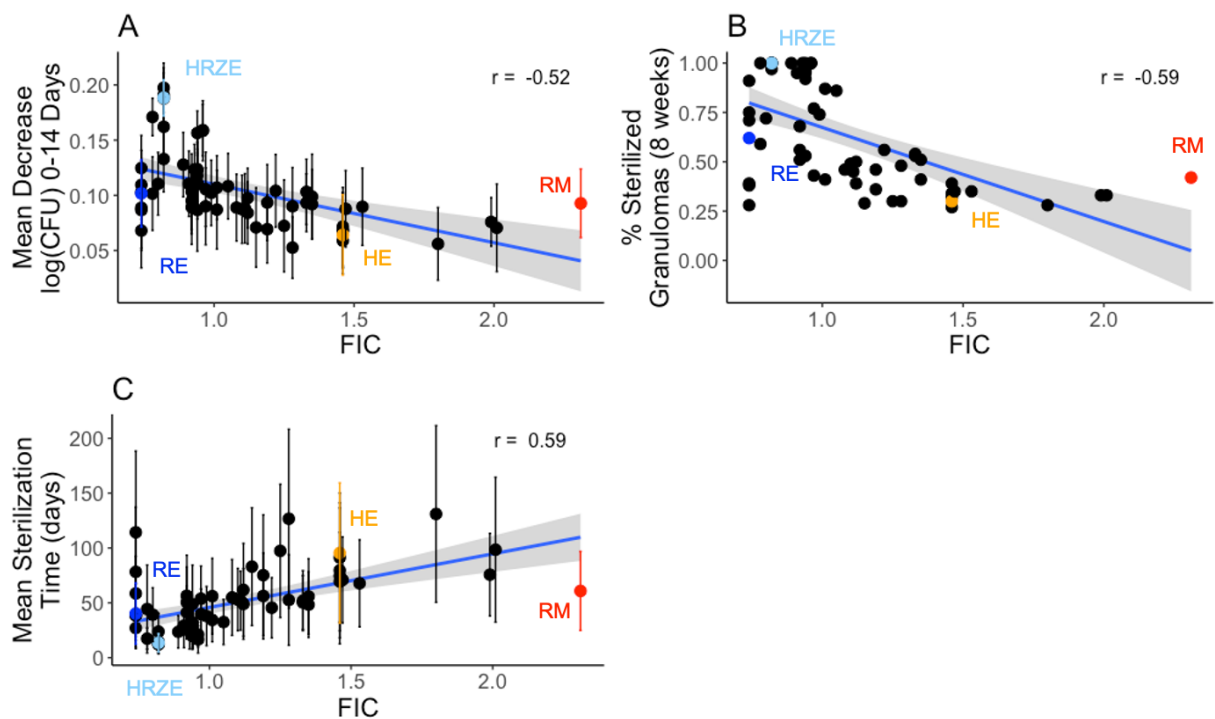
Figure 3.3 Regimen efficacy is correlated with FIC for 64 simulated drug regimens.
Mean decrease in log CFU (0-14 days) averaged over 100 granulomas simulated for each drug regimen (A) and percentage of sterilized (negative) granulomas after eight weeks of treatment (B) are negatively correlated with FIC values, with correlation coefficients of -0.52 and -0.59, respectively. Mean sterilization time for each regimen over 100 granulomas (C) is positively correlated with FIC with a correlation coefficient of 0.59. Each point represents the regimen outcome measurement for a given regimen and error bars indicate +/- standard deviation from the sample of 100 granulomas simulated. The 64 drug regimens simulated are listed in Table B.1 (Appendix B). The colored points correspond to the regimens HRZE (light blue), RE (dark blue), RM (red) and HE (orange) for emphasis.

3.4.2 The in vivo drug interaction score is predictive of treatment dynamics
The antibiotic killing rate is dependent not only on the FIC value, but also on local drug concentrations within a granuloma, the subpopulation of bacteria (intracellular, extracellular replicating, extracellular non-replicating), and the specific PD parameters of antibiotics involved. Based on the definition of the FIC, synergistic or antagonistic drug combinations result in a lower or higher effective concentration to achieve the same level of bacterial killing. To evaluate the overall impact of drug interactions on the calculated killing rate constant, we evaluate an *in vivo Drug Interaction Score* (iDIS) for the three subpopulations of bacteria. The iDIS measures the relative increase or decrease of the antibiotic killing rate constant due to the specific drug interaction. We calculate iDIS as the ratio of the antibiotic killing rate constant evaluated in the simulation to the rate constant if the interaction is simply additive (FIC equal to 1.0). This ratio provides a measure of how much the drug interaction impacts the killing rate constant and is unique for each individual mycobacterium within *GranSim* as drug concentrations change over time. At each time step during treatment, the average iDIS over all Mtb by subpopulation is evaluated as a model output.

Figure 3.4 shows the average iDIS for non-replicating Mtb over the first dose interval for each regimen, and its relationship to regimen outcomes. A value of 1 indicates the interaction has no impact on the killing rate constant; values greater than 1 or less than 1 indicate synergistic or antagonistic combinations, respectively.

The iDIS for each regimen is strongly correlated with the outcomes from our *GranSim* simulations: log decrease in CFU per day (R = 0.86), percentage of negative granulomas at eight weeks (R = 0.73), and the average sterilization time (R = -0.73) (Figure 3.4). The correlations are much stronger than those observed for FIC (Figure 3.3), indicating that measuring the iDIS, which is calculated for specific granuloma environments, provides more information on regimen efficacy than examining FIC values, which are calculated based on *in vitro* environments.
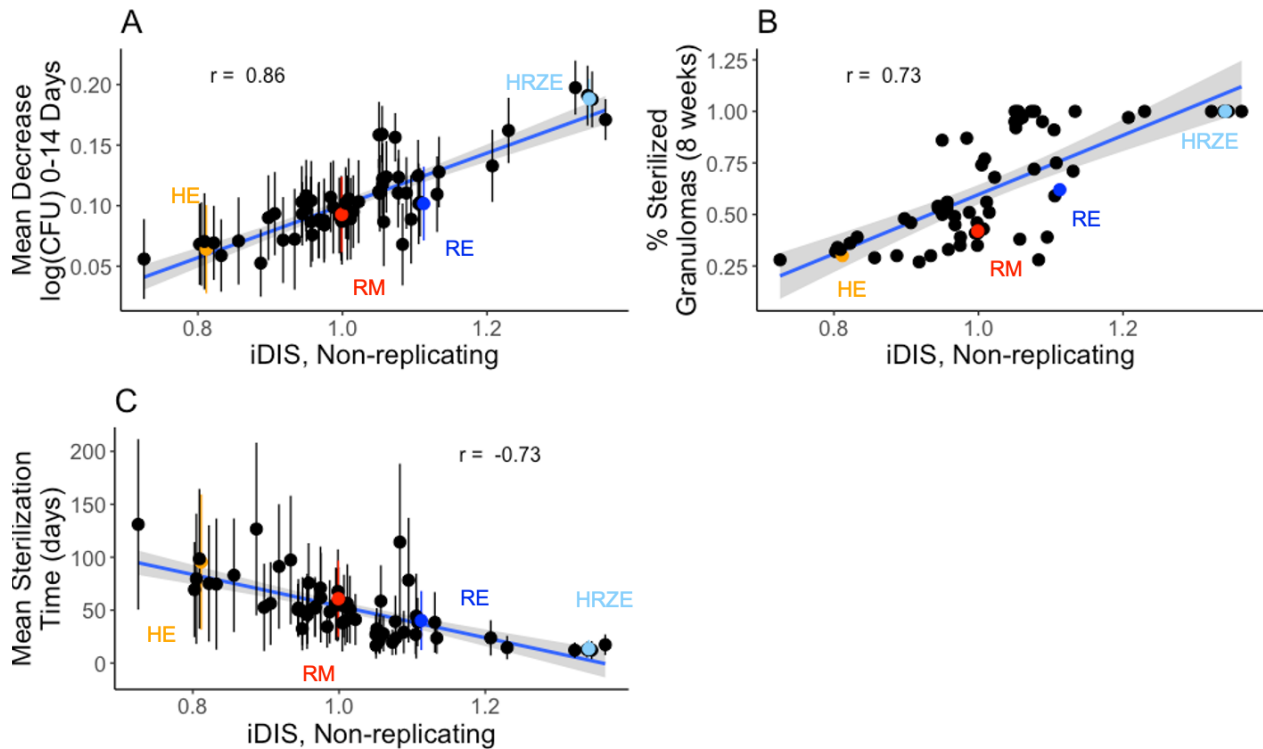
Figure 3.4 Regimen efficacy is correlated with the in vivo Drug Interaction Score (iDIS).
iDIS associated with non-replicating Mtb killing is evaluated for 3 measures over 64 simulated drug combination regimens. The decrease in log CFU (0-14) averaged over 100 granulomas simulated for each regimen (A) and percentage of sterilized (negative) granulomas after eight weeks of treatment (B) are positively correlated with iDIS of non-replicating Mtb during the first 24 hours of treatment (correlation coefficients of 0.86 and 0.73, respectively). Mean sterilization time for each regimen over 100 granulomas (C) is negatively correlated with iDIS of non-replicating Mtb (correlation coefficient of -0.73). Each point represents the regimen outcome measurement for a given regimen and error bars indicate +/- standard deviation from the sample of 100 granulomas simulated. The 64 drug regimens simulated are listed in Table B.1 (Appendix B). The colored points correspond to the regimens HRZE (light blue), RE (dark blue), RM (red) and HE (orange) for emphasis.

Each combination of antibiotics has a different absolute killing rate constant based on the specific combination of PD parameters associated with that combination together with the distribution of antibiotics within a granuloma. These results suggest that iDIS provides a more accurate representation of how well a given combination of antibiotics achieves sterilization as it accounts for the unique killing rate constant that each individual Mtb experiences and measures the impact that an FIC value has on that killing rate constant.

Antibiotics work stronger on replicating Mtb than against non-replicating Mtb. Antibiotic killing rate constants that are higher and closer to their overall E_{max} value are less impacted by drug interactions. We found that correlations between regimen outcomes

and the average iDIS associated with replicating extracellular and intracellular Mtb are weaker than when comparing regimen outcomes to the iDIS from non-replicating Mtb (Figures B.1 and B.2, Appendix B). The average iDIS measurements for replicating Mtb are closer to 1.0 and weaken the correlation with regimen outcomes. Hence, the strong correlation between drug interactions and clinical outcomes are primarily driven by drug action against non-replicating bacteria.

Figure 3.5 shows a heat map of the mean sterilization time, iDIS and FIC for each regimen, ordered by decreasing iDIS. In general, the regimens with the fastest sterilization times also have high iDIS. The top 17 regimens, as measured by shortest average sterilization time, all contain RIF, indicating that RIF is a very important addition to regimens. Another general trend is that two-drug combinations typically perform worse than 3- or 4-drug combinations. Fluoroquinolones tend to participate in more antagonistic combinations, as measured by the iDIS. For example, 22 of the 31 MXF or LVX containing regimens are above the median iDIS of all 64 regimens. Two regimens (R23.5E45dpw2 and R23.5E90dpw1) with synergistic iDIS measurements showed slow sterilization times, as they were dosed less frequently than a day.
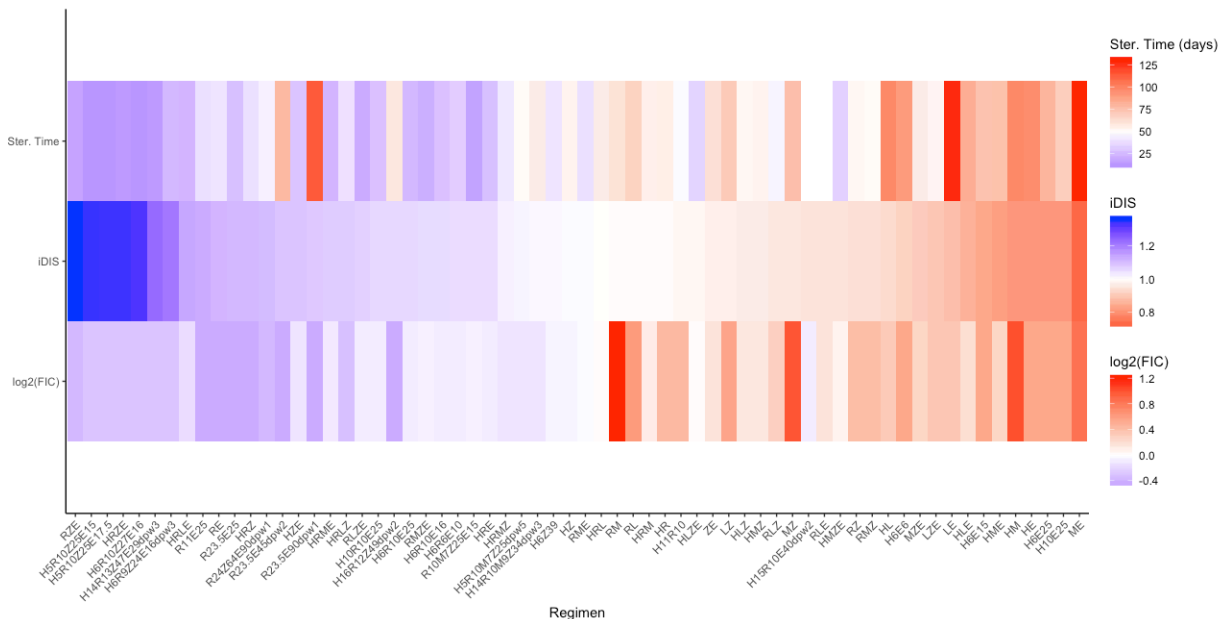
Figure 3.5 Heat map capturing three metrics for 64 different regimens.
The list of regimens is ordered by decreasing predicted iDIS (middle row). For each regimen, the $\log_2$(FIC) value (bottom row) and the average predicted granuloma sterilization time (top row) are also represented. For predicted iDIS and FIC, blue represents synergy, white represents additivity, and red represents antagonism. For sterilization time, blue represents shorter sterilization times and red represents longer.

3.4.3 INDIGO-MTB - GranSim regimen rankings are correlated with clinical rankings
To explore how our predictions of regimen efficacy compare to clinical results, we

compare our INDIGO-MTB - *GranSim* treatment simulations to results from TB drug

clinical trials. Drawing from the meta-analysis of phase II trials presented in Bonnet *et al*

(2017), we selected all regimens that reported sputum culture conversion in solid media

[45]. The efficacy metric presented for Phase IIb trials is the percent of patients with

negative sputum culture after 8 weeks of therapy. Since our simulations predict

treatment outcomes at the granuloma scale, we estimated how sterilization at the

granuloma level relates to host-level culture conversion. Figure B.3 (Appendix B) shows

the comparison of the upper and lower bound estimates for percent sputum conversion

from our simulation to clinical trial results for 26 regimens (Methods). For most

regimens, estimates of sterilization percentage compare closely to clinically measured

culture conversion. In general, *INDIGO-MTB - GranSim* simulations appear to

overpredict the rates of sterilization and most incorrect predictions fall into this category

(Figure B.3, Appendix B). This observed overprediction is likely due to the simplification

of predicting sterilization at the granuloma scale that does not include the full spectrum

of complex granuloma lesions, failed adherence to regimens, and other factors that

complicate TB treatment.

We next validate our simulation results by comparing the ranking of the efficacy of each

of the regimens with the corresponding ranking of the efficacy from clinical trials (Figure

3.6). The clinical rank is determined by ranking each regimen by the pooled culture

conversion after 8 weeks, so that a ranking of 1 is the regimen with the lowest culture

conversion. The simulation rank is determined by percentage of granulomas sterilized

after 8 weeks. We used the Spearman ranked correlation coefficient, weighted by the

number of patients in each pooled regimen result, and found a significantly strong

correlation between simulations and clinical trials (R = 0.72).
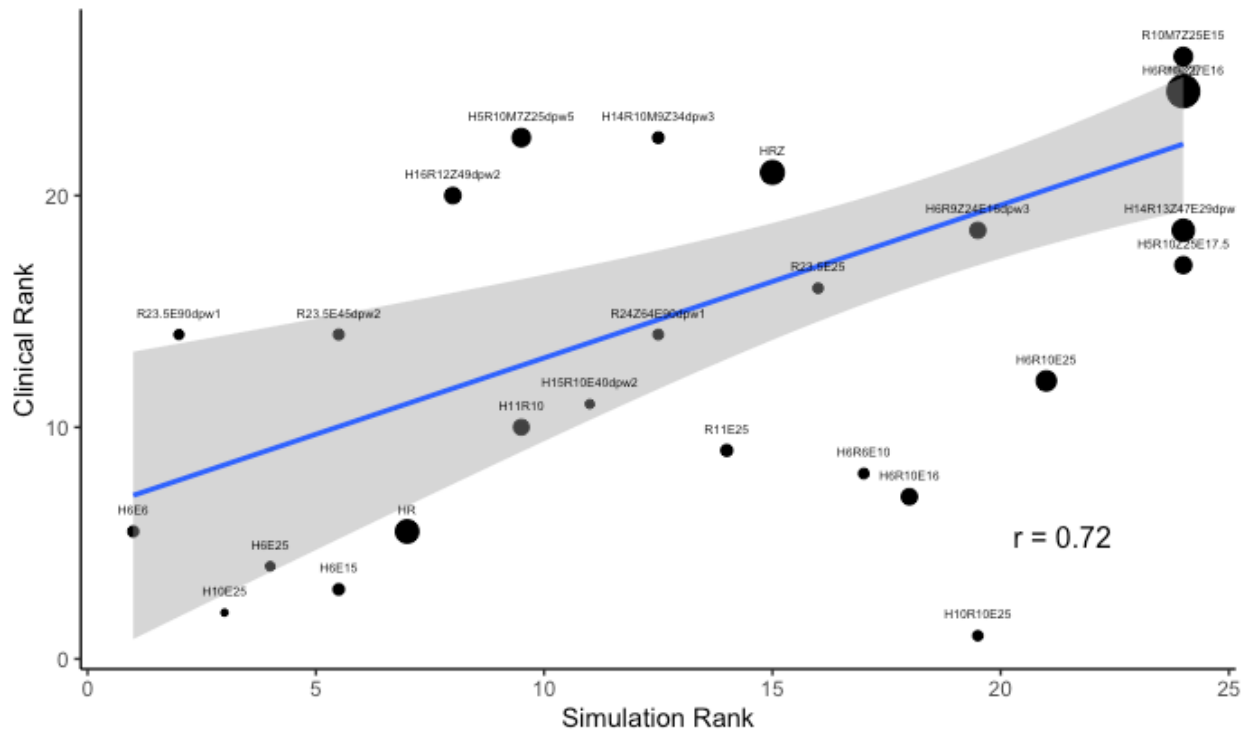
Figure 3.6 INDIGO-MTB-GranSim compared with clinical data.
Comparison and validation of treatment simulations with clinical trial results for 26 different regimens compiled in Bonnet *et al.* (2017) [45]. Predictions from *GranSim* simulations for 26 drug regimens correlate with clinical outcomes. The simulation rank, ranked by percentage of sterilized granulomas after 8 weeks, and clinical rank, ranked by clinically reported culture conversion, have a weighted correlation of 0.72, weighted by the number of patients treated with each regimen.

Recent phase III clinical trials have investigated the impact of introducing fluoroquinolones into treatment regimens to treat drug-susceptible TB, some with the additional intent of shortening treatment time from six months to four. Many of these trials have failed to show improvement in TB treatment, and often led to higher rates of unfavorable outcomes at the trial's endpoints [46–48]. These trends are reflected in our analysis of the drug interactions for various drug combinations. The control regimen, HRZE, is strongly synergistic as measured by iDIS, and we predict short average sterilization times (14 days, Figure 3.4). In contrast, fluoroquinolone containing regimens, such as HRMZ and RMZE, are closer to additive, and are predicted to have longer sterilization times of 41 and 21 days respectively. These trends indicate that our simulation predictions are consistent with phase III clinical trial observations. Thus INDIGO-MTB - *GranSim* simulations provide strong predictive measures of clinical outcome for different regimens.

Both iDIS and INDIGO-MTB FIC predictions for these regimens are also significantly correlated with their clinical ranking (Figure B.3, Appendix B). These simulated results are consistent with the correlation observed in a prior study between INDIGO-MTB FIC scores and percentage of patients with negative culture after treatment from 57 randomized clinical trials [8]. Based on these results, both interaction measurements have the potential to help predict the clinical efficacy of drug combination regimens.

The FIC value is one measure of drug interactions *in vitro*; however, there are many factors that impact regimen efficacy *in vivo* that FIC alone does not capture. Measuring the iDIS can incorporate changes in concentration due to PK variability, changes to dosing regimens, and heterogeneous antibiotic concentrations due to granuloma structure and the varying environments where bacteria reside impact the degree to which the drug interactions impact killing rates. It also includes effects of the immune responses occurring with granulomas.

3.4.4 Spatial variation in drug concentration influences iDIS in granulomas
Nonuniform drug distributions within granulomas arise due to barriers to diffusion that the cellular structure of granulomas creates [20–22,30]. The spatial variation in antibiotic concentrations within a granuloma leads to variations in local effective concentrations, and ultimately antibiotic killing rates and iDIS. The free drug concentrations available to induce bactericidal activity against Mtb are also influenced by binding to extracellular matrix as well as partitioning into macrophages [40]. Hence, we next focused on the contribution of the drug spatial variation to iDIS.

Figure 3.7 shows the spatial variation for effective drug concentrations normalized to the regimen's non-replicating Mtb C_{50} parameter and iDIS for four of the regimens simulated: HRZE, RE, HE and RM. These regimens demonstrate a mix of synergistic and antagonistic combinations that also exhibit both strong and weak iDIS values. For the two synergistic combinations, HRZE and RE, effective concentrations are lower within a granuloma than just outside it, lowering the killing rate constants. Because most

non-replicating Mtb are found within the hypoxic caseum which is typically located toward the center of the granuloma, the effective concentrations in those caseated regions and inside the granuloma are the concentrations that are relevant to predicting sterilization rates. However, lower effective concentrations inside granulomas and caseated regions can also result in higher iDIS (Figure 3.7). Because iDIS tends to be higher within granulomas where Mtb reside, this may contribute to synergistic combinations performing better than antagonistic combinations of similar effective concentrations.
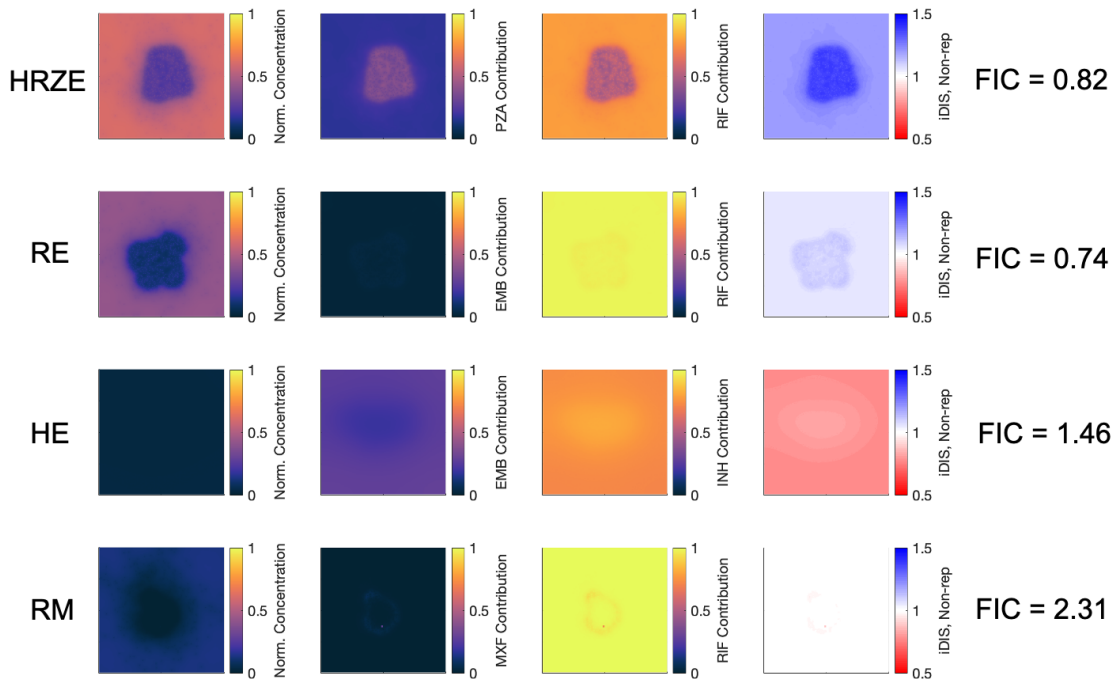
Figure 3.7 Contribution of individual antibiotics to the *in vivo* drug interaction score (iDIS).
Values of iDIS are associated with proportion of each antibiotic's contribution to the effective concentration. Four different regimens are shown: HRZE (first row), RE (second row), HE (third row), and RM (fourth row). Heat maps show the effective concentration normalized to the C_{50} for non-replicating Mtb of the combination (first column) and the fraction of each antibiotic's contribution to the effective concentration (second and third columns). The calculated iDIS value for non-replicating Mtb is shown in the fourth column, with the color bar representing the iDIS value with blue representing a synergy, white representing additivity, and red representing antagonism. All heat maps reflect conditions 6 hours after dosage with each antibiotic in the relevant regimen.

An additional aspect that influences the iDIS is the relative contribution of each antibiotic in the combinations (Figure 3.7, columns 2 and 3). Antibiotic combinations that contribute more equally to the effective concentration deviate more from additivity than combinations of antibiotic concentrations in which contributions are uneven (i.e. when

one antibiotic has a much higher adjusted concentration than the other antibiotics). Although RE has a more synergistic FIC than HRZE, the iDIS against non-replicating Mtb for HRZE is higher than RE, and HRZE has better efficacy than RE. This is partially due to R and Z contributing to the effective concentration in the granuloma evenly (R ~50% contribution, Z ~40% contribution). The contributions from R and E in RE, however, are more disproportionate, with >90% of the effective concentration due to R and <10% of the effective concentration from E.

A similar situation occurs with the two antagonistic combinations HE and RM. Although RM is predicted to be strongly antagonistic, its efficacy is still average compared across all regimens tested. HE, on the other hand, has a less antagonistic FIC, but performs more poorly than RM. When looking at both antibiotic contributions for these two regimens and the iDIS against non-replicating Mtb, we see that H accounts for ~75% of the effective concentration and E accounts for ~25%. Although not equal contributions, this still allows for an antagonistic interaction to occur. With the RM combination, R accounts for almost all of the contribution to the effective concentration because its levels are higher relative to its own C_{50}, resulting in almost no antagonistic interaction to occur with M, despite the high FIC. For antagonistic combinations, uneven contributions from the different antibiotics in the combination can mitigate the effect of the antagonistic interaction.

Due to this dependence on drug concentrations, the predicted iDIS varies for different doses and regimens of the same drug combination (Figure B.4, Appendix B). In contrast, the FIC interaction score is fixed for a combination irrespective of the dosage. As doses vary *in vivo*, the strength of the synergistic or antagonistic interactions can either increase or decrease, depending on the specific combination of antibiotics. One common trend is less frequent dosing tends to decrease the interaction strength, which we observe for both the HRZE and RE combinations.

3.4.5 Plasma clearance rates correlate with in vivo drug interaction score
Even for a given simulated granuloma and drug regimen, antibiotic concentrations can vary due to host-to-host PK variability [32]. This can also result in changes in iDIS. We picked four different regimens, ranging from synergistic to antagonistic (HRZE, RE, HE, RM) to exhaustively explore the impact of various PK parameters. The plasma clearance rate constant for many of the antibiotics in these regimens is significantly correlated with predicted iDIS, particularly the clearance rate constants for R, E and M (Table 3.1). A more detailed analysis of correlations between plasma PK parameters and iDIS is shown in Table B.3 (Appendix B). The R clearance rate constant is strongly correlated with iDIS, with coefficients between 0.8 and 0.9, depending on the regimen. The correlation coefficients for the clearance rate constant for R are positive for synergistic combinations (HRZE, RE), and negative for antagonistic combinations (RM). Because iDIS values that deviate further from 1 imply a stronger interaction, this means that faster clearance rates for R tend to increase the interaction strength. The opposite is true for the clearance rate constant of E. The correlation coefficient between the clearance rate constant for E and predicted iDIS is negative in synergistic combinations (HRZE, RE), and positive in the antagonistic combination (HE). While this may seem counterintuitive, it supports the idea that the iDIS value is dependent on relative in vivo drug concentrations. Faster clearance rates generally result in lower concentrations in plasma, and consequently lower concentrations in the granuloma. Because R tends to contribute more to effective concentrations than other antibiotics, increasing the clearance rates for R will strengthen the interaction by decreasing R concentration and allow for more even contributions. For E, whose contribution to effective concentration tends to be lower, increasing clearance rates result in lower E concentrations and contributions, and scenarios of even more lopsided contributions and less interaction. Relative drug concentrations inside the granuloma affect the strength of drug interactions, and these strong correlations indicate that interactions may be stronger or weaker for certain combinations depending on an individual's PK [32].

Table 3.1 Significant antibiotic clearance rate constants in determining iDIS
The relationship between clearance rate constants for different antibiotics is correlated with iDIS with non-replicating Mtb during the first dose of therapy. Table shows PRCC values relating the clearance rate constants to the predicted iDIS for the regimens HRZE, RE, HE and RM. The values shown represent PRCC values that are significant with $p < 0.01$.

Regimen	PRCC Values for predicted iDIS		
	R clearance	E clearance	M clearance
HRZE	0.89	-0.56	N/A
RE	0.90	-0.92	N/A
HE	N/A	0.88	N/A
RM	-0.83	N/A	0.99

3.5 Discussion

The need for multiple drug regimens to treat TB raises a number of issues that can be capitalized on to advance treatment for the world's worst killer by disease. In particular, understanding the role of interactions occurring in either a synergistic or antagonistic fashion between anti-TB antibiotics *in vivo* may provide a more rational approach to choosing novel combinations that have greater clinical efficacy. However, measuring drug interactions *in vivo* is challenging due to the limited throughput, cost, and time involved in testing drugs in model organisms. In this study, we introduce a computational pipeline that can simulate *in vivo* interactions by using datasets derived from individual drug-response transcriptomes and PK/PD, thereby greatly reducing cost and time. Our approach integrates interaction scores of combinations of antibiotics into a computational model that simulates drug delivery into the lung, spatial concentrations of drugs and pharmacodynamic effects within TB granulomas.

To evaluate drug regimens, we introduce a new metric called the *in vivo* drug interaction score (iDIS) that is dynamic and unique for each mycobacterium based on its location and metabolic state (i.e. replicating/non-replicating) within a granuloma. Unlike the *in vitro* drug interaction scores derived from checkerboard assays and INDIGO-MTB, which are fixed for given drug combinations, the *in vivo* score can provide a more nuanced impact of drug interactions on pathogen clearance. This allowed us to compare various drug regimens and rank them based on their *in vivo* interactions. We

found that our ranking of regimens is highly concordant with clinically observed efficacy of various drug combinations [45].

When simulating all regimens considered in this study, the FIC alone does correlate with the simulated and predicted outcomes from our model. However, there are a handful of regimens that do not fit the trend. Measuring the iDIS, which evaluates the relative increase or decrease in killing rate due to the interaction within the complex granuloma environment, provides a complementary measure of regimen outcome. This is because the effect that drug interactions have on killing rate constants is dependent on the balance of contributions from each single antibiotic. Combinations with highly synergistic or antagonistic FIC values may be closer to additive if only one antibiotic is present in sufficient quantities within a granuloma.

Our analysis of various drug regimens revealed ways of amplifying synergy as well mechanisms to mitigate antagonism *in vivo*. We found that some combinations with *in vitro* antagonism perform well clinically due to the distinct spatial distribution of the underlying drugs. Antagonistic interactions can be mitigated if the drugs have uneven distributions and effective concentrations or through less frequent dosing. Overall, we find that combinations with strong *in vitro* synergy remain synergistic or additive *in vivo*. Hence screening for synergy *in vitro* can be a useful strategy for identifying regimens with strong *in vivo* activity. In a minority of cases, this synergy may not be achieved *in vivo;* nevertheless, synergistic combinations generally outperform antagonistic regimens.

As part of this study, we wanted to determine which combinations of antibiotics are predicted to have strong synergy and antagonism, as well as which combinations are predicted to have high efficacy. We screened 64 combinations and regimens of front-line regimens (HRZE) along with M and L. The clinically used HRZE regimen does outperform other screened combinations, which highlights the need for new drugs to achieve the aim of improving TB treatment. Based on the INDIGO-MTB model, we previously identified drug combinations involving new TB drugs such as bedaquiline that

have better synergy than HRZE. Given the concordance between INDIGO-MTB FIC and various clinical metrics observed in this study, the synergistic combinations identified by INDIGO-MTB may be promising leads for further optimization using *GranSim* for reducing treatment time [16].

A limitation to our computational model is that the same FIC value is applied to all Mtb within a simulation, regardless of its environment or metabolic state. It is likely that the strength of a given interaction, or even whether it is synergistic or antagonistic, is dependent on the bacterium's microenvironment in the granuloma [50,51]. Additionally, these simulations represent treatment of primary granulomas in TB disease, and do not necessarily reflect the true and enormous complexity of granuloma lesions that occur during TB disease. Further, as the simulations are at the granuloma scale, relating the outcomes measured by the simulation to clinical outcomes is difficult. The final limitation is that we only considered combinations of six different antibiotics. There are many other antibiotics in use or in development for use to treat TB. Expanding our ability to accurately simulate the PK/PD of additional antibiotics will greatly increase our ability to answer how important drug interactions are in determining regimen efficacy.

In sum, our study addresses an important gap in current methods for identifying promising drug combinations for TB treatment by presenting a new pipeline for evaluating interactions between drugs *in vivo*. This pipeline provides an additional metric with which to evaluate novel combinations of antibiotics, explain mechanisms of failed regimens, and assist in optimization regimens as we expand our list of potential antibiotics.

3.6 References

1. Dheda K, Barry CE, Maartens G. Tuberculosis. Lancet. 2016;387: 1211–1226. doi:10.1016/S0140-6736(15)00151-8
2. Global tuberculosis report 2019. 2019.
3. Zumla A, Chakaya J, Centis R, D'Ambrosio L, Mwaba P, Bates M, et al. Tuberculosis treatment and management-an update on treatment regimens, trials, new drugs, and adjunct therapies. Lancet Respir Med. 2015;3: 220–234. doi:10.1016/S2213-2600(15)00063-6
4. Mdluli K, Kaneko T, Upton A. The Tuberculosis Drug Discovery and Development Pipeline and Emerging Drug Targets. Cold Spring Harb Perspect Med. 2015;5: a021154. doi:10.1101/cshperspect.a021154
5. Falzon D, Schünemann HJ, Harausz E, González-Angulo L, Lienhardt C, Jaramillo E, et al. World Health Organization treatment guidelines for drug-resistant tuberculosis, 2016 update. Eur Respir J. 2017;49. doi:10.1183/13993003.02308-2016
6. Conradie F, Diacon AH, Ngubane N, Howell P, Everitt D, Crook AM, et al. Treatment of highly drug-resistant pulmonary tuberculosis. N Engl J Med. 2020;382: 893–902. doi:10.1056/NEJMoa1901814
7. Xu J, Li SY, Almeida D V., Tasneen R, Barnes-Boyle K, Converse PJ, et al. Contribution of pretomanid to novel regimens containing bedaquiline with either linezolid or moxifloxacin and pyrazinamide in murine models of tuberculosis. Antimicrob Agents Chemother. 2019;63: 1–14. doi:10.1128/AAC.00021-19
8. Ma S, Jaipalli S, Larkins-Ford J, Lohmiller J, Aldridge BB, Sherman DR, et al. Transcriptomic signatures predict regulators of drug synergy and clinical regimen efficacy against tuberculosis. MBio. 2019;10: 1–16. doi:10.1128/mBio.02627-19
9. Berenbaum MC. A method for testing for synergy with any number of agents. J Infect Dis. 1978;137: 122–130. doi:10.1093/infdis/137.2.122
10. Berenbaum MC. What is Synergy? Pharmacol Rev. 1989;1989: 93–141.
11. Michel JB, Yeh PJ, Chait R, Moellering RC, Kishony R. Drug interactions modulate the potential for evolution of resistance. PNAS. 2008;105: 14918–14923. doi:10.1073/pnas.0800944105
12. Chandrasekaran S, Cokol-Cakmak M, Sahin N, Kazan H, Yilancioglu K, Collins JJ, et al. Chemogenomics and orthology-based design of antibiotic combination therapies. Mol Syst Biol. 2016;12: 872. doi:10.15252/msb.20156777
13. Silva A, Lee B-Y, Clemens DL, Kee T, Ding X, Ho C-M, et al. Output-driven feedback system control platform optimizes combinatorial therapy of tuberculosis using a macrophage cell culture model. PNAS. 2016;113: 2172–2179. doi:10.1073/pnas.1600812113
14. Cokol M, Kuru N, Bicak E, Larkins-Ford J, Aldridge BB. Efficient measurement and factorization of high-order drug interactions in Mycobacterium tuberculosis. Sci Adv. 2017;3: e1701881. doi:10.1126/sciadv.1701881
15. Yeh P, Tschumi AI, Kishony R. Functional classification of drugs by properties of their pairwise interactions. Nat Genet. 2006;38: 489–494. doi:10.1038/ng1755
16. Cicchese JM, Pienaar E, Kirschner DE, Linderman JJ. Applying Optimization Algorithms to Tuberculosis Antibiotic Treatment Regimens. Cell Mol Bioeng. 2017;10: 523–535. doi:10.1007/s12195-017-0507-6

17. Fonseca KL, Rodrigues PNS, Olsson IAS, Saraiva M. Experimental study of tuberculosis: From animal models to complex cell systems and organoids. PLoS Pathog. 2017;13: 1–13. doi:10.1371/journal.ppat.1006421

18. Lin PL, Rodgers M, Smith L, Bigbee M, Myers A, Bigbee C, et al. Quantitative comparison of active and latent tuberculosis in the cynomolgus macaque model. Infect Immun. 2009;77: 4631–4642. doi:10.1128/IAI.00592-09

19. Dartois V. The path of anti-tuberculosis drugs: from blood to lesions to mycobacterial cells. Nat Rev Microbiol. 2014;12: 159–167. doi:10.1038/nrmicro3200

20. Prideaux B, Via LE, Zimmerman MD, Eum S, Sarathy J, O'Brien P, et al. The association between sterilizing activity and drug distribution into tuberculosis lesions. Nat Med. 2015;21: 1223–7. doi:10.1038/nm.3937

21. Sarathy JP, Zuccotto F, Hsinpin H, Sandberg L, Via LE, Marriner GA, et al. Prediction of Drug Penetration in Tuberculosis Lesions. ACS Infect Dis. 2016;2: 552–563. doi:10.1021/acsinfecdis.6b00051

22. Pienaar E, Cilfone NA, Lin PL, Dartois V, Mattila JT, Butler JR, et al. A computational tool integrating host immunity with antibiotic dynamics to study tuberculosis treatment. J Theor Biol. 2015;367: 166–179. doi:10.1016/j.jtbi.2014.11.021

23. Sarathy JP, Via LE, Weiner D, Blanc L, Boshoff H, Eugenin EA, et al. Extreme drug tolerance of mycobacterium tuberculosis in Caseum. Antimicrob Agents Chemother. 2018;62: 1–11. doi:10.1128/AAC.02266-17

24. Bowness R, Chaplain MAJ, Powathil GG, Gillespie SH. Modelling the effects of bacterial cell state and spatial location on tuberculosis treatment: Insights from a hybrid multiscale cellular automaton model. J Theor Biol. 2018;446: 87–100. doi:10.1016/j.jtbi.2018.03.006

25. Chandrasekaran S. Predicting Drug Interactions From Chemogenomics Using INDIGO. Systems Chemical Biology Methods in Molecular Biology. 2019. pp. 219–231.

26. Segovia-Juarez JL, Ganguli S, Kirschner D. Identifying control mechanisms of granuloma formation during M. tuberculosis infection using an agent-based model. J Theor Biol. 2004;231: 357–376. doi:10.1016/j.jtbi.2004.06.031

27. Cilfone NA, Perry CR, Kirschner DE, Linderman JJ. Multi-scale modeling predicts a balance of tumor necrosis factor-a and interleukin-10 controls the granuloma environment during Mycobacterium truberculosis infection. PLoS One. 2013;8: e68680. doi:10.1371/journal.pone.0068680

28. Ray JCJ, Flynn JL, Kirschner DE. Synergy between individual TNF-dependent functions determines granuloma performance for controlling Mycobacterium tuberculosis infection. J Immunol. 2009;812: 3706–37017. doi:10.4049/jimmunol.0802297

29. Fallahi-Sichani M, El-Kebir M, Marino S, Kirschner DE, Linderman JJ. Multiscale computational modeling reveals a critical role for TNF-α receptor 1 dynamics in tuberculosis granuloma formation. J Immunol. 2011;186: 3472–3483. doi:10.4049/jimmunol.1003299

30. Pienaar E, Sarathy J, Prideaux B, Dietzold J, Dartois V, Kirschner DE, et al. Comparing efficacies of moxifloxacin, levofloxacin and gatifloxacin in tuberculosis

granulomas using a multi-scale systems pharmacology approach. PLOS Comput Biol. 2017;13. doi:10.1371/journal.pcbi.1005650

31. Pienaar E, Dartois V, Linderman JJ, Kirschner DE. In silico evaluation and exploration of antibiotic tuberculosis treatment regimens. BMC Syst Biol. 2015;9: 1–12. doi:10.1186/s12918-015-0221-8

32. Cicchese JM, Dartois V, Kirschner DE, Linderman JJ. Both Pharmacokinetic Variability and Granuloma Heterogeneity Impact the Ability of the First-Line Antibiotics to Sterilize Tuberculosis Granulomas. Front Pharmacol. 2020;11: 1–15. doi:10.3389/fphar.2020.00333

33. Strydom N, Gupta S V, Fox WS, Via LE, Bang H, Lee M, et al. Tuberculosis drugs' distribution and emergence of resistance in patient's lung lesions : A mechanistic model and tool for regimen and dose optimization. PLoS Med. 2019;16. doi:10.1371/journal.pmed.1002773

34. Aljayyoussi G, Jenkins VA, Sharma R, Ardrey A, Donnellan S, Ward SA, et al. Pharmacokinetic-Pharmacodynamic modelling of intracellular Mycobacterium tuberculosis growth and kill rates is predictive of clinical treatment duration. Sci Rep. 2017;7: 1–11. doi:10.1038/s41598-017-00529-6

35. Pasipanodya JG, McIlleron H, Burger A, Wash PA, Smith P, Gumbo T. Serum drug concentrations predictive of pulmonary tuberculosis outcomes. J Infect Dis. 2013;208: 1464–1473. doi:10.1093/infdis/jit352

36. GranSim. [cited 21 Aug 2020]. Available: http://malthus.micro.med.umich.edu/GranSim/

37. Pienaar E, Matern WM, Linderman JJ, Bader JS, Kirschner DE. Multiscale Model of Mycobacterium tuberculosis Infection Maps Metabolite and Gene Perturbations to Granuloma Sterilization. Infect Immun. 2016;84: 1650–1669. doi:10.1128/IAI.01438-15.Editor

38. Cilfone NA, Ford CB, Marino S, Mattila JT, Gideon HP, Flynn JL, et al. Computational modeling predicts IL-10 control of lesion sterilization by balancing early host immunity-mediated antimicrobial responses with caseation during mycobacterium tuberculosis infection. J Immunol. 2015;194: 664–77. doi:10.4049/jimmunol.1400734

39. Jonsson S, Davidse A, Wilkins J, Van Der Walt JS, Simonsson USH, Karlsson MO, et al. Population pharmacokinetics of ethambutol in South African tuberculosis patients. Antimicrob Agents Chemother. 2011;55: 4230–4237. doi:10.1128/AAC.00274-11

40. Zimmerman M, Lestner J, Prideaux B, O'Brien P, Dias-freedman I, Chen C, et al. Ethambutol Partitioning in Tuberculous Pulmonary Lesions Explains Its Clinical Efficacy. Antimicrob Agents Chemother. 2017;61: 1–12.

41. Greco WR, Bravo G, Parsons JC. The Search for Synergy: A Critical Review from a Response Surface Perspective. Pharmacol Rev. 1995;47: 331–385.

42. Hall MJ, Middleton RF, Westmacott D. The fractional inhibitory concentration (FIC) index as a measure of synergy. J Antimicrob Chemother. 1983;11: 427–433. doi:10.1093/jac/11.5.427

43. McKay AMD, Beckman RJ, Conover WJ. A Comparison of Three Methods for Selecting Values of Input Variables in the Analysis of Output from a Computer Code. Technometrics. 1979;21: 239–245. doi:doi:10.2307/1268522

44.	Marino S, Hogue IB, Ray CJ, Kirschner DE. A methodology for performing global uncertainty and sensitivity analysis in systems biology. J Theor Biol. 2008;254: 178–196. doi:10.1016/j.jtbi.2008.04.011

45.	Bonnett LJ, Ken-dror G, Koh GCKW, Davies GR. Comparing the Efficacy of Drug Regimens for Pulmonary Tuberculosis: Meta-analysis of Endpoints in Early-Phase Clinical Trials. Clin Infect Dis. 2017;65: 46–54. doi:10.1093/cid/cix247

46.	Gillespie SH, Crook AM, McHugh TD, Mendel CM, Meredith SK, Murray SR, et al. Four-Month Moxifloxacin-Based Regimens for Drug-Sensitive Tuberculosis. N Engl J Med. 2014;371: 1577–1587. doi:10.1056/NEJMoa1407426

47.	Jindani A, Harrison TS, Nunn AJ, Phillips PPJ, Churchyard GJ, Charalambous S, et al. High-Dose Rifapentine with Moxifloxacin for Pulmonary Tuberculosis. N Engl J Med. 2014;371: 1599–1608. doi:10.1056/NEJMoa1314210

48.	Pranger AD, van der Werf TS, Kosterink JGW, Alffenaar JWC. The Role of Fluoroquinolones in the Treatment of Tuberculosis in 2019. Drugs. 2019;79: 161–171. doi:10.1007/s40265-018-1043-y

49.	Renardy M, Hult C, Evans S, Linderman JJ, Kirschner DE. Global sensitivity analysis of biological multiscale models. Curr Opin Biomed Eng. 2019;11: 109–116. doi:10.1016/j.cobme.2019.09.012

50.	Cokol M, Li C, Chandrasekaran S. Chemogenomic model identifies synergistic drug combinations robust to the pathogen microenvironment. PLoS Comput Biol. 2018;14: 1–24. doi:10.1371/journal.pcbi.1006677

51.	Zimmermann M, Kogadeeva M, Gengenbacher M, McEwen G, Mollenkopf H-J, Zamboni N, et al. Integration of Metabolomics and Transcriptomics Reveals a Complex Diet of Mycobacterium tuberculosis during. mSystems. 2017;2: 1–18.

Chapter 4 Applying Optimization Algorithms to Tuberculosis Antibiotic Treatment Regimens

This chapter is a published work:

4.1 Abstract

Introduction: Tuberculosis (TB), one of the most common infectious diseases, requires treatment with multiple antibiotics taken over at least 6 months. This long treatment often results in poor patient-adherence, which can lead to the emergence of multi-drug resistant TB. New antibiotic treatment strategies are sorely needed. New antibiotics are being developed or repurposed to treat TB, but as there are numerous potential antibiotics, dosing sizes and potential schedules, the regimen design space for new treatments is too large to search exhaustively. Here we propose a method that combines an agent-based multi-scale model capturing TB granuloma formation with algorithms for mathematical optimization to identify optimal TB treatment regimens.

Methods: We define two different single-antibiotic treatments to compare the efficiency and accuracy in predicting optimal treatment regimens of two optimization algorithms: genetic algorithms (GA) and surrogate-assisted optimization through radial basis function (RBF) networks. We also illustrate the use of RBF networks to optimize double-antibiotic treatments.

Results: We found that while GAs can locate optimal treatment regimens more accurately, RBF networks provide a more practical strategy to TB treatment optimization with fewer simulations, and successfully estimated optimal double-antibiotic treatment regimens.

Conclusions: Our results indicate surrogate-assisted optimization can locate optimal TB treatment regimens from a larger set of antibiotics, doses and schedules, and could be applied to solve optimization problems in other areas of research using systems biology approaches. Our findings have important implications for the treatment of diseases like TB that have lengthy protocols or for any disease that requires multiple drugs.

4.2 Introduction

Tuberculosis (TB) is a disease caused by infection with *Mycobacterium tuberculosis*, and an estimated one fourth of the world's population has a latent *M. tuberculosis* infection [1]. In 2015, TB was responsible for 1.4 million deaths [2]. The typical treatment of drug-susceptible TB is a lengthy antibiotic regimen of at least six months beginning with four antibiotics for two months, namely isoniazid (INH), rifampin (RIF), ethambutol, and pyrazinamide. This regimen is followed by a continuation phase of two antibiotics (INH and RIF) for an additional four months [3]. Although largely considered a successful treatment for drug-susceptible TB, poor patient-adherence and the emergence of multi-drug-resistant TB indicate a need for better antibiotic treatments [3,4]. Programs such as DOT (directly observed treatment) have been put into place to track drug compliance, but this is costly and untenable for many TB patients world-wide [5,6]. Additional antibiotics are currently being developed or repurposed to treat TB [7,8]. Comparing treatments can involve large meta-analysis studies, and head-to-head comparisons of alternative protocols are often lacking [9,10]. Overall, the regimen design space for new antibiotic treatments, including combination treatments, is enormous and impossible to thoroughly examine in either an animal model or clinical setting (Figure 4.1). Identifying better antibiotic treatments (e.g. shorter, less toxic, cheaper, and/or more efficacious treatments) presents a challenging optimization problem of finding the best combination and regimen of antibiotics.

Regimen design space (RDS)

Treatment segments (M)	2
Number of drugs (c)	10
Drugs per segment (n)	4
Dose (D, mg/kg)	5
Frequency (F, week^{-1})	7

Number of possible regimens:

$$RDS = \left(\binom{c}{n} (D \times F)^n \right)^M = 9.9 \times 10^{16}$$

Figure 4.1 Estimating the size of the TB antibiotic regimen design space (RDS).
The number of potential antibiotic treatment regimens can be estimated by assuming values for the following variables: the number of treatment segments (M), such as an initial, intensive and continuation phase; number of antibiotics available for use (c); maximum number of antibiotics in each treatment segment (n); and available dose levels (D). Frequency (F) refers to the different possible dosing frequencies to be tested, e.g. once weekly, daily, etc.

There has been some effort to optimize TB treatment and clinical pharmacology of TB regimens [11–13]. In this work, we seek to formalize locating better antibiotic treatment regimens as an optimization problem. The goal of our treatment optimization problem is to identify the region of the regimen design space (combinations of antibiotics and treatment variable ranges) that contain optimal treatment protocols, rather than identify a single, optimal treatment with high precision. Optimal treatment variables (such as dose size or dosing frequency) identified with high precision would not necessarily translate to a clinical treatment, because clinical doses and dosing frequencies must be realistic to implement (e.g. using available dosages).

Systems biology has been used to study a wide array of topics [14] including systems pharmacology [15–17], vascular and muscle growth [18], or cancer development and therapy [19–21]. Computational modeling and systems biology approaches can help integrate large sets of data and provide additional biological insights, e.g. by using models to predict optimal conditions or to control model behavior [22–24]. As models that describe biological phenomena grow more complicated, there is a need for the proper tools to obtain the most out of these models.

In this work, we ask whether computational modeling of *M. tuberculosis* infection and antibiotic treatment can be used as an efficient strategy to identify better antibiotic treatment regimens. We have developed a hybrid, multi-scale model of granuloma formation to predict antibiotic efficacy [25,26]. Granulomas, regions of infected and inflamed lung tissue, form in response to *M. tuberculosis* lung infection. We simulate the dynamics of granuloma formation and function in the framework of a hybrid, multi-scale agent-based model [27–29]. These dynamics are crucial to understanding TB antibiotic efficacy, as the structure of granulomas influences antibiotic exposure to bacterial populations [26,30,31]. Although our model can assist in screening new antibiotic treatments, the computational complexity and number of granuloma simulations required to test all potential treatment regimens (Figure 4.1) prevents us from testing every possibility in the regimen design space. However, combining our granuloma model with optimization algorithms could provide a viable way to narrow the design space and guide animal and clinical trials.

A diverse set of optimization algorithms are applied in science, math and engineering [32,33]. Population-based algorithms, including the genetic algorithm (GA), can be used to solve optimization problems with objective functions that are functions of a computational model or simulation output [34]. GAs have been used to solve optimization problems in fields as varied as robotics, engineering design and pattern recognition, and cancer vaccination schedules in mice [32,35–38]. The GA utilizes ideas from natural selection to partially search a variable design space, and its framework allows for different ways to represent solutions as chromosomes, define objective functions, select parents and generate offspring [32]. The algorithm begins by generating a population of solutions and evaluating their objective function values. The best individuals from the population are selected to be parents, and a new population of solutions is generated through crossover operations between the parents and random mutations. New generations of solutions are generated until the algorithm converges on an optimum.

Optimization problems can also be solved through surrogate-assisted optimization, which generates a model to predict the value of an objective function throughout the

design space based on known objective function values. The surrogate model is then used to search for the optimal solution, which can be useful in situations where evaluating the objective function through experiments or running computational models is expensive or inefficient [39,40]. The surrogate model can be built through mathematical approximation or interpolation strategies, such as radial basis function (RBF) networks [41,42]. With this method, RBFs are used as interpolants between sample data points, so that a prediction of an unknown objective function can be expressed as a sum of all of the basis functions in the network. These RBF networks can be applied to efficiently predict the function response throughout the entire variable design space [41–43].

Here, we compare the application of GAs and RBF network surrogate models to optimize antibiotic treatment of TB. We rely on our published computational granuloma model to simulate the infection and immune response and a linked pharmacokinetic/pharmacodynamics (PK/PD) model to simulate drug treatment [25,26]. We first examine treatment with a single antibiotic to determine whether GAs or RBF network methods are better suited for treatment optimization. We then test the method of choice on the more complicated antibiotic optimization problem of two antibiotics administered simultaneously. Finally, we discuss barriers and approaches for solving higher dimensional problems (e.g. greater than two antibiotics) with these methods.

4.3 Model and Methods

4.3.1 Computational Granuloma Model
When *M. tuberculosis* infects lung tissue, an immune response occurs that leads to the formation of multiple granulomas, pockets of infected and inflamed tissue that are composed of various immune cells, dead cell debris and bacteria. These granulomas help prevent bacteria from spreading both by immunologically restraining and physically containing bacteria, but also present a physiological barrier to antibiotic diffusion [26,30,31]. We previously developed a computational model (*GranSim*) to study the formation of a granuloma by tracking immune cell and bacteria populations. Briefly, this multi-scale, hybrid model incorporates an agent-based model, ordinary differential equations (ODEs) and partial differential equations (PDEs) to describe and simulate

91

granuloma formation and function, and has been developed based on experimental data from *in vitro*, mouse and non-human primate models [27–29]. The agent-based model operates on the molecular and cellular levels and reads out at a tissue scale; individual immune cells (such as T cells and macrophages) are modeled as agents that are recruited and interact with each other according to a set of rules (see http://malthus.micro.med.umich.edu/GranSim/). ODEs and PDEs are used to describe molecular scale events, such as receptor-ligand binding or cytokine and antibiotic diffusion, which are solved through the implementation of efficient numerical solvers [44].

Previously, we incorporated antibiotics into *GranSim* to study how treatment with two first-line antibiotics, isoniazid (INH) and rifampin (RIF), affects sterilization of bacteria from a granuloma [25,26]. In the treatment model, concentrations of antibiotics in the plasma are described by a compartmental pharmacokinetic (PK) model that captures their distribution following oral administration [30]. A tissue PK model was used to determine intracellular and extracellular antibiotic concentrations in both uninfected lungs and granulomas, and antibiotic pharmacodynamic (PD) parameters determine killing of *M. tuberculosis* within granulomas. The PK and PD models are calibrated to experimental data from *M. tuberculosis* infected rabbits and nonhuman primates. Through both agent-based and PK model components, *GranSim* captures physiological organization and antibiotic distributions observed in granulomas, as shown in Figure 4.2.

To simulate antibiotic treatment, two variables per antibiotic are defined: the *dose size* and the *dosing frequency*. The dose size determines the amount of drug given at each dose, and the dosing frequency determines the number of doses per week. Each *GranSim* simulation provides time courses for all cellular and bacterial populations at the single granuloma scale. There are multiple additional model outputs from *GranSim* treatment simulations, but we will focus here on tracking the number of days of treatment required to kill all bacteria within a simulated granuloma, also termed "time to sterilization."
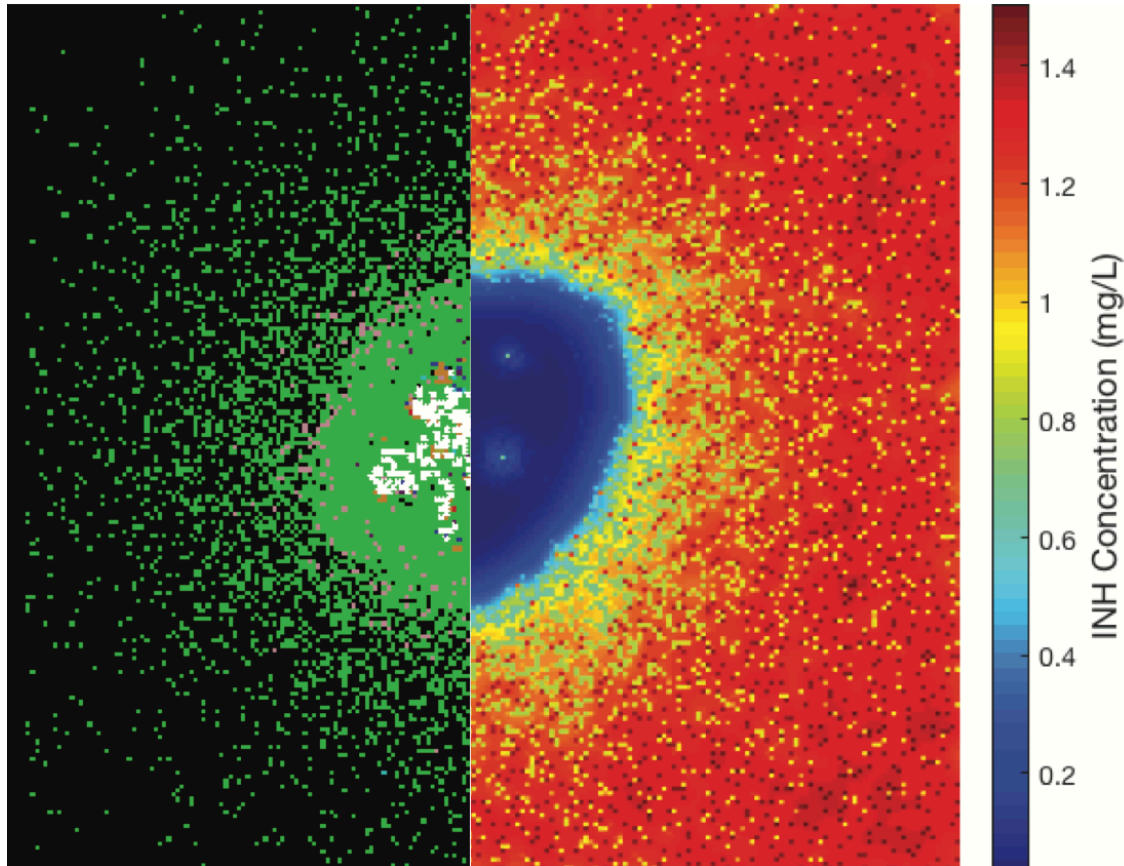
Figure 4.2 Visual representation of simulated granuloma.
The left side shows a snapshot of a granuloma simulation with each cell or compartment type: resting macrophages (green), activated macrophages (blue), infected macrophages (orange), chronically infected macrophages (red), caseation (white), and T-cells (purple, pink and light blue). The right shows unbound INH concentration on the simulation grid, with values ranging from about 0 to 1.5 mg/L (low concentration in blue, high concentration in red), illustrating the lack of antibiotic diffusion into granulomas. The entire snapshot represents an area of 16 mm^2 of lung tissue.

4.3.2 Defining the optimization problem

For optimizing TB antibiotic treatment regimens, the treatment variables and objective function must be defined. Figure 4.3 shows how the treatment variables can be expressed as a vector, with each element defined as one of the variables. In this definition, each antibiotic could be given at a different dose size and dosing frequency throughout the treatment. This vector could be lengthened to include different doses and frequencies over time to represent different treatment phases, such as the intensive and continuation phases of current TB treatments [3].

a. Treatment Variables

Regimen of n antibiotics ($2n$-dimensional)

Antibiotic 1 Dose

$$\boldsymbol{x} = \left\{ D_1, F_1, D_2, F_2 \dots D_N, F_N \right\}$$

Antibiotic 1 Dose Frequency

INH and RIF regimen (4-dimensional)

$$\boldsymbol{x} = \left\{ 10\ \text{mg/kg}, 7\ \text{wk}^{-1}, 15\ \text{mg/kg}, 2\ \text{wk}^{-1} \right\}$$

INH
10 mg/kg given
7 times per week

RIF
15 mg/kg given
2 times per week

b. Optimization Algorithm

Define treatment as variables and bounds

Define treatment objective function

Choose Algorithm

Genetic Algorithm

Optimization with RBF network

Initialize "population" of treatments

Evaluate "population" fitness

Select best treatments as "parents"

Generate new "population"

Select sample points

Generate RBF network

Converge on solution (optimal treatment)

Figure 4.3 Regimens as vectors and optimization algorithms
(a) The antibiotic treatment regimen can be expressed as a vector of individual variables. (b) Strategy to define and solve the TB antibiotic optimization problem. The process begins by defining the treatment variables and their bounds, and an objective function to evaluate treatment efficacy. Two optimization algorithms are considered: GA and surrogate-assisted optimization with an RBF network. Both optimization algorithms ultimately converge to an optimal treatment regimen prediction.

The goal of the objective function is to compare the efficacies of different antibiotic treatments. For a shorter treatment time, a goal could be to minimize the time to sterilization. However, only minimizing the time to sterilization would likely result in a regimen with the highest allowable dosage of antibiotic, and more adverse side effects in patients. With this in mind, our objective function should be one that balances finding a treatment with a fast time to sterilization while keeping dosages low. The objective function we define here takes as input the regimen of n potential antibiotics defined by

the input variable vector of length 2*n*. This objective function defines a surface in 2*n*-dimensional space where the global minimum of the surface corresponds to the "best" treatment regimen. The objective function value for a given antibiotic treatment is evaluated by simulating treatment of multiple granulomas with *GranSim*. The general form of the objective function we use is

$$f(x) = \frac{t(x)}{t_c} + \omega \frac{\sum_{i=1}^{n} D_i F_i}{\sum_{i=1}^{n} D_{i,max} F_{i,max}}$$

where $t(x)$ is the average time to sterilize a granuloma for a given antibiotic treatment x. Each treatment is simulated with multiple granulomas to account for host variability and model stochasticity. If a granuloma doesn't sterilize for a given treatment, the time to sterilization for that granuloma is set as the total simulated treatment length when calculating $t(x)$, as a way to inflate the average time to sterilization and increase the value objective function for a treatment that fails to sterilize multiple granulomas. D_i and F_i are the components of the input vector that correspond to the dose size and dose frequency, respectively, of antibiotic *i* (where *i* is the index for INH, RIF, or any other antibiotic). Both objective function terms are scaled to be of similar magnitude. The first term is divided by a characteristic time to sterilization, t_c, which is defined based on a typical average time to sterilization for a given treatment optimization problem. The second term is divided by the maximum amount of antibiotic based on the upper bounds of the treatment variables, $D_{i,max}$ and $F_{i,max}$. We seek to locate an antibiotic regimen that minimizes this objective function, implying that an optimal regimen is one that simulates a fast average time to sterilization, but also gives a relatively low dose of antibiotic. The dose-weight parameter, ω, can be adjusted to place varying emphasis on the amount of antibiotic given. To our knowledge, this is the first time an objective function has been defined for optimizing TB antibiotic regimens. In the future, there may be other important terms to consider including in the objective function. For example, it may be important to consider the percent of granulomas sterilized, whether there is excessive recruitment of immune cells, emergence of drug-resistance, and/or drug cost.

4.3.3 Genetic algorithm implementation
We used MATLAB's genetic algorithm (*ga*) function, and varied the settings for population size, generation stall limit, and a tolerance condition to test accuracy and convergence speed (MathWorks®, MATLAB 2015a). Figure 4.3 shows how GA can be implemented to solve treatment regimen optimization. Population size defines the number of individuals that are evaluated in each generation. The tolerance and generation stall limit are both stopping criteria. The generation stall limit defines the number of generations over which the average relative change in the best individual's fitness is calculated. If this average relative change is less than the tolerance, the algorithm stops searching. Two different settings are discussed here: default and relaxed settings. Default settings are MATLAB's built-in settings based on the type of problem and here define a population size and generation stall limit of 50, and a tolerance of 10^{-6}. The relaxed settings we determined through trial and error to increase convergence efficiency, resulting in a decrease in the accuracy of the solution. The relaxed settings have a population size of 12 individuals, generation stall limit of 5 individuals and a tolerance of 10^{-5}.

4.3.4 Surrogate-assisted optimization using radial basis function networks
For simplicity, we used an RBF network trained from a set of data points without resampling. Resampling can further improve the predictive and optimization power of the surrogate model [33,40,45,46]. We use the RBF networks here to predict the average time to sterilization from *GranSim* for any treatment, expressed as

$$\hat{t}(\boldsymbol{x}) = \sum_{j=1}^{k} w_j \phi_j(\boldsymbol{x}) \qquad \text{Eq. 4.2}$$

where $\boldsymbol{x}$ is the variable input vector (here $\boldsymbol{x}$ is the vector in Figure 4.3), and w_j are the weights on the radial basis functions ϕ_j. We use Gaussian RBFs centered at one of the sample points, with *k* representing the number of basis functions in the network. To find the optimal weights, the sum of the squared error is minimized between the predicted values and true value at each of the known sample points. To predict the value of the objective function for a given treatment, we evaluate Eq. 4.1 with the RBF network prediction of the time to sterilization for that treatment.

With a basis function centered at each sample point, the largest set of basis functions that could be used in the RBF network is equal to the number of sample points. However, using the full set can lead to over fitting. To avoid this, the RBF networks used in this study are built through forward selection, following the work of Orr [41]. The network begins with an empty set of basis functions and introduces whichever basis function minimizes the standard error the most. Basis functions are added one at a time until the standard error is lowered by < 0.01% over the last three basis function additions.

4.3.5 Single-antibiotic test problems

We crafted two test problems based on our published simulations of treatment to find optimal dose size and dosing frequency for a single antibiotic [25]. Thus we can propose two-dimensional optimization problems with known solutions, and use the optimization algorithms to solve the problem and test their performance. The data were generated by simulating antibiotic treatment with INH or RIF at five different dose sizes and seven dose frequencies to give 35 different treatments for each antibiotic. To do this, granuloma formation following infection was simulated for 100 days (no antibiotic treatment), with host variability included by simulating 82 granulomas with parameter values chosen from a uniform distribution. Antibiotic treatment for 180 days was then simulated, and the average time to sterilization all bacteria from all granulomas for each treatment regimen was calculated. Based on this average time to sterilization and the antibiotic regimen, the objective function value (Eq. 4.1) for each treatment can be evaluated, with t_c defined as the longest average time to sterilization from the set of 35 treatments. With the 35 objective function values, we generated an objective function response surface through linear interpolation between the known points. From this surface, we know the global minimum for each test problem, indicated by the circles in Figure 4.4a and Figure 4.4b corresponding to the treatment variables in Figure 4.4c. Because the recommended regimens for TB treatment consist of a combination of antibiotics, these single-antibiotic optimal treatments do not correspond to a practical treatment. Rather, these objective function response surfaces constitute the test problems we will use to determine the performance of different optimization algorithms.

a

b

c
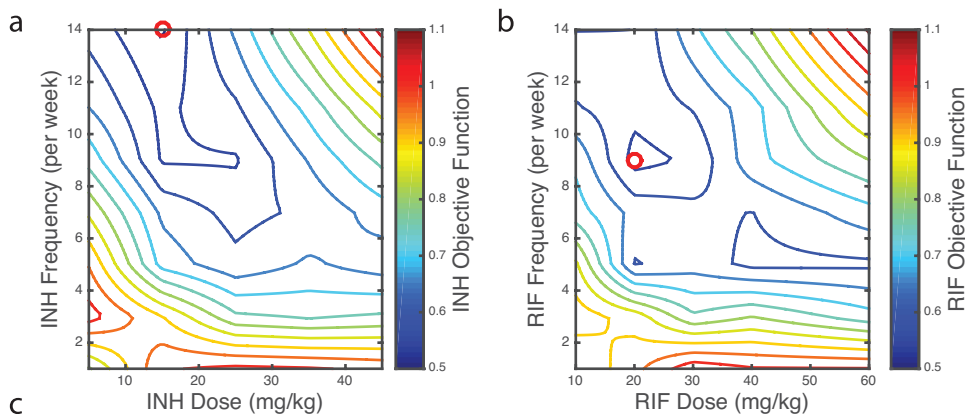
	Solution to Test Problem	
Test Problem	**Dose Size (mg/kg)**	**Dose Frequency (per week)**
INH Single-Antibiotic	15	14
RIF Single-Antibiotic	20	9

Figure 4.4 Contour plots for optimization test problems
Contour plots for INH (a) and RIF (b) single antibiotic treatment optimization test problems used to evaluate the performance of the genetic algorithms and RBF networks. Different treatments (35 for each antibiotic) were simulated by varying the dose size at five different levels (5, 15, 25, 35, and 45 mg/kg for INH; 10, 20, 30, 40, and 60 mg/kg for RIF) and seven dosing frequencies (1, 3, 5, 7, 9, 11, 14 doses per week) of the antibiotic, encompassing a realistic range for TB treatment. This range was chosen to encompass human equivalent doses in non-human primates (note, however, that treatment of humans with a single antibiotic is not standard-of-care). The objective function value (Eqn. 1) was determined for each treatment, and contour plots were generated to represent the objective function response surface defined by the 35 treatments and linear interpolation between them. The circle on each contour plot shows the location of the global minimum for that test problem, which corresponds to the antibiotic treatments given in the table (c).

4.3.6 Double-antibiotic treatment optimization implementation

Optimizing the dose size and dosing frequency when treating with two antibiotics (INH and RIF) is a four-dimensional optimization problem with variables INH dose size, INH dosing interval, RIF dose size and RIF dosing interval. We optimized double-antibiotic treatments using two RBF network surrogate models trained from two sets of data. The first, referred to as the *training set*, contains 45 treatments generated through Latin Hypercube Sampling (LHS) [47,48]. The second set of data is our *edge-supplemented training set*. Because RBF networks interpolate between the training points, we sampled 81 treatments to define the edges of the regimen design space to improve the RBF network accuracy near the design space edges. We generated all possible combinations of the four treatment variables at three discrete values for each variable: the variable's lower bound, an intermediate value, and its upper bound. The edge-supplemented set consists of the same 45 treatments of the training set plus the 81

edge treatments (i.e., 126 different treatments). The number of treatments in the training set was chosen based on a general rule of using about 10 points for every dimension of the optimization problem [49,50]. In addition to the two training sets just defined, we simulated a *test set* of 45 treatments chosen using LHS to validate the RBF network. We set variable ranges so that INH dose size could range from 0 to 45 mg/kg, RIF dose size from 0 to 60 mg/kg, and INH and RIF dosing frequencies from 1 to 14 doses per week. Because the plasma PK model is calibrated to non-human primate data, we chose these treatment boundaries as a range of non-human primate doses that yield human-equivalent exposure similar to clinical doses [3,25,51].

We treated a set of 73 granulomas, each with a different granuloma parameter set, with each of the 126 treatments and calculated the average time to sterilization for each treatment. With both the training set and edge-supplemented training set, we generated RBF networks to predict the average time to sterilization for any possible treatment variable combination. We used these RBF networks to search for local optima at discretely evaluated predictions of the objective function given by Eq 4.1, with a characteristic time to sterilization t_c defined as 120 days. Unlike the single-antibiotic test problems where we defined the longest average time to sterilization as t_c, we do not know the shape of the objective function with double-antibiotic treatments, so the maximum average time to sterilization in the regimen design space is unknown. We chose 120 days as the characteristic time to sterilization based on our experience that most granuloma treatment simulations would sterilize within this time frame. We varied the dose-weight parameter   to investigate how the balance between quickly sterilizing the granuloma and antibiotic dose effects the predicted optimal treatment.

4.4 Results and Discussion

4.4.1 Using RBF networks is more efficient but GA is more accurate when solving single-antibiotic treatment optimization

For antibiotic treatment optimization, it is our goal to locate the region of the regimen design space representing treatments that quickly kill all bacteria (a fast time to sterilization) while minimizing the amount of antibiotic given. To test whether GA or RBF networks are more appropriate for TB treatment optimization, we generated two test

problems to optimize single-antibiotic treatments. These two-dimensional test problems have known solutions, shown in Figure 4.4 and are based on our previous published simulations with *GranSim* [25]. We optimized dose size and dosing frequency for INH or RIF using either a GA or an RBF network prediction (Figure 4.3). To optimize using an RBF network prediction, we train the RBF networks using 21 treatments chosen using LHS and their associated objective function values sampled from the test-problem objective function response surface. We performed 30 independent optimizations on both test problems with both optimization algorithms to capture the variation in solutions of each algorithm. The optimal treatments obtained for each method are shown in Figure 4.5.

Optimization using an RBF network lacks the accuracy to precisely find the known solution to the test problems, although most of the solutions are found in the same region as the known solution (Figure 4.5a and Figure 4.5d). In contrast, using GA, with default stopping criteria (Figure 4.5b and Figure 4.5e), we accurately identified the global minimum of the test problem. All 30 runs yielded the known solution for the INH test problem, and almost all known solutions for the RIF test problem. Relaxing the stopping criteria for the GA can decrease the number of function evaluations, but at the expense of accuracy in finding the global minimum, as shown by the variation in solutions shown in Figure 4.5c and Figure 4.5f.
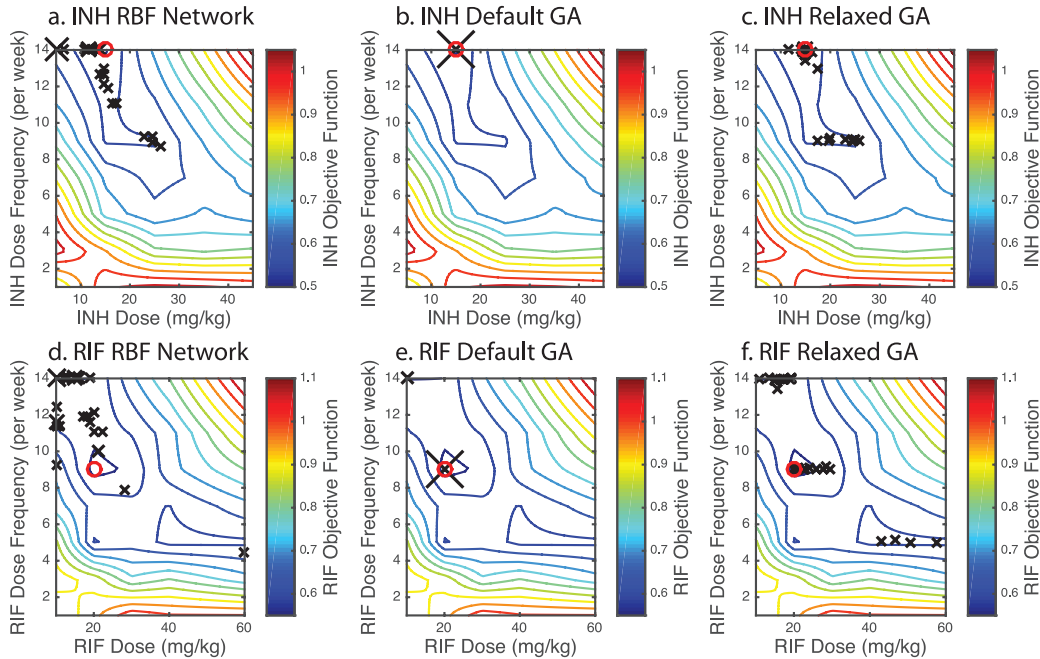
Figure 4.5 Comparing solutions using RBF network predictions and GA
Each test problem was solved using RBF network predictions (a and d) and GA with the default (b and e) and relaxed settings (c and f) with 30 independent optimizations. The location of the global minimum found with each optimization is represented by an "x" on the contour plots. Larger "x's" indicate that multiple runs found a global minimum at that location.

Based on accuracy, the GA has an advantage over the RBF networks. However, one of the defining characteristics of our TB treatment optimization problem is that each simulation is computationally expensive. Evaluating the efficacy of a single antibiotic treatment regimen requires multiple granuloma simulations and based on the time per granuloma simulation, uses between 300 and 400 CPU-hours (based on run times on XSEDE Comet). Because of this, the number of function evaluations (number of different treatments simulated) associated with each method is important in determining performance of the optimization algorithms. The RBF networks generate their solution with far fewer function evaluations, especially when compared to the default GA stopping criteria (Table 4.1). Even with relaxed stopping criteria, the GA solutions require orders of magnitude more function evaluations on average than the RBF networks.

If the overall goal is to identify the region of the design space that provides the best solutions rather than a unique location, which is the case with our treatment optimization

problem, then RBF network predictions can be effective. Although the RBF networks provide less accuracy, one benefit is that they provide a predicted response surface at any point in the regimen design space. With this information, the user can identify the region of the design space where the global minimum might occur, even if the predicted global minimum is not exactly accurate.

The objective function for the single-antibiotic test problems was chosen with the goal to locate a treatment that can quickly sterilize a granuloma while keeping antibiotic doses relatively low. However, different optimal treatment regimens could be defined based on different goals with different objective functions. For example, if toxicity or drug cost is a higher concern, then higher weights could be placed on the amount of antibiotics given. Adding a penalty based on the percentage of granulomas that did not sterilize would emphasize searching for treatments that have higher probabilities of sterilizing every granuloma in a host. Using RBF networks to locate optimal treatments allows for easy comparison of additional objective functions. With a set of treatments simulated with *GranSim,* different outputs or statistics from the model can be combined in different ways to generate different objective function response surfaces, without having to repeat treatment simulations.

4.4.2 RBF networks can be used to predict optimum double-antibiotic treatments
We next predicted optimal treatment regions when administering both INH and RIF simultaneously to study whether utilizing optimization would extend to a higher dimensional problem (more antibiotics). Based on our single-antibiotic treatment optimization results, we chose RBF networks rather than GA for this problem. We generated two different RBF networks from our training set and edge-supplemented training set to predict the average time to sterilization for a treatment. Using these two RBF networks, we evaluated their accuracy by comparing the predicted average time to sterilization and the simulated average time to sterilization at the test set treatments. Varying the dose-weight parameter, we located multiple, local optimal treatments based on the objective function in Eq. 4.1 and the average time to sterilization predictions from both RBF networks. The training set RBF network identified 8 optimal treatments, and the edge-supplemented RBF network identified 7 optimal treatments.

The edge-supplemented training set RBF network is more accurate and has a higher correlation coefficient when predicting average time to sterilization than the training set RBF network (Figure 4.6). This is not surprising as the edge-supplemented training set has more training points. We next compared prediction accuracy by simulating each of the optimal treatments identified by the RBF networks. We found that the RBF network generated with the edge-supplemented training set provides a more accurate prediction of the 7 optimal treatments it identified when compared to the accuracy of the training set RBF network at predicting its 8 optimal treatments (Figure 4.6c). The presence of training points along the edge of the regimen design space reduces the amount of error and thus yields more accurate optimal treatment identification.
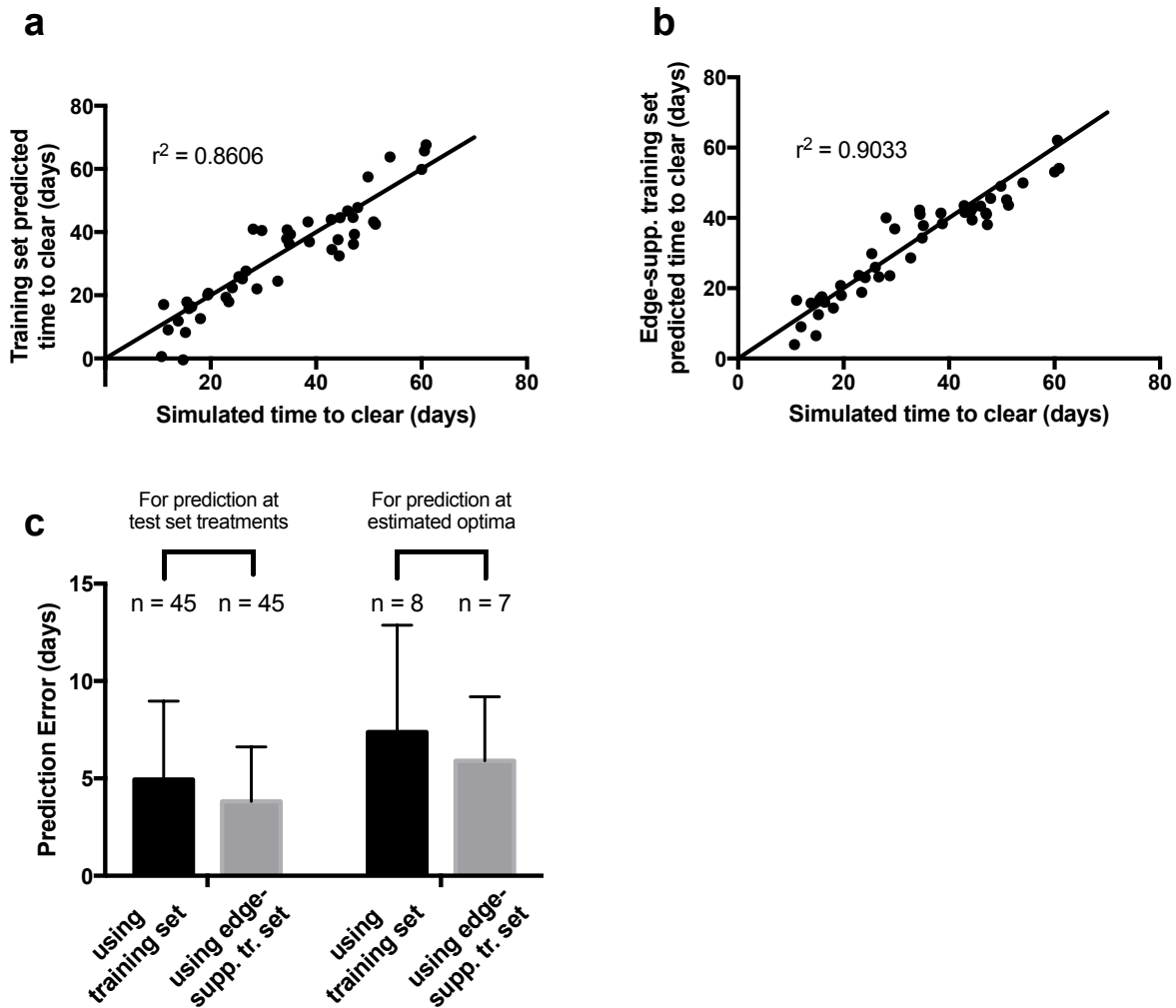
Figure 4.6 Testing the accuracy of RBF network generated solutions

(a,b) The simulated average time to sterilization vs. the RBF-predicted average time to sterilization is shown for each of the 45 test set treatments using the training set RBF network (a) and the edge-supplemented training set RBF network (b). The edge-supplemented training set RBF network is a more accurate predictor of average time to sterilization, indicated by the higher coefficient of determination. (c) The average prediction error and standard deviation (mean ± SD) are shown for the test set treatments (as in parts a and b) and at the estimated optimal treatments for the training set RBF network (n=8) and the edge-supplemented RBF network (n=7, optimal treatments with predicted and simulated times to sterilization listed in Table 4.2). The edge-supplemented training set RBF network has a lower average error at its estimated optimal treatments than the training set RBF network.

The optimal treatments from the edge-supplemented training set RBF network are listed in Table 4.2. Optimal treatments were located with dose-size weights of 0.75, 1, 2, and 3. As the dose-weight parameter is varied from 0.75 to 3, there are two general regions where optimal treatments are located. The first optimal region is a dose of INH between ~20-25 mg/kg given once a day with a low dose of RIF given about twice a week. The second optimum treatment is a similar dose size of INH given only once a week with an intermediate dose of RIF given every 1-2 days (Table 4.2), which shows similar dose sizes to non-human primate human-equivalent doses for recommended CDC regimens [3,51]. With this information, the two optimum treatments can be compared, and the best treatment can be chosen based on other criteria, such as the predicted time to sterilization or clinical practicality. For each toxicity weight, the daily INH doses with twice weekly RIF doses gives a faster time to sterilization than the other optimum treatment (Table 4.2).

RBF networks interpolate between known data points, so training the network with only the 45 points chosen using LHS can lead to inaccurate predictions along the edge of the design space. Adding training points along the edges can fix this but presents a barrier when scaling to optimization problems in higher dimensions. With optimization of more than two antibiotics or greater than four dimensions, evaluating every possible point along the edge of the design space becomes inefficient. To solve higher dimensional problems, resampling the objective function after an initial surrogate model is built can provide an efficient way of minimizing the objective function with the fewest number of sample points [33,39,40,45,46]. We plan to use these more complex sampling and resampling methods to improve the predictive and optimization power of the surrogate model in future studies of optimization treatments adding in additional antibiotics.

The surrogate models we build here are based solely on simulated data, using a model we developed based on a variety of animal data. However, surrogate modeling can be applied to data obtained through physical experiments as well. As with simulated data, the most frequent limiting factor to developing an accurate surrogate model is the density of data points within the design space. A low estimate for the number of data points required to build an accurate surrogate model is 10 for each design variable in the optimization problem, although 2 or 3 times as many points may be required depending on the specific problem and the desired accuracy of the surrogate model [49,50]. For many experimental studies, achieving this resolution of data may be infeasible. In these cases, there are a few possible solutions. One solution is to reduce the number of design variables to the most important and hold all others constant. Estimating optima of objective functions with one or two variables requires significantly fewer points than objective functions using three or more variables. Another solution is to use multi-fidelity surrogate modeling and combine the sparsely collected experimental data with larger sets of simulated data [52,53].

There are other antibiotics that are being considered for new TB therapy, including fluoroquinolones and oxazolidinones. We plan to investigate these as candidates for optimizing TB treatment with the optimization framework presented here. As we consider additional antibiotics, optimizing treatments with *GranSim* can provide predictions on whether antibiotic treatments will be successful in human clinical trials. While the simulations presented here represent treatment of a single granuloma, simulations with additional antibiotics will need to consider treatment of multiple granulomas in a single host. Providing this information could help prevent wasted resources arising from failed clinical trials and could help drugs reach the clinic more rapidly. Some antibiotics, such as moxifloxacin, showed promise in shortening TB treatment in animal trials, but failed to do so in human trials [54–56]. Using the optimization framework outlined here, we could identify treatments that have a higher probability of succeeding in human trials.

4.5 Conclusions

Current TB treatment is long and has many complications that indicate the need for better therapies. Based on the number of combination regimens of all potential antibiotics for TB, finding the best treatment regimen presents a challenging optimization problem. We presented a framework of combining our multi-scale, hybrid model of granuloma formation and treatment with optimization algorithms to predict optimal treatment regimens. Because each treatment simulation is computationally expensive, using an efficient algorithm is necessary for treatment optimization. We show that using a RBF network surrogate model is more suitable for predicting optimal treatments than GA. Using this framework we can guide experimental testing of new antibiotic regimens.

Table 4.1 Average number of function evaluations required to solve each of the test problems with each optimization method.

The RBF network predictions were always generated with 21 sample points. For GA optimizations, the number of function evaluations was averaged over the 30 independent optimizations. The average number of granuloma simulations required to find the optimum treatment is equal to the average number of function evaluations times the number of granulomas (in this problem, 82) simulated per treatment.

Optimization Method	Average Number of Function Evaluations Required	
	INH Test Problem	RIF Test Problem
RBF Network	21	21
Default Genetic Algorithm	3,855	4,085
Relaxed Genetic Algorithm	347.2	263.6

Table 4.2 The local optima located for the objective function to evaluate INH/RIF antibiotic treatments for the different weight parameters.

Because we identified local optimal treatments, multiple optima can be identified for a single dose-size weight. As the weight parameter increases, the local optima tend towards treatments that have lower total weekly doses and a higher predicted time to sterilization. Predictions were tested by running simulations at those points, giving the simulated time to sterilization.

Dose-weight Parameter (ω)	INH Dose (mg/kg)	INH Dose Freq. (week^{-1})	RIF Dose (mg/kg)	RIF Dose Freq. (week^{-1})	Weekly INH Dose (mg/kg)	Weekly RIF Dose (mg/kg)	Total Weekly Dose (mg/kg)	Predicted Time to Sterilize (days)	Simulated Time to Sterilize (days)
0.75	28.9	7.3	8.6	1.9	210.7	16.1	226.8	10.2	16.3
1	22.5	1.1	25.7	4.9	25.9	125.8	151.8	17.3	21.9
	25.7	7.3	8.6	1.9	187.4	16.1	203.4	11.8	16.8
2	22.5	1.1	17.1	3.7	24.1	63.3	87.4	25.9	31.0
	22.5	7.3	4.3	1.9	171.2	8.0	179.2	15.5	21.9
3	19.3	1.1	12.9	3.7	20.7	47.8	68.4	30.2	42.4
	19.3	4.9	4.3	1.9	94.5	8.0	102.5	29.9	31.4

4.6 References

1.   Houben RMGJ, Dodd PJ. The Global Burden of Latent Tuberculosis Infection: A Re-estimation Using Mathematical Modelling. PLoS Med. 2016;13: 1–13. doi:10.1371/journal.pmed.1002152
2.   Global tuberculosis report. Geneva; 2018.
3.   CDC. Treatment of Tuberculosis. Arch Intern Med. 2003. doi:10.1001/archinte.1956.00250190115011
4.   Munro SA, Lewin SA, Smith HJ, Engel ME, Fretheim A, Volmink J. Patient Adherence to Tuberculosis Treatment: A Systematic Review of Qualitative Research. PloS Med. 2007;4: 1230–1245. doi:10.1371/journal.pmed.0040238
5.   Steffen R, Menzies D, Oxlade O, Pinto M, de Castro AZ, Monteiro P, et al. Patients' costs and cost-effectiveness of tuberculosis treatment in DOT and non-DOT facilities in Rio de Janeiro, Brazil. PLoS One. 2010;5: 1–7. doi:10.1371/journal.pone.0014014
6.   McLaren ZM, Milliken AA, Meyer AJ, Sharp AR. Does directly observed therapy improve tuberculosis treatment? More evidence is needed to guide tuberculosis policy. BMC Infect Dis. 2016;16. doi:10.1186/s12879-016-1862-y
7.   Zumla A, Nahid P, Cole ST. Advances in the development of new tuberculosis drugs and treatment regimens. Nat Rev Drug Discov. 2013;12: 388–404. doi:10.1038/nrd4001
8.   Zumla AI, Gillespie SH, Hoelscher M, Philips PPJ, Cole ST, Abubakar I, et al. New antituberculosis drugs, regimens, and adjunct therapies: Needs, advances, and future prospects. Lancet Infect Dis. 2014;14: 327–340. doi:10.1016/S1473-3099(13)70328-1
9.   Menzies D, Benedetti A, Paydar A, Martin I, Royce S, Pai M, et al. Effect of duration and intermittency of rifampin on tuberculosis treatment outcomes: A systematic review and meta-analysis. PLoS Med. 2009;6: 1–18. doi:10.1371/journal.pmed.1000146
10.   Chang KC, Leung CC, Grosset J, Yew WW. Treatment of tuberculosis and optimal dosing schedules. Thorax. 2011;66: 997–1007. doi:10.1136/thx.2010.148585
11.   Egelund EF, Alsultan A, Peloquin CA. Optimizing the Clinical Pharmacology of Tuberculosis Medications. Clin Pharmacol Ther. 2015;98: 387–393. doi:10.1002/cpt.180
12.   Silva A, Lee B-Y, Clemens DL, Kee T, Ding X, Ho C-M, et al. Output-driven feedback system control platform optimizes combinatorial therapy of tuberculosis using a macrophage cell culture model. PNAS. 2016;113: 2172–2179. doi:10.1073/pnas.1600812113
13.   Lee B-Y, Clemens DL, Silva A, Dillon BJ, Masleša-Galić S, Nava S, et al. Drug regimens identified and optimized by output-driven platform markedly reduce tuberculosis treatment time. Nat Commun. 2017;8. doi:10.1038/ncomms14183
14.   Walpole J, Papin JA, Peirce SM. Multiscale Computational Models of Complex Biological Systems. Annu Rev Biomed Eng. 2013;15: 137–154. doi:10.1146/annurev-bioeng-071811-150104
15.   Cosgrove J, Butler J, Alden K, Read M, Kumar V, Cucurull-Sanchez L, et al. Agent-Based Modeling in Systems Pharmacology. CPT Pharmacometrics Syst

Pharmacol. 2015;4: 615–629. doi:10.1002/psp4.12018

16. Hunt CA, Kennedy RC, Kim SHJ, Ropella GEP. Agent-based modeling: A systematic assessment of use cases and requirements for enhancing pharmaceutical research and development productivity. WIREs Syst Biol Med. 2013;5: 461–480. doi:10.1002/wsbm.1222

17. An G, Mi Q, Dutta-Moscato J, Vodovotz Y. Agent-based models in translational systems biology. Wiley Interdiscip Rev Syst Biol Med. 2009;1: 159–171. doi:10.1002/wsbm.45

18. Martin KS, Virgilio KM, Peirce SM, Blemker SS. Computational modeling of muscle regeneration and adaptation to advance muscle tissue regeneration strategies. Cells Tissues Organs. 2015;202: 250–266. doi:10.1159/000443635

19. Chapa J, An G, Kulkarni SA. Examining the relationship between pre-malignant breast lesions, carcinogenesis and tumor evolution in the mammary epithelium using an agent-based model. PLoS One. 2016;11: 1–24. doi:10.1371/journal.pone.0152298

20. Wang Z, Butner JD, Cristini V, Deisboeck TS. Integrated PK-PD and agent-based modeling in oncology. J Pharmacokinet Pharmacodyn. 2015;42: 179–189. doi:10.1007/s10928-015-9403-7

21. Finley SD, Chu L-H, Popel AS. Computational systems biology approaches to anti-angiogenic cancer therapeutics. Drug Discov Today. 2015;20: 187–197. doi:10.1016/j.drudis.2014.09.026

22. An G, Fitzpatrick BG, Christley S, Federico P, Kanarek A, Miller Neilan R, et al. Optimization and control of agent-based models in biology: a perspective. Bull Math Biol. 2017;79: 63–87. doi:10.1007/s11538-016-0225-6

23. Stephenson B, Lanzas C, Lenhart S, Day J. Optimal control of vaccination rate in an epidemiological model of Clostridium difficile transmission. J Math Biol. 2017. doi:10.1007/s00285-017-1133-6

24. Kirschner D, Lenhart S, Serbin S. Optimal control of the chemotherapy of HIV. J Math Biol. 1997;35: 775–792. doi:10.1007/s002850050076

25. Pienaar E, Dartois V, Linderman JJ, Kirschner DE. In silico evaluation and exploration of antibiotic tuberculosis treatment regimens. BMC Syst Biol. 2015;9: 1–12. doi:10.1186/s12918-015-0221-8

26. Pienaar E, Cilfone NA, Lin PL, Dartois V, Mattila JT, Butler JR, et al. A computational tool integrating host immunity with antibiotic dynamics to study tuberculosis treatment. J Theor Biol. 2015;367: 166–179. doi:10.1016/j.jtbi.2014.11.021

27. Cilfone NA, Perry CR, Kirschner DE, Linderman JJ. Multi-scale modeling predicts a balance of tumor necrosis factor-a and interleukin-10 controls the granuloma environment during Mycobacterium truberculosis infection. PLoS One. 2013;8: e68680. doi:10.1371/journal.pone.0068680

28. Fallahi-Sichani M, El-Kebir M, Marino S, Kirschner DE, Linderman JJ. Multiscale computational modeling reveals a critical role for TNF-α receptor 1 dynamics in tuberculosis granuloma formation. J Immunol. 2011;186: 3472–3483. doi:10.4049/jimmunol.1003299

29. Linderman JJ, Cilfone NA, Pienaar E, Gong C, Kirschner DE. A multi-scale approach to designing therapeutics for tuberculosis. Integr Biol. 2015;7: 591–609.

doi:10.1039/C4IB00295D

30. Kjellsson MC, Via LE, Goh A, Weiner D, Low KM, Kern S, et al. Pharmacokinetic evaluation of the penetration of antituberculosis agents in rabbit pulmonary lesions. Antimicrob Agents Chemother. 2012;56: 446–457. doi:10.1128/AAC.05208-11

31. Prideaux B, Dartois V, Staab D, Weiner DM, Goh A, Via LE, et al. High-sensitivity MALDI-MRM-MS imaging of moxifloxacin distribution in tuberculosis-infected rabbit lungs and granulomatous lesions. Anal Chem. 2011;83: 2112–2118. doi:10.1021/ac1029049

32. Man KF, Tang KS, Kwong S. Genetic algorithms: Concepts and applications. IEEE Trans Ind Electron. 1996;43: 519–534. doi:10.1109/41.538609

33. Jin Y. Surrogate-assisted evolutionary computation : Recent advances and future challenges. Swarm Evol Comput. 2011;1: 61–70. doi:10.1016/j.swevo.2011.05.001

34. Alba E, Luque G, Nesmachnow S. Parallel metaheuristics: recent advances and new trends. Int Trans Oper Res. 2013;20: 1–48. doi:10.1111/j.1475-3995.2012.00862.x

35. Kia R, Khaksar-Haghani F, Javadian N, Tavakkoli-Moghaddam R. Solving a multi-floor layout design model of a dynamic cellular manufacturing system by an efficient genetic algorithm. J Manuf Syst. 2014;33: 218–232. doi:10.1016/j.jmsy.2013.12.005

36. Melin P, Castillo O. A review on type-2 fuzzy logic applications in clustering, classification and pattern recognition. Appl Soft Comput J. 2014;21: 568–577. doi:10.1016/j.asoc.2014.04.017

37. Lollini P-L, Motta S, Pappalardo F. Discovery of cancer vaccination protocols with a genetic algorithm driving an agent based simulator. BMC Bioinformatics. 2006;7: 352. doi:10.1186/1471-2105-7-352

38. Palladini A, Nicoletti G, Pappalardo F, Murgo A, Grosso V, Stivani V, et al. In silico modeling and in vivo efficacy of cancer-preventive vaccinations. Cancer Res. 2010;70: 7755–7763. doi:10.1158/0008-5472.CAN-10-0701

39. Forrester AIJ, Sóbester A, Keane AJ. Engineering Design via Surrogate Modelling: A Practical Guide. John Wiley & Sons; 2008.

40. Sóbester A, Forrester AIJ, Toal DJJ, Tresidder E, Tucker S. Engineering design applications of surrogate-assisted optimization techniques. Optim Eng. 2014;15: 243–265. doi:10.1007/s11081-012-9199-x

41. Orr MJL. Introduction to radial basis function networks. 1996. Available: http://citeseerx.ist.psu.edu/viewdoc/summary?doi=10.1.1.133.7043

42. Gutmann HM. A Radial Basis Function Method for Global Optimization. J Glob Optim. 2001;19: 201–227. doi:10.1023/A:1011255519438

43. Jones DR. A Taxonomy of Global Optimization Methods Based on Response Surfaces. J Glob Optim. 2001;21: 345–383. doi:10.1023/A:1012771025575

44. Cilfone NA, Kirschner DE, Linderman JJ. Strategies for Efficient Numerical Implementation of Hybrid Multi-scale Agent-Based Models to Describe Biological Systems. Cell Mol Bioeng. 2015;8: 119–136. doi:10.1007/s12195-014-0363-6

45. Akhtar T, Shoemaker CA. Multi objective optimization of computationally expensive multi-modal functions with RBF surrogates and multi-rule selection. J

Glob Optim. 2016;64: 17–32. doi:10.1007/s10898-015-0270-y

46. Diaz-Manriquez A, Toscano-Pulido G, Gomez-Flores W. On the selection of surrogate models in evolutionary optimization algorithms. 2011 IEEE Congr Evol Comput CEC. 2011; 2155–2162. doi:10.1109/CEC.2011.5949881

47. McKay AMD, Beckman RJ, Conover WJ. A Comparison of Three Methods for Selecting Values of Input Variables in the Analysis of Output from a Computer Code. Technometrics. 1979;21: 239–245. doi:doi:10.2307/1268522

48. Marino S, Hogue IB, Ray CJ, Kirschner DE. A methodology for performing global uncertainty and sensitivity analysis in systems biology. J Theor Biol. 2008;254: 178–196. doi:10.1016/j.jtbi.2008.04.011

49. Jones DR, Schonlau M, William J. Efficient Global Optimization of Expensive Black-Box Functions. J Glob Optim. 1998;13: 455–492. doi:10.1023/a:1008306431147

50. Forrester AIJ, Sóbester A, Keane AJ. Multi-fidelity optimization via surrogate modelling. Proc R Soc A. 2007;463: 3251–3269. doi:10.2307/20209374

51. Lin PL, Dartois V, Johnston PJ, Janssen C, Via L, Goodwin MB, et al. Metronidazole prevents reactivation of latent Mycobacterium tuberculosis infection in macaques. Proc Natl Acad Sci. 2012;109: 14188–14193. doi:10.1073/pnas.1121497109

52. Kuya Y, Takeda K, Zhang X, Forrester AIJ. Multifidelity Surrogate Modeling of Experimental and Computational Aerodynamic Data Sets. AIAA J. 2011;49: 289–298. doi:10.2514/1.J050384

53. Reese CS, Wilson AG, Hamada M, Martz HF, Ryan KJ. Integrated Analysis of Computer and Physical Experiments. Technometrics. 2004;46: 153–164. doi:10.1198/004017004000000211

54. Nuermberger EL, Yoshimatsu T, Tyagi S, Williams K, Rosenthal I, O'Brien RJ, et al. Moxifloxacin-containing regimens of reduced duration produce a stable cure in murine tuberculosis. Am J Respir Crit Care Med. 2004;170: 1131–1134. doi:10.1164/rccm.200407-885OC

55. Nuermberger EL, Yoshimatsu T, Tyagi S, O'Brien RJ, Vernon AN, Chaisson RE, et al. Moxifloxacin-containing regimen greatly reduces time to culture conversion in murine tuberculosis. Am J Respir Crit Care Med. 2004;169: 421–266. doi:10.1164/rccm.200310-1380OC

56. Gillespie SH, Crook AM, McHugh TD, Mendel CM, Meredith SK, Murray SR, et al. Four-Month Moxifloxacin-Based Regimens for Drug-Sensitive Tuberculosis. N Engl J Med. 2014;371: 1577–1587. doi:10.1056/NEJMoa1407426

Chapter 5 Optimizing Doses of First-line Tuberculosis Antibiotics Identifies Alternative Regimens with High Efficacy in Virtual Clinical Trials

5.1 Introduction

Even though tuberculosis (TB) has been around for thousands of years, we have treated TB disease with primarily the same drugs for close to 50 years [1]. Caused by the pathogen *Mycobacterium tuberculosis* (Mtb), the preferred, standard antibiotic regimen is estimated to have a success rate of ~95% [2,3]. With ~5% treatment failure rate, the standard regimen alone has not provided a significant decrease in the global TB burden. TB is one of the world's deadliest infectious diseases, evaluated by number of annual deaths, and the World Health Organization aims to decrease the number of TB-related deaths by 90% by 2030 [4]. While vaccination efforts can also reduce the number of new TB cases, a highly efficacious drug regimen will continue to be needed to treat TB until its eradication, and changes to the existing regimen for drug-sensitive TB may help achieve this goal.

When Mtb infects lung tissue, the immune response results in the formation of a granuloma. The granuloma is a collection of immune cells recruited to the site of infection to control the pathogen [5]. The granuloma contains Mtb and is therefore the target for antibiotic treatment. Different subpopulations of Mtb, such as extracellular or intracellular (inside macrophages or neutrophils) and replicating or non-replicating, exist in the granuloma depending on the microenvironment. The structure of the granuloma can act as a mechanism to control infection, but it also presents a physiological barrier to antibiotic diffusion [6–8].

The current standard regimen for drug-susceptible TB involves up to 6 months or more of therapy with the antibiotics isoniazid (H), rifampin (R), ethambutol (E), and

pyrazinamide (Z). New regimens attempting to shorten TB treatment have been clinically tested, but with limited success. Efforts to introduce fluoroquinolones, such as gatifloxacin and moxifloxacin (M), into regimens for drug-susceptible TB to shorten treatment from 6 months to 4 months failed to show noninferiority to control regimens [2,3,9].

Multiple factors limit the ability to shorten the standard regimen for drug-susceptible TB. First, the structure of the granuloma influences both antibiotic distribution and can result in lower concentrations inside the granuloma [7,8]. Second, microenvironments can promote Mtb to shift towards phenotypic states that are tolerant towards antibiotics [10] For example, Mtb collected from granuloma caseum, material consisting of dead cell debris, show high levels of tolerance to antibiotics [11]. Third, host-to-host variability in drug absorption and metabolism kinetics leads to PK variability that has been clinically linked to worse outcomes in TB treatment [12].

A goal for identifying better regimens for TB treatment involves finding a regimen that can manage and overcome all three of these complications: the heterogeneity in granulomas and antibiotic distribution, antibiotic-tolerant Mtb, and host-to-host PK variability. By addressing these complications, a better regimen is one that would successfully treat more individuals with a shorter treatment duration. Efforts to utilize experimental PK data to determine optimal doses can consider some factors that complicate treatment but rely on the existence of good experimental data and are resource-limited in the number of regimens that can be experimentally or clinically tested [13].

Using computational modeling to predict regimen efficacy provides a more efficient way of predicting regimen efficacy and determining optimal doses. We have previously shown how our computational simulation of granuloma formation, function and treatment can simulate efficacies of different TB regimens (Chapters 2 and 3) [7,14,15]. This computational simulation, called *GranSim*, can simulate granuloma heterogeneous environments that impact antibiotic distribution, and shows that different granuloma

types sterilize at varying rates even with the same drug regimen [7,14,15]. By accounting for the mechanisms that complicate TB treatment, we can accurately predict granuloma sterilization with different regimens. Formalizing the goal of optimizing antibiotic regimens as finding the optimal dosing schedule that minimizes both the time to sterilize a granuloma and total antibiotic dose, we have shown that we can utilize surrogate-assisted optimization algorithms to accurately and efficiently predict optimal regimens (Chapter 4) [16]. Using *GranSim*, we can predict granuloma-level sterilization when simulating TB treatment, but we are ultimately interested in predicting how a regimen treats an individual, and how the regimen performs in an entire population.

I have two goals in this chapter. First, I examine the standard HRZE regimen and whether more optimal doses of these drugs can be identified. To do this I optimize the doses for HRZE at the granuloma scale using a surrogate-assisted optimization algorithm (Chapter 4) and compare the efficacies of optimal regimens identified. I also present a process of generating a virtual population to simulate a virtual clinical trial (VCT) that captures the heterogeneity and variability in both granulomas and plasma PK and examine predicted optimal HRZE regimens in this population.

Second, I ask whether improvements to the standard HRZE regimen could be obtained by substituting moxifloxacin for isoniazid or rifampin. Fluoroquinolones are frequently prescribed for treating multi-drug resistant TB [17]. A study comparing three fluoroquinolones predicted that moxifloxacin has better and more robust sterilizing activity compared to levofloxacin and gatifloxacin [8]. Substituting isoniazid or rifampin with moxifloxacin has been investigated as a way to potentially shorten treatment, or as an alternative for TB cases with resistance to isoniazid or rifampin. Clinical trials have been conducted to test whether the inclusion of moxifloxacin in place of isoniazid or rifampin could shorten treatment regimens [3,18]. However, many of these clinical trials failed to show an advantage over the HRZE regimen. To investigate the performance of these alternative regimens, here, I simulate the HRZE regimen and regimens where moxifloxacin (M) replaces H or R (HMZE and RMZE) in non-human primates (NHPs). Although these simulations are at the granuloma scale, they are useful for predicting

outcomes of NHP experiments currently being performed in the lab of our collaborator, Professor Joanne Flynn at the University of Pittsburgh. In addition to predicting outcomes for these regimens, we can predict which alternative regimens are interesting candidates for future experimental studies.

5.2 Methods

5.2.1 GranSim and pharmacokinetic/pharmacodynamic modeling

As a basis for the granuloma treatment optimization and hosts for the virtual clinical trial, I utilize our computational model of granuloma formation and function, *GranSim*. This model is described briefly below and in previous chapters (Chapters 2, 3 and 4). *GranSim* is an agent-based model that simulates the immune response in TB disease with granuloma formation as an emergent behavior [7,19–22]. Agents in this agent-based model include immune cells, such as macrophages and T-cells, and individual Mtb that interact with each other according to a set of rules (for more complete description of rules, see http://malthus.micro.med.umich.edu/GranSim/). For the purpose of this work, *GranSim* provides a simulation that can recreate the heterogeneity and PK variability associated with TB treatment in a granuloma and can simulate the spatial distribution of antibiotics and sterilizing ability of different antibiotic regimens (Chapter 2) [7,8,14,15].

The PK/PD model within *GranSim* simulates the plasma concentration over time following oral doses of antibiotics, the subsequent spatial concentration in the simulated granuloma, and the bactericidal activity based on the local concentration. The plasma PK model uses a compartmental, ordinary differential equation model to simulate absorption through transit compartments into the plasma, exchange with peripheral tissue, and first-order elimination from the plasma [7,23]. Plasma PK parameters for H, R, E and Z were calibrated based on human plasma measurements [14,24]. The tissue PK model references the concentration in the plasma to calculate flux through vascular sources in the computational grid, diffusion through tissue, binding to caseum, and partitioning into macrophages [7,15,25]. The PD model uses a Hill curve to determine the concentration dependent antibiotic killing rate constant [26], to determine the rate of

death per time step. The concentration used in the Hill curve is an effective concentration, calculated as the sum of all antibiotic concentrations converted to the equipotent concentration of the antibiotic of the highest maximal killing rate constant. Based on the predicted fractional inhibitory concentration, the effective concentration is adjusted to account for synergistic or antagonistic concentrations (Chapter 3) [27,28].

5.2.2 HRZE dose multi-objective optimization problem
Defining an optimization requires defining the objective function (or multiple objective functions, see next section) whose values are to be minimized, and the design variables that define the domain of those objective functions. For the purpose of optimizing the doses for HRZE, the variables include the individual doses for each antibiotic. The sampling ranges for each dose variable were set to range from 0 mg/kg to double the standard CDC dose [1]. Maximum doses for each antibiotic were set to 10, 20, 40 and 50 mg/kg for H, R, E, and Z, respectively. Because the ranges for these doses are different, the design variables used to define the objective function domains are normalized to range from 0 to 1. The objective functions include minimizing the total antibiotic dose and the sterilization time for that combination of doses. The total antibiotic dose is evaluated as the sum of the normalized antibiotic doses. The sterilization time is evaluated as the time to completely sterilize a granuloma, averaged over a set of granulomas. Granulomas that fail to sterilize are assigned a sterilization time of 180 days (length of treatment) to ensure they have the highest objective function value.

5.2.3 Multi-objective Surrogate-assisted Optimization Algorithm
The goal of multi-objective optimization is to find the optimal trade-off between two or more objectives by identifying the variable combinations that make up that optimal trade-off [29]. Using a surrogate-assisted framework involves predicting each objective based on the outcomes of the already sampled regimens. The surrogate predictions of each objective can then be used as a computationally-inexpensive alternative to predict the objective functions throughout the whole design space. Here, I use a kriging-based surrogate model to generate the objective function predictions. This kriging-based prediction and optimization algorithm is based on a set of open source MATLAB

functions developed by Forrester and Sóbester [30,31]. Using a surrogate-assisted framework provides an efficient and accurate way to thoroughly investigate the regimen design space and predict optimal doses (Chapter 4) [16].

First, the algorithm samples the antibiotic doses to generate a set of initial regimens for simulating treatment (Figure 5.1). A Latin hypercube sampling (LHS) design samples the doses to evenly distribute throughout the regimen design space [31,32]. Then, *GranSim* simulates treatment with each of these regimens on a set of 30 granulomas, and records the day when all Mtb are dead evaluate the sterilization time, reported as the average time when all Mtb are dead over the 30 granulomas (see section below for description of the 30 granulomas).

Second, based on the sampled regimens and the calculated values of the corresponding objective functions, the algorithm builds a kriging-based surrogate model to predict the values of the objective functions at any point in the variable design space. The kriging model operates by assuming that the value of a function *f* of *n* variables at any *n*-dimensional vector **x** can be stated as the sum of some unknown mean (μ) and an error term that is a function of position (Eq. 5.1) [33].

$$f(\boldsymbol{x}) = \mu + \epsilon(\boldsymbol{x}) \qquad \text{Eq. 5.1}$$

To provide an estimate for the error at any given **x**, we assume the errors at two points are correlated based on the distance between those two points. The correlation in error between points *i* and *j*, equal to component R_{ij} in the correlation matrix **R**, exponentially decays with respect to the weighted distance between them (Eq. 5.2).

$$R_{ij} = Corr\left[\epsilon\left(x^{(i)}\right), \epsilon\left(x^{(j)}\right)\right] = \exp\left[-\sum_{h=1}^{n} \theta_h \left|x_h^{(i)} - x_h^{(j)}\right|^2\right] \quad (\theta_h \geq 0) \qquad \text{Eq. 5.2}$$

Given *k* sample data points of *f* throughout the design space, the model maximizes the likelihood function (Eq. 5.3, Eq. 5.4, Eq. 5.5) by varying the weight parameters θ_h and p_h to

obtain the best fit. The vector **y** of length k has entries with the values of the observed function at each of the sample points. With the optimized parameters θ_h and p_h, the value of f at any point **x*** is predicted with Eq. 5.6, where the vector **r** of length k is given such that its entry i is given as the correlation in error between sample point $\mathbf{x}^{(i)}$ and **x***.

$$l = \frac{1}{(2\pi\hat{\sigma}^2)^{k/2}|\boldsymbol{R}|^{1/2}} \exp\left[-\frac{(\boldsymbol{y} - \mathbf{1}\hat{\mu})'\boldsymbol{R}^{-1}(\boldsymbol{y} - \mathbf{1}\hat{\mu})}{2\hat{\sigma}^2}\right] \qquad \text{Eq. 5.3}$$

$$\hat{\mu} = \frac{\mathbf{1}'\boldsymbol{R}^{-1}\boldsymbol{y}}{\mathbf{1}'\boldsymbol{R}^{-1}\mathbf{1}} \qquad \text{Eq. 5.4}$$

$$\hat{\sigma}^2 = \frac{(\boldsymbol{y} - \mathbf{1}\hat{\mu})'\boldsymbol{R}^{-1}(\boldsymbol{y} - \mathbf{1}\hat{\mu})}{k} \qquad \text{Eq. 5.5}$$

$$\hat{f}(\boldsymbol{x}^*) = \hat{\mu} + \boldsymbol{r}'\boldsymbol{R}^{-1}(\boldsymbol{y} - \mathbf{1}\hat{\mu}) \qquad \text{Eq. 5.6}$$

Once the kriging model for each objective is tuned, the algorithm resamples the design space to select the regimen that maximizes the likelihood of expected improvement of the objective functions. The expected improvement criterion seeks the set of design variables that maximizes the expected distance from the points currently in the Pareto front [31,34]. At this point, *GranSim* simulates the sampled regimen that maximizes the likelihood of improving the values. An iterative process continues, where the algorithm adds new regimen results to the set of sampled regimens and objective functions and updates the kriging model until the algorithm samples the number of specified regimens.

To visualize the results of the optimization algorithm, we can plot both objective function outcomes for each regimen against each other. If the regimen design space is well-sampled, and the algorithm successfully identifies regimens that provide the trade-off between the two objectives, sterilization time and total dose, this plot provides a visualization of the Pareto front. The Pareto front is the set of regimens contained in the Pareto set, which is defined as regimens that have non-dominated objective function values [35]. In other words, the set of non-dominated solutions represent the

compromise between the two objective functions, where no regimen in the set has a higher value for both objectives when compared to the other solutions in the non-dominated set.
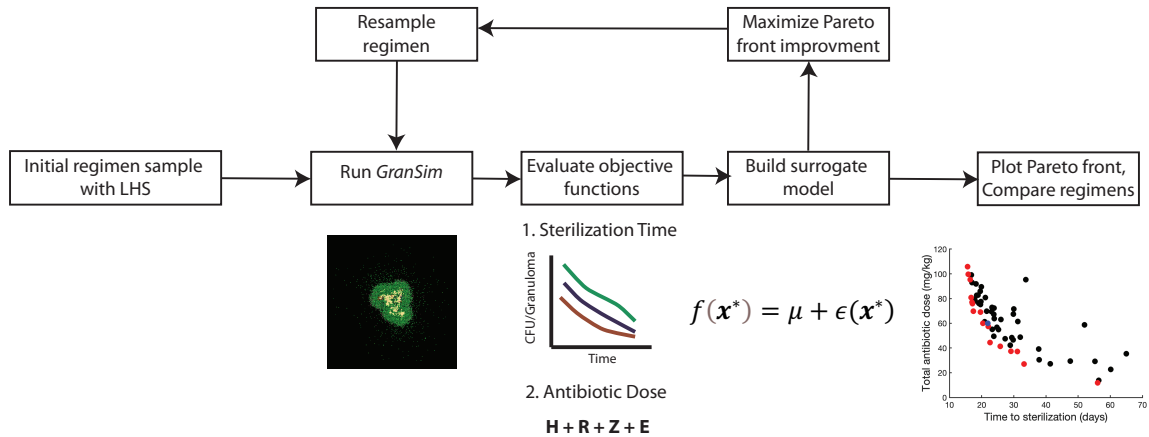
Figure 5.1 Surrogate-assisted optimization algorithm
The surrogate-assisted optimization algorithm begins by sampling the variable domain defined by the dose range for each antibiotic using LHS. Based on the initial set of regimens, treatment is simulated on a set of granulomas using *GranSim*. The outputs of *GranSim* are then used to calculate the objective function values for each regimen. The multi-objective scheme here uses the average granuloma sterilization time and the total antibiotic dose as the two objectives to minimize. Based on the sampled regimens and their objective function values, the surrogate models are tuned. Until the specified number of regimens is sampled, an iterative process occurs where new regimens are sampled from the variable domain. New regimens are selected by maximizing the predicted improvement to the existing Pareto front. Once all regimens are sampled, the full Pareto front, and all objective function values for the sampled regimens can be plotted to evaluate the performance of each regimen and identify optimal trade-offs.

5.2.4 Set of granulomas for dose optimization
To evaluate the average sterilization time objective function, we need a set of granulomas to simulate each regimen. Because the optimization algorithm involves an iterative process, and samples numerous regimens, computational expense and efficiency is a concern. We simulate a set of 500 granulomas, with immune parameter ranges listed for granulomas with low colony forming unit (CFU, number of bacteria) measures in Table 2.1. Because we simulate these granulomas on a 200x200 grid instead of the 300x300 grid required of the high-CFU granulomas, the low-CFU granulomas are much less computationally expensive. To find an optimal regimen, we want to find a regimen that is able to sterilize the worst granulomas. To do this, we selected the 30 granulomas with the highest CFU from the set of 500 simulated granulomas to represent the hardest to treat granulomas that are still able to be run on

120

the 200x200 grid. We treated these granulomas with the sampled set of regimens, varying doses of the four first-line antibiotics. For optimization with the four-first line antibiotics, we simulate these 30 granulomas with both low plasma PK exposure (low PK) and average PK exposure by setting the plasma PK parameters according to the low and average levels listed in Table 2.2.

5.2.5 Host formation and virtual clinical trial population
To explore how these regimens perform in a whole infected host, we need to create a simulation that represents a group of granulomas as a whole infected lung. TB disease in primates results in the formation of multiple granulomas, and successful treatments must sterilize the entire lung [36]. Here, we define a host as a collection of granulomas with the same plasma PK parameters. This definition assumes a granuloma develops independently of the status of the other granulomas in the host but captures the primary host-level characteristic by allowing for the same PK within a host and variable PK throughout the population. To build the population of hosts, we first created an *in silico* repository of granulomas, ranging from low to high CFU, using two sets of immune parameter ranges to generate the low and high CFU granulomas, based on the parameter ranges for these two groups in Table 2.1. These granulomas are a different set than the set of 30 granulomas used for optimization and include a greater diversity of granulomas. Because the number of overall granuloma simulations in the host simulations is smaller than the number required for dose optimization, we can afford to include the higher CFU granulomas on the 300x300 which provides a greater diversity of granuloma types into the hosts. We simulate the low-CFU granulomas on a 200x200 grid with 500 different parameter sets for 500 different granulomas. We simulate the high-CFU granulomas on a 300x300 grid, due to their tendency to have larger diameters, with 200 different parameter sets [14]. A total of 514 granulomas were unsterilized after simulating 300 days (354 low-CFU and 160 high-CFU).

To generate the list of granulomas that comprise a host, we use measurements of CFU per granuloma from 623 granulomas from 38 non-human primates (NHP) to determine the relative probability a granuloma has a certain level of bacteria burden. These

granulomas are compiled from numerous studies [37–41], and the complete set has been used for model calibration in a previous study [42]. Animals were infected with a low dose Mtb and necropsy was performed according to previously described protocols [36, 38]. The age of the granulomas excised during necropsy for bacterial burden measurement varies, depending on the study, but ranges from 4-17 weeks after initial Mtb infection. Figure 5.2 shows the CFU/granuloma distributions for both simulated granulomas and NHP granulomas.

We next binned the NHP granulomas into 4 different levels: less than 10^3 CFU (36% of granulomas), between 10^3 and 10^4 CFU (33% of granulomas), between 10^4 and 10^5 CFU (26% of granulomas), and greater than 10^5 CFU (5% of granulomas). We similarly binned the *in silico* granulomas sampled from those bins with the relative probabilities based on the NHP granulomas to generate a collection of 10 granulomas for each host. We generated a total of 400 hosts and randomly placed them into four treatment groups (Figure 5.3). To introduce plasma PK variability, we sampled 400 parameter sets using LHS from the plasma PK ranges that capture the range of human plasma concentration (Table 2.2), and assigned each parameter set to a host. We simulate the hosts in each treatment group with one of four regimens. The four regimens include one control group that is the regimen with the standard, recommended doses, and the other three are regimens identified as potential optimal regimens using the surrogate-assisted optimization algorithm. We statistically compare the differences in host sterilization times between each treatment group and the control group using a t-test with a significance level of $p < 0.01$.

5.2.6 Non-human primate granulomas for moxifloxacin treatment simulation
To predict regimen efficacy in non-human primates (NHPs), we simulate a set of 500 granulomas, with immune parameter ranges for the low-CFU granulomas (Table 2.1). To match the timeline of infection and treatment based on NHP experiments, we simulate these granulomas for 100 days in the absence of antibiotics to allow for granuloma formation. After day 100, we treat granulomas with different regimens for an additional 100 days, or until granuloma sterilization. The simulated regimens include the

standard combination of antibiotics (HRZE), and regimens where moxifloxacin (M) is used to replace R in the regimen (HMZE) or H in the regimen (RMZE). We calibrate plasma PK parameters for M to NHP plasma concentrations following a dose of 50 mg/kg (see Appendix D for parameters and calibration). Tissue PK parameters for M were calibrated and established in a previously published study [8]. We use doses for each antibiotic with daily administration at the NHP equivalent dose to the human recommended doses: H, 15 mg/kg; R, 20 mg/kg; M, 35 mg/kg; Z, 50 mg/kg; E 55 mg/kg [43].

5.2.7 Surrogate-model prediction behavior
To check that the kriging-model produces realistic predictions of the objective functions, we evaluate the objective function predictions for both the average granuloma sterilization time and total daily dose. Holding the three other variable doses constant at their standard dose, the kriging-model predicts the average sterilization time and total daily dose for the full range of the fourth antibiotic dose. The surrogate models for average sterilization and total antibiotic dose were built based on a sample of 40 initial regimens, and 20 infill sampled regimens.

Figure 5.4 shows the surrogate model predictions of average granuloma sterilization time and total daily antibiotic dose while varying each antibiotic. As expected, the relationship between antibiotic dose and total daily dose is linear, and the range of responses corresponds to the expected linear prediction for each antibiotic. The prediction for the average granuloma sterilization time also shows the expected trend. In general, as antibiotic dose increases the sterilization time decreases. However, some of the predictions show that as antibiotic dose is increased, there is no additional gain in sterilization time, and the sterilization time levels. This provides some indication that there may be an optimal trade-off between antibiotic dose and sterilization time, and that for some antibiotics, increasing the dose does not translate to a shorter sterilization time.
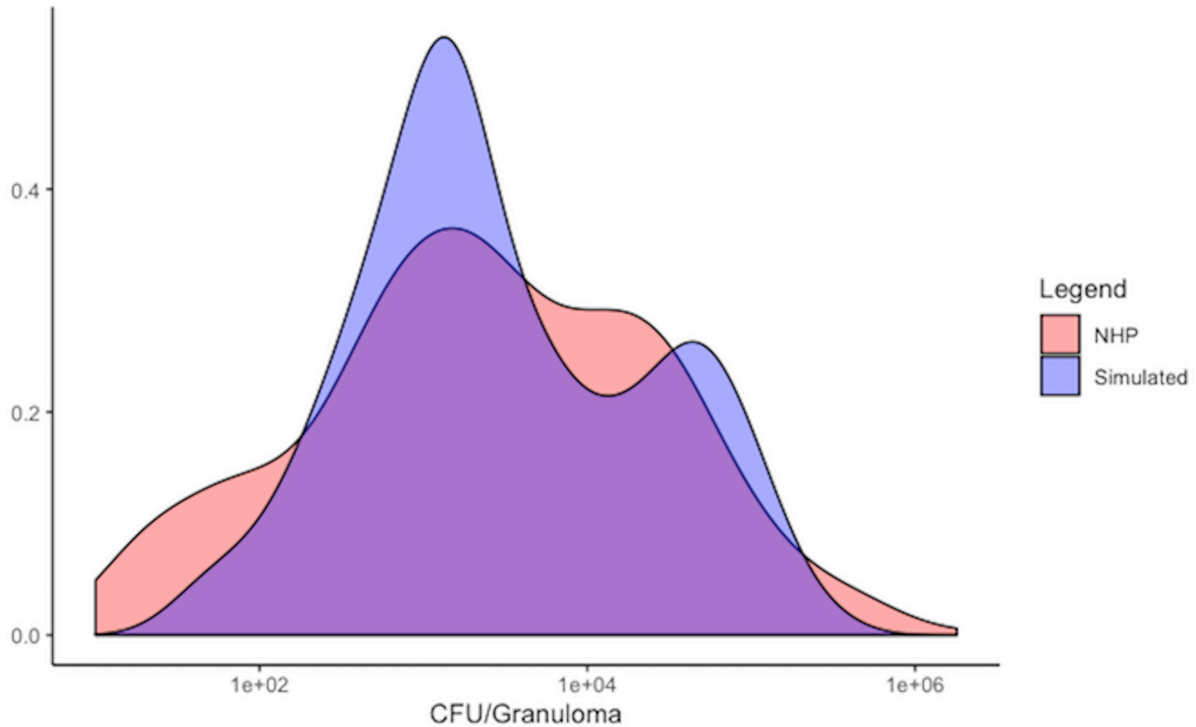
Figure 5.2 Granuloma CFU Distributions
The CFU/granuloma distributions for experimentally measured non-human primate granulomas (red, NHP), and simulated granulomas (blue). The distributions represent CFU/granuloma measurements from 623 granulomas from 38 NHP and 514 simulated granulomas. The NHP granulomas are compiled from numerous studies [37–41], and represent granulomas that came from NHPs at timepoints ranging from 4-17 weeks after infection.
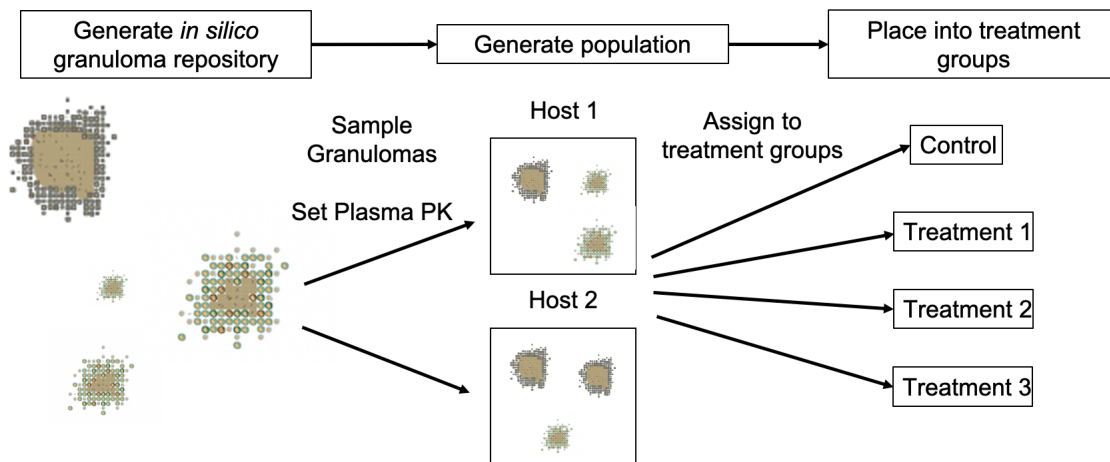
Figure 5.3 Virtual population from in silico granulomas
In silico granulomas are generated by simulating *GranSim* by sampling 500 low-CFU granulomas and 200 high-CFU granulomas based on immune parameter ranges defined in Chapter 2. Granulomas are simulated for 300 days, and then any non-sterilized granulomas are included the granuloma repository. Then, 10 granulomas are sampled with relative probabilities to match CFU/granuloma distributions from non-human primate granulomas. These individual in silico granulomas are then grouped into virtual hosts. Each host is assigned plasma PK parameters to generate PK variability in the virtual population., Finally, hosts are sorted into treatment groups for a virtual clinical trial.

A

B
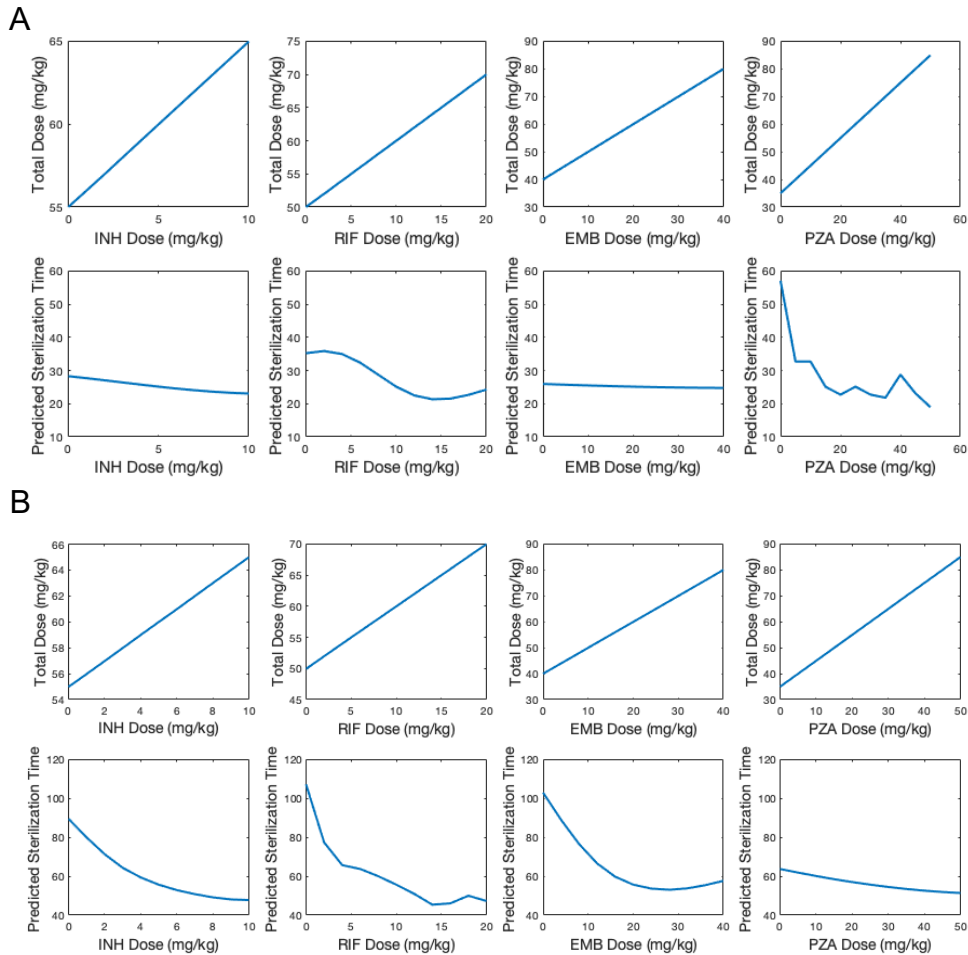
Figure 5.4 Surrogate model predictions
The kriging-based surrogate model predicts the total antibiotic dose and average sterilization time for different regimens as doses vary. While holding every other antibiotic dose constant, the objective function prediction while varying a single antibiotic's dose shows the general relationship between antibiotic dose and objective output. Surrogate model predictions were made based on 60 regimens simulated in 30 granulomas with average PK exposure (A) and low PK exposure (B).

5.3 Results

5.3.1 Pareto-fronts predict potential optimal regimens for average and low plasma concentrations

To identify optimal regimens to test in our virtual clinical trial, there are a number of goals in mind, and they correspond closely with the objective functions used for optimization. The first is to try and find a regimen that decreases the sterilization time, while simultaneously attempting to decrease total antibiotic dose. The other goal is to try and identify a regimen that will perform well with low plasma antibiotic concentrations individuals (referred to as low PK), while not significantly increasing sterilization time or antibiotic dose in average plasma concentrations (referred to as average PK). The

multi-objective optimization problem uses objectives of minimizing both the average granuloma sterilization time and total daily antibiotic dose. To find the optimal doses for the HRZE regimen, we trained the kriging-based surrogate model by initially sampling 40 regimens and adding 20 regimens iteratively resampled. The variables used to define the regimens are the dosages for each antibiotic (total of 4 variables). The optimization algorithm resamples points by maximizing the expected improvement of both objectives and improving the Pareto front (Methods). We performed optimization on 30 granulomas and evaluate the average sterilization time for these 30 granulomas as the first objective function. The second objective function is the sum of the dosage parameters for each antibiotic. HRZE doses are optimized under two different sets of simulations. The first involved optimizing doses on the 30 granulomas with average plasma PK exposure and concentrations. The second was on the same 30 granulomas with plasma low PK concentrations.

Based on the sampled regimens identified through the optimization algorithm, we identify a number of non-dominated solutions on the Pareto front. Figure 5.5 shows the simulated objective function outcome for each sampled regimen, with the non-dominated solutions in red. Additionally, the standard dose simulation is shown for comparison.

For the average PK optimization, the standard regimen is identified as near the predicted Pareto front. This implies that the standard doses are already near optimal for individuals with average PK exposure. At the same time, there are some regimens that appear to provide similar average sterilization times while simultaneously decreasing the overall antibiotic dose. For low PK optimization, the predicted Pareto front pushes further towards lower antibiotic doses and sterilization times than the current regimen with standard doses. This indicates that individuals with low PK exposure may have regimens available that provide shorter average sterilization times while simultaneously allowing for a lower total dose, and that the current regimen may not necessarily be optimal for all individuals.
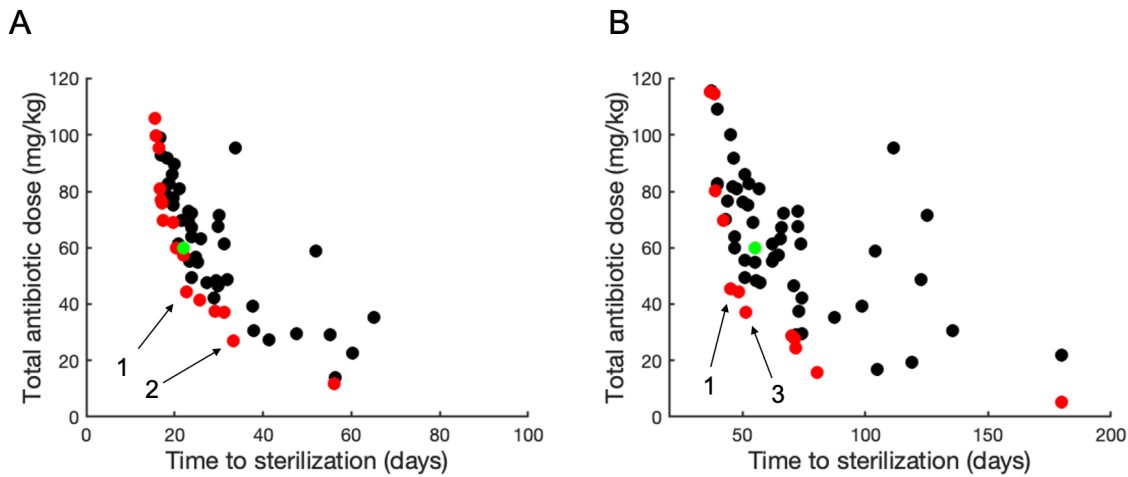
Figure 5.5 Pareto fronts for HRZE dose optimization
Each of the objective function outcomes for the 60 regimens simulated in 30 average PK (A) and low PK (B) granulomas plotted against each other represent the trade-off between the two objectives. Each point represents a given regimen with a unique combination of doses for the four antibiotics: H, R, E and Z. Points in red indicate non-dominated regimens on the predicted Pareto front. The green point is the regimen based on the doses currently used, standardized doses. Potential alternative regimens listed in Table 5.1 are indicated by arrows in the plots.

Based on the Pareto front predictions in Figure 5.5, there are a few regimens that satisfy some of the goals of regimen optimization. These regimens are indicated by arrows on the Pareto front plots, and their doses are listed in Table 5.1. Treatment 1 appears as a regimen in both the average and low PK Pareto fronts. For average PK individuals, Treatment 1 is predicted to slightly decrease the total antibiotic dose while barely affecting the average time to sterilization. For low PK individuals, Treatment 1 is predicted to both decrease the total antibiotic dose and shorten the average time to sterilization. In other words, although the current antibiotic regimen doses are predicted to be suboptimal for low PK individuals, it is possible there is a regimen that is optimal for both average and low PK individuals.

Treatment 2 was selected as another potential regimen of interest. Although it is predicted to sterilize granulomas approximately 10 days slower than the control or Treatment 1, it has a much lower overall antibiotic dose. Treatment 3 was selected because it has low antibiotic doses for all four drugs and is predicted to have roughly equivalent sterilization times compared to Treatment 1 in low PK individuals.

127

Table 5.1 Doses for each regimen identified for the treatment groups, and pointed in the Pareto fronts in Figure 5.5.

	H dose (mg/kg)	R dose (mg/kg)	E dose (mg/kg)	Z dose (mg/kg)
Control	5	10	20	25
Treatment 1	7	15	3	20
Treatment 2	7	9	6	5
Treatment 3	6	18	10	3

5.3.2 Testing optimal regimens at the granuloma scale shows slightly faster sterilization times as compared to the standard HRZE regimen

Using the optimal regimens selected from the Pareto fronts in Figure 5.5 and listed in Table 5.1, we tested the efficacy of each against the control at the granuloma scale. The set of granulomas consisted of the 160 high-CFU granulomas generated for the host library (Methods). To compare efficacy at the granuloma scale, we focused on simulating treatment in these granulomas that would be hardest to treat. We simulated this set of 160 granulomas under three different PK conditions. The first is simulating each granuloma with average PK exposure for every antibiotic. The second is repeating the simulations, but with every antibiotic set to have low PK exposure. The third scenario is simulating the granulomas with each granuloma assigned a variable PK exposure, sampled from the full ranges of plasma PK parameters (Appendix C, Table C.1) to determine whether differences in regimens only exist at certain levels of PK exposure, or if they are detectable within the whole range of PK exposure.

Treatment outcomes, measured as the sterilization time for each granuloma, for each treatment group and PK pairing, are shown in Figure 5.6. We first examined granulomas when average PK parameters were used. None of the identified optimal regimens outperform the control treatment. Treatments 2 and 3 are predicted to have slower sterilization times on average when compared to the control. Treatment 1 and the control treatment generate statistically identical sterilization time distributions. When the

same set of granulomas is simulated with low PK exposure parameters, Treatment 1 shows statistically significant improvement in sterilization time when compared to the control treatment. However, when PK variability is introduced back into the simulations, the results converge on the same distributions as constant average PK, and there is no statistical difference between Treatment 1 and the control. This is unsurprising, since we saw little or no differences in the average and low PK scenarios, but also indicates that differences will likely be small in a virtual population.
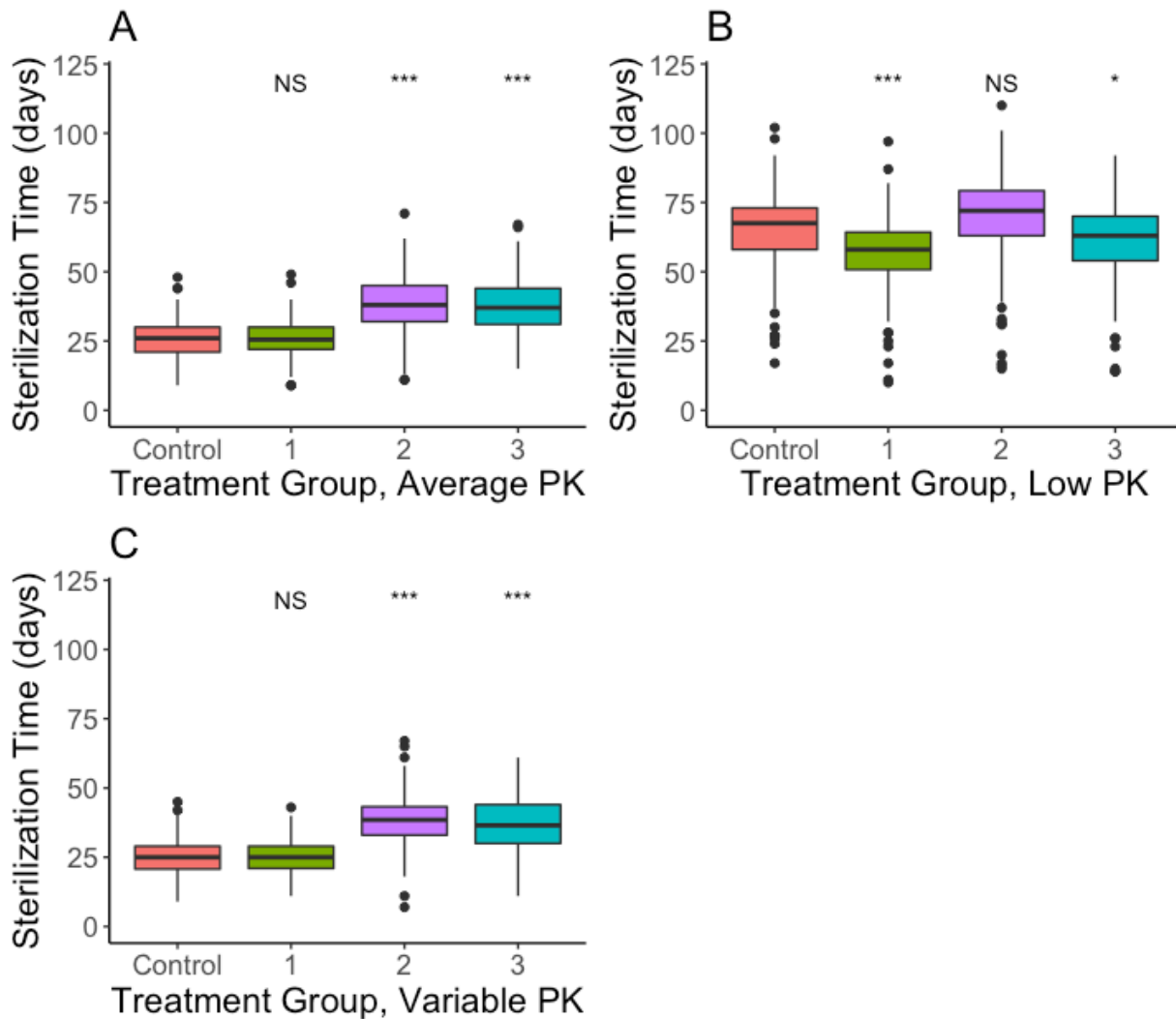
Figure 5.6 Granuloma level outcomes for the optimal treatment regimens
The sterilization time distribution for the set of large, caseous granulomas treated when given average PK (A), low PK (B) and variable PK (C) exposures for all four antibiotics. The treatment groups and numbers refer the treatment regimens defined by the doses listed Table 5.1. Statistical significance between mean sterilization time in each treatment group and the control is determined with a t-test with significance levels labeled above each treatment group (NS $p > 0.01$; * $p < 0.01$; ** $p < 0.001$; *** $p < 0.0001$).

5.3.3 Variability of virtual clinical trials weakens ability to differentiate between regimen efficacies

We observe that the regimens compared at the granuloma scale may show small improvements when compared to the control regimen under low plasma antibiotic concentrations, but that difference is obscured when variability in PK exposure is introduced. Next, we seek to find if any differences in the regimens is detectable in a virtual population when evaluating host sterilization times. Comparing the regimens of Table 5.1 in a virtual clinical trial setting introduces additional sources of variability that exist in a real population, including the heterogeneity of granulomas that exist within and across hosts and the variability in PK exposure for different antibiotics. We generate the virtual hosts and sort them into treatment groups according to Figure 5.3. Because granulomas are grouped into hosts, we use the overall host sterilization time used as the primary outcome for the virtual clinical trial.

Figure 5.7 shows the distribution of host sterilization times for each treatment group regimen. Like the average and variable PK granuloma outcomes in Figure 5.6, Treatment group 1 shows no statistically significant difference when comparing the average sterilization time to the control group. The regimens for VCT treatment groups 2 and 3 show small but statistically significant increases of about 2 days in average host sterilization times as compared to control. Thus, unless hosts with low PK can be identified pre-treatment, the HRZE regimens identified in Table 5.1 do not offer a significant advantage over the standard HRZE regimen.
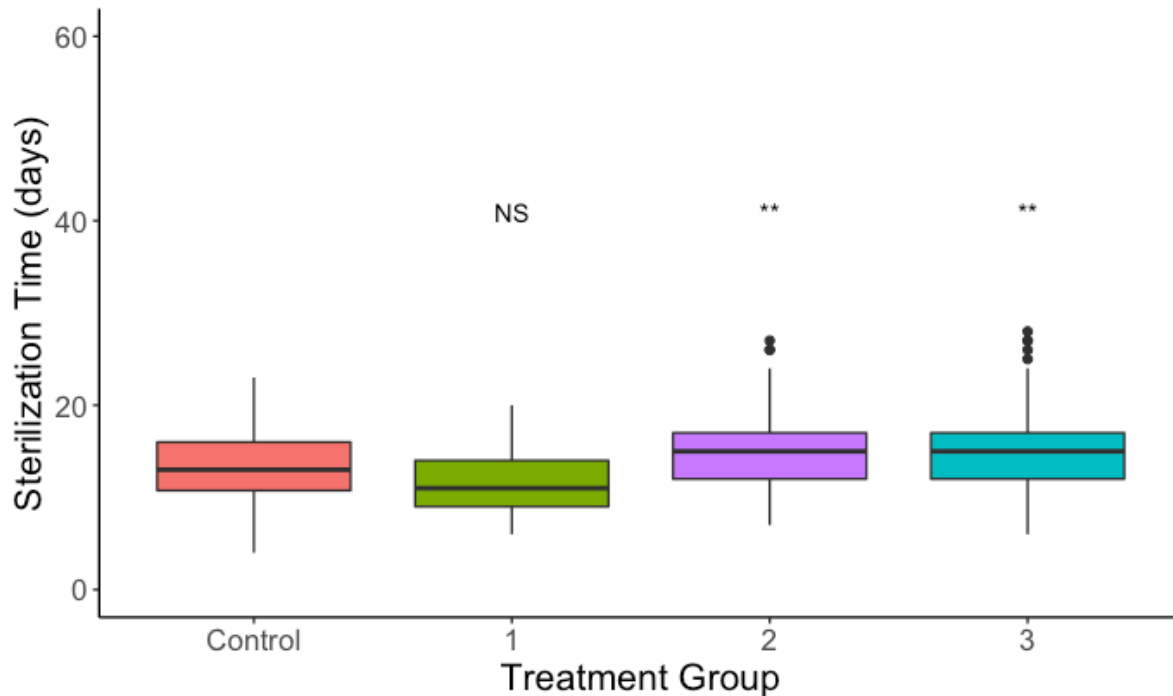
Figure 5.7 Host sterilization time in virtual clinical trial
The host sterilization times in days following treatment start for the control group and each of the three treatment group regimens defined by the doses listed Table 5.1. Treatment groups are given different regimens with varying doses of HRZE, and each group represents the sterilization times from 100 hosts. Statistical significance between mean sterilization time in each treatment group and the control is determined with a t-test with significance levels labeled above each treatment group (NS $p > 0.01$; * $p < 0.01$; ** $p < 0.001$).

5.3.4 Moxifloxacin-containing regimens present an additional alternative to successful treatment of drug-sensitive TB

We next turned to designing better regimens for drug-susceptible TB by using different antibiotics. Fluoroquinolones are frequently prescribed for treating multi-drug resistant TB [17]. A study comparing three fluoroquinolones predicted that moxifloxacin has better and more robust sterilizing activity compared to levofloxacin and gatifloxacin [8]. Substituting isoniazid or rifampin with moxifloxacin has been investigated as a way to potentially shorten treatment, or as an alternative for TB cases with resistance to isoniazid or rifampin. Clinical trials have been conducted to test whether the inclusion of moxifloxacin in place of isoniazid or rifampin could shorten treatment regimens [3,18]. However, many of these clinical trials failed to show an advantage over the HRZE regimen.

We can better understand the results from these clinical trials, and perhaps suggest more fruitful directions for treatment optimization, by simulating these same antibiotic

131

regimens, and predict outcomes to help inform non-human primate (NHP) experiments. To simulate the conditions of NHP treatment, we simulated a set of 334 granulomas for 100 days following infection and treated with three different regimens: HMZE, RMZE, and HRZE. We use doses for each antibiotic with daily administration at the NHP equivalent dose to the human recommended doses: H, 15 mg/kg; R, 20 mg/kg; M, 35 mg/kg; Z, 50 mg/kg; E 55 mg/kg [43]. We calibrated the plasma PK parameters for each antibiotic non-human primate plasma concentrations and doses (see Appendix C for parameters and calibration for M) [7,42]. Figure 5.8 shows the percentage of granulomas sterilized over the course of treatment for each regimen. During the first week, the number of granulomas sterilized is similar for each regimen. After a week of treatment, however, HMZE is only able to sterilize a few more granulomas, and only sterilizes 46% of granulomas after 100 days. In contrast, RMZE and HRZE sterilize all granulomas before 50 days of treatment. Comparing the percentage of granulomas sterilized over time, RMZE and HRZE perform similarly, and RMZE may be a useful alternative in patients with adverse reactions to H or with mono-H resistant TB. We predict HMZE is an inferior regimen on the basis of percentage of sterilized granulomas after 100 days. However, its ability to rapidly sterilize some granulomas early in treatment means that early measurements in clinical trials (such as early bactericidal activity), or short term *in vitro* measurements, could be misleading in predicting its overall efficacy *in vivo*.
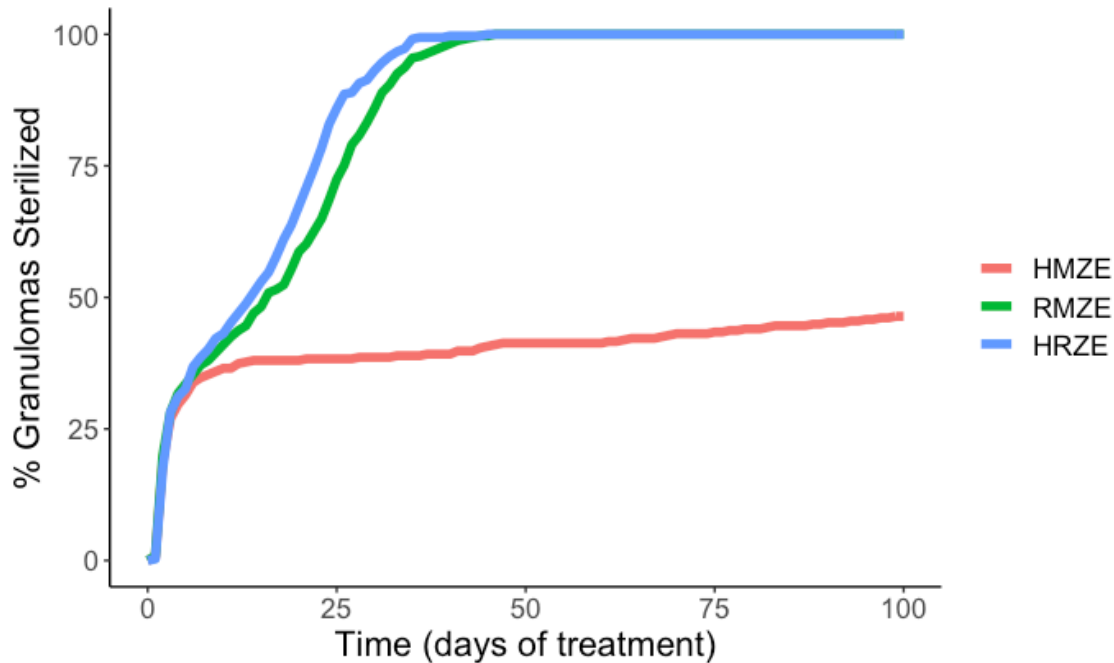
Figure 5.8 NHP treatment moxifloxacin-containing regimens
The percentage of granulomas (n = 334) sterilized over 100 days of treatment for NHP granulomas treated with HMZE, RMZE and HRZE regimens. Panel B shows the boxplot of sterilization times for granulomas that sterilized with 100 days (unsterilized granulomas are excluded) for each regimen.

5.4 Discussion

New drug regimens are desperately needed for TB to combat the long length and side effects of current treatments and to improve efficacy. Successful clinical trials are a requirement for new regimens and treatments to be approved. Generally, the population of interest in clinical trials of new TB regimens is all individuals with TB. However, populations of individuals have varying disease severity, types of granulomas, and PK exposure through varying drug absorption and metabolism/elimination kinetics. The corresponding groups of individuals sampled to represent a population in clinical trials also includes this same heterogeneity. In general, this is useful, because it allows us to ensure the regimen tested is successful in a general population.

In this chapter, we first sought to optimize the doses for HRZE to identify the optimal trade-off between sterilization time and total antibiotic dose. Because *GranSim* is a simulation at the scale of an individual TB granuloma, the optimization algorithm finds optimal doses for granuloma level treatment. But ultimately these regimens need to be successful at the host scale, and then in an entire population. The results presented

address how optimization at the granuloma scale compares to one measure of efficacy (sterilization time) of regimens tested in heterogenous and non-heterogenous populations of both granulomas and hosts.

Looking at the Pareto front predictions, generated from sampled regimens simulated to treat granulomas with average and low PK antibiotic parameters, we see that the standard HRZE regimen is already near optimal and close to the predicted Pareto front for individuals with average PK concentrations (Figure 5.5). However, for individuals with low PK concentrations, the control regimen is further from the Pareto front, and there are a number of potential regimens that could simultaneously decrease overall antibiotic dose and decrease average sterilization time. Selecting three different regimens as potential alternatives to the control regimen and comparing efficacies at the granuloma level, we confirm the predictions from the Pareto front. The control regimen is not outperformed by any treatment, unless it is compared while treating granulomas that have both high CFU and parameters causing low PK exposure. Under average or variable PK conditions, the control regimen is as good or better than the potential alternatives. This trend observed for the average and variable PK granulomas extends to the virtual population. This is unsurprising, because the virtual population has the same amount of PK variability as the granuloma-level comparisons of Figure 5.6.

Although these regimens fail to significantly outperform the standard (control) HRZE regimen regarding average sterilization time, we predicted they both have acceptable levels of efficacy. In particular, Treatment 1 is never statistically worse than the control treatment, whether comparing at the granuloma or host level. While these results do not suggest replacing the standard regimen, they do provide a way of identifying potential regimens that could be used as alternatives. For some of the treatment groups, doses for E and Z are low, and indicate that these could be useful regimens in situations where administration of either of those drugs to a given patient is not advised or not possible. This could be due to existing allergies to the antibiotic, the onset of adverse-drug reactions, or unavailability of the antibiotic.

Another important observation from these results is that the current regimen is already near-optimal. This is not surprising, as although optimization schemes were not performed to determine the regimen, this regimen has undergone extensive research within patients over decades to ensure doses corresponding to appropriate levels of antibiotic to achieve their intended therapeutic effect. Using the Pareto front predictions, we see that the average individual does not have many alternative doses to improve the sterilization time without significantly increasing antibiotic doses. And when comparing efficacies in a heterogenous virtual clinical trial, the control does not get outperformed. If we are to shorten drug-susceptible TB treatment, it will likely require the use of novel antibiotics.

As a potential alternative combination of antibiotics, replacing either isoniazid of rifampin with moxifloxacin has been tested clinically. When comparing the HMZE and RMZE regimens to the preferred HRZE into our simulated non-human primate granulomas, we also confirm that introducing moxifloxacin does not outperform the standard regimen. However, a third regimen, RMZE, sterilizes granulomas at a similar rate as HRZE, and could be a suitable alternative when isoniazid is ineffective, due to resistance or adverse drug reactions.

Although these results do not necessarily identify a regimen that will outperform the currently used regimen, we were able to quickly identify promising alternatives, and potentially a new regimen (Treatment 1) that could improve treatment for individuals with whose own PK parameters lead to lower plasma concentrations. Importantly, using simulations to evaluate optimal doses and combinations of antibiotics provides a rapid and inexpensive way to identify regimens for further testing, and could reduce the resources and number of clinical trials required to develop and approve new antibiotic regimens for TB treatment.

These results also highlight the idea that identifying differences in regimens in a clinical trial setting is difficult when looking at the full heterogeneity of a population. Yet, even if two regimens appear the same on average at the population level, that doesn't mean

they are the same for an individual. That Treatment 1 outperforms the standard regimen in granulomas with low antibiotic exposure indicates that applying personalized medicine to TB treatment could be beneficial. While designing a regimen for every TB patient is not yet feasible, treating different groups of TB patients with different regimens could improve efficacy, reduce side effects, and decrease the TB global burden. In order to do this, we need to identify ways to measure which patients have more severe, complicated TB lesions, and whether they are at risk for low plasma antibiotic concentrations. PET/CT scans can provide a way towards this goal, but the equipment is expensive, so other routes should be tried [39]. Using measurements that evaluate disease severity and pharmacokinetics as requirements for inclusion into a given clinical trial could help to reduce the heterogeneity of the population, allowing a better chance to identify higher efficacy treatments for the subpopulation of interest.

5.5 References

1. Nahid P, Dorman SE, Alipanah N, Barry PM, Brozek JL, Cattamanchi A, et al. Official American Thoracic Society/Centers for Disease Control and Prevention/Infectious Diseases Society of America Clinical Practice Guidelines: Treatment of Drug-Susceptible Tuberculosis. Clin Infect Dis. 2016;63: 853–867. doi:10.1093/cid/ciw566

2. Jindani A, Harrison TS, Nunn AJ, Phillips PPJ, Churchyard GJ, Charalambous S, et al. High-Dose Rifapentine with Moxifloxacin for Pulmonary Tuberculosis. N Engl J Med. 2014;371: 1599–1608. doi:10.1056/NEJMoa1314210

3. Gillespie SH, Crook AM, McHugh TD, Mendel CM, Meredith SK, Murray SR, et al. Four-Month Moxifloxacin-Based Regimens for Drug-Sensitive Tuberculosis. N Engl J Med. 2014;371: 1577–1587. doi:10.1056/NEJMoa1407426

4. Global tuberculosis report 2019. 2019.

5. Ramakrishnan L. Revisiting the role of the granuloma in tuberculosis. Nat Rev Immunol. 2012;12: 352–66. doi:10.1038/nri3211

6. Dartois V. The path of anti-tuberculosis drugs: from blood to lesions to mycobacterial cells. Nat Rev Microbiol. 2014;12: 159–167. doi:10.1038/nrmicro3200

7. Pienaar E, Cilfone NA, Lin PL, Dartois V, Mattila JT, Butler JR, et al. A computational tool integrating host immunity with antibiotic dynamics to study tuberculosis treatment. J Theor Biol. 2015;367: 166–179. doi:10.1016/j.jtbi.2014.11.021

8. Pienaar E, Sarathy J, Prideaux B, Dietzold J, Dartois V, Kirschner DE, et al. Comparing efficacies of moxifloxacin, levofloxacin and gatifloxacin in tuberculosis granulomas using a multi-scale systems pharmacology approach. PLOS Comput Biol. 2017;13. doi:10.1371/journal.pcbi.1005650

9. Merle CS, Fielding K, Sow OB, Gninafon M, Lo MB, Mthiyane T, et al. A Four-Month Gatifloxacin-Containing Regimen for Treating Tuberculosis. N Engl J Med. 2014;371: 1588–1598. doi:10.1056/NEJMoa1315817

10. Sacchettini JC, Rubin EJ, Freundlich JS. Drugs versus bugs: In pursuit of the persistent predator Mycobacterium tuberculosis. Nat Rev Microbiol. 2008;6: 41–52. doi:10.1038/nrmicro1816

11. Sarathy JP, Via LE, Weiner D, Blanc L, Boshoff H, Eugenin EA, et al. Extreme drug tolerance of mycobacterium tuberculosis in Caseum. Antimicrob Agents Chemother. 2018;62: 1–11. doi:10.1128/AAC.02266-17

12. Pasipanodya JG, McIlleron H, Burger A, Wash PA, Smith P, Gumbo T. Serum drug concentrations predictive of pulmonary tuberculosis outcomes. J Infect Dis. 2013;208: 1464–1473. doi:10.1093/infdis/jit352

13. Chang KC, Leung CC, Grosset J, Yew WW. Treatment of tuberculosis and optimal dosing schedules. Thorax. 2011;66: 997–1007. doi:10.1136/thx.2010.148585

14. Cicchese JM, Dartois V, Kirschner DE, Linderman JJ. Both Pharmacokinetic Variability and Granuloma Heterogeneity Impact the Ability of the First-Line Antibiotics to Sterilize Tuberculosis Granulomas. Front Pharmacol. 2020;11: 1–15. doi:10.3389/fphar.2020.00333

15. Pienaar E, Dartois V, Linderman JJ, Kirschner DE. In silico evaluation and

exploration of antibiotic tuberculosis treatment regimens. BMC Syst Biol. 2015;9: 1–12. doi:10.1186/s12918-015-0221-8

16. Cicchese JM, Pienaar E, Kirschner DE, Linderman JJ. Applying Optimization Algorithms to Tuberculosis Antibiotic Treatment Regimens. Cell Mol Bioeng. 2017;10: 523–535. doi:10.1007/s12195-017-0507-6

17. Nahid P, Mase SR, Migliori GB, Sotgiu G, Bothamley GH, Brozek JL, et al. Treatment of drug-resistant tuberculosis. An official ATS/CDC/ERS/IDSA clinical practice guideline. American Journal of Respiratory and Critical Care Medicine. 2019. doi:10.1164/rccm.201909-1874ST

18. Pranger AD, van der Werf TS, Kosterink JGW, Alffenaar JWC. The Role of Fluoroquinolones in the Treatment of Tuberculosis in 2019. Drugs. 2019;79: 161–171. doi:10.1007/s40265-018-1043-y

19. Segovia-Juarez JL, Ganguli S, Kirschner D. Identifying control mechanisms of granuloma formation during M. tuberculosis infection using an agent-based model. J Theor Biol. 2004;231: 357–376. doi:10.1016/j.jtbi.2004.06.031

20. Ray JCJ, Flynn JL, Kirschner DE. Synergy between individual TNF-dependent functions determines granuloma performance for controlling Mycobacterium tuberculosis infection. J Immunol. 2009;812: 3706–37017. doi:10.4049/jimmunol.0802297

21. Fallahi-Sichani M, El-Kebir M, Marino S, Kirschner DE, Linderman JJ. Multiscale computational modeling reveals a critical role for TNF-α receptor 1 dynamics in tuberculosis granuloma formation. J Immunol. 2011;186: 3472–3483. doi:10.4049/jimmunol.1003299

22. Cilfone NA, Perry CR, Kirschner DE, Linderman JJ. Multi-scale modeling predicts a balance of tumor necrosis factor-a and interleukin-10 controls the granuloma environment during Mycobacterium truberculosis infection. PLoS One. 2013;8: e68680. doi:10.1371/journal.pone.0068680

23. Kjellsson MC, Via LE, Goh A, Weiner D, Low KM, Kern S, et al. Pharmacokinetic evaluation of the penetration of antituberculosis agents in rabbit pulmonary lesions. Antimicrob Agents Chemother. 2012;56: 446–457. doi:10.1128/AAC.05208-11

24. Prideaux B, Via LE, Zimmerman MD, Eum S, Sarathy J, O'Brien P, et al. The association between sterilizing activity and drug distribution into tuberculosis lesions. Nat Med. 2015;21: 1223–7. doi:10.1038/nm.3937

25. Cilfone NA, Kirschner DE, Linderman JJ. Strategies for Efficient Numerical Implementation of Hybrid Multi-scale Agent-Based Models to Describe Biological Systems. Cell Mol Bioeng. 2015;8: 119–136. doi:10.1007/s12195-014-0363-6

26. Ankomah P, Levin BR. Two-drug antimicrobial chemotherapy: A mathematical model and experiments with Mycobacterium marinum. PLoS Pathog. 2012;8. doi:10.1371/journal.ppat.1002487

27. Cokol M, Li C, Chandrasekaran S. Chemogenomic model identifies synergistic drug combinations robust to the pathogen microenvironment. PLoS Comput Biol. 2018;14: 1–24. doi:10.1371/journal.pcbi.1006677

28. Chandrasekaran S. Predicting Drug Interactions From Chemogenomics Using INDIGO. Systems Chemical Biology Methods in Molecular Biology. 2019. pp. 219–231.

29. Akhtar T, Shoemaker CA. Multi objective optimization of computationally expensive multi-modal functions with RBF surrogates and multi-rule selection. J Glob Optim. 2016;64: 17–32. doi:10.1007/s10898-015-0270-y

30. Sóbester A, Forrester AIJ, Toal DJJ, Tresidder E, Tucker S. Engineering design applications of surrogate-assisted optimization techniques. Optim Eng. 2014;15: 243–265. doi:10.1007/s11081-012-9199-x

31. Forrester AIJ, Sóbester A, Keane AJ. Engineering Design via Surrogate Modelling: A Practical Guide. John Wiley & Sons; 2008.

32. McKay AMD, Beckman RJ, Conover WJ. A Comparison of Three Methods for Selecting Values of Input Variables in the Analysis of Output from a Computer Code. Technometrics. 1979;21: 239–245. doi:doi:10.2307/1268522

33. Jones DR, Schonlau M, William J. Efficient Global Optimization of Expensive Black-Box Functions. J Glob Optim. 1998;13: 455–492. doi:10.1023/a:1008306431147

34. Keane AJ. Statistical improvement criteria for use in multiobjective design optimization. AIAA J. 2006;44: 879–891. doi:10.2514/1.16875

35. Bao C, Xu L, Goodman ED, Cao L. A novel non-dominated sorting algorithm for evolutionary multi-objective optimization. J Comput Sci. 2017;23: 31–43. doi:10.1016/j.jocs.2017.09.015

36. Lin PL, Rodgers M, Smith L, Bigbee M, Myers A, Bigbee C, et al. Quantitative comparison of active and latent tuberculosis in the cynomolgus macaque model. Infect Immun. 2009;77: 4631–4642. doi:10.1128/IAI.00592-09

37. Marino S, Gideon HP, Gong C, Mankad S, McCrone JT, Lin PL, et al. Computational and Empirical Studies Predict Mycobacterium tuberculosis-Specific T Cells as a Biomarker for Infection Outcome. PLoS Comput Biol. 2016;12: 1–30. doi:10.1371/journal.pcbi.1004804

38. Gideon HP, Phuah J, Myers AJ, Bryson BD, Rodgers MA, Coleman MT, et al. Variability in tuberculosis granuloma T cell responses exists, but a balance of pro- and anti-inflammatory cytokines is associated with sterilization. PLoS Pathog. 2015;11. doi:10.1371/journal.ppat.1004603

39. Lin PL, Coleman T, Carney JPJ, Lopresti BJ, Tomko J, Fillmore D, et al. Radiologic responses in cynomolgus macaques for assessing tuberculosis chemotherapy regimens. Antimicrob Agents Chemother. 2013;57: 4237–4244. doi:10.1128/AAC.00277-13

40. Cadena AM, Hopkins FF, Maiello P, Carey AF, Wong EA, Martin CJ, et al. Concurrent infection with Mycobacterium tuberculosis confers robust protection against secondary infection in macaques. PLoS Pathog. 2018;14: 1–17. doi:10.1371/journal.ppat.1007305

41. Darrah PA, DiFazio RM, Maiello P, Gideon HP, Myers AJ, Rodgers MA, et al. Boosting BCG with proteins or rAd5 does not enhance protection against tuberculosis in rhesus macaques. npj Vaccines. 2019;4. doi:10.1038/s41541-019-0113-9

42. Wessler T, Joslyn LR, Jacob Borish H, Gideon HP, Flynn JAL, Kirschner DE, et al. A computational model tracks whole-lung Mycobacterium tuberculosis infection and predicts factors that inhibit dissemination. PLoS Comput Biol. 2020;16: 1–25. doi:10.1371/journal.pcbi.1007280

43. Lin PL, Dartois V, Johnston PJ, Janssen C, Via L, Goodwin MB, et al. Metronidazole prevents reactivation of latent Mycobacterium tuberculosis infection in macaques. Proc Natl Acad Sci. 2012;109: 14188–14193. doi:10.1073/pnas.1121497109

Chapter 6 Conclusions

6.1 Summary of research findings

Improving antibiotic treatment for tuberculosis (TB) could help to significantly decrease global TB deaths and disease burden. Caused by the pathogen *Mycobacterium tuberculosis* (Mtb), lesions in the lungs called granulomas form in response to infection with Mtb. Because variability in plasma pharmacokinetics (PK) and granuloma heterogeneity impact antibiotic distribution in granulomas and overall regimen efficacy, considering these aspects in new antibiotic regimen design is critical. This thesis presents methodologies for modeling antibiotic treatment and predicting regimen efficacy and optimal regimens. This work presents a method of incorporating and modeling the variability observed in antibiotic concentrations into PK models, the heterogeneity of granulomas, and drug-drug interactions to predict antibiotic regimen efficacy. Using *GranSim*, our computational model of granuloma formation and function, we can apply optimization algorithms to predict optimal antibiotic doses and compare different regimens from the granuloma to population scales.

6.1.1 Integrating plasma pharmacokinetic variability into granuloma-level pharmacokinetics

Natural variability in the population in how individuals absorb, distribute and eliminate antibiotics from the body impacts antibiotic concentrations in the granuloma. Incorporating this PK variability into computational models of TB treatment is necessary for accurate predictions of antibiotic distributions in granulomas and regimen efficacies. Because the source of PK variability occurs at the host scale, when calibrating tissue specific PK parameters to experimentally measured granuloma concentrations, this variability must be accounted for. In Chapter 2, we present a process of utilizing *GranSim* to calibrate antibiotic tissue PK parameters based on average granuloma concentrations. By appropriately accounting for this variability, and accurately

141

calibrating the tissue PK parameters, we can recreate the qualitative distributions of antibiotics in granulomas.

6.1.2 Modeling the effect of drug-drug interactions on antibiotic killing rates

Drug-drug interactions can play an important role in selecting the best combination of drugs for treatment. With TB antibiotics, the fractional inhibitory concentration (FIC), is a commonly used measurement to evaluate the strength of the synergistic or antagonistic interaction [1]. In Chapter 3, we develop a model for integrating the FIC for a combination of antibiotics into our PD model by defining an effective concentration that incorporates the contribution of each antibiotic and adjusts the effective concentration according to the strength of the interaction. This adjustment in the effective concentration results in a consequent increase or decrease in the antibiotic killing rate constant. Using this model, we can efficiently simulate a large number of antibiotic combinations and measure the effect that drug-drug interactions have on antibiotic killing rates and overall granuloma sterilization. This model has the important characteristic that the strength of the interaction weakens when antibiotic concentrations are uneven (e.g. when one antibiotic has a much higher concentration than the others). Because of this, we can predict the actual *in vivo* effect of the drug-drug interaction on the antibiotic killing rate.

6.1.3 Defining improving antibiotic regimens as an optimization problem

With the incorporation of PK variability, granuloma heterogeneity, and drug-drug interactions into a computational model, we can predict the efficacy of a given regimen at the granuloma scale. But with this model, how do we find optimal regimens, when defining a regimen by its antibiotic dose and dosing frequency, in the high dimensional regimen design space? Evolutionary algorithms are powerful in finding global optima in high dimensional spaces, even in multi-modal functions with numerous local optima. However, they sample the design space inefficiently, and require the iterative evolution of populations of samples that make their limit their use when optimizing computationally expensive functions. Surrogate-assisted optimization is a class of alternative algorithms that allows for efficient exploration of the design space and accurate prediction of objective function values and optima. Surrogate-assisted

optimization algorithms may not be as useful at predicting and optimizing over multi-modal, rapidly changing surfaces, but they can be useful in predicting optimal regimens. The relationship between the variables describing regimens and their objective functions are frequently simple surfaces, often monotonically increasing or decreasing.

In Chapter 4, we show that we can use surrogate-assisted optimization to predict regimens that still maintain clinical relevance [2]. We can improve the accuracy of predicting objective functions using surrogate models by adding resampling schemes and resampling the design space in regions that either have high levels of uncertainty, or by sampling areas with higher probabilities of containing global optima [3]. Additionally, by using a multi-objective optimization scheme, we can compare two competing objectives without imposing a weight on those objectives. In this way, we can identify the optimal trade-off between the objectives. In other words, we can identify the point when increasing antibiotic dose no longer results in a decrease in sterilization time.

6.1.4 Variability in pharmacokinetics and granuloma heterogeneity impact granuloma sterilization

With an antibiotic regimen such as the standard therapy for drug-susceptible TB that has a relatively high level of success when treating disease, understanding the mechanisms and conditions of failure is important to understanding how to improve efficacy. Based on the results presented in Chapter 2, it is clear that natural variability in the population regarding how antibiotics are absorbed, distributed, and eliminated from the body can create conditions of treatment failure. Currently used regimens are successful for the average individual, but still fail to cure TB in some individuals. When parameters causing low antibiotic concentrations in plasma are paired with high bacterial burden, and lesions that inhibit antibiotic diffusion and accumulation, we show that these create conditions where granulomas fail to sterilize. The results of Chapter 2 reinforce another important concept in TB treatment. Antibiotics can distribute differently in a granuloma, and will complement each when given in combination, by accumulating in different regions of the granuloma and having different levels of bactericidal activity against different subpopulations of Mtb [4].

6.1.5 Antibiotic concentrations in granulomas impact the strength of synergistic and antagonistic antibiotic combinations

Specialization in the spatial distributions of antibiotics is not the only way that antibiotics given in combination can complement each other. Drug-drug interactions between antibiotics can also generate synergistic and antagonistic interactions that produce higher or lower levels of bactericidal activity, especially when observed *in vitro*. However, are these same interactions observed in a granuloma, and do they impact sterilizing ability? A relationship exists between the fractional inhibitory concentration of a combination of antibiotics and its observed clinical efficacy [5], but does not completely explain the efficacy of all antibiotic combinations. In Chapter 3, we show that by using computational modeling to measure the real impact these drug interactions have on the antibiotic killing rate constant, based on predicted *in vivo* concentrations of the antibiotics, we generate a much stronger predictor of *in vivo* efficacy. This is an important finding because some combinations that are strongly antagonistic interactions *in vitro* could still be efficacious regimens. And similarly, a strong synergistic interaction is not enough to result in highly efficacious regimen.

6.1.6 Predicting optimal regimens in a virtual population

In Chapter 5, we use a multi-objective, surrogate-assisted optimization scheme to optimize the doses for the four first-line TB antibiotics: isoniazid, rifampin, pyrazinamide and ethambutol. We optimize these doses for granulomas with different levels of antibiotic concentrations in plasma. We find that the currently used doses are near-optimal for the four first-line antibiotics when they are able to achieve average levels of concentration in plasma and the granuloma. However, we predict that granulomas simulated with low plasma antibiotic concentrations have alternative regimens with higher levels of efficacy, while also allowing for lower overall doses of antibiotics. This indicates that there may be alternative regimens that improve treatment in individuals with pharmacokinetics that result in low plasma antibiotic concentrations. This result is connected to our findings in Chapter 2, where we observe that PK variability can create conditions that result in granulomas that fail to sterilize with antibiotic treatment. Using computational modeling, coupled with surrogate-assisted optimization algorithms, we

predict there may be alternative doses that can improve treatment under these conditions. However, performing clinical trials to detect the differences between alternative regimens in a diverse population may be difficult. We show that when these regimens are tested in a virtual clinical trial accounting for the range of PK variability and granuloma heterogeneity, alternative regimens only show equal sterilization rates when compared to the control regimen consisting of the currently recommended doses.

6.2 Future directions

Computational modeling of in-host dynamics of Mtb infection and immune response in TB disease has made numerous contributions to the field from studying immunological mechanisms, analyzing disease progression, and simulating antibiotic treatment [6]. Certainly, computational modeling is a long way from completely replacing these experimental alternatives, but computational modeling can provide a vital role in accelerating experimental research by predicting promising routes and helping to avoid investing in failed therapies. The continual advancement of these models to include additional features can improve their ability to recapitulate the behavior in the biological system. In terms of modeling work presented in this thesis, this could include simulating more complex lesion types, improving pharmacodynamic models, and modeling new antibiotics and therapies. Adding new objectives when optimizing antibiotic regimens can diversify the types of optimal regimens identified and improve treatment in a diverse population.

6.2.1 Improvements to GranSim

There are three improvements to *GranSim* that could further improve its ability to describe and predict antibiotic efficacy. First, the simulations we present in this work do not explicitly include fibrosis, the depositing of connective tissue such as collagen during pathological would healing, although *GranSim* has been used to simulate fibrosis [7]. Fibrotic granulomas are often associated with healing granulomas and fibrosis frequently arises with antibiotic treatment [8–10]. This could present an even more impermeable barrier to diffusion than the cells within a granuloma alone. Fibrosis is potentially an important part of why drug treatment takes so long and can fail to sterilize

145

granulomas. As the granuloma starts to heal, it may wall off remaining Mtb, limiting antibiotic diffusion to those regions. Second, cavitation is another pathological manifestation of TB disease that is related to more severe disease and higher rates of treatment failure and formation of resistance, and occurs when the granuloma structure begins to degrade and liquify, forming cavities in the lungs [11–14]. Modeling how Mtb persist in cavity walls, and the pharmacokinetics of cavities, would provide another potentially critical understanding of how treatments fail. Third, while we have addressed TB mostly as a pulmonary disease, existing in granulomas in the lungs, extrapulmonary involvement is not uncommon [15]. In particular, granuloma formation and involvement in lymph nodes in macaques is associated with more severe disease and dissemination events [16,17]. Extending plasma PK models to include a lymph node compartment that receives antibiotic from peripheral tissue and adds antibiotic back into a plasma compartment would provide an organ-level prediction of antibiotic concentration in lymph nodes. Within the lymph, the same tissue PK phenomena that govern antibiotic distribution in lungs and granulomas could be used to describe the distribution of antibiotics in lymph node granulomas. Because granulomas in lymph nodes tend to have limited ability to kill Mtb and often associated with higher Mtb burden in non-human primate models [16,18], modeling lymph node treatment could increase our understanding of TB treatment failure and inform better regimen design.

6.2.2 Improvements to the pharmacodynamic model
The relationship between antibiotic concentration and pharmacodynamic effect is critical to determining antibiotic treatment efficacy. In this thesis, we utilize a Hill curve to describe this effect, which is a widely used model to describe the pharmacodynamics of therapeutic agents, and in this research describes the relationship between antibiotic concentration and the killing rate constant [19–21]. However, there are often distinct concentration levels that exhibit bacteriostatic and bactericidal effect of TB antibiotics [22]. Capturing the pharmacodynamic effect of both growth inhibition and bactericidal effects could enhance the ability to predict an antibiotic regimen's efficacy. Because *GranSim* already includes the bactericidal effect with the Hill curve, a potential option for modeling growth inhibition would involve utilizing another Hill curve that evaluates the

reduction in Mtb growth rate. This bacteriostatic function could evaluate how much the growth rate decreases as a function of the concentration, with parameters influenced by minimum inhibitory concentration measurements [22]. Because non-replicating Mtb are typically more tolerant to a variety of antibiotics [23], a potential consequence of introducing this bacteriostatic effect would result in lower overall killing activity when one antibiotic is exhibiting a bacteriostatic effect. The ability to simulate the conditions when this phenomenon occurs could improve our ability to predict regimens that have higher risks of treatment failure.

The drug-drug interactions modeled in Chapter 3 use fractional inhibitory concentrations that are constant for the given combination of antibiotics. However, the conditions within a granuloma, and the microenvironments that impact bacterial metabolism and phenotypic state can also impact the synergistic or antagonistic interactions [24]. *GranSim* is well suited to accommodate these changes in interactions due to microenvironments, through either course-grained representation based on variable growth rate of Mtb in the model, or fine-grained calculation of the metabolites and nutrients in a granuloma [25]. Introducing these environment dependent interactions would improve *GranSim's* ability to predict how drug interactions impact sterilization rate and regimen efficacy.

6.2.3 Host-directed therapies

Many pathological characteristics of TB disease are caused by the body's own immune response. Host-directed therapies that modulate immune responses could limit harmful inflammation or improve the efficacy of antibiotic therapy. The formation of the granuloma, and consequent tissue damage, are mostly dictated by the level and control of the inflammatory responses, and a proper balance between pro- and anti-inflammatory responses is necessary for granuloma maintenance [26–28]. Modulating the immune response can alter the progression of TB disease. For example, anti-TNF therapies (such as those given for the treatment of rheumatoid arthritis) can result in reactivation of latent infections [29–31]. Studies in non-human primates suggest there may be some host-directed therapies that could be beneficial in improving responses to

drug treatment. Neutralization of IL-10 in non-human primates during Mtb infection does not change overall disease outcomes compared to untreated non-human primates, but results in immunologically different granulomas that could potentially impact antibiotic activity [32]. The use of IL-1 receptor antagonists together with linezolid treatment in non-human primates is a potential host-directed therapy to reduce linezolid toxicity and reduce TB-associated inflammation in the lungs [33]. If the granuloma is the product of an immune response, can we discover additional ways to modulate the immune response to adjust the structure of the granuloma, and improve antibiotic accumulation in granulomas? Or is it possible that relieving some of the immune pressure can shift Mtb out of a phenotypic state that is more tolerant to antibiotics to a state where that is more susceptible? Potential host-directed therapies could prove useful in conjunction with antibiotics, but the inflammatory balance that is required to maintain a granuloma and control Mtb infection is delicate, and there is potential for these therapies to do more harm than good.

6.2.4 Additional antibiotics to simulate new regimens
The antibiotics studied in this work included the four-first line antibiotics (isoniazid, rifampin, ethambutol, and pyrazinamide), and the fluoroquinolones moxifloxacin and levofloxacin. However, there are numerous other antibiotics in the TB drug pipeline that would be useful introductions into the model. Perhaps the most exciting antibiotics are included in the Nix-TB, or BPaL regimen, consisting of bedaquiline, pretomanid, and linezolid. Each of these are newer antibiotics that have shown success in clinical trials at reducing the treatment duration of extensively drug resistant TB (XDR-TB) from 24 months to 6 months [34]. Bedaquiline is a diarylquinoline that is highly active against replicating and non-replicating bacterial population [35], and has promise in being a useful antibiotic in treating TB despite its high caseum binding fraction and limited transport into caseous lesions [36]. Linezolid is a potent antibiotic, but has many associated toxicities, particularly bone marrow suppression. A recent study showed that co-administration of IL-1 receptor antagonistic could reduce inflammation and linezolid associated toxicity [33]. While these are some of the most exciting drugs that have made it through the gauntlet of studies to clinical testing clinically, there are many other

candidates in the pipeline [37,38]. Modeling new antibiotics as they are being developed gives another tool in identifying the best regimens and identify the best experiments and trails to conduct when investigating new regimens.

6.2.5 New objectives for optimization and regimen evaluation
Using alternative objectives to evaluate and optimize antibiotic regimens would provide additional treatment options that can achieve different goals. Considering other events during TB treatment, such as antibiotic toxicity and the formation of resistant Mtb could be additional objectives to consider in regimen optimization. Evaluating regimens based on the time required to sterilize a granuloma or host, as implemented here, is a logical choice. Not only does faster sterilization mean that one is less likely to fail to completely sterilize and relapse, but it also means that treatment durations could potentially shorten. Balancing sterilization time with total antibiotic dose is necessary, because minimizing sterilization time would only result in an optimization algorithm finding the highest allowable dose of antibiotic. Minimizing toxicity is an important objective and related to antibiotic dose. As toxicity and adverse drug reactions occur in TB treatment, patient adherence and regimen efficacy decrease [39]. Designing a regimen that minimizes the frequency or probability of adverse-drug reactions could be beneficial at increasing overall treatment success rates. Measuring and modeling toxicity, either through the explicit modeling of toxic antibiotic metabolites, or by relating long-term drug exposure to risk of adverse-drug events, would be a useful objective [40,41].

An additional objective could be minimizing the risk of resistance development. Antibiotic resistance is a very concerning aspect of TB treatment [42,43]. Although the simulations presented in this thesis did not involve any resistant Mtb, it is a functionality built into our model for isoniazid and rifampin, and has been used to study the emergence and treatment of resistant Mtb [44]. The ability to simulate the spatial distribution of antibiotics in granulomas is so important in evaluating resistance risk. Even if average granuloma concentrations are above concentrations that could reduce development of resistant Mtb [45], the distribution of certain antibiotics may create microenvironments that meet the criteria for resistance selection. Sub-therapeutic

concentrations have the potential to promote resistance [46]. Measuring the amount of time Mtb spend at concentrations that pose higher risks of resistance formation could be an additional objective to minimize. Minimizing the risk of resistance would allow for the selection of optimal regimens that are good at sterilizing granulomas, but also mitigate the growing threat of rising antibiotic resistance in TB disease.

6.2.6 Improving therapy in a heterogeneous population
Modern research in medicine and health sciences has promoted the idea of personalized medicine [47]. Understanding the specifics of an individual's disease, whether it is a specific type of mutation in cancerous tissue or the severity of the disease, could allow physicians to design a treatment course specific to that individual. Many findings in this thesis would support the role of personalized medicine for TB treatment. If PK variability is important in determining treatment success and changing doses could create regimens that are more optimal for people with low levels of plasma antibiotic concentrations, tailoring a regimen to that individual has the potential for being the best option.

However, applying personalized medicine in practice has a couple of major limitations. The first is that each individual requires attention from medical professionals, and those medical professionals need to spend the time and resources to evaluate the personalized regimen for that patient. Given the global scale, and prevalence in low-resource regions of our world, this type of personalized attention is not feasible. The second limitation is that personalized medicine requires some type of biomarker that is easily measured, so we would need biomarkers predictive of disease progression, reactivation, and treatment success [48].

A more realistic approach to applying personalized medicine in TB treatment would be using a stratified approach. Stratified medicine involves treating subgroups of patients similarly, depending on some characteristic of their disease [49]. Based on the findings of this work, those groups could stratify based on average PK exposure versus low PK exposure, or complex TB lesions versus smaller granulomas. Again, a barrier to

implementing stratified medicine in the clinic is determining the metrics with which to stratify the patients. Advancing our ability to determine the prognosis of TB patients and monitor antibiotic concentrations through already used diagnostics and tests, such as chest X-rays, sputum cultures, time to positivity measurements, and drug sensitivity tests could all be pieces of information with which to stratify individuals [50]. The required research pipeline to realize the clinical application of stratified medicine techniques involves identifying easily measurable metrics through which to stratify patients, followed by clinical testing and monitoring of programs that utilize these methods.

Designing better antibiotic regimens for TB treatment should involve ensuring that the antibiotic regimen is efficacious for all individuals. Whether its designing one regimen that works for an entire heterogenous population, or finding regimens that work best in stratified groups, using computational modeling can help to design these regimens. Representing the complexity in the immune response, disease progression, and treatment with a computational model can help us to understand the underlying mechanisms that determine regimen efficacy. Through the use of optimization algorithms to screen new antibiotic combinations and doses, we can identify the trade-off between different objectives when designing antibiotic regimens and use this information to tailor new regimens to specific groups of TB patients.

6.3 References

1. Cokol M, Kuru N, Bicak E, Larkins-Ford J, Aldridge BB. Efficient measurement and factorization of high-order drug interactions in Mycobacterium tuberculosis. Sci Adv. 2017;3: e1701881. doi:10.1126/sciadv.1701881

2. Cicchese JM, Pienaar E, Kirschner DE, Linderman JJ. Applying Optimization Algorithms to Tuberculosis Antibiotic Treatment Regimens. Cell Mol Bioeng. 2017;10: 523–535. doi:10.1007/s12195-017-0507-6

3. Forrester AIJ, Sóbester A, Keane AJ. Engineering Design via Surrogate Modelling: A Practical Guide. John Wiley & Sons; 2008.

4. Cicchese JM, Dartois V, Kirschner DE, Linderman JJ. Both Pharmacokinetic Variability and Granuloma Heterogeneity Impact the Ability of the First-Line Antibiotics to Sterilize Tuberculosis Granulomas. Front Pharmacol. 2020;11: 1–15. doi:10.3389/fphar.2020.00333

5. Ma S, Jaipalli S, Larkins-Ford J, Lohmiller J, Aldridge BB, Sherman DR, et al. Transcriptomic signatures predict regulators of drug synergy and clinical regimen efficacy against tuberculosis. MBio. 2019;10: 1–16. doi:10.1128/mBio.02627-19

6. Kirschner D, Pienaar E, Marino S, Linderman JJ. A review of computational and mathematical modeling contributions to our understanding of Mycobacterium tuberculosis within-host infection and treatment. Curr Opin Syst Biol. 2017;3: 170–185. doi:10.1016/j.coisb.2017.05.014

7. Warsinske HC, DiFazio RM, Linderman JJ, Flynn JL, Kirschner DE. Identifying mechanisms driving formation of granuloma-associated fibrosis during Mycobacterium tuberculosis infection. J Theor Biol. 2017;429: 1–17. doi:10.1016/j.jtbi.2017.06.017.Identifying

8. Dheda K, Booth H, Huggett JF, Johnson MA, Zumla A, Rook GAW. Lung remodeling in pulmonary tuberculosis. J Infect Dis. 2005;192: 1201–1210. doi:10.1086/444545

9. Difazio RM, Mattila JT, Klein EC, Cirrincione LR, Howard M, Wong EA, et al. Active transforming growth factor-β is associated with phenotypic changes in granulomas after drug treatment in pulmonary tuberculosis. Fibrogenesis Tissue Repair. 2016;24: 1–11. doi:10.1186/s13069-016-0043-3

10. Gil O, Díaz I, Vilaplana C, Tapia G, Díaz J, Fort M, et al. Granuloma encapsulation is a key factor for containing tuberculosis infection in minipigs. PLoS One. 2010;5: e10030. doi:10.1371/journal.pone.0010030

11. Kempker RR, Heinrichs TM, Nikolaishvili K, Sabulua I, Bablishvili N, Gogishbili S, et al. Lung Tissue Concentrations of Pyrazinamide among Patients with Tuberculosis. Antimicrob Agents Chemother. 2017;61: 1–11. doi:10.1128/AAC.00226-17

12. Chatterjee A, D'Souza D, Vira T, Bamne A, Ambe GT, Nicol MP, et al. Strains of Mycobacterium tuberculosis from Western Maharashtra, India, exhibit a high degree of diversity and strain-specific associations with drug resistance, cavitary disease, and treatment failure. J Clin Microbiol. 2010;48: 3593–3599. doi:10.1128/JCM.00430-10

13. Ong CWM, Elkington PT, Friedland JS. Tuberculosis, pulmonary cavitation, and matrix metalloproteinases. Am J Respir Crit Care Med. 2014;190: 9–18. doi:10.1164/rccm.201311-2106PP

14. Converse PJ, Dannenberg AM, Estep JE, Sugisaki K, Abe Y, Schofield BH, et al. Cavitary Tuberculosis Produced in Rabbits by Aerosolized Virulent Tubercle Bacilli. Infect Immun. 1996;64: 4776–4787.
15. Lee JY. Diagnosis and treatment of extrapulmonary tuberculosis. Tuberc Respir Dis (Seoul). 2015;78: 47–55. doi:10.4046/trd.2015.78.2.47
16. Ganchua SKC, Cadena AM, Maiello P, Gideon HP, Myers AJ, Junecko BF, et al. Lymph nodes are sites of prolonged bacterial persistence during Mycobacterium tuberculosis infection in macaques. PLoS Pathog. 2018;14: 1–28. doi:10.1371/journal.ppat.1007337
17. Maiello P, DiFazio RM, Cadena AM, Rodgers MA, Lin PL, Scanga CA, et al. Rhesus macaques are more susceptible to progressive tuberculosis than cynomolgus macaques: A quantitative comparison. Infect Immun. 2018;86: 1–14. doi:10.1128/IAI.00505-17
18. Ganchua SKC, White AG, Klein EC, Flynn JAL. Lymph nodes—The neglected battlefield in tuberculosis. PLoS Pathog. 2020;16: 1–19. doi:10.1371/JOURNAL.PPAT.1008632
19. Regoes RR, Wiuff C, Zappala RM, Garner KN, Baquero F, Levin BR. Pharmacodynamic Functions : a Multiparameter Approach to the Design of Antibiotic Treatment Regimens. Antimicrob Agents Chemother. 2004;48: 3670–3676. doi:10.1128/AAC.48.10.3670
20. Ankomah P, Levin BR. Two-drug antimicrobial chemotherapy: A mathematical model and experiments with Mycobacterium marinum. PLoS Pathog. 2012;8. doi:10.1371/journal.ppat.1002487
21. Pienaar E, Cilfone NA, Lin PL, Dartois V, Mattila JT, Butler JR, et al. A computational tool integrating host immunity with antibiotic dynamics to study tuberculosis treatment. J Theor Biol. 2015;367: 166–179. doi:10.1016/j.jtbi.2014.11.021
22. Lakshminarayana SB, Huat TB, Ho PC, Manjunatha UH, Dartois V, Dick T, et al. Comprehensive physicochemical, pharmacokinetic and activity profiling of anti-TB agents. J Antimicrob Chemother. 2015;70: 857–867. doi:10.1093/jac/dku457
23. Sarathy JP, Via LE, Weiner D, Blanc L, Boshoff H, Eugenin EA, et al. Extreme drug tolerance of mycobacterium tuberculosis in Caseum. Antimicrob Agents Chemother. 2018;62: 1–11. doi:10.1128/AAC.02266-17
24. Cokol M, Li C, Chandrasekaran S. Chemogenomic model identifies synergistic drug combinations robust to the pathogen microenvironment. PLoS Comput Biol. 2018;14: 1–24. doi:10.1371/journal.pcbi.1006677
25. Pienaar E, Matern WM, Linderman JJ, Bader JS, Kirschner DE. Multiscale Model of Mycobacterium tuberculosis Infection Maps Metabolite and Gene Perturbations to Granuloma Sterilization. Infect Immun. 2016;84: 1650–1669. doi:10.1128/IAI.01438-15.Editor
26. Cicchese JM, Evans S, Hult C, Joslyn LR, Wessler T, Millar JA, et al. Dynamic balance of pro- and anti-inflammatory signals controls disease and limits pathology. Immunol Rev. 2018;285: 147–167. doi:10.1111/imr.12671
27. Gideon HP, Phuah J, Myers AJ, Bryson BD, Rodgers MA, Coleman MT, et al. Variability in tuberculosis granuloma T cell responses exists, but a balance of pro- and anti-inflammatory cytokines is associated with sterilization. PLoS Pathog.

2015;11. doi:10.1371/journal.ppat.1004603

28.   Cilfone NA, Perry CR, Kirschner DE, Linderman JJ. Multi-scale modeling predicts a balance of tumor necrosis factor-a and interleukin-10 controls the granuloma environment during Mycobacterium truberculosis infection. PLoS One. 2013;8: e68680. doi:10.1371/journal.pone.0068680

29.   Lin PL, Myers A, Smith L, Bigbee C, Bigbee M, Fuhrman C, et al. Tumor necrosis factor neutralization results in disseminated disease in acute and latent Mycobacterium tuberculosis infection with normal granuloma structure in a cynomolgus macaque model. Arthritis Rheum. 2010;62: 340–350. doi:10.1002/art.27271

30.   Fallahi-Sichani M, Flynn JL, Linderman JJ, Kirschner DE. Differential Risk of Tuberculosis Reactivation among Anti-TNF Therapies Is Due to Drug Binding Kinetics and Permeability. J Immunol. 2012;188: 3169–3178. doi:10.4049/jimmunol.1103298

31.   Marino S, Sud D, Plessner H, Lin PL, Chan J, Flynn JL, et al. Differences in reactivation of tuberculosis induced from anti-tNF treatments are based on bioavailability in granulomatous tissue. PLoS Comput Biol. 2007;3: 1909–1924. doi:10.1371/journal.pcbi.0030194

32.   Wong EA, Evans S, Kraus CR, Engelman KD, Maiello P, Flores WJ, et al. IL-10 Impairs Local Immune Response in Lung Granulomas and Lymph Nodes during Early Mycobacterium tuberculosis Infection . J Immunol. 2020;204: 644–659. doi:10.4049/jimmunol.1901211

33.   Winchell CG, Mishra BB, Phuah JY, Saqib M, Nelson SJ, Maiello P, et al. Evaluation of IL-1 Blockade as an Adjunct to Linezolid Therapy for Tuberculosis in Mice and Macaques. Front Immunol. 2020;11: 1–18. doi:10.3389/fimmu.2020.00891

34.   Conradie F, Diacon AH, Ngubane N, Howell P, Everitt D, Crook AM, et al. Treatment of highly drug-resistant pulmonary tuberculosis. N Engl J Med. 2020;382: 893–902. doi:10.1056/NEJMoa1901814

35.   Koul A, Vranckx L, Dendouga N, Balemans W, Van Den Wyngaert I, Vergauwen K, et al. Diarylquinolines are bactericidal for dormant mycobacteria as a result of disturbed ATP homeostasis. J Biol Chem. 2008;283: 25273–25280. doi:10.1074/jbc.M803899200

36.   Irwin SM, Prideaux B, Lyon ER, Zimmerman MD, Brooks EJ, Schrupp CA, et al. Bedaquiline and Pyrazinamide Treatment Responses Are Affected by Pulmonary Lesion Heterogeneity in Mycobacterium tuberculosis Infected C3HeB/FeJ Mice. ACS Infect Dis. 2016;2: 251–267. doi:10.1021/acsinfecdis.5b00127

37.   Zumla AI, Gillespie SH, Hoelscher M, Philips PPJ, Cole ST, Abubakar I, et al. New antituberculosis drugs, regimens, and adjunct therapies: Needs, advances, and future prospects. Lancet Infect Dis. 2014;14: 327–340. doi:10.1016/S1473-3099(13)70328-1

38.   Zumla A, Nahid P, Cole ST. Advances in the development of new tuberculosis drugs and treatment regimens. Nat Rev Drug Discov. 2013;12: 388–404. doi:10.1038/nrd4001

39.   Munro SA, Lewin SA, Smith HJ, Engel ME, Fretheim A, Volmink J. Patient Adherence to Tuberculosis Treatment: A Systematic Review of Qualitative

Research. PloS Med. 2007;4: 1230–1245. doi:10.1371/journal.pmed.0040238

40. Lyons MA, Reisfeld B, Yang RSH, Lenaerts AJ. A physiologically based pharmacokinetic model of rifampin in mice. Antimicrob Agents Chemother. 2013;57: 1763–1771. doi:10.1128/AAC.01567-12

41. Cordes H, Thiel C, Aschmann HE, Baier V, Blank LM, Kuepfer L. A physiologically based pharmacokinetic model of isoniazid and its application in individualizing tuberculosis chemotherapy. Antimicrob Agents Chemother. 2016;60: 6134–6145. doi:10.1128/AAC.00508-16

42. Global tuberculosis report 2019. 2019.

43. Nahid P, Mase SR, Migliori GB, Sotgiu G, Bothamley GH, Brozek JL, et al. Treatment of drug-resistant tuberculosis. An official ATS/CDC/ERS/IDSA clinical practice guideline. American Journal of Respiratory and Critical Care Medicine. 2019. doi:10.1164/rccm.201909-1874ST

44. Pienaar E, Linderman JJ, Kirschner DE. Emergence and selection of isoniazid and rifampin resistance in tuberculosis granulomas. PLoS One. 2018;13: 1–29. doi:10.1371/journal.pone.0196322

45. Dheda K, Lenders L, Magombedze G, Srivastava S, Raj P, Arning E, et al. Drug-penetration gradients associated with acquired drug resistance in patients with tuberculosis. Am J Respir Crit Care Med. 2018;198: 1208–1219. doi:10.1164/rccm.201711-2333OC

46. Gumbo T, Louie A, Liu W, Brown D, Ambrose PG, Bhavnani SM, et al. Isoniazid bactericidal activity and resistance emergence: Integrating pharmacodynamics and pharmacogenomics to predict efficacy in different ethnic populations. Antimicrob Agents Chemother. 2007;51: 2329–2336. doi:10.1128/AAC.00185-07

47. Ginsburg GS, Phillips KA. Precision medicine: From science to value. Health Aff. 2018;37: 694–701. doi:10.1377/hlthaff.2017.1624

48. Gideon HP, Skinner JA, Baldwin N, Flynn JL, Lin PL. Early Whole Blood Transcriptional Signatures Are Associated with Severity of Lung Inflammation in Cynomolgus Macaques with *Mycobacterium tuberculosis* Infection. J Immunol. 2016; 1601138. doi:10.4049/jimmunol.1601138

49. Britten N, Pope C, Halford S, Richeldi L. What if we made stratified medicine work for patients? Lancet Respir Med. 2016;4: 8–10. doi:10.1016/S2213-2600(15)00499-3

50. Babalik A, Mannix S, Francis D, Menzies D. Therapeutic drug monitoring in the treatment of active tuberculosis. Can Respir J. 2011;18: 225–229. doi:10.1155/2011/307150

Appendices

Appendix A Supplementary Information for Chapter 2
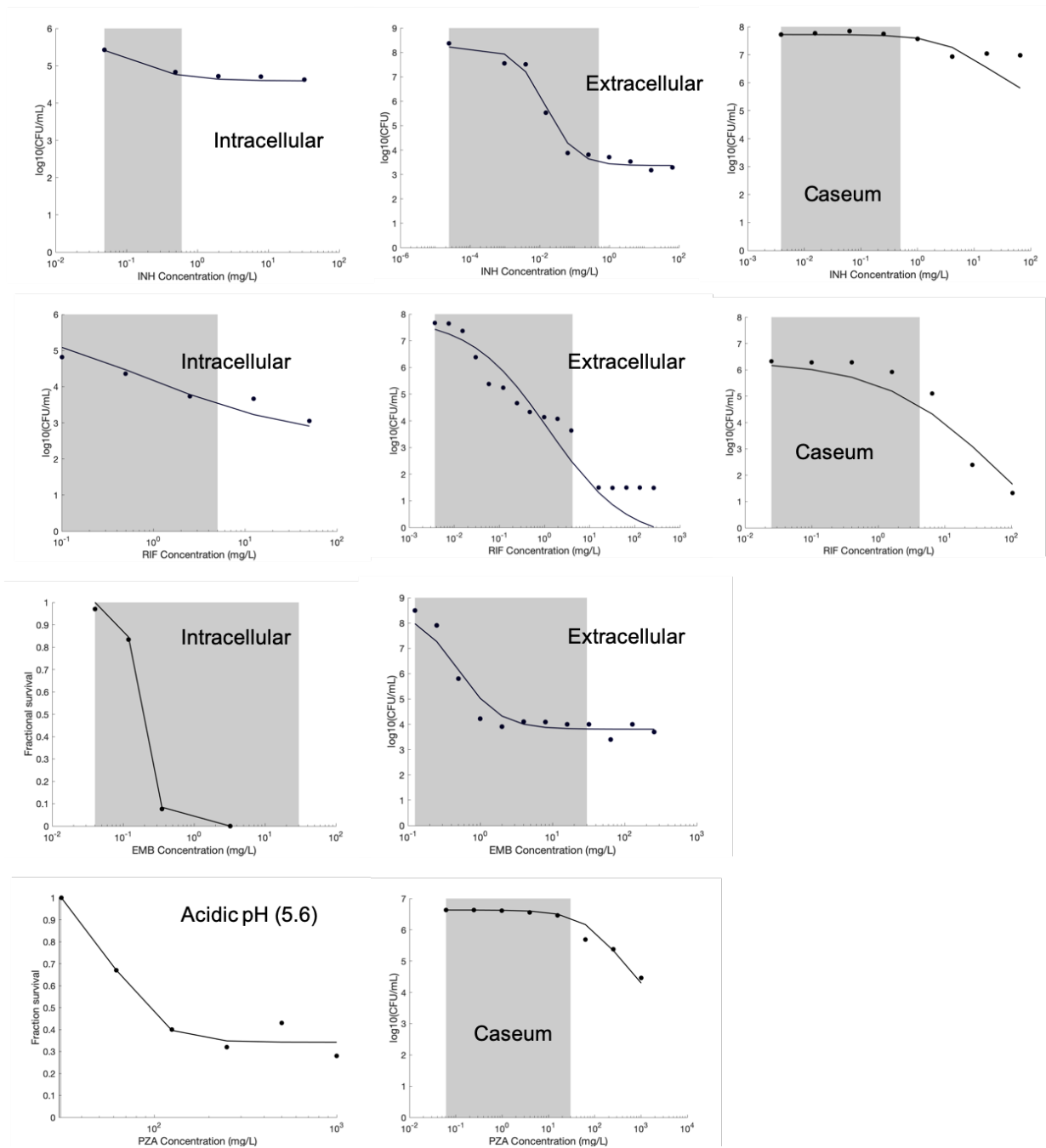
Figure A.1 Calibrated dose response curves
Calibrated dose-response curves (lines) to *in vitro* data (dots) of dose response assays from individual experiments from the literature for each antibiotic under various culture conditions. References for the data sets are listed in Table 2.3. Calibrated curves for antibiotics are presented in rows in the order INH, RIF, EMB and PZA from top to bottom. Gray shaded regions indicate concentration values reached in granulomas.
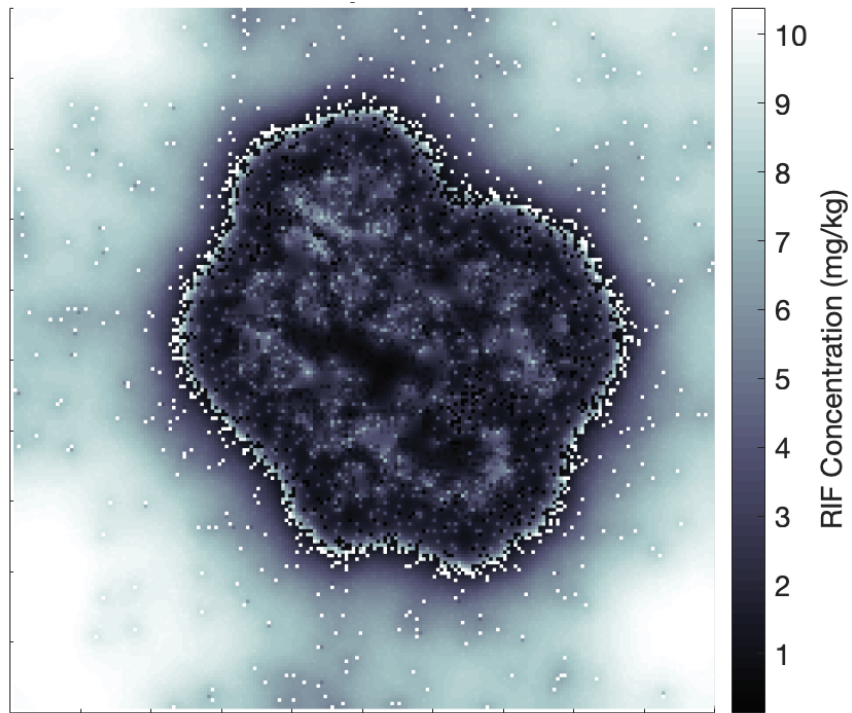
Figure A.2 Simulated spatial RIF distribution
The simulated spatial distribution of RIF in a granuloma with larger amounts of caseum. Concentrations shown are based on those observed after six hours following a fifth daily dose of 10 mg/kg RIF. The granuloma is simulated on a 200x200 simulation grid representing 4 mm x 4 mm of lung tissue. Compared to the single-dose RIF concentration in a smaller granuloma, accumulation of RIF is observed in caseated regions of the granuloma (lighter pockets dispersed throughout the center of the granuloma).
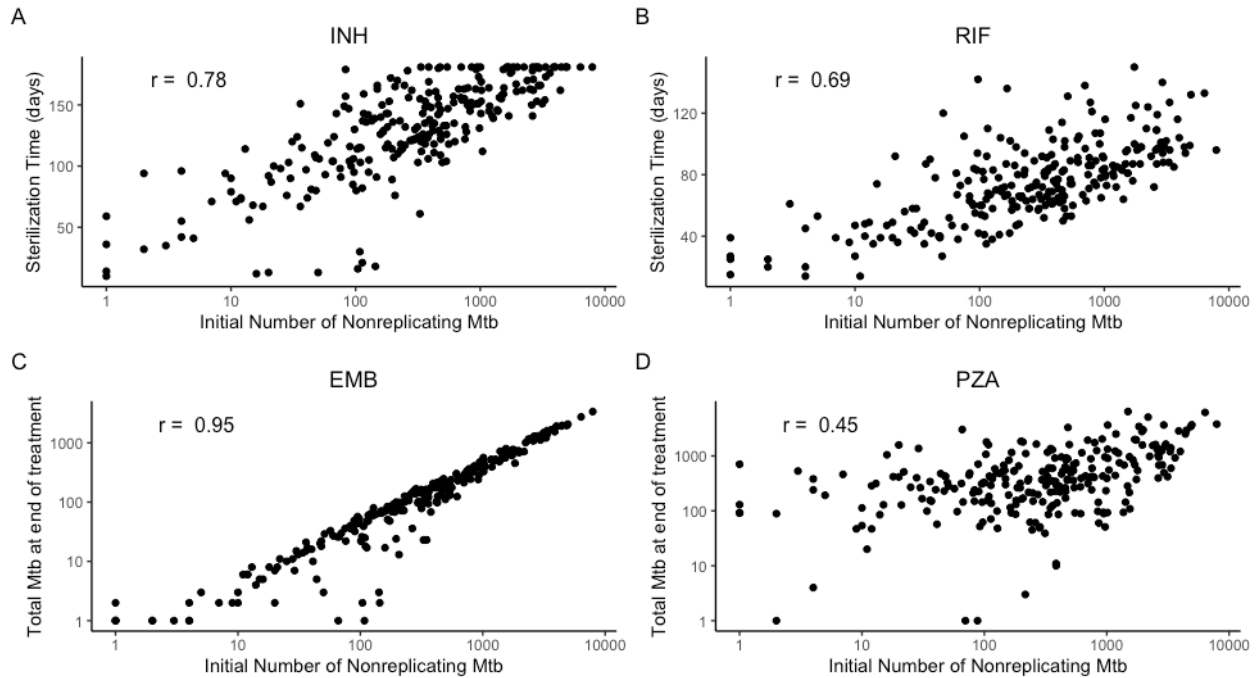
Figure A.3 Non-replicating Mtb are correlated with treatment outcomes
The number of non-replicating Mtb at the beginning of therapy (300 days post infection) is positively correlated with sterilization time or number of remaining Mtb at the end of treatment (180 days of treatment). (INH, A; RIF, B; EMB, C; PZA, D). INH and EMB show strong positive relationships with correlation coefficients 0.78 and 0.95 respectively. The correlations are for RIF and PZA, with coefficients of 0.69 and 0.45 respectively. RIF has the best ability to kill non-replicating Mtb, so the sterilization time is less dependent on that subpopulation's size. PZA shows little sterilizing activity in granulomas, so the number left at the end of treatment is more correlated with the initial number of Mtb.
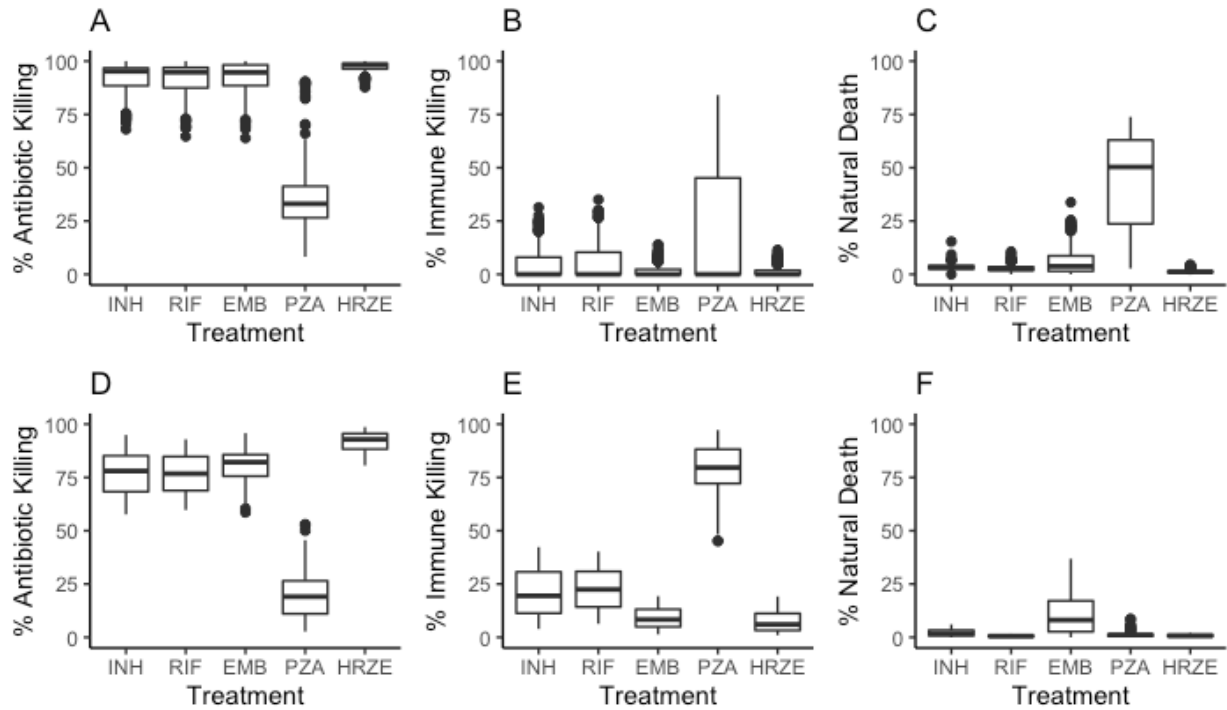
Figure A.4 The type of bacterial death during each treatment with average PK for low-CFU
The type of bacterial death during each treatment with average PK for low-CFU (A, B and C) and high-CFU (D, E, and F) granulomas. Figure shows the distribution of the percentrage of bacteria that die due to various causes over all granulomas. The types of death displayed are bacteria that died due to antibiotics (A and D), bacteria that died due to an immune response (B and E), and bacteria that died due to natural death through either starvation or death in caseum (C and F).
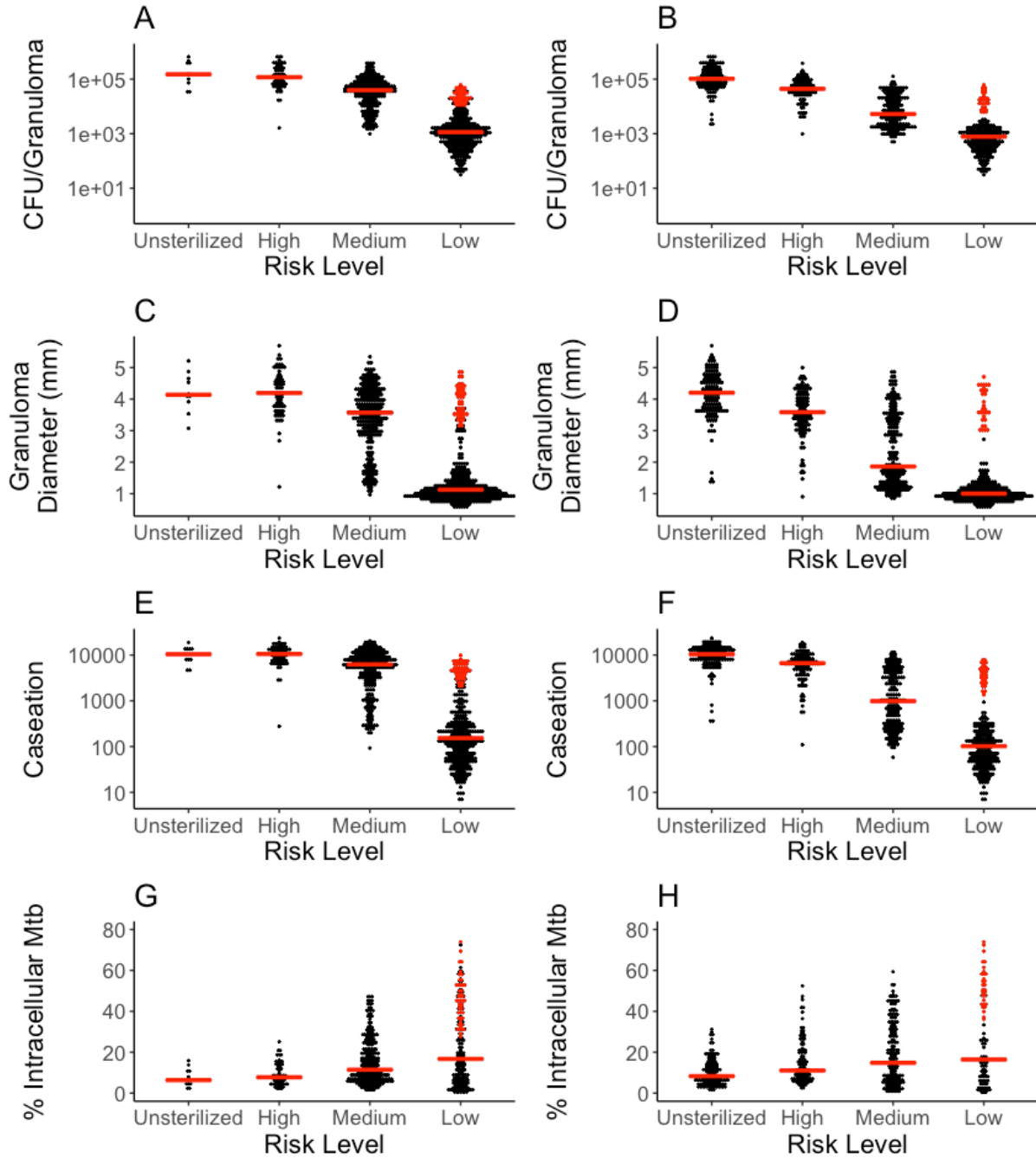
Figure A.5 Risk of granuloma treatment failure.
Simulated granulomas were classified into four risk of treatment failure categories based on sterilization time when treated with HRZE with average (A, C, E, G) and low (B, D, F, H) PK exposure. The four categories were unsterile (failed to sterilize), high (sterilized after 150 days), medium (sterilized between 90 and 150 days), and low (sterilized before 90 days). The plots show the distribution of pretreatment CFU/granuloma, diameter, amount of caseation (measured in number of caseated compartments in the simulation), and percentage of intracellular Mtb, for each risk category, with the median value indicated by the red line. Each dot is a single granuloma. Red dots indicate granulomas that are low risk but have characteristics similar to unsterilized or high-risk granulomas.

Appendix B Supplementary Information for Chapter 3

Table B.1 List of regimens simulated and their corresponding fractional inhibitory concentrations (FIC).
The antibiotics included and their abbreviations and standard doses are isoniazid (H, 5 mg/kg), rifampin (R, 10 mg/kg), ethambutol (E, 20 mg/kg), pyrazinamide (Z, 25 mg/kg), moxifloxacin (M, 7 mg/kg), and levofloxacin (L, 17 mg/kg). The regimen names give the single letter abbreviation, followed by the dose in mg/kg for that antibiotic. If no number is listed, the standard dose was used. The doses per week (dpw) are listed at the end of the regimen. If no doses per week is listed, doses were simulated as administered daily. The regimens used for validation of the model are labeled with an asterisk, corresponding to the regimens listed in Figure 3.4 and referenced from Bonnet *et al.* (2017)[1]

Regimen	FIC
HRZE	0.82
HR	1.35
HZ	0.97
HE	1.46
RZ	1.33
ZE	1.12
RE	0.74
HRZ	0.74
HRE	0.94
HZE	0.91
RZE	0.78
HMZE	1.05
RMZE	0.96
HM	2.01
RM	2.31
MZ	1.99
ME	1.8
HRM	1.08
HMZ	1.1
HME	1.19
RMZ	1.33
RME	0.99
MZE	1.19
HRMZ	0.92
HRME	0.93

HL	1.25
RL	1.53
LZ	1.47
LE	1.28
HRL	1.01
HLZ	1.11
HLE	1.15
RLZ	1.22
RLE	1.12
LZE	1.28
HRLZ	0.8
HRLE	0.89
HLZE	1.01
RLZE	0.94
H6E15*	1.46
H6E25*	1.46
R11E25*	0.74
R23.5E25*	0.74
H11R10*	1.35
H6R10E16*	0.94
H6R10E25*	0.94
H10R10E25*	0.94
R24Z64E90dpw1*	0.78
H16R12Z49dpw2*	0.74
H6R10Z27E16*	0.82
H5R10M7Z25dpw5*	0.92
R10M7Z25E15*	0.96
H14R10M9Z34dpw3*	0.92
H6E6*	1.46
H10E25*	1.46
R23.5E45dpw2*	0.74
R23.5E90dpw1*	0.74
H6R6E10*	0.94
H15R10E40dpw2*	0.94
H5R10Z25E17.5*	0.82
H6R9Z24E16dpw3*	0.82
H14R13Z47E29dpw3*	0.82

*Used for validation

164

Table B.2 Host immune parameters used with *GranSim* to generate the granuloma bio-repository.
Timestep units represent 10-minute time steps in the agent-based simulation. The minimum and maximum values for parameter ranges used in sampling are listed. Parameters are based on previous *GranSim* studies [2,3].

Parameter Definition	Units	Min	Max
# immune cell deaths causing compartment caseation		6	10
Time to heal caseated compartment	Timesteps	909	1365
TNF threshold for causing immune cell apoptosis	Molecules	690	1035
Rate constant for TNF-induced apoptosis	1/s	1.36e-6	2.04e-6
Minimum chemokine concentration to induce chemotaxis	Molecules	0.27	0.41
Maximum chemokine concentration to induce chemotaxis	Molecules	392	588
Initial density of macrophages	Fraction of grid compartments	0.019	0.029
Time between resting macrophage movements	Timesteps	4	6
Time between active macrophage movements	Timesteps	15	23
Time between infected macrophage movements	Timesteps	169	255
TNF threshold to induce NFkB activation	Molecules	42.8	64.1
Rate constant for NFkB activation	1/s	6.77e-6	1.01e-5
Probability resting macrophage kills extracellular Mtb		0.0738	0.111
Killing probability adjustment for resting macrophages with NFkB activation		0.129	0.194
# bacteria to cause NFkB activation		236	354

|			
# bacteria for macrophage to become chronically infected		12	18
# bacteria to cause macrophage to burst		19	29
# bacteria activated macrophage can phagocytose		3	5
Probability activated macrophage will will heal a caseated compartment		0.00459	0.00687
Probability a T-cell will move to same compartment as a macrophage		0.0367	0.0550
Probability IFNγ producing T-cell induces Fas/FasL apoptosis		0.0293	0.0439
Probability IFNγ producing T-cell also produces TNF		0.0514	0.0770
Probability cytotoxic T-cell kills macrophage		0.00505	0.0121
Probability cytotoxic T-cell kills a macrophage and all its intracellular bacteria		0.619	0.928
Probability regulatory T-cell deactivates macrophage		0.00584	0.00876
Time when T-cell recruitment begins	Timesteps	3225	4722
Time delay after T-cell recruitment begins until maximal recruitment rate	Timesteps	650	976
Macrophage maximal recruitment probability		0.0241	0.0361
Macrophage threshold for recruitment by chemokines	Molecules	0.641	0.960
Macrophage threshold for recruitment by TNF	Molecules	0.00859	0.0129
Macrophage half saturation for recruitment by TNF	Molecules	1.22	1.82

Macrophage half saturation for recruitment by chemokine	Molecules	1.68	2.52
IFNγ producing T-cell maximal recruitment probability		0.0484	0.0726
IFNγ producing T-cell threshold for recruitment by chemokine	Molecules	0.0535	0.0802
IFNγ producing T-cell threshold for recruitment by TNF	Molecules	1.01	1.51
IFNγ producing T-cell half saturation for recruitment by TNF	Molecules	1.22	1.82
IFNγ producing T-cell half saturation for recruitment by chemokine	Molecules	1.64	2.46
Probability a IFNγ producing T-cell is cognate		0.0437	0.0655
Cytotoxic T-cell maximal recruitment probability		0.0370	0.0554
Cytotoxic T-cell threshold for recruitment by chemokine	Molecules	3.55	5.32
Cytotoxic T-cell threshold for recruitment by TNF	Molecules	0.920	1.38
Cytotoxic T-cell half saturation for recruitment by TNF	Molecules	0.715	1.07
Cytotoxic T-cell half saturation for recruitment by chemokine	Molecules	5.24	7.86
Probability a cytotoxic T-cell is cognate		0.0414	0.0620
Regulatory T-cell maximal recruitment probability		0.0246	0.0369
Regulatory T-cell threshold for recruitment by chemokine	Molecules	2.03	3.04
Regulatory T-cell threshold for recruitment by TNF	Molecules	1.65	2.47

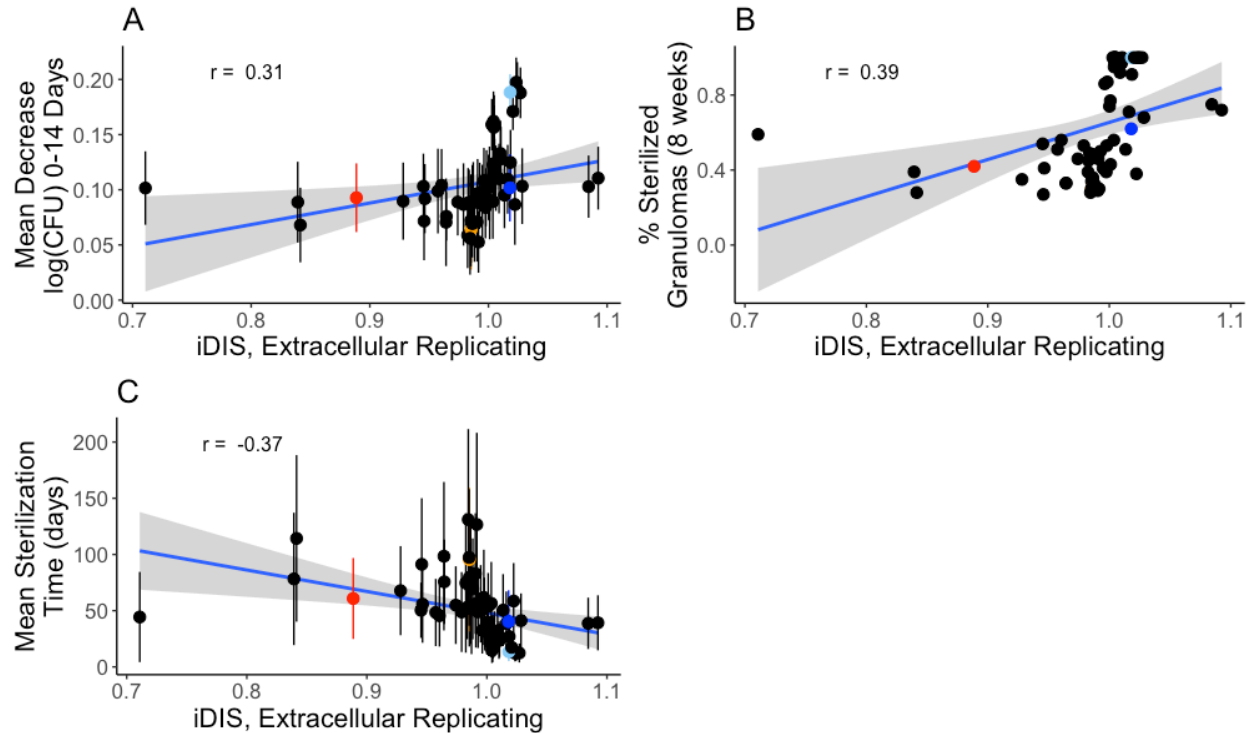|			
Regulatory T-cell half saturation for recruitment by TNF	Molecules	2.00	3.00
Regulatory T-cell half saturation for recruitment by chemokine	Molecules	1.23	1.84
Probability a regulatory T-cell is cognate		0.0400	0.0600

Table B.3 Plasma PK PRCC Values

For four regimens (HRZE, RE, HE and RM), the table shows the PRCC values relating the plasma PK parameters to the predicted iDIS for non-replicating Mtb during the first dose of treatment. All PRCC values reported are significant with p<0.01 and NS designates that the parameter was not significant. The parameters for each antibiotic listed include the absorption rate constant (kAbs), the intercompartmental clearance (Q), the volume of distribution for the plasma (central) compartment (Vol. Dist. Cent.), the volume of distribution for the peripheral compartment (Vol. Dist. Periph.), and the clearance rate constant (CL).

	INH					RIF					EMB					PZA					MXF				
	kAbs	Q	Vol. Dist. Cent	Vol. Dist. Periph	CL	kAbs	Q	Vol. Dist. Cent	Vol. Dist. Periph	CL	kAbs	Q	Vol. Dist. Cent	Vol. Dist. Periph	CL	kAbs	Q	Vol. Dist. Cent	Vol. Dist. Periph	CL	kAbs	Q	Vol. Dist. Cent	Vol. Dist. Periph	CL
HRZE	NS	-0.66	0.34	-0.18	-0.20	0.28	NS	NS	NS	0.89	0.43	NS	-0.26	NS	-0.56	NS	NS	0.54	NS	0.21					
RE						NS	NS	NS	NS	0.90	0.74	-0.27	-0.23	-0.20	-0.92										
HE	-0.31	-0.87	0.67	-0.33	-0.39						-0.68	0.26	0.30	0.20	0.88										
RM						NS	NS	NS	-0.26	-0.83											NS	0.12	0.19	-0.95	0.99
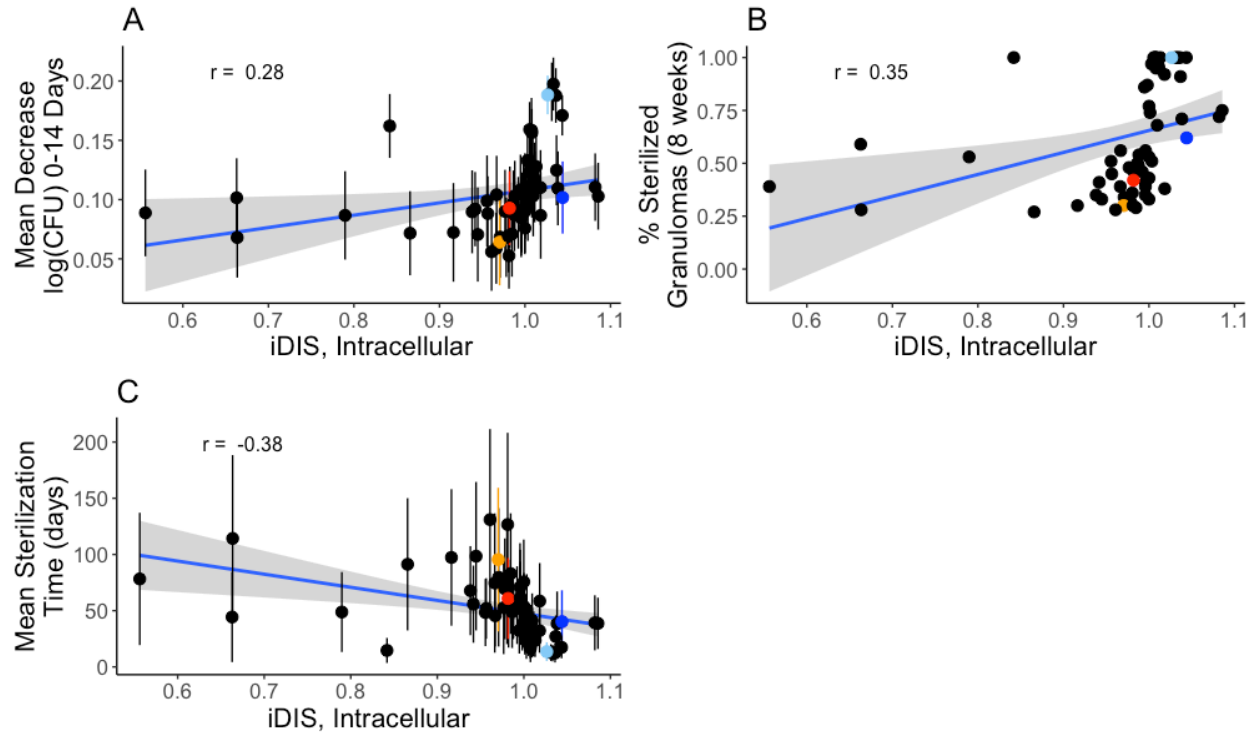
Figure B.1 Measures of regimen efficacy are correlated with interaction strength associated with intracellular replicating Mtb killing rate for 64 regimens.
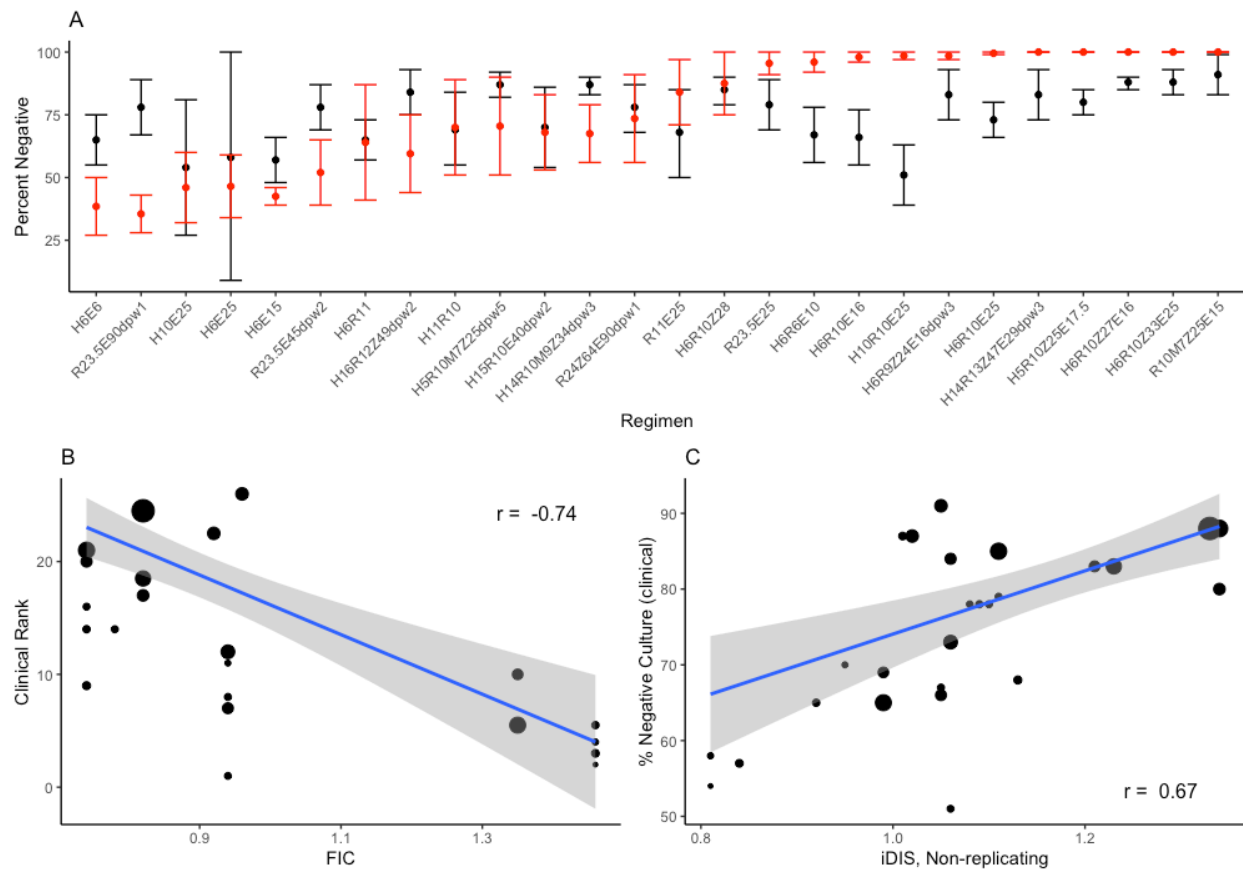
The mean decrease in log CFU (0-14) averaged over each 100 granulomas simulated for each regimen (A) and percentage of sterilized (negative) granulomas after eight weeks of treatment (B) are weakly positively correlated with the average interaction strength experienced by non-replicating Mtb during the first 24 hours of treatment with correlation coefficients of 0.28 and 0.35 respectively. Mean sterilization time for each regimen over 100 granulomas (C) is negatively correlated with the average interaction strength with a correlation coefficient of -0.38. Each point represents the regimen outcome measurement for a given regimen and error bars indicate +/- standard deviation from the sample of 100 granulomas simulated. The colored points correspond to the regimens HRZE (light blue), RE (dark blue), RM (red) and HE (orange).

170

Figure B.2 Measures of regimen efficacy are correlated with interaction strength associated with extracellular replicating Mtb killing rate for 64 regimens.

The mean decrease in log CFU (0-14) averaged over each 100 granulomas simulated for each regimen (A) and percentage of sterilized (negative) granulomas after eight weeks of treatment (B) are weakly positively correlated with the average interaction strength experienced by non-replicating Mtb during the first 24 hours of treatment with correlation coefficients of 0.28 and 0.35 respectively. Mean sterilization time for each regimen over 100 granulomas (C) is negatively correlated with the average interaction strength with a correlation coefficient of -0.38. Each point represents the regimen outcome measurement for a given regimen and error bars indicate +/- standard deviation from the sample of 100 granulomas simulated. The colored points correspond to the regimens HRZE (light blue), RE (dark blue), RM (red) and HE (orange).

Figure B.3 Comparison of treatment simulations with clinical trial results
Comparison of treatment simulations with clinical trial results for 26 different regimens compiled in Bonnet *et al.*
(2017)[1]. The clinical regimen efficacy metric used is solid culture conversion following 8 weeks of therapy. We
compare the confidence intervals (black) to the percent of simulated granulomas that sterilized (lower red bar) or had
fewer than 10 CFU after 8 weeks of therapy (upper red bar, red dot average of error bars) for all 26 regimens (A).
Regimens are abbreviated by the single antibiotic abbreviation, followed by the dose in mg/kg for that antibiotic, with
the doses per week (dpw) listed at the end of the regimen abbreviation. FIC is negatively correlated with clinical rank
with a weighted correlation of -0.74 (B), and iDIS is positively correlated with clinical rank with a weighted correlation
of 0.67 (C). Each dot represents an individual regimen, its size is linearly scaled by the number of patients treated (B
and C)
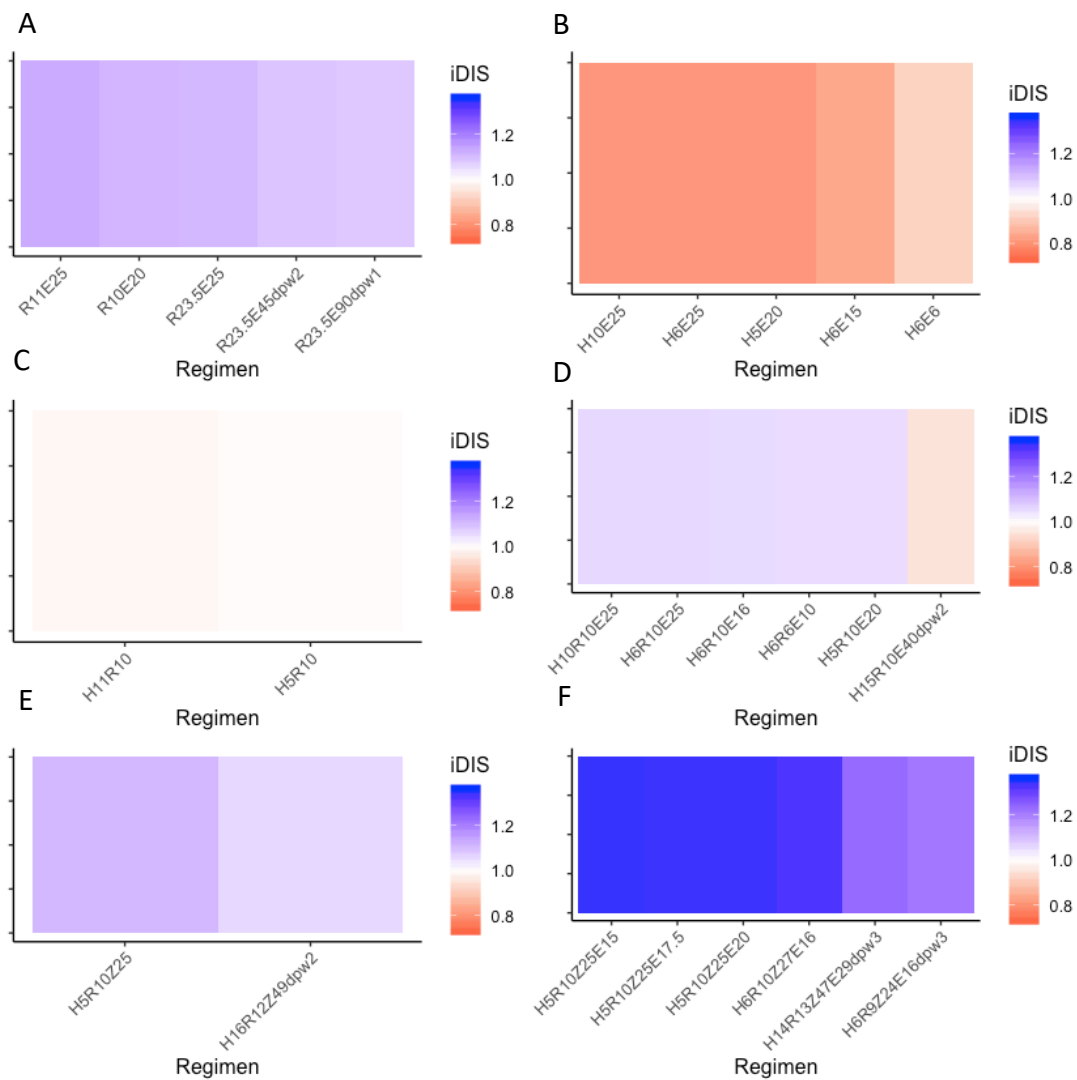
Figure B.4 Heat map of predicted iDIS value for different regimens of the same antibiotic combination.
The list of regimens is ordered by decreasing predicted in vivo DIS for regimens involving the antibiotic combination RE (A), HE (B), HR (C), HRE (D), HRZ (E) and HRZE (F). For predicated IDIS blue represents synergy, white represents additivity, and red represents antagonism.

References

1. Bonnett LJ, Ken-dror G, Koh GCKW, Davies GR. Comparing the Efficacy of Drug Regimens for Pulmonary Tuberculosis: Meta-analysis of Endpoints in Early-Phase Clinical Trials. Clin Infect Dis. 2017;65: 46–54. doi:10.1093/cid/cix247
2. Pienaar E, Cilfone NA, Lin PL, Dartois V, Mattila JT, Butler JR, et al. A computational tool integrating host immunity with antibiotic dynamics to study tuberculosis treatment. J Theor Biol. 2015;367: 166–179. doi:10.1016/j.jtbi.2014.11.021
3. Cicchese JM, Dartois V, Kirschner DE, Linderman JJ. Both Pharmacokinetic Variability and Granuloma Heterogeneity Impact the Ability of the First-Line Antibiotics to Sterilize Tuberculosis Granulomas. Front Pharmacol. 2020;11: 1–15. doi:10.3389/fphar.2020.00333

Appendix C Supplementary Information for Chapter 5

Table C.1 NHP plasma PK parameters.
The ranges for the plasma PK parameters calibrated to NHP plasma data. Parameters calibrated in previously published studies [1,2], except for moxifloxacin, whose data and calibrated curves are shown in Figure C.1.

Parameter	Units	INH	RIF	MXF	EMB	PZA
Absorption rate constant	1/h	[0.3, 1.2]	[0.50,0.74]	[0.1,0.4]	[0.1,0.6]	[1.4,1.6]
Intercompartmental clearance rate constant	L/(h*kg)	[0.05,0.3]	[0.1,0.5]	[0.2,1.0]	[0.5,1.4]	[3.5,4.5]
Central compartment volume of distribution	L/kg	[1,3]	[0.56,0.66]	[4.5,10]	[1,4]	[0.3,0.7]
Peripheral compartment volume of distribution	L/kg	[15,35]	[0.05,0.15]	[15,25]	[2,10]	[0.2,0.4]
Plasma clearance rate constant	L/(h*kg)	[1.2,2.2]	[0.70,0.092]	[0.3,1.3]	[2,3]	[0.25,0.35]
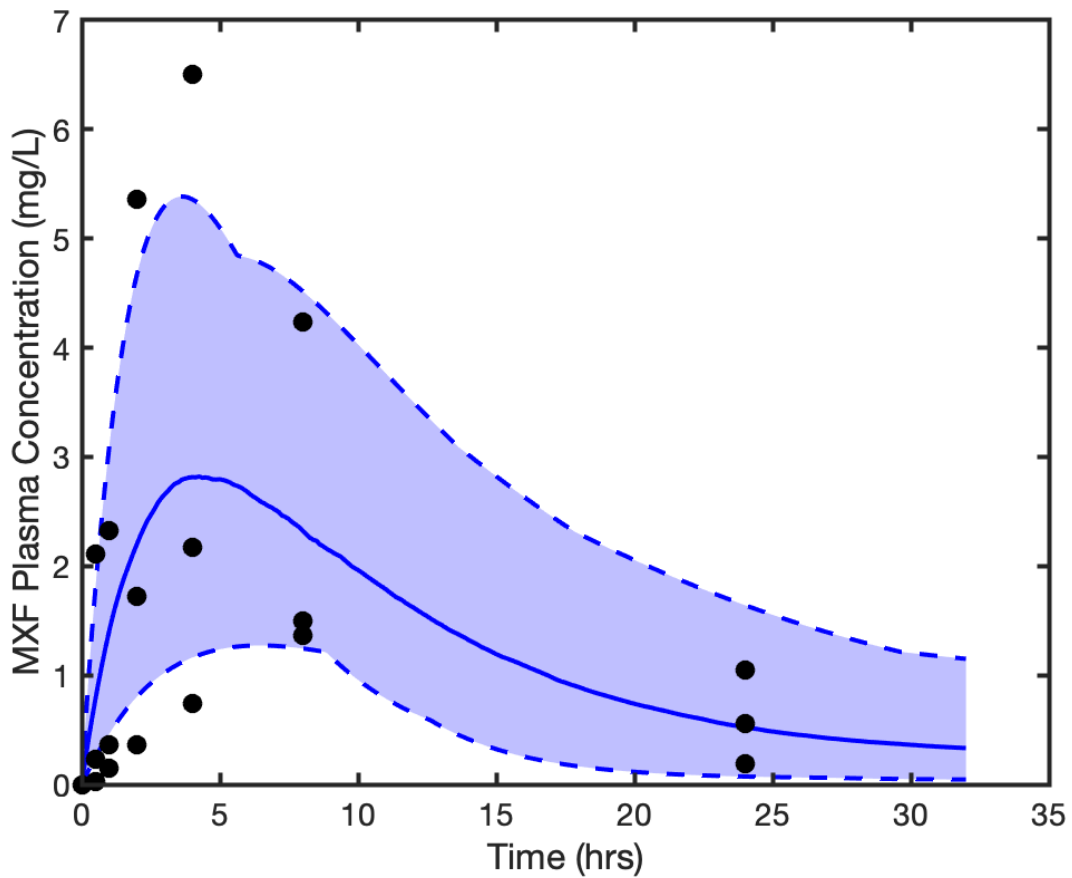
Figure C.1 NHP plasma PK calibration for MXF
The calibrated ranges for the plasma PK parameters calibrated to NHP plasma data (black dots) and the range of simulation outcomes (blue shaded area) with median concentration (blue line). Median plasma PK parameter calibrated to minimize the sum of the squared error between data and simulation outcome, and the ranges for parameters were set to capture full range of observed data. Data from NHP were obtained by administering a single oral dose of 50 mg/kg to three subjects, and serial blood draws at 0.5, 1, 2, 4, 8 and 24 hours (data unpublished).

References

1.   Pienaar E, Cilfone NA, Lin PL, Dartois V, Mattila JT, Butler JR, et al. A computational tool integrating host immunity with antibiotic dynamics to study tuberculosis treatment. J Theor Biol. 2015;367: 166–179. doi:10.1016/j.jtbi.2014.11.021

2.   Lin PL, Dartois V, Johnston PJ, Janssen C, Via L, Goodwin MB, et al. Metronidazole prevents reactivation of latent Mycobacterium tuberculosis infection in macaques. Proc Natl Acad Sci. 2012;109: 14188–14193. doi:10.1073/pnas.1121497109